PROPERTIES OF INFRARED-LUMINOUS GALAXIES,

or, How I Spent Seven Summer Vacations

A thesis by

David Paul Carico

In partial fulfillment of the requirements for the degree of

Doctor of Philosophy

California Institute of Technology

Pasadena, California

1991

Submitted August 9, 1990

God offers for every mind the choice
between truth and repose.

– Ralph Waldo Emerson

Whatever furnishes the semblance of an idea governed by
its Principle, furnishes food for thought.

– Mary Baker Eddy

It's OK to be a bum...just be an educated bum.

– Sachi Fujikawa
(my high–school English teacher)

DEDICATION

This thesis, everything that has gone into it, and everything that may ever come from it, is dedicated to:

— My family: Cal, Donna, and Joel Carico —

whose overwhelming love and support (financial, and otherwise!) has literally made this possible;

and

— Marion Kalb —

without whose insightful love and concern, I'm sure I'd still *be designing fuel pumps...*

ACKNOWLEDGEMENTS

It is a rare opportunity when one has a forum in which to express gratitude for a lifetime's influence and support from friends, colleagues, and family. I consider this thesis – representing the culmination of more than 23 years of formal education – to be such an opportunity. Please forgive the following spate of verbosity, then – I've been looking forward to this for many years, and have many folks to thank!

As this is an academic work, a good place to begin these acknowledgements of gratitude is with the various schools and teachers who have brought me through these years. The public schools which I attended throughout my childhood and years as a teenager – Apperson Street Elementary School; Mount Gleason Junior High School; Verdugo Hills High School – and the colleges/universities which provided the bulk of my adult academic education – Pierce Community College; the University of California, Berkeley; the California Institute of Technology – have all provided me with the solid educational background that I needed at each level, as well as many fond memories. I am truly thankful to each and every one of the teachers that I have had at these schools; although I may not have recognized it at the time, they have all given me something which I carry with me to this day, and I deeply appreciate their efforts in what is all too often, particularly at the pre–college level, a difficult and seemingly thankless job.

There are, of course, a number of teachers who stand out in my thought as especially helpful and/or influential in my life, and I wish to thank each of them directly: From high school, Mr. Newton, who was perhaps the best math teacher I have had anywhere and whose talents were generally not appreciated as they should have been, and Mr. Frank Simpson and Ms. Fujikawa, both of whom challenged my intellect by forcing me to think in new ways – a *very* worthwhile excercise, which is too often ignored in the classroom. From Pierce College, I extend special thanks to Dr. Duxler for my first fascinating experience with physics; to Dr. Kuljian (the great Dr. K!) for so successfully creating that most difficult combination – a chemistry course which was both intensely educational *and* the most fun I've ever had in a classroom! to Larry Small, for his enthusiastic support which has continued throughout my educational career; and to my dad, Cal Carico, and everyone else at the Pierce math department for helping to make those three semesters so enjoyable.

I join with probably every other Berkeley physics student in thanking Sumner Davis for his tremendous example of enthusiasm and love for the students, for teaching, and for physics. And at Caltech, my deepest thanks go to Eugene Cowan, for patiently helping me through what was, for me, a very difficult and frustrating subject; to Frank Porter, for maintaining such a friendly "open–door" policy, always finding time to talk with a confused student; and to Kip Thorne, for making the dryest and most challenging subject matter both fascinating and intelligible. Also, although I never had formal classes

with them, both Richard Feynman and Stephen Hawking presented several lectures which I was able to attend during my stay at Caltech, and these remain the most inspiring scientific lectures I have yet heard.

It is certainly true, particularly at the graduate level, that most of one's ultimate scientific education comes from research, rather than the classroom. In this regard, my education owes as much to my colleagues of the last several years as to my course instructors. At Berkeley, I benefited immensely from my involvement with the Berkeley Automated Supernova Search, and thank Rich Muller for providing that opportunity, and all of the team members, but particularly Carl Pennypacker and Shane Burns, for their friendship, assistance and support. Here at Caltech, my thanks go out to Gerry Neugebauer, Dave Sanders, Keith Matthews, James Graham, Erich Grossman, Jocelyn Keene, and especially Dan Watson (I can never thank you enough for helping to pull me through the worst night of my educational career!), all of whom have helped me at one time or another with my graduate research; also, thanks are due Pat Neill for help with more things than I could possibly mention; and without Taco's help, God knows where any of us would be – thanks a million! My appreciation also goes to all of the grad students whom I've come to know here, most especially my friends and tennis partners Erich Grossman and Todd Groesbeck, and Paul Kinney, wherever he is, for his friendship and for teaching me the wonders of *C*. I thank Gerry Neugebauer for the opportunity to be a part of the "IRA", and for financial support; and most importantly, Tom Soifer, my "official" and/or "unofficial" adviser, in the real meaning of the word, for the last seven years (your simple gesture of *not* telling the Director of Palomar that a certain first–year grad student had accidently shut down the 200 inch, meant more to me than you can imagine – I am forever indebted!) Finally, my deepest appreciation goes to Tom Soifer, Paul Robinson, Laurance Doyle, Nick Scoville, Carl Pennypacker, Shane Burns, Sumner Davis, Ed Danielson...and any other colleague whose kindness, patience, and humanity have enabled me to maintain my conviction that science and compassion are *not* mutually exclusive.

Despite the time and effort which has been required in my education, the most important aspects of my life have always been outside of the academic environment. Hence, it is most important to me that I express my gratitude for many years of wonderful, inspiring friends and relationships. In this regard, I won't attempt to go back through my entire life, nor can I possibly include every non–academic acquaintance which has been of value to me. But I want to thank those that are most prominent in my thoughts right now for their support and love, which I shall continually endeavor to return: Barbara Clarke; Greg and B.J. Chandler; Rich and Marilyn Tradewell; Carin Stout; Paul Peterson (it's been a while, but few people have had a greater impact on my life); Ruth Heffernan (the wonderful and talented E–mail correspondent!); Cathy Hubbell; Lisa McDermid; Laurance Doyle; Paul Robinson; Judith Barnett; Duncan and Susan Weathers; Jeff and Dora Roeca; Tina Lamperts; Christina Petersen; Jim and Carrie Wood; Chris and Nanette Burns (Teitelbaum? I'm sorry – I just can't get used to it!); and, finally, Greg and Rob, and everyone who contributed to the two best summers of my life! (Nurn, W. Germany,

has never been the same, guys...)

Of course, these acknowledgements would not be complete without mention of my extended family, who have loved and supported me, in person or in spirit, throughout my life: Shirley Dallas, Gordon and Anne Signor, Tim and Barbara Dallas, Chris Dallas, Bob and Mary Jane Carico, Susie and Carol Carico, and Margaret Carico.

Finally, there are those few individuals whose value in my life has truly been immeasurable, and for them it is impossible for me to do justice in words to my appreciation. Suffice it to say that my life has literally been shaped by their love and friendship. My heart therefore goes out to:

Brian Wright, whose love and inspiration are truly and continually boundless.

Jerry Mosley – friend, house–mate, landlord, philosopher, geographer–extraordinaire, and one of the wisest people I've known (who *still* can't figure out how to work the VCR!).

Kim Sindelar, and the first children I've ever grown to love, Jason and Kameryn – what an experience! You've taught me more about Life and Love than you'll probably ever imagine. You, your love, and friendship, are genuinely precious.

Pam Shanley Daube, my friend, confidante, one–woman support team, and the source of such unlimited joy and vitality! Thanks for more than I could possibly mention.

Marion Kalb, whose priceless love, friendship, and caring throughout so many years, and despite some seemingly overwhelming obstacles, has always been unfailing.

My family, Cal, Donna, and Joel – as wonderful a family as anyone has ever had.

For life and all the marvels that go with it, my infinite gratitude to the Creator.

ABSTRACT

Galaxies selected from the *IRAS* database having unusually high $60 - 100\mu m$ luminosities are studied at wavelengths ranging from $\sim 1 - 1000\mu m$. It is found that these galaxies differ significantly from normal, optically–selected galaxies, not only in their far–infrared luminosities, but in their near–infrared properties as well. A substantial excess emission at near–infrared wavelengths is attributed to emission from hot dust, with temperatures $\sim 500 - 1000$ K. Furthermore, this hot dust emission is confined to the central nuclear regions, within characteristic scale sizes $\sim 1 - 3$ kpc. This suggests that the bulk of the infrared luminosity, and hence the processes responsible for the extreme activity in infrared–luminous galaxies, is highly localized about galaxy nuclei. High resolution images of a number of these nuclei reveals a high percentage of double–nucleus sources amongst the most luminous galaxies, giving evidence that galaxy–galaxy interactions play a significant role in the generation of high infrared luminosities.

The distribution of the mass of, and luminosity from, dust in infrared–luminous galaxies is analyzed as a function of the temperature of the dust. It is found that, in galaxies for which the entire energy distribution is dominated by emission from dust heated to a steady–state, the mass of dust scales with steady–state temperature as $M \propto T^{-\alpha}$, where α is typically in the range $6 - 6.5$. Dust continues to contribute substantially to the total luminosity up to temperatures in excess of 300 K above the temperatures responsible for the peak in the infrared luminosity. At the lowest temperatures, however, it is very difficult to constrain the contribution to the observed emission: For the galaxies studied, the observations are consistent with models in which the amount of very cold dust ranges from essentially non–existent, to the dominant component of the total dust mass.

TABLE OF CONTENTS

Chapter THREE: The IRAS Bright Galaxy Sample: Multi–Beam Photometry of Galaxies With $L_{IR} \geq 10^{11} L_{\odot}$

Chapter FOUR: The Near–Infrared Morphology of Ultraluminous Infrared Galaxies

Chapter FIVE: The Temperature Distribution of Dust in Infrared Galaxies

LIST OF FIGURES

LIST OF TABLES

INTRODUCTION

The purpose of this thesis is to gain a better understanding of the nature and evolution of galaxies, by studying the infrared emission from galaxies which have been selected on the basis of being bright at 60 microns (μm). As will be shown, such an approach provides information on galaxies which cannot be obtained through optical studies, in that it enables a more direct analysis of the interstellar medium – that is, the material between the stars – rather than the stars themselves. This material can be a significant component of the mass of a galaxy, and it's emission often provides vital clues to the energetics and dynamics in a galaxy.

This chapter begins with a brief background on the history and terminology relevent to extragalactic infrared research; then, a discussion of infrared–selected galaxies is given; this is followed by a summary of the key results of this thesis; and finally, the results are interpreted in terms of their relevence to our understanding of galaxies in general.

I. Background on extra–galactic infrared astronomy

The study of galaxies at infrared wavelengths (which, throughout this thesis, will refer to wavelengths between roughly 1 μm and 1000 μm) essentially began as a scientific field during the mid–to–late 1960s. Early studies of individual galaxies can be found in the work of Johnson (1966), and Pacholczyk and Wisniewski (1967), while the first analysis at infrared wavelengths of a statistically significant number of galaxies was reported by Kleinmann and Low (1970), who detected strong infrared emission from 15 galaxies, and provided important evidence that *all* galaxies emit significant quantities of infrared radiation, and furthermore that, in some galaxies, the infrared luminosity dominates the energy distribution, and exceeds the entire luminosity of a normal galaxy. This was followed by a study of 50 extragalactic sources by Rieke and Low (1972), which confirmed the findings of Kleinmann and Low, identifying a number of galaxies whose infrared luminosities span the entire range from normal, low–luminosity galaxies, to quasars, which had for some years been recognized as the most luminous objects in the Universe. Galaxies with high infrared luminosities that dominate their energy output, and

equal or exceed the total luminosity of normal galaxies, are generally referred to as "infrared–luminous galaxies," or simply "infrared galaxies;" this terminology will be maintained throughout this work.

Unfortunately, infrared astronomy in general has from the start suffered from two severe difficulties – namely, the thermal emission from the earth's atmosphere, which imposes high background noise at infrared wavelengths, and the effectiveness of the atmosphere at absorbing radiation over much of the infrared range. Because of these considerations, ground–based work must of necessity be limited to a few select wavelength bands, wherein the atmosphere is, if not transparent, at least somewhat less opaque. The wavelength bands most suitable for ground–based observations are in the so–called "near–infrared" range, between roughly $1\mu m$ and $10\mu m$. Specifically, atmospheric transmission bands exist at mean wavelengths of approximately $1.3\mu m$, $1.6\mu m$, $2.2\mu m$, $3.7\mu m$, $4.7\mu m$, and $10\mu m$. Almost all of the early infrared work was done through one or more of these "windows." Additional translucent windows also exist at longer wavelengths, near $20\mu m$ and at $\sim 30 - 40\mu m$, and some significant early research was accomplished by utilizing these (see, e.g., Kleinmann and Low 1970; Rieke and Low 1975). But for the most part, at wavelengths beyond roughly $10\mu m$, measurements from the earth are, depending on the precise wavelength, either difficult or impossible.

Although various attempts were made to circumvent this limitation through airborn observations (see, e.g., Telesco, Harper, and Loewenstein 1976; Smith 1982), there is little doubt that the greatest breakthrough in extra–galactic infrared astronomy came in January of 1983 with the launch of the *Infrared Astronomical Satellite* (*IRAS*; see Neugebauer *et al.* 1984). During its 10 months of data collection, the instrument succeeded in surveying 96% of the sky at $12\mu m$, $25\mu m$, $60\mu m$, and $100\mu m$, and sent back a wealth of data, including measurements of many thousands of galaxies, a large fraction of which had never before been catalogued.

II. The galaxies studied in this thesis

As mentioned previously, much can be learned about the nature and evolution of galaxies by studying their interstellar medium. One way to facilitate such a study, is to measure the galaxies at infrared wavelengths. This is simply because the emission from a stellar population, being essentially

a population of thermally emitting "blackbodies" at temperatures ranging from a few thousand degrees, up to a few tens–of–thousands of degrees (see, e.g., Mihalas and Binney 1968, p.111), is effectively limited to wavelengths less than a few microns. Longward of this wavelength, the energy distribution for most[1] galaxies is dominated by thermal emission from "dust" grains – small particles (sizes $\lesssim 0.25 \mu m$), generally considered to be of graphitic and/or silicate composition (see Draine and Lee 1984, and references therein), that are often seen distributed throughout the interstellar medium, as well as in clouds or disks centered about individual stars ("circumstellar dust"), and in "HII–regions" (regions of high density/temperature gas and particles). Thus, a study of galaxies at infrared wavelengths is effectively a study of the interstellar dust in those galaxies.

The *IRAS* data provided an ideal opportunity for undertaking such a study, by providing the means for generating large, statistically complete samples of galaxies selected solely on the basis of their brightness at infrared wavelengths. The first such sample of infrared–selected galaxies was the *IRAS Minisurvey Sample*, presented by Soifer *et al.* (1984). The sample consists of 86 galaxies, selected on the basis of their $60 \mu m$ emission, from the *IRAS* minisurvey, a preliminary survey of a small region of the sky done prior to the complete all–sky survey (see Rowan–Robinson *et al.* 1984). A similar but considerably larger sample of infrared galaxies selected from the entire *IRAS* database was presented by Soifer *et al.* (1987). This sample, the *IRAS Bright Galaxy Sample* (hereafter referred to as the BG Sample), contains 313 galaxies (based on a revised version of the sample presented by Soifer *et al.* 1989) also selected on the basis of their 60 μm emission; it is statistically complete at $60 \mu m$ down to a flux density limit of 5.24 Jy,[2] and is one of the largest complete samples of infrared–selected galaxies.

With the exception of Chapter 1, the galaxies studied in this thesis are amongst the most luminous galaxies in the BG Sample, selected to have infrared luminosities[3] $L_{IR} \geq 10^{11} L_{\odot}$; hereafter these

[1] The class of galaxies known as *Seyfert* galaxies are believed to contain a substantial, if not dominant, contribution from non–thermal emission at infrared wavelengths; see Sanders *et al.* 1989, Osterbrock 1990.

[2] 1 Jy $\equiv 10^{-26}$ Watts m^{-2} Hz^{-1}.

[3] L_{IR} is an estimate of the luminosity between $8 \mu m$ and $1000 \mu m$; see Chapter 2. $L_{\odot}$ is the solar bolometric luminosity, 3.83×10^{26} Watts.

galaxies will be referred to as the luminous Bright Galaxies, or LBGs. As it is useful to have a sample of lower–luminosity galaxies to be used for comparison, an analysis of the Minisurvey galaxies is given in Chapter 1, and frequent reference to this sample is made throughout the later chapters. The Minisurvey galaxies are used as representative of lower luminosity galaxies rather than the rest of the BG Sample for two reasons: First, although the *IRAS* data are available for the entire BG Sample, a large part of this thesis involves analysis of the near–infrared emission as well, and there was not sufficient observing time to obtain measurements of a significant fraction of the Bright Galaxies. Second, the combination of the fact that the Minisurvey Sample had a factor of 10 lower flux density cutoff than the BG Sample, and the fact that the LBGs are, on average, a factor of 10 more luminous than the Minisurvey galaxies, gives the result that the two samples – the LBGs and the *entire* Minisurvey Sample – have virtually identical median redshifts: 0.0246 for the high luminosity Bright Galaxies, and 0.0272 for the Minisurvey galaxies. Hence, identical beam diameters used to measure the two samples of galaxies will, on average, measure regions in those galaxies of the same *physical* size.

Of course, the validity of this straight comparison between the Bright Galaxies and the Minisurvey galaxies requires that the two samples are equivalent representations of infrared galaxies. That this is so can be seen in Figure 1, which shows the distributions of the far–infrared luminosity in the two samples (Figure 1a), and the flux density ratio $f_\nu(60\mu m)/f_\nu(100\mu m)$ (Figure 1b), which relates to the temperature of the dust grains responsible for the bulk of the infrared emission, and hence characterizes the intensity of the radiation field heating those grains.

It is seen that, in regards to both properties, the two samples are indeed quite close. The median infrared luminosities for the two samples differ by only 30%, even though the distributions range over three orders of magnitude; and the median $f_\nu(60\mu m)/f_\nu(100\mu m)$ ratios differ by less than 10%. The only noticeable difference between the two samples appears to be the higher percentage of very high luminosity galaxies in the BG Sample: 69 of the 313 Bright Galaxies, or 22%, have $L_{FIR} \geq 10^{11}\ L_\odot$, whereas only 10 of the Minisurvey galaxies, or 12%, have such high far–infrared luminosities. The statistical significance of this distinction has not been investigated.

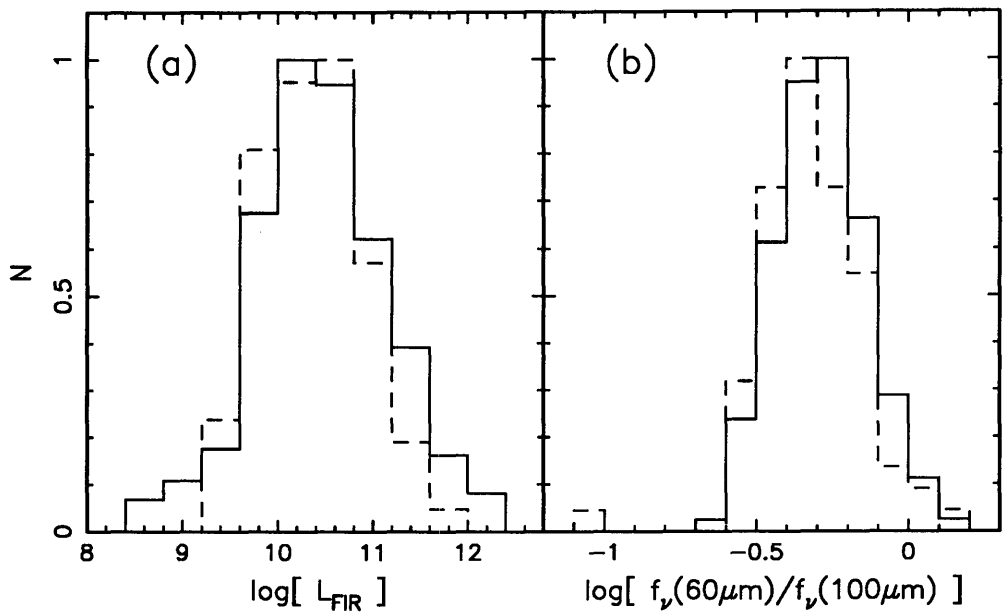

Fig. 1. The distribution of far–infrared luminosities (*a*) and flux density ratios $f_\nu(60\mu m)/f_\nu(100\mu m)$ (*b*) for the Bright Galaxies (***solid line***) and the Minisurvey galaxies (***dashed line***). For the BG Sample, the values of L_{FIR} are from Soifer (1990, private communication), and the values of the flux density ratios are from Soifer *et al.* (1989). The data for the Minisurvey galaxies are from Chapter 1 of this thesis. The distributions have been normalized to a maximum of 1.

A number of interesting results concerning infrared galaxies have come from the study of one or the other of these samples prior to this thesis. In particular, there is the not–surprising fact that both the Minisurvey galaxies and the Bright Galaxies have infrared–to–visible luminosity ratios which are generally higher, sometimes much higher, than those of normal, optically selected galaxies. For comparison, normal galaxies typically have infrared luminosities which are less than or comparable to their visible luminosities; for the Minisurvey galaxies, however, the infrared–to–visible luminosity ratios range up to more than 50, and for the most luminous Bright Galaxies, this ratio can be well over 100.

Another interesting result regarding infrared galaxies is the apparent connection between infrared activity and galaxy–galaxy interactions (throughout this thesis "infrared activity" will refer to the physical processes responsible for unusually high infrared emission, as observed, for example, in a high infrared–to–visible luminosity ratio). Soifer *et al.* (1984) pointed out the large fraction of interacting systems in the Minisurvey Sample; also, Lonsdale, Persson, and Matthews (1984) investigated the

issue in depth, through a comparison of the morphological characteristics of the Minisurvey galaxies and the infrared properties of a sample of optically–selected interacting systems. They found not only an unusually high fraction of galaxies in the Minisurvey Sample whose infrared emission was likely due to galaxy interactions, but substantially higher than normal infrared luminosities amongst the optically–selected interacting galaxies.

Toomre and Toomre (1972) pointed out that galaxy interactions provide a simple and likely means of funneling a sudden increased supply of material into the nucleus of one or the other of the galaxies involved, thereby triggering a burst of energetic activity, such as an abrupt and violent increase in star formation. Gunn (1979) provided the theoretical justification that infalling gas and dust in the center of a galaxy could provide sufficient fuel to "feed" the massive black hole in an active galactic nucleus (AGN),[4] and then went on to suggest that this infall of material might be triggered by a galaxy–galaxy collision or merger. It is thus possible that the unusually high interaction rate amongst infrared galaxies is causally connected to their unusually high degree of infrared activity.

The evidence for such a connection is strong: In addition to the results of Lonsdale, Persson, and Matthews (1984), Sanders *et al.* (1988) presented deep optical images of the ten galaxies from the BG Sample with infrared luminosities $L_{IR} \geq 10^{12}\ L_{\odot}$ (the "ultraluminous" infrared galaxies), and found that *all* of the galaxies show signs of recent tidal interaction, either in the existence of distinct multiple nuclei, or irregular tail–like structures (see Toomre and Toomre 1972). Furthermore, visible images (unpublished) taken by the author, in collaboration with Sanders, of a sample of 26 of the LBGs, show evidence for interaction in 65% of the galaxies.

It thus seems probable that, at the highest luminosities, galaxy–galaxy interactions trigger highly energetic activity which, in galaxies with significant quantities of dust, appears as increased infrared luminosity. What is *not* clear, and has been under debate for a number of years, is the nature of the energetic activity that actually gets triggered by the interaction. One possibility is an AGN in the most luminous infrared galaxies, which increases in infrared luminosity as the result of the infall of material

[4] Throughout this thesis, the term "active galactic nucleus" will refer to a quasar–like energy source; see Weedman (1986).

triggered by an interaction, as in the analysis of Gunn (1979). There is some evidence for this, in that samples of infrared galaxies tend to contain high percentages of Seyfert galaxies (de Grijp *et al.* 1985). Furthermore, based on a detailed study of the ten ultraluminous galaxies from the BG Sample, which included not only the optical images of these galaxies mentioned previously, but optical spectra and millimeter measurements of the molecular gas content, Sanders *et al.* (1988) argued that the primary energy source in the most luminous infrared is essentially a dust–enshrouded quasar.

On the other hand, the infrared emission from most of the LBGs is substantially extended, with significant emission seen out to at least several hundred parsecs[5] in radius (Chapter 2). Also, Rieke (1988) has pointed out that the X–ray emission from the ultraluminous galaxies is too low to attibute the predominant source of energy to a standard quasar. As an alternative, he has suggested that the observations can be satisfied by a moderate luminosity AGN, responsible for the observed quasar–like properties, coupled with intense circumnuclear star formation, responsible for the bulk of the infrared luminosity. Still another alternative has been suggested by Harwit *et al.* (1987), who argue that the extreme luminosities can be generated simply through collisional heating of the molecular gas through cloud–cloud interactions within the merging system.

None of these proposals can yet be considered proven correct, nor can any be entirely ruled out. The question of the source of the luminosity in the most extreme infrared galaxies, and the ultimate nature of the relation between galaxy collisions and infrared emission, remains a subject of active research and debate.

III. Summary of the thesis

This thesis consists of five chapters, identified as follows. Note that the first four have been previously published, and the corresponding references are given.

Chapter 1: Near–infrared observations of IRAS minisurvey galaxies.

Reference: Carico, D.P., B.T. Soifer, C. Beichman, J.H. Elias, K. Matthews, and G.

[5] 1 parsec = 3.26 light–years = 3.09×10^{18} cm; see, e.g., Mihalas and Binney 1968, for the origin of this unit.

Neugebauer, 1986. Near–infrared observations of *IRAS* minisurvey galaxies, *Astronom. J.*, **92**, 1254.

Chapter 2: The IRAS Bright Galaxy Sample: 1 – 10μm observations and coadded IRAS data for galaxies with $L_{IR} \geq 10^{11} L_{\odot}$.

Reference: Carico, D.P., D.B. Sanders, B.T. Soifer, J.H. Elias, K. Matthews, and G. Neugebauer, 1988. The *IRAS* Bright Galaxy Sample. III. $1 - 10\ \mu m$ observations and coadded *IRAS* data for galaxies with $L_{IR} \geq 10^{11}\ L_{\odot}$, *Astronom. J.*, **95**, 356.

Chapter 3: The IRAS Bright Galaxy Sample: Multi–beam photometry of galaxies with $L_{IR} \geq 10^{11} L_{\odot}$.

Reference: Carico, D.P., D.B. Sanders, B.T. Soifer, K. Matthews, and G. Neugebauer, 1990. The *IRAS* Bright Galaxy Sample. V. Multi–beam photometry of galaxies with $L_{IR} \geq 10^{11}\ L_{\odot}$, *Astronom. J.*, **100**, 70.

Chapter 4: The near–infrared morphology of ultraluminous infrared galaxies.

Reference: Carico, D.P., J.R. Graham, K. Matthews, T.D. Wilson, B.T. Soifer, G. Neugebauer, and D.B. Sanders, 1990. The near–infrared morphology of ultraluminous infrared galaxies, *Astrophys. J. (Letters)*, **349**, L39.

Chapter 5: The temperature distribution of dust in infrared galaxies.

The data utilized in each of these chapters were obtained from a variety of sources, and span the entire range of infrared wavelengths. These sources and wavelengths, and the relevence of each, will now be discussed briefly.

III.1 The data

As is implied by the choice of galaxy samples, the common thread tying all of the galaxies together is the IRAS data. For the Minisurvey galaxies, the $60\mu m$ and $100\mu m$ *IRAS* measurements are presented in Chapter 1 (most of these galaxies were not detected by *IRAS* at $12\mu m$ and $25\mu m$). For the BG

Sample, all of the galaxies discussed in Chapters 2 – 5 have *IRAS* flux densities at $25\mu m$, $60\mu m$, and $100\mu m$, and for most of the sources $12\mu m$ measurements are also available (see the individual chapters); these data are given in Chapter 2.

The *IRAS* data are perhaps the most fundamental to an understanding of dust emission from the most luminous galaxies; the energy distributions generally peak between $60\mu m$ and $100\mu m$ (Chapter 2), and it appears that beyond $\sim 100\mu m$, the distributions drop off extremely rapidly with increasing wavelength (Chapter 5). However, with only the four *IRAS* data points, many questions for any particular galaxy are still left unanswered. Hence, much of the effort behind this thesis has gone into obtaining follow–up measurements of the galaxies at other wavelengths, to obtain a more complete picture of the infrared emission.

The additional measurements have been taken primarily at near–infrared wavelengths. In Chapter 1, measurements at $1.25\mu m$, $1.65\mu m$, and $2.2\mu m$ are presented for 82 of the 86 Minisurvey galaxies; in Chapter 2, measurements at these same wavelengths, plus wavelengths of $3.7\mu m$ and $10.1\mu m$, are presented for the high luminosity Bright Galaxies. These measurements were all obtained at the Palomar Observatory 200 inch Hale Telescope.

Chapter 3 addresses a problem which has not yet been mentioned, namely the effect of the different beam sizes used for the measurements at different wavelengths. The size of the *IRAS* beams for the various detector arrays typically ranged from $0.76' \times 4.5'$ at $12\mu m$, to $3.0' \times 5.0'$ at $100\mu m$ (see the *IRAS Explanatory Supplement* 1988, p.II–12), whereas the beams used for the ground–based measurements at other wavelengths are typically much smaller: For comparison, the near–infrared measurements made at the Hale telescope generally used $5''$ diameter beams. This clearly creates a problem in comparing the short wavelength emission to the *IRAS* flux densities. In an effort to solve this problem, Chapter 3 presents near–infrared measurements at $1.25\mu m$, $1.65\mu m$, and $2.2\mu m$ of a sub–sample of the high luminosity galaxies presented in Chapter 2, taken at the Palomar Observatory 60 inch telescope utilizing beam diameters of $17''$, $33''$, and $55''$. These data are used in conjunction with the small diameter beam measurements from Chapter 2 to study the spatial distribution of the near–infrared emission, and as a

means of comparing the *total* near–infrared emission from infrared galaxies to their far–infrared emission as measured by *IRAS*.

Chapter 4 presents results obtained using an infrared imaging camera, developed recently at the Downs Laboratory of Physics at Caltech. The camera was used at the Hale telescope to obtain $2.2\mu m$ images, roughly 18″ square, of the nuclei of 9 of the most luminous galaxies from the BG Sample, all of which have infrared luminosities exceeding $10^{12}\ L_{\odot}$.

Finally, Chapter 5 includes measurements at 1.25 mm from the recently completed Caltech Submillimeter Observatory on Mauna Kea, in Hawaii. Measurements were obtained for 17 Bright Galaxies selected primarily for expected brightness at this wavelength, and secondarily for having a high infrared luminosity.

III.2 Results

Some of the key results from this thesis are:

(1) **From Chapters 1 and 2:** The near–infrared properties of infrared galaxies span the entire range of observed properties of extra–galactic sources – from those typical of normal, quiescent galaxies, to those of "starburst"[6] and Seyfert nuclei, and quasars.

(2) **From Chapter 3:** For those galaxies with unusual near–infrared emission, the physical processes responsible for that emission are confined within the central 1 – 3 kiloparsecs (kpc) about the galaxy nucleus; that is, *extreme infrared activity in galaxies is primarily a nuclear phenomenon.*

(3) **From Chapters 1, 2, and 5:** The primary *observable* effect of the nuclear activity can be attributed to an increase in the total mass of dust emitting at high temperatures. Although the bulk of the infrared luminosity is emitted from dust at temperatures ~30 – 50 K (Soifer *et al.* 1989), the near–infrared emission (Chapters 1 and 2) suggests that dust at temperatures as high as ~800 K is contributing at those wavelengths. Furthermore, a detailed analysis of the distribution of the dust

[6] Starburst nuclei are characterized by extreme levels of star formation activity which are believed to be short–lived (hence the term "burst"); see Weedman (1987), Balzano (1983).

mass as a function of temperature (Chapter 5) shows that a substantial fraction of the *total* infrared luminosity in some of the most luminous Bright Galaxies is emitted by dust at temperatures $\sim$ 100 – 300 K.

(4) **From Chapter 4:** Two of the nine ultraluminous galaxies imaged at 2.2 μm have previously undetected double nuclei, doubling the number of galaxies in the ultraluminous sample known to have double nuclei. Furthermore, three of these four double–nucleus sources have unusually red flux density ratios[7]

IV. Interpretation and implications of the results

Result (1) above, that the observed properties of infrared galaxies span the range from those of normal galaxies to those of starburst galaxies, Seyfert galaxies, and quasars, suggests that infrared galaxies are *not* an entirely new category of object; rather, they fill the gap between previously well–studied but seemingly disparate classes of objects. This result is consistent with the findings of Soifer *et al.* (1987) that a significant fraction, perhaps as high as 50%, of the total population of galaxies in the Universe may at some period in their lifetime undergo a period of high infrared activity. However, the current result extends this somewhat by suggesting the possibility that infrared galaxies may actually represent an evolutionary stage in the development of one or more of these other highly energetic systems.

The possibility that extreme infrared activity represents a phase in the development of a starburst nucleus or an AGN gains further evidence from results (2) and (3) above, which, taken together, indicate that extreme infrared activity is coupled with a greatly enhanced concentration of very hot dust in the galaxy nuclei. Since the expected temperature for dust grains in the general interstellar medium is $\sim$10 – 20 K (see, e.g., Draine and Lee 1984), dust grains heated to temperatures of several hundred degrees must be immersed in an extremely intense radiation field. The primary source of the radiation heating the hot dust in most of the LBGs cannot be a central AGN: The reason is simply that the dust emitting at temperatures $\sim$100 – 300 K would have to be well within roughly 100 parsecs of the AGN, whereas

[7] A "red" flux density ratio refers to an excess of emission at the longer wavelength.

Chapter 2 demonstrates that the 10 μm emission from most of the LBGs has a substantial component which is extended over regions at least several hundred parsecs in diameter. Thus, the luminosity source primarily responsible for the dust heating in these galaxies is more likely star formation. It follows, then, that the star formation must be extremely intense: For dust at 100 – 300 K, the radiation field must be equivalent to that from a hot star seen from a distance of 10^{16-17} cm – much less than a parsec. Thus, the hot stars in the nucleus must form a very dense population. This is further indicated by the results of Chapter 3, which show that the near–infrared luminosities within the central 2 kpc of the LBGs, although typically lower than those of Seyfert nuclei, are nonetheless considerably higher than those of starburst nuclei.

Rieke *et al.* (1980) have estimated that the lifetime of a non–recurring starburst phase in galaxies lasts for a time $\lesssim 10^8$ yrs. If this is true, and given that the extreme infrared activity is coupled with hot dust in the galaxy nucleus which is heated by intense star formation activity, the question of how this dust becomes concentrated in the nucleus needs to be addressed. The most straightforward solution is presumably that discussed in some detail in Section II, namely that the dust falls into the nucleus from its origin in the surrounding disk, and that this infall is triggered by tidal effects from a galaxy–galaxy interaction. The empirical evidence for this possibility, and the theoretical justification, have been brought out previously (Section II). Further evidence is given by result (4) above, that two previously undetected double–nuclei have been found amongst the ultraluminous galaxies. It is also known that higher–resolution follow–up observations of one of these galaxies (*Arp 220*) by Graham *et al.* (1990) yielded yet another double–nucleus in this group. Since the presence of a double nucleus is the strongest evidence for an on–going interaction, these results add further to the probable connection between galaxy interactions and infrared activity.

Although the evidence is strong that infrared activity is primarily triggered by galaxy interactions, this does not imply that galaxy interactions necessarily result in enhanced infrared activity. Haynes and Herter (1988) have addressed this very question by comparing the infrared properties of a sample of isolated single galaxies and a sample of isolated galaxy pairs. They find essentially no evidence for

enhanced infrared emission in the sample of galaxy pairs, and conclude that galaxy interactions do *not* generally imply substantial infrared effects.

One possible explanation for the results of Haynes and Herter (1988) is that enhanced infrared activity is *primarily* brought about as a result of the interaction of two galaxies, *both* of which already have enhanced dust masses in their disks prior to the interaction. This situation was stated by Sanders *et al.* (1988) as a necessary condition for the formation of the ultraluminous galaxies, and holds up fairly well in the results of Chapter 4 [result (4) above] in which 3 of the 4 double–nucleus sources were found to have enhanced infrared emission in both of their nuclei. It is interesting also to note that Haynes and Herter point out that the majority of their galaxy pairs show enhanced activity in only *one* of the galaxies. With this interpretation, the results of Haynes and Herter essentially provide a severe constraint on the fraction of galaxies which have sufficient dust in their disks to fuel a significant burst in infrared emission.

REFERENCES

Balzano, V.A., 1983. Star–burst galactic nuclei, *Astrophys. J.*, **268**, 602.

de Grijp, M.H.K., G.K. Miley, J. Lub, and T. de Jong, 1985. Infrared Seyferts: a new population of active galaxies?, *Nature*, **314**, 240.

Draine, B.T., and H.M. Lee, 1984. Optical properties of interstellar graphite and silicate grains, *Astrophys. J.*, **285**, 89.

Graham, J.R., D.P. Carico, K. Matthews, G. Neugebauer, B.T. Soifer, and T.D. Wilson, 1990. The double nucleus of Arp 220 unveiled, *Astrophys. J. (Letters)*, **354**, L5.

Gunn, J.E., 1979. Feeding the monster: gas discs in elliptical galaxies, in *Active Galactic Nuclei*, C. Hazard and S. Mitton (Eds.), Cambridge University Press, Cambridge, p.213.

Harwit, M., J.R. Houck, B.T. Soifer, and G.G.C. Palumbo, 1987. The most luminous far–infrared extragalactic sources, *Astrophys. J.*, **315**, 28.

Haynes, M.P., and T. Herter, 1988. Far–infrared emission in single and binary galaxies, *Astronom. J.*, **96**, 504.

Infrared Astronomical Satellite (IRAS) Catalogs and Atlases: *Explanatory Supplement*, 1988. C.A. Beichman, G. Neugebauer, H.J. Habing, P.E. Clegg, and T.J. Chester (Eds.), National Aeronautics and Space Administration, Washington D.C..

Johnson, H.L., 1966. *Astrophys. J.*, **143**, 187.

Kleinmann, D.E., and F.J. Low, 1970. Observations of infrared galaxies, *Astrophys. J. (Letters)*, **159**, L165.

Lonsdale, C.J., S.E. Persson, and K. Matthews, 1984. Infrared observations of interacting/merging galaxies, *Astrophys. J.*, **287**, 95.

Mihalas, D., and J. Binney, 1968. *Galactic Astronomy: Structure and Kinematics*, Freeman, San Francisco.

Neugebauer, G., *et al.*, 1984. The Infrared Astronomical Satellite (IRAS) mission, *Astrophys. J. (Letters)*, **278**, L1.

Osterbrock, D.E., 1990. Active galactic nuclei, *Reports on Progress in Physics*, submitted.

Pacholczyk, A.G., and W.Z. Wisniewski, 1967. Infrared radiation from the Seyfert galaxy NGC 1068, *Astrophys. J. (Letters)*, **147**, L394.

Rieke, G.H., 1988. Hard X–ray observations of ultraluminous infrared galaxies, *Astrophys. J. (Letters)*, **331**, L5.

Rieke, G.H., M.J. Lebofsky, R.I. Thompson, F.J, Low, and A.T. Tokunaga, 1980. *Astrophys. J.*, **238**, 24.

Rieke, G.H., and F.J. Low, 1972. Infrared photometry of extragalactic sources, *Astrophys. J. (Letters)*, **176**, L95.

Rieke, G.H., and F.J. Low, 1975. Measurements of galactic nuclei at 34μm, *Astrophys. J. (Letters)*, **200**, L67.

Rowan–Robinson, M., *et al.*, 1984. The IRAS minisurvey, *Astrophys. J. (Letters)*, **278**, L7.

Sanders, D.B., Phinney, E.S., Neugebauer, G., Soifer, B.T., and Matthews, K., 1989. Continuum energy distributions of quasars: shapes and origins, *Astrophys. J.*, **347**, 29.

Sanders, D.B., B.T. Soifer, J.H. Elias, B.F. Madore, K. Matthews, G. Neugebauer, and N.Z. Scoville, 1988. Ultraluminous infrared galaxies and the origin of quasars, *Astrophys. J.*, **325**, 74.

Smith, J., 1982. The far–infrared disk of M 51, *Astrophys. J.*, **261**, 463.

Soifer, B.T., L. Boehmer, G. Neugebauer, and D.B. Sanders, 1989. The *IRAS* Bright Galaxy Sample. IV. Complete *IRAS* observations, *Astronom. J.*, **98**, 766.

Soifer, B.T., D.B. Sanders, B.F. Madore, G. Neugebauer, G.E. Danielson, J.H. Elias, C.J. Lonsdale, and W.L. Rice, 1987. The IRAS Bright Galaxy Sample. II. The sample and luminosity function, *Astrophys. J.*, **320**, 238.

Soifer, B.T., *et al.*, 1984. Infrared galaxies in the IRAS minisurvey, *Astrophys. J. (Letters)*, **278**, L71.

Telesco, C.M., D.A. Harper, and R.F. Loewenstein, 1976. Far–infrared photometry of NGC 1068, *Astrophys. J. (Letters)*, **203**, L53.

Toomre, A., and J. Toomre, 1972. Galactic bridges and tails, *Astrophys. J.*, **178**, 623.

Weedman, D. W., 1986. *Quasar Astronomy*, Cambridge University Press, Cambridge.

Weedman, D.W., 1987. Starburst galaxies, in *Star Formation in Galaxies*, C.J. Lonsdale (Ed.), US Government Printing Office, Washington D.C., p. 351.

Chapter ONE:

Near–Infrared Observations of IRAS Minisurvey Galaxies

This article has previously appeared in
the *Astronomical Journal*, Vol. **92**, p.1254 (1986).
Coauthors: B.T. Soifer, C. Beichman, J.H. Elias,
K. Matthews, and G. Neugebauer.

ABSTRACT

Near-infrared photometry at J, H, and K has been obtained for 82 galaxies from the IRAS minisurvey, a sample of infrared selected galaxies. The near-infrared colors of these galaxies are similar to those of normal field spiral galaxies, but cover a larger range in $J - H$ and $H - K$. There is evidence of a tighter correlation between the near- and far-infrared emission than exists between the far-infrared and the visible emission. These results suggest that hot dust emission contributes to the 2.2 μm luminosity, and extinction by dust affects both the near-infrared colors and the visible luminosities. In addition, there is an indication that the far-infrared emission in many of the minisurvey galaxies is coming from a strong nuclear component.

I. INTRODUCTION

The IRAS minisurvey contained 86 galaxies that were detected at 60 μm and have Galactic latitude $|b| > 20°$ and visible counterparts on the Palomar Observatory Sky Survey (POSS) (see Soifer *et al.* 1984, as well as Rowan-Robinson *et al.* 1984, for an explanation of the IRAS minisurvey). As such, the galaxies in that survey represent a complete far-infrared selected sample of galaxies. Excess infrared emission in galaxies can be produced through various mechanisms, including (1) dust in the source galaxy which preferentially absorbs short wavelength radiation, with re-emission by dust of the absorbed starlight; this reemission can be either in the far-infrared, for cold intersellar dust, or the near-infrared, for hot circumstellar dust, and (2) non-thermal emission in the source galaxy. In order to study the general characteristics of far-infrared-bright galaxies in the near-infrared in an effort to better understand the possible source of the infrared luminosity in such galaxies, this paper presents near-infrared observations of the IRAS minisurvey galaxies and, utilizing also the available IRAS data, provides an analysis of the near- and far-infrared properties of the minisurvey sample of far-infrared-bright galaxies.

II. OBSERVATIONS AND DATA REDUCTION

II.1 Near–infrared observations

The 86 galaxies analyzed by Soifer *et al.* (1984) which comprise the minisurvey sample are listed in *IRAS Circular No. 6* (1984). Of these, 82 were observed at 1.25 μm (J), 1.65 μm (H) and 2.2 μm (K) using the 5 m Hale telescope at Palomar Observatory; these galaxies are listed in Table 1. A solid nitrogen cooled InSb detector was used for the observations, and for most of the galaxies a 10″ diameter beam was used. There were three observations (of 17153+1141, 17152+1940, and 17223+1906) which used a 5″ diameter beam, and one (of 18064+3942) which used an 8″ diameter beam; possible beam size effects are discussed below. Sky subtraction was achieved by chopping to reference positions 15″ north and south of the galaxy. The statistical uncertainties in the observed magnitudes are <0.08 mag, and are due primarily to errors in centering the beam on the nucleus of the galaxy. Since the corresponding colors are relatively insensitive to the beam position, their statistical uncertainties are <0.04 mag.

There were four galaxies from the original sample of Soifer *et al.* (1984) which were not observed in the near–infrared. Of these, one galaxy, 18056+3533 (1805+356P06), is too large for a measurement appropriate for this analysis to be made with the 5 m telescope. The remaining three are discussed below (Section II.2).

For several of the IRAS sources, there was more than one object within a 3σ uncertainty radius ($\sim$1') of the IRAS position. In such cases, near–infrared measurements were taken for all nearby objects which were not obviously point–like, and various methods were subsequently used to associate a single object with the IRAS source. For some cases, the near–infrared colors showed objects to be foreground stars. In other cases, accurate radio positions (S. Eales 1986) were used to identify the IRAS source on the assumption that the radio source and the IRAS source are the same (see, e.g., Helou, Soifer, and Rowan–Robinson 1985, and Sanders and Mirabel 1985). When radio positions were not available, the object which was closest in position to the IRAS source was taken to be the infrared source, provided that it was at least comparable in size and brightness to the other nearby object(s). For cases in which a single galaxy could not be selected positionally, the galaxy which was significantly brighter at 2.2 μm was chosen. If no unambiguous determination could be made, positionally or otherwise, the flux densities at each wavelength for each non–stellar object within 1' of the IRAS position were added together. The cases where multiple objects were found near the IRAS position are listed in the notes to Table 1.

Heliocentric redshifts have been obtained or were available in the literature for 80 of the 82 galaxies that were observed in the near–infrared. Most of these redshifts were obtained using either the double spectrograph (Oke and Gunn 1982) mounted at the Cassegrain focus of the Palomar 5 m telescope, or the Grism spectrometer on the 2.2 m telescope on Mauna Kea. The redshifts and their source are listed in Table 1.

Corrections were applied to the measured magnitudes of each galaxy to take into account wavelength dependent distortions in the beam profiles. Two–dimensional representations of the beam shapes for each wavelength were made by combining beam profiles obtained from north–south

and east–west scans across a star, and these two–dimensional representations were then numerically convolved with the de Vaucouleurs $r^{1/4}$ law (de Vaucouleurs 1948). The scale lengths in the de Vaucouleurs law for each galaxy profile were taken as $D_o/2$, where D_o is the galaxy major axis diameter as determined from the POSS blue prints by visually estimating the radius at which the galaxy brightness equals the sky background. The corresponding corrections subtracted from each observed magnitude were $0.03 - 0.07$ mag in J, $0.02 - 0.05$ mag in H, and $0.01 - 0.02$ mag in K, with uncertainties of $0.01 - 0.02$ mag. The resulting corrections to the near–infrared colors caused a decrease of $0.02 - 0.03$ mag in $J - H$ and $0 - 0.03$ mag in $H - K$, with uncertainties in the corrections on the order of 0.03 mag.

Corrections for Galactic reddening and redshift (K–corrections) were also applied to the observed magnitudes. The Galactic reddening corrections, A_λ, were obtained for each galaxy from the reddening maps of Burstein and Heiles (1982) using the reddening law of Cohen *et al.* (1981). The K–corrections, K_λ, were obtained by linearly interpolating between the K–corrections of S. E. Persson as given by Neugebauer *et al.* (1985). Using the convention that the corrected magnitude, $m_{o\lambda}$, and the measured magnitude, m, are related by $m_{o\lambda} = m - A_\lambda - K_\lambda$, the following mean values for the corrections and their corresponding dispersions were obtained: $A_J = 0.08 \pm 0.04$ mag, $A_H = 0.05 \pm 0.02$ mag, $A_K = 0.03 \pm 0.01$ mag, and $K_J = 0.02 \pm 0.02$ mag, $K_H = 0.00 \pm 0.01$ mag, $K_K = -0.12 \pm 0.08$ mag.

No correction for beam size has been made. Table 1 gives the values of $\log(A/D_o)$ for the minisurvey galaxies, where A is the beam diameter and D_o is as described above. Although the individual measurements of D_o are crude, they are nevertheless sufficient to indicate any significant effects that may exist in the sample as a whole. No evidence of any correlation between size and near–infrared colors was apparent. The observed and corrected K magnitudes and near–infrared colors are tabulated in Table 1. The two galaxies for which redshifts are not available have not been included in any of the following analysis; nevertheless, their observed near–infrared magnitudes and colors have been included in Table 1.

Elston *et al.* (1985) have published J, H, and K measurements for eight of the minisurvey galaxies. In almost every case their color measurements are significantly discrepant with the corresponding

measurements presented in this paper. For three of the galaxies for which the greatest discrepancy exists (17218+2110, 17519+3351, and 17526+3253), we have repeated the observations, and in each case these repeat measurements were in good agreement with the original Palomar results. The discrepancies are not due to different sources being selected as the correct IRAS source since none of the objects observed from Palomar can account for the extreme near–infrared colors reported by Elston *et al.*, and only two of the eight minisurvey galaxies for which Elston *et al.* report J, H, and K measurements have other objects nearby which could lead to such confusion.

II.2 IRAS data

The IRAS data used for this analysis were taken from the *IRAS Point Source Catalog* (1985, hereafter PSC) and are listed in Table 1. The data used by Soifer *et al.* (1984) in their analysis involved flux estimates which were revised prior to publication of the PSC. Two of the galaxies present in Soifer's sample, 0418+058P06 and 1751+319P06, did not qualify for inclusion in the PSC, and a third galaxy, 04203+0425 (0420+044P06), has only a limit listed in the PSC for the 60 μm flux density. These galaxies have been excluded from this paper. A fourth galaxy from Soifer's sample, 1733+803P06, was also excluded from the PSC, but in this case the IRAS observations were judged valid (Chester 1985). The 60 μm and 100 μm flux densities from the IRAS working survey data base for this galaxy are also listed in Table 1. The *IRAS Explanatory Supplement* (1985) includes a complete discussion of the uncertainties in the IRAS data.

Sixteen of the minisurvey galaxies have only limits in the PSC for the 100 μm flux density. For these galaxies, which are flagged in Table 1, the improved 100 μm or 60 μm flux densities or limits have been obtained from coaddition of IRAS survey data.

III. RESULTS

III.1 Near–infrared colors

The near–infrared colors for the minisurvey galaxies are plotted in Figure 1. There is one galaxy, 04210+0400, which is distinct from the rest of the sample with $J - H = 0.81$ and $H - K = 0.87$.

These measurements are appropriate for a galaxy with contributions at K of roughly 90% Seyfert nucleus and 10% normal galaxy (Glass 1981), and are consistent with the findings of Beichman *et al.* (1985) who speculate that this galaxy represents the first observational evidence for a transitional stage between Seyfert galaxies and narrow–line radio galaxies.

The region in Figure 1 enclosed by a dashed line is the region occupied by the normal spiral galaxies of Aaronson (1977), converted to the CIT photometric system of Frogel *et al.* (1978). The Aaronson sample was not intended as a statistically complete sample, but consists of 91 galaxies that were selected on the basis of being bright, well observed at other wavelengths, and covering a wide range of morphological types. Nevertheless, we will use Aaronson's sample as representative of normal field spiral galaxies.

It can be seen from Figure 1 that a large fraction of the minisurvey galaxies would be well fitted by the normal galaxy region were it not for a slight shift, amounting to roughly 0.02 mag in both $J - H$ and $H - K$. We consider such a small systematic effect with skepticism in view of the systematic uncertainties inherent in the comparison between the two samples. The effect can also be viewed as a somewhat larger shift of $\sim$0.05 mag in $H - K$ alone, making it consistent with a contribution to the 2.2 μm flux from dust emission. However, a conclusive determination as to whether this shift is a real effect would require measurements of both the minisurvey sample and a set of normal spiral galaxies using the same photometric system and is beyond the limits of this study.

The minisurvey galaxies are redder, on average, than the Aaronson galaxies and show a larger dispersion in $J - H$ and $H - K$. As is indicated in Figure 1, this can be understood by invoking the presence of dust in the minisurvey galaxies, affecting the near–infrared colors of a normal stellar population through absorption with visual optical depths up to about 5, coupled with emission by hot dust. The large internal extinction needed to account for these colors is consistent with the considerable internal extinction in a sample of late-type spiral galaxy nuclei studied by Frogel (1985), and with the finding by De Jong *et al.* (1984) that most IRAS galaxies are late-type spirals.

A possible alternate source for excess reddening in near–infrared colors is nonthermal infrared

continuum emission. To consider this possibility, it would be worthwhile to know what fraction of the minisurvey galaxies may be Seyfert nuclei. The spectral indices between 60 and 100 μm for the minisurvey galaxies have been compared to those in a sample of known Seyfert galaxies studied by Miley, Neugebauer, and Soifer (1985). The spectra of the minisurvey galaxies between 60 and 100 μm do appear to be statistically somewhat steeper than would be expected for Seyfert nuclei, but the difference is only marginally significant and of itself is insufficient to provide a reliable estimate of the Seyfert contribution to the minisurvey sample. De Grijp *et al.* (1985) have shown that the selection criterion $0.5 < \alpha(60,25) < 1.25$ (where α is defined by $f_\nu \propto \nu^{-\alpha}$) is a very efficient means of finding previously unknown Seyfert galaxies (see also Osterbrock and De Robertis 1985). Unfortunately, only 21 of the minisurvey galaxies have firm IRAS detections at 25 μm. Nevertheless, for those 21 galaxies the median spectral index is $\alpha(60,25) = 2.1$, which can be compared to the results of Miley, Neugebauer, and Soifer (1985) who find median 60 to 25 μm spectral indices for Seyfert 1 and Seyfert 2 galaxies of 1.0 and 1.2, respectively. Although not conclusive, this suggests that the minisurvey probably does not contain a substantial Seyfert population.

It may be possible to identify Seyfert nuclei based on their near–infrared properties. Balzano and Weedman (1981), by analyzing samples of Seyfert, emission line, and bright compact nuclei, conclude that a value of $J - K > 1.1$ mag for a galaxy nucleus indicates an 80% probability that the nucleus will show indicators of a nonthermal source. The results of Balzano and Weedman, however, are based in large part on an analysis of known Seyfert nuclei, for which the near–infrared colors tend to have a larger $H - K$ than do the minisurvey galaxies. Ten of the minisurvey galaxies have $J - K > 1.1$ mag, but, because the distribution of the minisurvey galaxies corresponds well with the effect of internal extinction from dust absorption, we believe that nonthermal continuum does not contribute substantially to the near–infrared colors of the minisurvey galaxies. Nevertheless, this possibility cannot be entirely ruled out based on the data in this paper.

III.2 Near– and far–infrared luminosity correlation

The near– and far–infrared luminosities are tabulated in Table 1 for all of the galaxies for which

redshifts are available. For these calculations, the near–infrared flux is taken as $F_{NIR} = \nu f_\nu$ (2.2 μm) while the far–infrared flux is taken as the flux between 42 μm and 122 μm (see Appendix B of *Cataloged Galaxies and Quasars Observed in the IRAS Survey* (1985)). The luminosities were calculated for $H_o = 75$ km sec^{-1} Mpc^{-1} and $q_o = 1/2$. The distribution of near–infrared luminosities has a mean $log(L_{NIR}/L_\odot) = 9.6$ (where $L_\odot$ is the solar luminosity) with a disperson of $log(L_{NIR}/L_\odot)$ of $\sigma_{NIR} = 0.5$, and the far–infrared luminosity distribution has a mean $log(L_{FIR}/L_\odot) = 10.4$ with a dispersion of $log(L_{FIR}/L_\odot)$ of $\sigma_{FIR} = 0.5$.

Figure 2a shows the distribution of $log(L_{FIR}/L_{NIR})$ for the minisurvey galaxies; the distribution has a mean $log(L_{FIR}/L_{NIR}) = 0.8$, and a dispersion of $log(L_{FIR}/L_{NIR})$ of $\sigma = 0.2$. It would be useful to compare the distributions of $log(L_{FIR}/L_{NIR})$ and $log(L_{FIR}/L_B)$, where L_B is the blue luminosity, for the minisurvey galaxies to determine if the far–infrared luminosity is better correlated with the near–infrared or the blue luminosity. However, these galaxies have not yet been systematically measured at visible wavelengths; the blue magnitudes used by Soifer *et al.* (1984) were crude estimates. Soifer *et al.* (1986b), however, have compiled a complete sample of 341 IRAS galaxies which have 60 μm flux densities greater than 5 Jy, Galactic latitude $|b| > 30°$, and declination $\delta > -20°$. This sample, the IRAS bright galaxy sample, is similar to that obtained in the minisurvey in that it represents a complete, flux–limited sample of infrared selected galaxies; we assume that these galaxies will have similar properties to those in the minisurvey. In Figure 2b the distribution of $log(L_{FIR}/L_B)$ for the bright galaxy sample is plotted. It has a dispersion of $log(L_{FIR}/L_B)$ of $\sigma_{bg} = 0.6$ centered about a mean $log(L_{FIR}/L_B) = 0.6$.

Clearly, fluctuations and sample size will effect the widths of the distributions. Additional scatter can also be expected in the bright galaxy sample distribution since the blue luminosities for the bright galaxy sample were derived from the blue magnitudes listed in the Zwicky Catalog (Zwicky *et al.* 1961–8). These effects have been considered by adding an additional uncertainty to the L_{NIR} measurements, comparable to the uncertainties in the Zwicky magnitudes (which are <0.5 mag; see, e.g., Giovanelli and Haynes 1984, or Huchra 1981), and then using an F–distribution test to compare

the effect of the additional scatter in the minisurvey distribution to the bright galaxy sample distribution. The result is that, to the 99% confidence level, the quantities σ and σ_{bg} do not represent dispersions of equivalent parent populations. Thus, to the extent that the minisurvey and the bright galaxy sample provide equivalent representations of far–infrared–bright galaxies, such galaxies do in fact have a tighter correlation between their far– and near–infrared emission than between their far–infrared and blue light.

Such a tighter correlation in the far–infrared to 2.2 μm luminosity again suggests that extinction by dust significantly affects the visible luminosity of far–infrared–bright galaxies. However, an alternate explanation (Frogel 1986) can be formulated by assuming that a number of the minisurvey galaxies have undergone a period of active star formation in the past 10^8 yr. Such enhanced star formation would produce relatively bright optical magnitudes and blue UBV colors, but would not necessarily produce correspondingly high far–infrared emission. Furthermore, the enhanced optical emission would not be well correlated with the near–infrared emission, which is due primarily to older stars. Without more detailed information on the types of galaxies in the minisurvey, it is not possible to distinguish conclusively between these two possible explanations.

In Figure 2c, the distribution of $log(L_{FIR}/L_{NIR})$ for the minisurvey galaxies is again shown, where the near–infrared luminosities have been corrected to A/D_o = 1.0 using the growth curve given by Frogel *et al.* (1978); the corresponding corrections to the K magnitudes are typically in the range from 0 to 1 magnitude. This distribution has a mean $log(L_{FIR}/L_{NIR})$ = 0.5, with a dispersion of $log(L_{FIR}/L_{NIR})$ of $\sigma_{1.0}$ = 0.3. An F–distribution test again indicates that the increase in scatter in this distribution relative to the distribution in Figure 2a is statistically significant to the 90% confidence level, implying that the far–infrared emission in the majority of the minisurvey galaxies may have a strong nuclear component.

The use of the near–infrared colors as an indicator of far–infrared activity in the minisurvey galaxies has been investigated in the color–color plots of Figure 3. In each of these plots, the intent has been to identify some parameter involving the far–infrared luminosity which would divide the sample into distinct groups such that the near–infrared colors for each group would be distinguishable.

In Figure 3a, the galaxies have been divided into three groups according to whether their far–infrared luminosity lies in the upper, middle, or lower range of the far–infrared luminosities for the entire sample. The luminosity cutoff for each group was determined so as to have as nearly equal numbers of galaxies in each group as possible. In Figure 3b, a similar division of the sample into three roughly equal size groups has been done, where the galaxies have been separated by the ratio L_{FIR}/L_{NIR}. In Figure 3c, the sample has been separated in a similar manner using the quantity $L_{FIR}/(D_o)^2$, effectively the far–infrared surface brightness. In all cases, the parameters, which should be clear indicators of far–infrared activity, are ineffective in distinguishing the near–infrared colors as a function of the far–infrared emission.

This result, that there is no clear correlation between near–infrared colors and far–infrared activity, is not surprising if the far–infrared luminosity in these galaxies is not dominated by the emission from the dust which is responsible for the extinction seen in the near–infrared. In particular, if the near–infrared luminosity is extended throughout the disk, as would be expected for a normal stellar population, then the relatively broad–beam near–infrared measurements (with $A/D_o > 0.2$ for more than 90% of the sample) will be dominated by disk emission which, considering the above discussion, would not necessarily correlate well with the primarily nuclear far–infrared emission.

IV. CONCLUSIONS

Near-infrared observations of 80 galaxies from the IRAS minisurvey have produced the following results:

1) The near-infrared colors of far-infrared-bright galaxies are similar to those of normal field spiral galaxies, but show a larger range in $J-H$ and $H-K$ and slightly redder colors, possibly indicating the presence of dust in far-infrared-bright galaxies. For the minisurvey sample, there is evidence for dust absorption of visual optical depths up to about 5, coupled with hot dust emission.

2) The far-infrared emission of far-infrared-bright galaxies appears to be more tightly correlated with the near-infrared emission than with the visible emission. This suggests the possibility of a

significant effect from dust aborption on the visible luminosity of these galaxies, but can also be explained in terms of recent active star formation.

3) There is an indication that the far-infrared-bright galaxies emit a significant fraction of their far-infrared luminosity primarily from a strong nuclear component.

As the manuscript of this paper was being submitted, near-infrared measurements of 22 of the 86 minisurvey galaxies were published by Moorwood, Veron-Cetty, and Glass (1986). Their results are consistent with the results presented in this paper.

ACKNOWLEDGEMENTS

The authors extend special thanks to C. G. Wynn-Williams for helpful suggestions on a preliminary version of the manuscript. We also thank E. E. Becklin, J. N. Heasley, G. J. Hill, and C. G. Wynn-Williams of the Institute for Astronomy, University of Hawaii, as well as S. E. Persson of Mount Wilson and Las Campanas Observatories and C. J. Persson of the Infrared Processing and Analysis Center, for generously supplying a number of the redshifts reported in this paper. Steve Eales, also of the Institute for Astronomy, University of Hawaii, provided radio positions to clear up several positional ambiguities. Finally, we gratefully acknowledge a number of useful comments from the referee, Jay Frogel. The research presented in this paper was supported in part by the National Science Foundation grant AST 83-12699 and in part by the NASA IRAS extended mission program.

REFERENCES

Aaronson, J., 1977. Infrared observations of galaxies, Ph.D. thesis, Harvard University.

Balzano, V.A., and D.W. Weedman, 1981. The near–infrared properties of galactic nuclei, *Astrophys. J.*, **243**, 756.

Beichman, C., *et al.*, 1985. The *IRAS* galaxy 0421+040P06: an active spiral (?) galaxy with extended radio lobes, *Astrophys.J.*, **293**, 148.

Burstein, D., and C. Heiles, 1982. *Astron. J.*, **87**, 1165.

Chester, T., 1985, private communication.

Cohen, J.G., J.A. Frogel, S.E. Persson, and J.H. Elias, 1981. *Astrophys. J.*, **249**, 481.

de Grijp, M.H.K., *et al.*, 1985. Infrared Seyferts: a new population of active galaxies?, *Nature*, **314**, 240.

de Jong, T., P.E. Clegg, B.T. Soifer, M. Rowan–Robinson, H.J. Habing, J.R. Houck, H.H. Aumann, and E. Raimon, 1984. *IRAS* observations of Shapley–Ames galaxies, *Astrophys. J. (Letters)*, **278**, L67.

De Vaucouleurs, G., 1948. *Ann. d' Astrophys.*, **11**, 247.

Eales, S., 1986, private communication.

Elston, R., M.E. Cornell, and M.J. Lebofsky, 1985. The properties of far–infrared luminous galaxies. I. Spectroscopic and near–infrared observations, *Astrophys. J.*, **296**, 106.

Frogel, J.A., S.E. Persson, M. Aaronson, and K. Matthews, 1978. Photometric studies of composite stellar systems. I. CO and JHK observations of E and SO galaxies, *Astrophys. J.*, **220**, 75.

Frogel, J.A., 1986. Private communication.

Frogel, J.A., 1985. The stellar content of the nuclei of late–type spiral galaxies, *Astrophys. J.*, **298**, 528.

Giovanelli, R., and M.P. Haynes, 1984. *Astron.J.*, **89**, 1.

Glass, I.S., 1981. JHK observations of quasars and BL Lac objects, *Mon. Not. R. Astron. Soc.*, **194**, 795.

Helou, G., B.T. Soifer, M. Rowan-Robinson, 1985. Thermal infrared and non–termal radio: remarkable correlation in disks of galaxies, *Astrophys. J. (Letters)*, **298**, L7.

Huchra, J., 1976. *Astron. J.*, **81**, 952.

Infrared Astronomical Satellite (IRAS) Catalogs and Atlases: *Cataloged Galaxies and Quasars Observed in the IRAS Survey*, 1985. C.J. Lonsdale, G. Helou, J.C. Good, and W. Rice (Eds.), National Aeronautics and Space Administration, Washington D.C..

Infrared Astronomical Satellite (IRAS) Catalogs and Atlases: *Explanatory Supplement*, 1988. C.A. Beichman, G. Neugebauer, H.J. Habing, P.E. Clegg, and T.J. Chester (Eds.), National Aeronautics and Space Administration, Washington D.C..

Infrared Astronomical Satellite (IRAS) Catalogs and Atlases: *The Point Source Catalog*, 1985. National Aeronautics and Space Administration, Washington D.C..

Infrared Astronomical Satellite (IRAS) Circular No. 6, 1984. *Astron. Astrophys.*, **131**, C1.

Miley, G.K., G. Neugebauer, and B.T. Soifer, 1985. *IRAS* observations of Seyfert galaxies, *AstrophysJ. (Letters)*, **293**, L11.

Moorwood, A.F.M., M.P. Veron-Cetty, and I.S. Glass, 1986. Optical and near–infrared observations of *IRAS* galaxies, *Astron. Astrophys.*, **160**, 39.

Neugebauer, G., K. Matthews, B.T. Soifer, and J.H. Elias, 1985. Infrared photometry of the nebulosity around quasars, *Astrophys. J.*, **298**, 275.

Oke, J.B., and J.E. Gunn, 1982. *Pub. Astron. Soc. Pac.*, **94**, 586.

Persson, S.E., and C.J. Persson, 1986. In preparation.

Rood, H.J., 1980. *A Catalog Of Galaxy Redshifts* (unpublished).

Rowan–Robinson, M., *et al.*, 1984. The *IRAS* Minisurvey, *Astrophys. J. (Letters)*, **278**, L7.

Sanders, D.B., and I.F. Mirabel, 1985. *Astrophs. J. (Letters)*, **298**, L31.

Soifer, B.T., *et al.*, 1986a. In preparation.

Soifer, B.T., *et al.*, 1986b. The luminosity function and space density of the most luminous galaxies in the *IRAS* survey, *Astrophys. J. (Letters)*, **303**, L41.

Soifer, B.T., *et al.*, 1984. Infrared galaxies in the *IRAS* minisurvey, *Astrophys. J. (Letters)*, **278**, L71.

Zwicky, F., and E. Herzog, 1963-1968. *Catalog of Galaxies and Clusters of Galaxies*, Vol. 2 (1963), Vol. 3 (1966), and Vol. 4 (1968), California Institute of Technology Press, Pasadena.

Zwicky, F., E. Herzog, and P. Wild, 1961. *Catalog of Galaxies and Clusters of Galaxies*, Vol. 1, California Institute of Technology Press, Pasadena.

Zwicky, F., M. Karpowicz, and C.T. Kowal, 1968. *Catalog of Galaxies and Clusters of Galaxies*, Vol. 5, California Institute of Technology Press, Pasadena.

Zwicky, F., and C.T. Kowal, 1968. *Catalog of Galaxies and Clusters of Galaxies*, Vol. 6, California Institute of Technology Press, Pasadena.

Figure Captions

Figure 1: Near-infrared colors for the IRAS minisurvey galaxies. The region enclosed by a dashed line is that occupied by the normal spiral galaxies of Aaronson (1977). The solid lines **A** through **D** represent contributions to the near-infrared colors as follows: **A** corresponds to a reddening screen of purely absorbing dust, drawn as a function of τ_V, the optical depth at V; **B** to reddening from dust that is uniformly mixed with the emitting source, also drawn as a function of τ_V; **C**, **D** to 600 K and 1000 K dust, respectively, with emissivity, ϵ, varying as $\epsilon \propto \nu^2$, where ν is the frequency. Lines **C** and **D** are labeled according to the fractional contribution to the 2.2 μm emission, assuming zero contribution from dust emission for a normal stellar population. All of the lines **A** through **D** are taken from Aaronson (1977).

Figure 2: (a) The distribution of $log(L_{FIR}/L_{2.2})$ for the minisurvey galaxies. L_{FIR} and L_{NIR} are the far- and near-infrared luminosities, respectively (see text), and f is the fraction of galaxies, normalized to 1 at the peak in the distribution. (b) The distribution of $log(L_{FIR}/L_B)$ for the IRAS bright galaxy sample (Soifer *et al.*, 1986b), normalized to the peak in the distribution. (c) The same as (a), but with the near-infrared luminosites adjusted to $A/D_o = 1.0$ using the growth curve given by Frogel *et al.* (1978). A is the beam diameter and D_o is the galaxy major axis diameter as measured on the Palomar Observatory Sky Survey prints (see text).

Figure 3: The near-infrared colors for the minisurvey galaxies. (a) The galaxies are separated according to their far-infrared luminosities, where the symbols $\triangle$, $\bigcirc$, and + represent $log(L_{FIR}/L_\odot) > 10.61$, $10.10 < log(L_{FIR}/L_\odot) < 10.61$, and $log(L_{FIR}/L_\odot) < 10.10$, respectively. (b) The galaxies are separated according to the ratio of their far-infrared to near-infrared luminosities, where the symbols $\triangle$, $\bigcirc$, and + represent $log(L_{FIR}/L_{NIR}) > 0.87$, $0.64 < log(L_{FIR}/L_{NIR}) < 0.87$, and $log(L_{FIR}/L_{NIR}) < 0.64$, respectively. (c) The galaxies are separated according to the effective far-infrared surface brightness, $L_{FIR}/(D_o)^2$, where D_o is the galaxy major axis diameter as measured on the Palomar Observatory Sky Survey blue prints (see text). The symbols $\triangle$, $\bigcirc$, and + represent $log(L_{FIR}/(L_\odot D_o^2)) > 7.97$, $7.10 < log(L_{FIR}/(L_\odot D_o^2)) < 7.96$, and $log(L_{FIR}/(L_\odot D_o^2)) < 7.10$,

respectively.

For each of the above plots, the cutoffs in the luminosity parameter were determined so as to give roughly equal numbers of galaxies in each of the three groups.

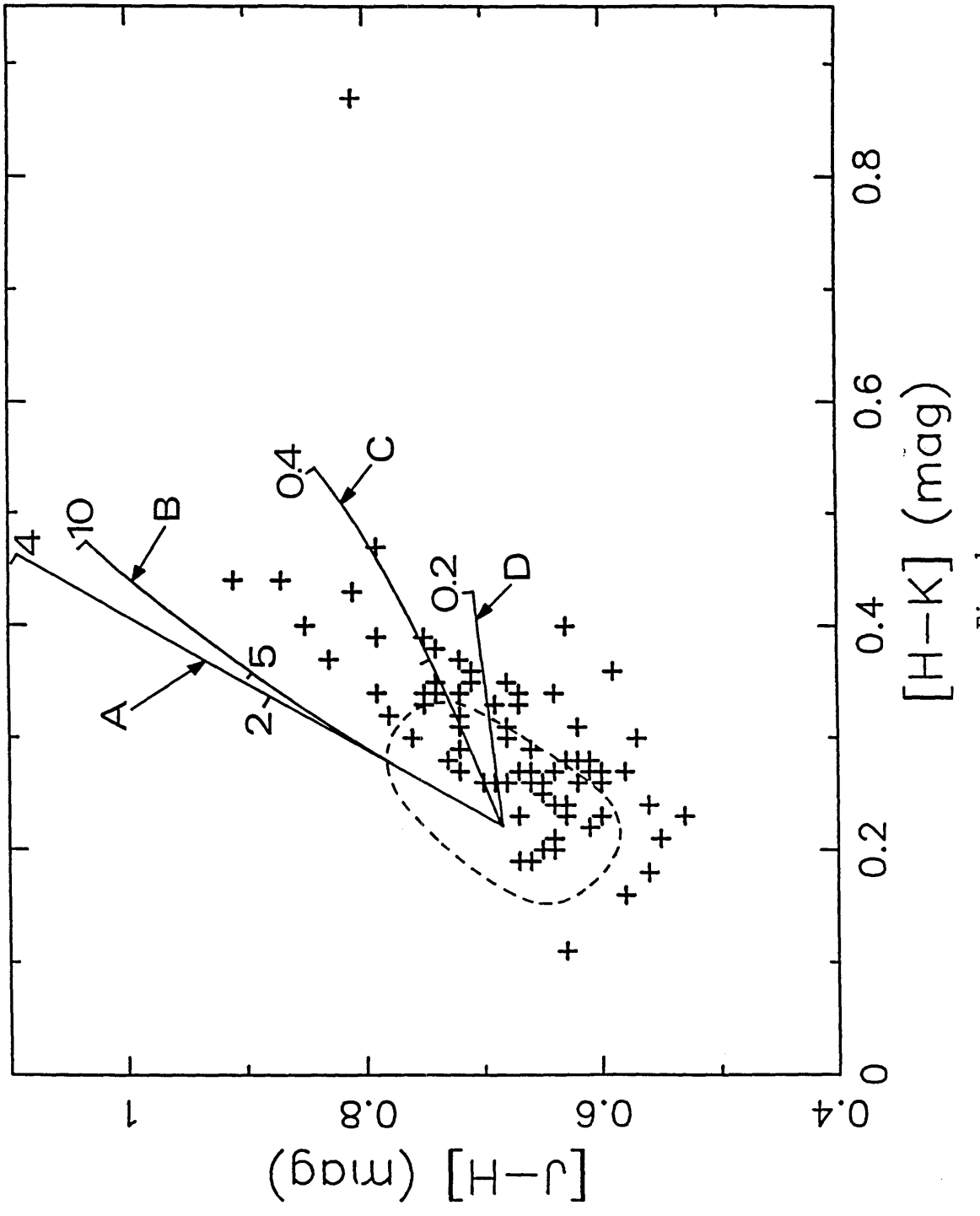

Fig. 1

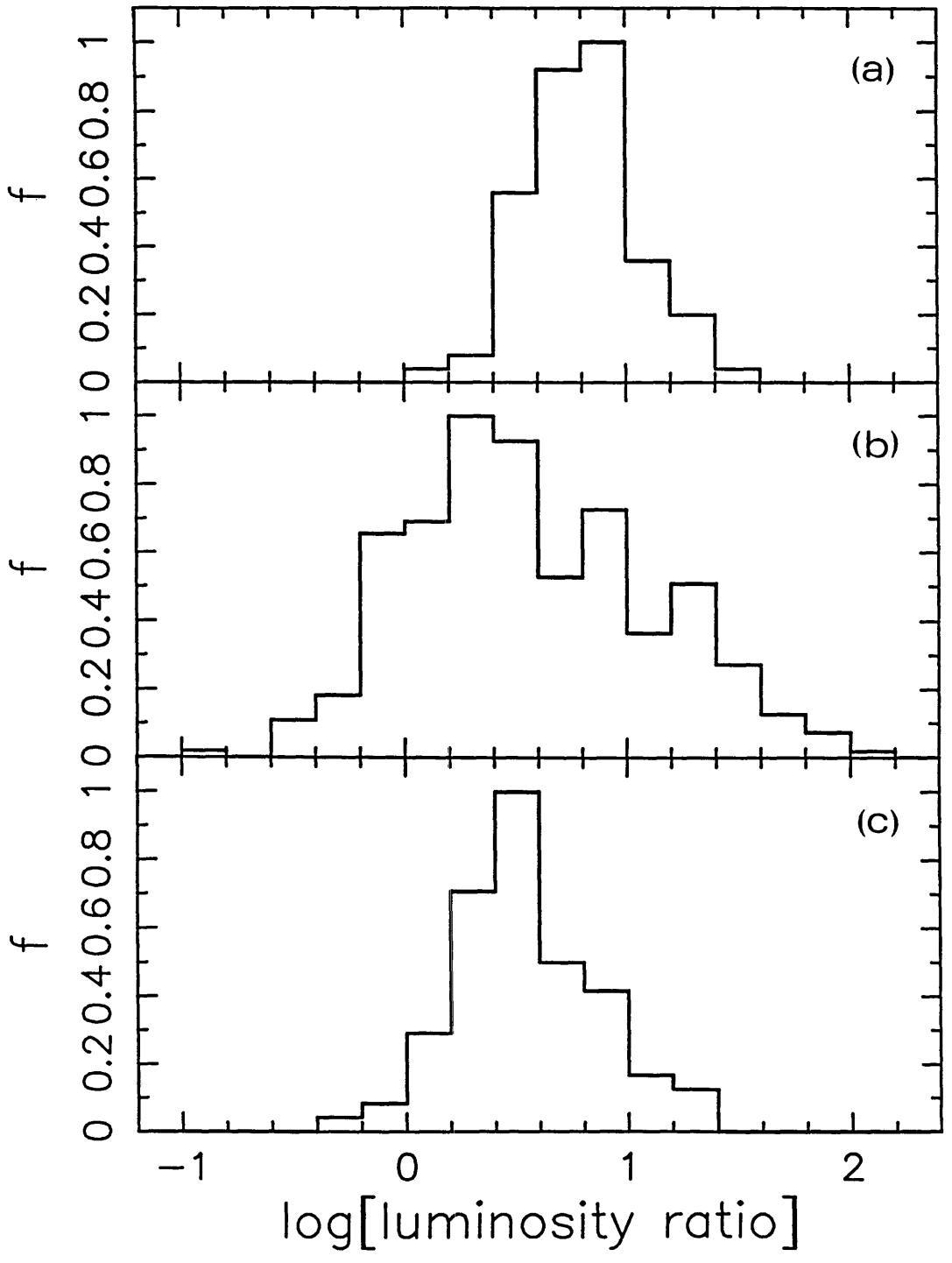

Fig. 2

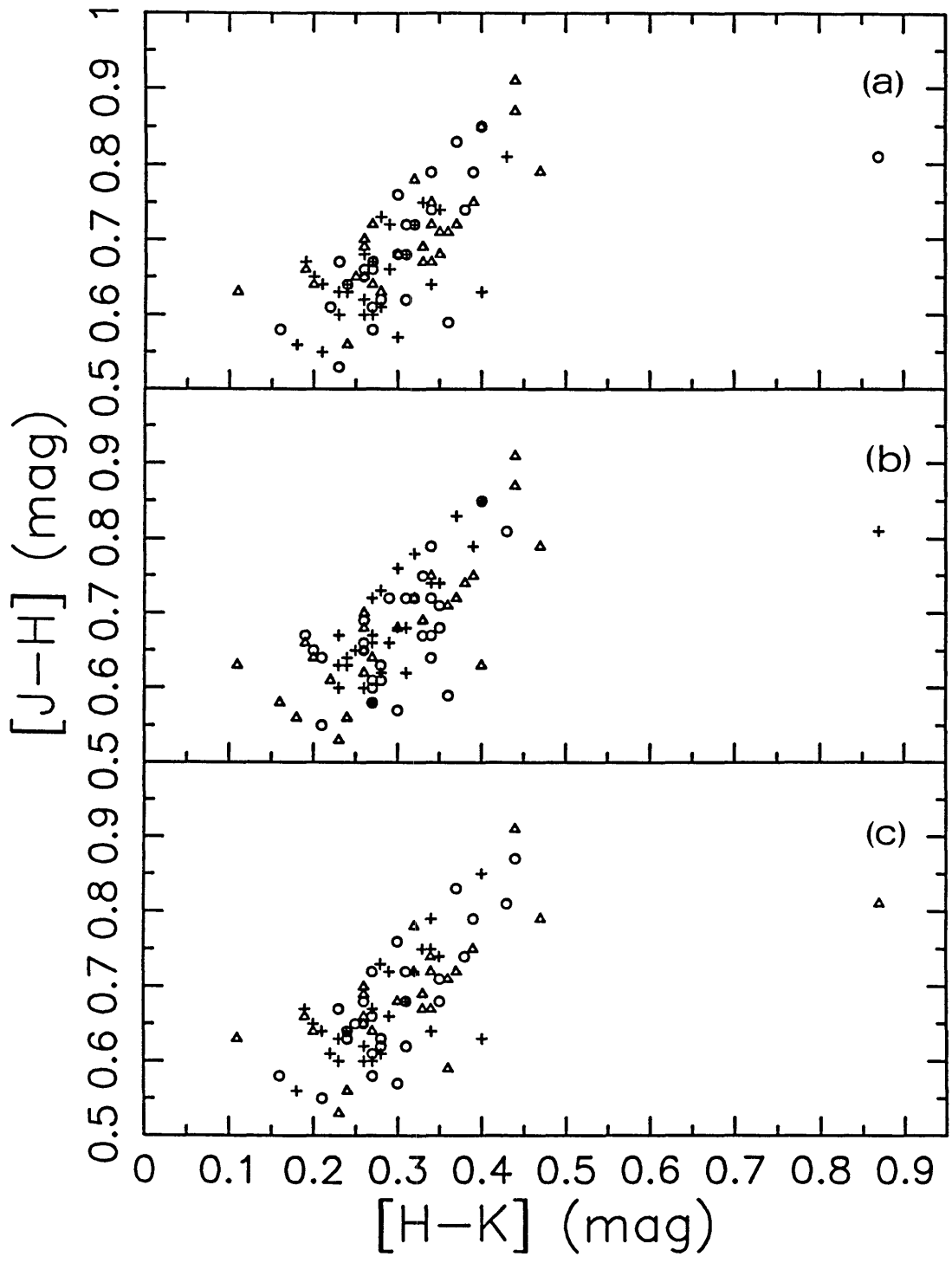

Fig. 3

Table 1

NAME		REDSHIFT		MAGNITUDES AND COLORS								IRAS DATA[h]		LUMINOSITIES[i]	
						OBSERVED[f]			CORRECTED[g]						
IRAS PSC[a]	CIRC #6[b]	z	ref[c]	E^{d}_{B-V} (mag)	LOG[A/D_o][e]	K	[J–H]	[H–K]	K_c	$[J-H]_c$	$[H-K]_c$	f_{60}	f_{100}	LOG[$L_{NIR}/L_\odot$]	LOG[$L_{FIR}/L_\odot$]
						(mag)						(Jy)			
01254+8445	0125+848P03	0.0158	P	0.12	–0.48	11.46	0.72	0.35	11.48	0.67	0.27	0.49±0.06	1.71±0.21	9.45	9.67
03533+2606	0353+261P06	0.1883	P	0.10	0.00	13.72	0.76	0.72	14.18	0.64	0.20	0.49±0.06	1.35±0.49†	10.55	11.77
03553+1826	0355+184P06	0.0237	P	0.24	–0.40	12.85	0.66	0.33	12.86	0.56	0.20	0.57±0.05	1.05±0.35†	9.25	9.95
03560+2012	0356+202P06	0.0481	P	0.20	–0.18	13.24	0.67	0.44	13.35	0.56	0.24	0.56±0.07	<2.10†	9.67	10.71
03565+2139	0356+217P03	0.0254	P	0.18	–0.48	11.77	0.67	0.38	11.80	0.59	0.26	0.66±0.05	1.49±0.18	9.73	10.11
03577+2054	0357+209P06	0.0218	P	0.18	–0.40	12.66	0.66	0.40	12.68	0.58	0.29	0.60±0.05	<1.22†	9.25	9.92
03598+1401	0359+140P06	–	–	0.22	–0.48	12.25	0.70	0.43	–	–	–	0.70±0.06	1.48±0.49†	–	–
04009+2446	0400+248P06	0.0763	P	0.12	0.00	12.99	0.78	0.59	13.19	0.69	0.33	0.73±0.09	<1.65†	10.14	11.11
04023+2114	0402+212P03	0.0285	P	0.20	–0.48	11.75	0.89	0.52	11.79	0.80	0.39	1.02±0.08	2.04±0.24	9.84	10.25
04028+1109	0402+112P06	0.010	UH	0.20	–0.30	12.03	0.74	0.36	12.01	0.66	0.29	0.65±0.05	1.79:±0.29	8.84	9.47
04064+0831	0406+085P03	0.0120	P	0.18	–0.70	11.73	0.68	0.30	11.72	0.61	0.22	3.37±0.27	6.88±0.55	9.11	10.15
04097+0525	0409+054P03	0.0188	P	0.14	–0.60	10.85	0.93	0.53	10.87	0.87	0.44	8.32±0.67	15.70±1.26	9.84	10.92
04120+0622	0412+064P06	0.0333	P	0.12	0.00	12.50	0.75	0.43	12.58	0.68	0.30	0.66±0.05	1.13±0.31†	9.66	10.29
04133+0803	0413+081P03	0.0056	P	0.18	–0.70	11.54	0.70	0.46	11.51	0.63	0.40	4.58±0.55	5.33±0.64	8.53	9.52
04139+0238	0413+026P06	0.0111	P	0.13	–0.90	11.76	0.69	0.29	11.76	0.64	0.23	0.67±0.08	2.31±0.18	9.02	9.50
04140+0103	0414+011P03	0.0739	P	0.09	–0.18	12.61	0.80	0.59	12.82	0.72	0.34	0.80±0.06	1.79±0.21	10.26	11.13
04141+0008	0414+001P03	0.033	E	0.09	0.00	13.16	0.81	0.52	13.25	0.75	0.40	1.81±0.14	2.82±0.23	9.38	10.71
04144+1020	0414+103P03	0.0257	P	0.21	–0.30	11.56	0.81	0.50	11.59	0.72	0.37	2.58±0.21	6.25±0.75	9.83	10.73
04145+0439	0414+047P06	0.011	UH	0.14	–0.65	11.29	0.80	0.41	11.29	0.74	0.35	0.59±0.05	1.22:±0.24	9.20	9.32
04147+0218††	0414+023P06	0.0121	P	0.12	–0.70	12.29	0.67	0.32	12.30	0.62	0.26	1.42±0.11	3.55±0.43	8.89	9.82
04151+0126††	0415+014P06	0.0170	P	0.09	–0.40	11.76	0.79	0.45	11.79	0.74	0.38	2.79±0.22	5.02±0.60	9.39	10.35
04161+0306	0416+031P03	0.023	UH	0.13	–0.60	11.85	0.91	0.50	11.89	0.85	0.40	0.68±0.05	2.13±0.17	9.61	10.11
04172–0111	0417–012P06	0.0481	P	0.07	0.00	12.88	0.72	0.43	13.02	0.66	0.26	0.54±0.04	1.04:±0.12	9.81	10.55
04175–0106	0417–011P06	0.0338	P	0.07	–0.48	12.10	0.79	0.44	12.19	0.74	0.32	0.75±0.06	1.79±0.14	9.83	10.43
04175+0005	0417+001P06	0.016	UH	0.08	–0.48	12.08	0.85	0.50	12.11	0.81	0.43	1.37±0.11	3.75±0.30	9.21	10.07
04172+0158	0417+020P06	0.0143	P	0.12	–0.60	13.45	0.61	0.25	13.46	0.56	0.18	0.88±0.07	1.93±0.15	8.56	9.73
04180–0208	0418–021P06	0.015	UH	0.03	–0.30	12.67	0.62	0.28	12.71	0.60	0.23	0.48±0.06	1.21±0.15	8.91	9.54
04187+0042	0418+007P06	0.0426	P	0.09	–0.18	11.98	0.80	0.50	12.10	0.73	0.35	0.63±0.05	1.48±0.18	10.07	10.55
04192+0355††	0419+039P06	0.023	UH	0.17	–0.54	11.78	0.73	0.37	11.81	0.65	0.26	2.00±0.16	4.11±0.33	9.64	10.49
04194–0055	0419–009P06	0.0343	P	0.07	–0.60	12.43	0.73	0.44	12.53	0.68	0.32	0.51±0.06	1.31±0.16	9.70	10.29
04210+0400	0421+040P06	0.0463	P	0.17	0.00	12.46	0.91	1.05	12.57	0.81	0.87	0.59±0.05	1.35:±0.16	9.95	10.58
16487–0222	1648–024P06	0.0244	P	0.12	–0.60	11.55	0.79	0.41	11.60	0.73	0.31	2.47±0.20	4.40±0.35	9.78	10.60
16501–0210	1650–022P06	0.0249	P	0.12	–0.18	14.10	0.75	0.36	14.15	0.69	0.26	0.53±0.06	0.86±0.37†	8.78	9.94
16534–0110	1653–012P06	0.0410	P	0.12	–0.60	12.61	0.99	0.59	12.71	0.91	0.43	3.77±0.30	5.96±0.72	9.79	11.22
16547+0257	1654+030P06	0.0304	P	0.08	–0.18	12.71	0.78	0.43	12.79	0.73	0.32	1.70±0.14	1.66±0.13	9.50	10.54
16572+0234	1657+026P06	0.029	P	0.08	–0.70	12.41	0.70	0.35	12.49	0.65	0.24	0.51±0.06	1.17±>0.23	9.57	10.12
16583–0146	1658–018P06	0.031	UH	0.14	–0.60	12.83	0.87	0.47	12.90	0.80	0.34	0.46±0.06	1.18±0.24	9.46	10.15
16587+0655	1658+069P06	0.0224	P	0.12	–0.40	11.92	0.68	0.38	11.96	0.62	0.28	1.33±0.11	1.32±0.16	9.56	10.18
16589+0521	1658+054P06	0.0503	P	0.08	–0.18	11.73	0.74	0.52	11.88	0.67	0.34	1.95±0.16	3.09±0.25	10.30	11.11
17002+7702††	1700+770P06	0.0555	P	0.05	–0.30	12.44	0.78	0.46	12.61	0.72	0.27	0.44:±0.05	1.29±0.10	10.10	10.68

Table 1 (continued)

NAME		REDSHIFT				MAGNITUDES AND COLORS OBSERVED[f]			CORRECTED[g]			IRAS DATA[h]		LUMINOSITIES[i]	
IRAS PSC[a]	CIRC #6[b]	z	ref[c]	E^{d}_{B-V} (mag)	LOG[A/D$_o$][e]	K	[J–H]	[H–K]	K_c	$[J-H]_c$	$[H-K]_c$	f_{60} (Jy)	f_{100}	LOG[$L_{NIR}/L_{\odot}$]	LOG[$L_{FIR}/L_{\odot}$]
17012+0418	1701+043P06	0.022	UH	0.07	–0.60	13.39	0.76	0.37	13.44	0.72	0.29	0.50±0.06	0.76±0.16†	8.91	9.75
17015+0300	1701+030P06	0.0957	P	0.09	0.00	13.19	0.73	0.57	13.45	0.65	0.25	0.67±0.05	0.98±0.17†	10.24	11.19
17019+7714	1702+772P06	0.0678	P	0.06	0.00	12.44	0.75	0.49	12.64	0.69	0.26	0.61±0.05	1.56±0.12	10.26	10.96
17026+0959	1702+100P06	0.022	UH	0.08	–0.40	12.45	0.65	0.35	12.48	0.61	0.28	0.56:±0.07	1.79±0.21	9.11	9.77
17027+0803	1702+081P06	0.032	UH	0.08	–0.48	11.82	0.69	0.40	11.91	0.64	0.28	2.31±0.18	2.86±0.23	9.89	10.76
17039+1026	1703+104P06	0.012	P	0.08	–0.60	11.83	0.68	0.40	11.85	0.64	0.34	1.95±0.16	4.24±0.34	9.06	9.93
17041+0636	1704+066P06	0.063	P	0.08	–0.48	12.63	0.73	0.46	12.81	0.66	0.24	0.42:±0.05	1.27±0.15	10.13	10.77
17062+0406	1706+041P06	0.020	P	0.06	–0.60	12.53	0.63	0.35	12.58	0.59	0.27	0.84±0.07	1.92±0.15	9.21	10.01
17091+0803	1709+081P06	0.0086	UH	0.08	–0.78	11.39	0.75	0.36	11.40	0.72	0.32	3.01±0.24	4.07±0.33	8.95	9.74
17101+1637	1710+166P06	0.0297	P	0.10	–0.48	13.12	0.67	0.38	13.19	0.61	0.26	0.47±0.06	1.50±0.12	9.32	10.17
17118+1253††	1711+129P06	0.0304	UH	0.13	0.00	12.96	0.71	0.40	13.03	0.64	0.28	0.56±0.04	4.51±1.25†	9.40	10.62
17118+7849	1711+788P06	0.0398	P	0.05	–0.30	12.76	0.72	0.37	12.88	0.67	0.23	0.50±0.08	0.75±0.17†	9.70	10.31
17152+1940	1715+197P06	0.036	UH	0.09	–0.60	12.27	0.74	0.44	12.37	0.68	0.31	2.07±0.17	3.11±0.25	9.81	10.84
17153+1141††	1715+117P06	0.030	UH	0.15	–0.60	13.06	0.83	0.47	13.19	0.75	0.34	1.69±0.14	3.07±0.37	9.35	10.62
17156+1238	1715+126P06	0.113	E	0.15	–0.18	13.72	0.73	0.48	14.01	0.62	0.11	0.77±0.06	<0.54†	10.16	11.30
17176+1642	1717+167P06	0.0205	R	0.09	–0.85	12.48	0.72	0.27	12.52	0.67	0.19	0.67±0.05	1.96±0.16	9.26	9.99
17218+2110	1721+212P06	0.023	UH	0.08	–0.60	11.20	0.87	0.47	11.26	0.82	0.38	2.16±0.17	3.97±0.32	9.86	10.50
17223+1906	1722+191P06	0.054	UH	0.08	–0.30	13.65	0.60	0.42	13.81	0.53	0.23	0.61±0.05	<0.67†	9.59	10.61
17253+2108	1725+211P06	0.025	P	0.09	–0.18	11.98	0.71	0.37	12.04	0.66	0.27	0.84±0.07	1.22±0.20	9.62	10.12
17300+2009	1730+202P06	0.050	UH	0.08	–0.18	12.38	0.85	0.50	12.53	0.78	0.32	0.48±0.06	1.36±0.22	10.04	10.62
–	1733+803P06††	0.057	E	0.06	0.00	13.10	0.77	0.55	13.27	0.71	0.36	0.78	1.41	9.85	10.84
17353+2616	1735+263P06	0.0198	P	0.06	–0.30	12.37	0.66	0.32	12.42	0.62	0.24	0.48±0.06	1.21:±>0.24	9.27	9.78
17364+2458	1736+250P06	0.018	P	0.07	–0.54	11.60	0.77	0.35	11.64	0.73	0.28	1.13±0.09	1.75±0.14	9.50	9.98
17377+2845††	1737+287P06	0.023	UH	0.05	–0.18	12.16	0.72	0.39	12.22	0.68	0.31	0.60±0.05	1.13±0.14	9.48	9.95
17386+2908	1738+291P06	0.046	UH	0.05	–0.30	12.38	0.67	0.47	12.52	0.62	0.31	0.61±0.05	0.95±0.17†	9.97	10.52
17400+2538	1740+256P06	0.024	UH	0.07	–0.60	11.96	0.71	0.36	12.02	0.67	0.27	1.10±0.09	1.83±0.15	9.59	10.23
17445+3043	1744+307P06	0.0153	P	0.06	–0.70	11.93	0.72	0.43	12.14	0.65	0.19	1.76±0.14	4.10±0.33	10.52	11.47
17519+3351††	1751+339P06	0.063	UH	0.05	–0.18	13.24	0.85	0.68	13.43	0.79	0.47	1.27±0.10	2.03±0.16	9.88	11.13
17526+3253††	1752+329P06	0.0258	P	0.05	–0.95	11.23	0.89	0.49	11.30	0.85	0.40	3.42±0.27	6.81±0.54	9.94	10.81
17530+3446	1753+348P06	0.0160	P	0.05	–0.70	10.58	0.71	0.41	10.62	0.68	0.35	5.84±0.47	13.03±1.56	9.80	10.66
17550+3238	1755+326P06	0.0159	R	0.05	–0.95	12.75	0.68	0.26	12.79	0.65	0.20	0.52±0.06	1.63±0.13	8.93	9.67
17557+3117††	1755+313P06	–	–	0.05	–0.18	12.68	0.71	0.60	–	–	–	0.59±0.05	1.11±0.18	–	–
18039+3349	1803+338P06	0.031	UH	0.07	–0.18	12.89	0.63	0.39	12.98	0.58	0.28	0.64±0.05	1.37±0.11	9.44	10.26
18039+3444	1803+347P06	0.024	UH	0.07	–0.48	12.03	0.68	0.33	12.09	0.64	0.24	0.63±0.08	1.62±0.13	9.57	10.07
18040+3400††	1804+340P06	0.024	UH	0.07	–0.78	12.95	0.68	0.30	13.01	0.64	0.21	0.45±0.05	1.46±0.12	9.20	9.98
18060+3552	1806+359P06	0.021	UH	0.06	–0.48	12.23	0.63	0.34	12.28	0.59	0.26	0.77±0.06	1.71±0.14	9.38	10.01
18064+3942	1806+397P06	0.1081	P	0.05	–0.27	13.24	0.78	0.59	13.54	0.71	0.25	0.69±0.06	0.91:±0.11	10.31	11.30
18130+3720††	1813+373P06	0.057	UH	0.05	0.00	12.65	0.73	0.52	12.82	0.67	0.33	0.79±0.06	1.41±0.11	10.03	10.85
18164+3948	1816+398P06	0.030	UH	0.06	–0.60	12.68	0.63	0.26	12.76	0.58	0.15	0.73±0.15	2.36±0.19	9.49	10.38
18203+4133	1820+416P06	0.050	UH	0.05	0.00	12.81	0.65	0.51	12.97	0.59	0.34	0.49±0.05	1.22±0.15	9.86	10.60
21263+8705	2126+871P06	0.0183	P	0.08	–0.48	12.78	0.79	0.41	12.82	0.75	0.33	0.64±0.05	<1.13†	9.04	9.76
23272+8518††	2327+853P06	0.0369	P	0.09	–0.48	11.75	0.77	0.49	11.85	0.71	0.35	1.53±0.12	4.77±0.57	10.04	10.87

[a] *Infrared Astronomical Satellite (IRAS) Catalogs and Atlases: The Point Source Catalog.* 1985, (Washington: US Government Printing Office).

[b] 1984, *Astr. Ap.*, **131**, C1.

[c] Reference for redshifts: P = Persson and Persson (1986); UH = University of Hawaii Institute for Astronomy (see text); E = Elston *et al.* (1985); R = Rood (1980).

[d] The color excess taken from the reddening maps of Burstein and Heiles (1982).

[e] The logarithm of the ratio of the beam size to the galaxy size. A is the beam diameter (generally 10"; see text) and D_o is the galaxy major axis diameter as determined from the Palomar Observatory Sky Survey blue prints by visually estimating the radius at which the galaxy brightness equals the sky background.

[f] The values quoted have been corrected for wavelength dependent distortions in the beam profiles (see text). The statistical uncertainties in the observed magnitudes and colors are believed to be <0.08 mag and <0.04 mag, respectively.

[g] corrected for redshift and Galactic reddening

[h] From the *IRAS Point Source Catalog* (PSC) 1985. The uncertainties quoted are calculated from the largest values for each uncertainty range given in the PSC. The symbol $\pm>$ indicates that the quoted uncertainty is a lower limit. A colon following the flux density refers to a "moderate quality" measurement; no colon indicates a "high quality" measurement. See the *IRAS Explanatory Supplement* (1985) for a complete discussion of the uncertainties and quality of the IRAS measurements. Flux densities obtained from coaddition of IRAS survey data are indicated by $\dagger$; cases where only an improved limit could be obtained are indicated by $<$.

[i] L_{NIR} and L_{FIR} are the near and far-infrared luminosities, respectively, as defined in the text, and $L_\odot$ is the solar luminosity.

††Notes to Table 1

(offset positions given here are only approximate)

04147+0218: There are two galaxies in the field. The galaxy chosen as the minisurvey galaxy lies within 5" of the IRAS position, and is almost 2 magnitudes brighter at K and considerably larger than the second galaxy, which is 20"E and 60"N of the IRAS position.

04151+0126: There is a foreground star lying 40"E, 15"N of the IRAS position. The galaxy is 90"W, 60"S of the IRAS position.

04192+0355: There are two non-stellar nuclei within a few arc-seconds of the IRAS position; their near-infrared flux densities have been added.

17002+7702: There are three objects visible near the IRAS position. One at 20"W, 15"S is a foreground star. The other two, at 0"E, 15"N and 20"W, 0"N, are non-stellar; the source at 20"W, 0"N was chosen as the IRAS source based on the radio source position (Eales, 1986).

17118+1253: There are two non-stellar objects, one at 60"W, 20"N and a second at 50"W, 0"N; the latter was chosen as the minisurvey galaxy since it is 1.6 magnitudes brighter at K, and its position agrees with the radio source position (Eales, 1986).

17153+1141: A foreground star lies 50"E, 20"S of the IRAS position. The minisurvey galaxy is at 15"W, 0"N, with a second foreground star lying to the immediate northwest.

1733+803P06: This galaxy was not included in the *IRAS Point Source Catalog*. However, the IRAS flux densities for this galaxy were considered valid despite their exclusion from the PSC (see text). The 60 μm and 100 μm flux densities have been taken as the average of those quantities for the IRAS sources 17329+8016 and 17331+8016 from the IRAS working survey data base.

17377+2845: The minisurvey galaxy is at 5"E, 25"N, with a foreground star lying to the immediate southwest.

17519+3351: The minisurvey galaxy is at 0"E, 0"N; there is a second galaxy at 10"W, 60"S.

17526+3253: There are two non-stellar nuclei within a few arc-seconds of the IRAS position; both nuclei correspond to radio source positions (Eales, 1986). The near-infrared flux densities for both sources have been added together.

17557+3117: There are two galaxies in the field, one at 20"E, 0"N and another at 10"E, 5"N. They are of comparable size and brightness, and both galaxies correspond to radio source positions (Eales, 1986). The near-infrared flux densities for both galaxies been added together.

18040+3400: There are two non-stellar nuclei within a few arc-seconds of the IRAS position; their near-infrared flux densities have been added together.

18130+3720: There are two galaxies in the field, one at 5"W, 0"N and another at 10"W, 20"N. They are of comparable size and brightness, and their near-infrared flux densities have been added together. There is also a foreground star at 10"W, 15"N.

23272+8518: There are two galaxies in the field, one at 10"E, 0"N and another at 5"W, 15"N. They are of comparable size and brightness, and their near-infrared flux densities have been added together. There is also a foreground star at 30"W, 0"N.

Chapter TWO:

The IRAS Bright Galaxy Sample: 1 – 10 μm Observations and Coadded IRAS Data for Galaxies With $L_{IR} \geq 10^{11} L_{\odot}$

This article has previously appeared in
the *Astronomical Journal*, Vol. **95**, p.356 (1988).
Coauthors: D.B. Sanders, B.T. Soifer, J.H. Elias,
K. Matthews, and G. Neugebauer.

ABSTRACT

Galaxies from the IRAS Bright Galaxy Sample with infrared luminosities $L_{IR} \geq 10^{11}\ L_{\odot}$ have been measured at 1.3, 1.6, 2.2, 3.7, and 10 μm. In addition, coadded IRAS measurements at all four IRAS bands have been obtained. It is found that an increase in the total infrared luminosity above $L_{IR} \sim 10^{11}\ L_{\odot}$ is correlated with increased emission from hot dust with characteristic temperatures $\sim$ 800 K contributing a substantial fraction of the 2.2 and 3.7 μm emission. This hot dust emission appears to "turn on" at luminosities of roughly $10^{11}\ L_{\odot}$.

The far–infrared emission cannot be modeled with a single dust temperature, but requires a cold ($T \sim 30 - 50\ K$) component coupled with a warmer ($T \gtrsim 70\ K$) component. Although the relative contribution from the cold component decreases with increasing luminosity, the temperature of the warmer component is independent of luminosity. The $f_{\nu}(12\ \mu m)/f_{\nu}(25\ \mu m)$ ratios for the galaxies in this sample are small compared with other extra-galactic objects, indicating that the radiation at 12 and 25 μm is dominated by emission from large dust grains radiating at high temperatures, rather than PAHs.

The spatial distribution of the 10 μm emission indicates a substantial extended component for most of the galaxies in this sample, implying that star formation processes contribute significantly to the luminosities. However, one third of the galaxies have exponential scale sizes characteristic of compact sources, and half of the galaxies have 10 μm emission consistent with a contribution of 50% or more from a central point source.

I. INTRODUCTION

The IRAS Bright Galaxy Sample (Soifer *et al.* 1987, hereafter Paper I) has helped demonstrate the importance of infrared emission in the energy budget of the local Universe. The space density of IRAS galaxies is comparable to or greater than that of starburst or Seyfert galaxies, and, at the highest infrared luminosities, IRAS galaxies appear to be the most numerous objects known (Paper I). Understanding the nature of this infrared emission is clearly of great importance.

Various analyses have concluded that the excess infrared emission in the vast majority of low to moderately high infrared luminosity galaxies ($L_{IR} \lesssim 10^{11}\ L_{\odot}$;[1] L_{IR} is defined in Section III) is due to star formation processes, rather than active nuclei (see, e.g., Eales *et al.* 1987; Carico *et al.* 1986; Elston, Cornell, and Lebofsky 1985; Rieke *et al.* 1980). However, at the highest luminosities ($L_{IR} \gtrsim 10^{12}\ L_{\odot}$), evidence suggests that active nuclei may be important in infrared galaxies (Becklin and Wynn-Williams 1987; Hill, Wynn-Williams, and Becklin 1987; Sanders *et al.* 1988), and that such galaxies may represent a phase in the formation of quasars (Sanders *et al.* 1988). These results suggest that the luminosity range $10^{11}\ L_{\odot} \lesssim L_{IR} < 10^{12}\ L_{\odot}$ is a transition range wherein the emergence of active nuclei occurs.

The current paper is one in a series of papers analyzing the properties of the Bright Galaxy Sample. The results of $1 - 10\ \mu m$ observations, as well as coadded IRAS data, of 61 galaxies from the Bright Galaxy Sample are presented. All of the 61 galaxies have $L_{IR} \geq 10^{11}\ L_{\odot}$; thus, they are representative of the most extreme luminosities known. By comparing the galaxies in the current sample with galaxies of both lower luminosity ($L_{IR} < 10^{11}\ L_{\odot}$) and the highest luminosities ($L_{IR} \gtrsim 10^{12}\ L_{\odot}$), it is the intent of this work to investigate the nature of the transition from normal galaxy properties to the extreme properties reported for galaxies with $L_{IR} \geq 10^{12}\ L_{\odot}$, and in particular to determine whether the unusual properties of galaxies with $L_{IR} \geq 10^{12}\ L_{\odot}$ are found, to a lesser degree, in infrared galaxies at lower luminosities.

---

[1] Throughout the text, H_o is taken as 75 $km\ sec^{-1}\ Mpc^{-1}$; $L_{\odot}$ is the solar bolometric luminosity, 3.83×10^{26} Watts

II. THE SAMPLE

The galaxies analyzed in this paper are a subset of the IRAS Bright Galaxy Sample (Paper I), which contains 324 galaxies, and represents all extragalactic objects with IRAS 60 μm flux densities greater than 5.4 Jy in an area of $\sim$ 14,500 square degrees, with Galactic latitude $|b| > 30°$, and declination $\delta > -30°$ for 0-12 hr, $\delta > -15°$ for 12-14 hr, and $\delta > -20°$ for 14-24 hr (Paper I).

The selection of galaxies for inclusion in this analysis was based on the far-infrared luminosity, L_{FIR}, which is tabulated in Paper I for the Bright Galaxy Sample, and which utilizes the IRAS 60 and 100 μm data to obtain an estimate of the luminosity between 40 and 400 μm (see Appendix B of *Cataloged Galaxies and Quasars Observed in the IRAS Survey (1985)*). In order to focus on the most luminous infrared galaxies, a list was compiled of all galaxies from the Bright Galaxy Sample with $L_{FIR} \geq 10^{11}\ L_{\odot}$. These galaxies, of which there are 69, will hereafter be referred to as the luminous bright galaxies, or LBGs; they are tabulated in Table 1, along with their coordinates and redshifts, reprinted from Paper I, and their optical diameters as measured from the Palomar Observatory Sky Survey prints. Of these 69 galaxies, 8 were not observable at the time the Palomar observations were being done. The remaining 61 galaxies, analyzed in this paper, therefore represent an unbiased and nearly complete sample of luminous infrared galaxies.

III. OBSERVATIONS AND DATA REDUCTION

The $1 - 10$ μm measurements were made at the Cassegrain f/70 focus of the Hale 5 m telescope at Palomar Observatory, using a solid nitrogen cooled InSb detector system for the $1.3 - 3.7$ μm measurements, and a helium cooled germanium bolometer for the 10 μm measurements. Beam sizes ranged from 4.6″ to 10″ in diameter, and sky subtraction was achieved by chopping to reference positions 15″ north and south of the galaxy. Sixty-one galaxies were observed at 1.27 μm (J), 1.65 μm (H), and 2.23 μm (K); 58 were observed at 3.69 μm (L'); and 59 were observed at 10.6 μm (N). The bandwidths of the filters used are $\Delta\lambda$ = 0.24 μm, $\Delta\lambda$ = 0.30 μm, $\Delta\lambda$ = 0.41 μm, $\Delta\lambda$ = 0.64 μm, and $\Delta\lambda$ = 4.7 μm, respectively. The measurements between 1.27 and 3.69 μm were calibrated using standard stars from Elias *et al.* (1982); the 10.6 μm measurements were calibrated at 10.1 μm, using standard

stars which are effectively on the system of Tokunaga (1984).

In general, observations were made by first locating the position of maximum flux at 2.2 μm in the beam (the instantaneous signal was always large enough to do this), then measuring fluxes at that location at all wavelengths. The photometric uncertainties for the 1.3, 1.6, and 2.2 μm measurements are generally $< 8\%$, and are due primarily to difficulties in accurately centering in the beam the position of maximum emission in the galaxy. Since the near–infrared flux density ratios (colors) are relatively independent of beam position, the uncertainties in the ratios are considerably less than those in the individual flux densities. For the 3.7 and 10 μm measurements, the photometric uncertainties are typically $\lesssim 15\ and\ 20\%$, respectively, but range up to 50% for some sources due to the increased background noise at longer infrared wavelenghts.

The LBGs have a broad range of energy distributions. Hence, individual corrections for redshift (K-corrections) have been made for each galaxy by using the measured flux densities to estimate by interpolation the flux densities at the filter wavelengths for an equivalent galaxy with zero heliocentric velocity. This process systematically overestimates the flux densities at 3.7 μm, so at that wavelength the interpolated flux density was averaged with the measured flux density for each galaxy to obtain the K-correction. Also, this process does not provide corrections for the 10 μm data; however, the uncertainties in the 10 μm data are large enough, and the redshifts small enough, that any correction at 10 μm would be inappropriate. Since the Bright Galaxy Sample was defined to have Galactic latitude $|b| > 30°$, where Galactic extinction is generally small, no corrections have been made for extinction within our own galaxy. Furthermore, no correction was made for internal extinction, because a large fraction of the galaxies in this sample are highly disturbed, and corrections would be difficult to estimate.

A large number of the LBGs contain optically obvious multiple nuclei. In such cases, near–infrared measurements were taken on each nucleus. These individual measurements have been used in calculating the near–infrared flux density ratios; however, when comparing a 10 μm flux density to IRAS data (where typical beam sizes were $1.5' \times 4.75'$), an estimate of the total 10 μm emission, obtained by

adding the individual flux densities from all measured positions, has been used. For all of the galaxies there is clearly a problem when attempting to relate the near–infrared ratios to IRAS measurements because of the difference in beam sizes. To minimize this problem, an effort was made to use flux density ratios from only that position within each source whose near–infrared emission was clearly dominant. However, for 11 of the LBGs, no such dominant position was found, so that both sets of near–infrared measurements have been used throughout the paper, and it is assumed that the infrared luminosity is distributed roughly equally between the individual objects.

Many of the LBGs have only limits listed in the IRAS Point Source Catalog (1985) for the 12 μm flux density. The original IRAS scans over the galaxies were therefore coadded, providing flux density estimates down to $\sim$ 0.4 Jy, which is below the sensitivity limit (0.5 Jy) of the Point Source Catalog. For completeness, this procedure was applied to all four IRAS bands, although the resulting deviations from the data in Paper I at 60 and 100 μm are small.

Although the LBG sample was selected on the basis of the far-infrared luminosity, L_{FIR} (see Section II), for all subsequent analyses the luminosity was adjusted for each galaxy using the method of Perault *et al.* (1986) to estimate L_{IR}, the luminosity between 8 and 1000 μm, utilizing all four IRAS bands. The resulting luminosity, which will be used throughout the rest of this paper, provides a better estimate of the total infrared luminosity and is systematically higher than L_{FIR}; the sample mean and dispersion of L_{IR}/L_{FIR} for the LBGs is 1.30 ± 0.14.

The observed near–infrared and IRAS flux densities, as well as the near–infrared beam diameters, are tabulated in Table 2, and the K-corrected near–infrared flux densities are given in Table 3. Table 4 lists the near–infrared and IRAS flux density ratios used in the analysis, as well as the infrared luminosities, L_{IR}.

IV. DISCUSSION

IV.1 1.3 – 3.7 μm measurements: the source of the near–infrared emission

Figure 1 shows the dependence of the near–infrared emission on luminosity for infrared galaxies by plotting the logarithms of the flux density ratios $R(1.3/1.6) \equiv f_\nu(1.27\ \mu m)/f_\nu(1.65\ \mu m)$ and

$R(2.2/1.6) \equiv f_\nu(2.23\ \mu m)/f_\nu(1.65\ \mu m)$ versus luminosity for a broad range of luminosities, where $f_\nu(\lambda)$ is the flux density at wavelength λ. Throughout this paper, the notation $R(\lambda_1/\lambda_2)$ will refer to the appropriate flux density ratio. The lower luminosity data ($L_{IR} < 10^{11}\ L_\odot$) are from Carico *et al.* (1986), and represent a sample of IRAS galaxies (the IRAS Minisurvey Sample; see Soifer *et al.* 1984) which was flux density-limited at 0.5 Jy and 60 μm, a factor of 10 fainter than the limit used to define the LBG sample. The two samples have the same mean redshift (the systematically higher luminosity of the LBGs is offset by the higher flux density limit as compared to the lower luminosity sample), and hence the only relevent difference in the selection criteria between the lower luminosity galaxies and the LBG sample is the luminosity cutoff used to define the latter sample. Since 12 and 25 μm data are not available for the lower luminosity galaxies, the infrared luminosity, L_{IR}, for those galaxies has been taken as $L_{IR} = 1.3 \times L_{FIR}$, adopting the mean L_{IR}/L_{FIR} for the LBGs given above; L_{IR}/L_{FIR} is not correlated with L_{IR} for the LBGs. The dashed lines in Figure 1, at $log[R(1.3/1.6)] = -0.09$ and $log[R(2.2/1.6)] = -0.12$, represent the ratios appropriate for normal spiral galaxies (Aaronson 1977).

From Figure 1 it is clear that the extreme $8 - 1000\ \mu m$ luminosities of the LBGs are also reflected in the near–infrared emission. The near–infrared flux density ratios deviate more from normal galaxy colors with increasing wavelength, as evidenced by the larger change in R(2.2/1.6) compared to R(1.3/1.6) for $L_{IR} \gtrsim 10^{11}\ L_\odot$. Further, Figure 1b suggests that the mechanisms effecting the near–infrared emission "turn on" at luminosities of roughly $10^{11}\ L_\odot$. This indicates a means of selecting highly luminous galaxies based on near–infrared emission alone. By using $R(2.2/1.6) \sim 1$ ($log[R(2.2/1.6)] \sim 0$ *or* $[H - K] \sim 0.5$ mag) as a rough cutoff, one should be able, on average, to separate out unusually infrared-luminous galaxies from more normal objects. As this procedure would require only broad-band 1.6 and 2.2 μm measurements, it may prove extremely useful, particularly since such infrared-luminous galaxies generally have large amounts of visual extinction, making the optical spectra more difficult to obtain.

The near-infrared flux density ratios R(1.3/1.6), R(2.2/1.6), and R(3.7/1.6) for the LBGs are shown in Figure 2. This figure is a three-dimensional representation, where the ratios are plotted on the x, y,

and z-axes, respectively, of a standard right-handed coordinate system. To eliminate ambiguities in the apparent position of the data in this three-dimensional space, the projection of the data onto each of the axis planes is also shown.

Figure 2 shows that the dispersion in the near–infrared properties of the LBGs is largest at 3.7 μm (note the different scale used for the R(3.7/1.6) axis in Figure 2). This effect cannot be attributed entirely to the larger statistical uncertainties in the 3.7 μm data; the dispersion in R(3.7/1.6) due to the uncertainties in the measurements is roughly twice that in R(2.2/1.6), whereas the observed range in R(3.7/1.6) is almost four times that in R(2.2/1.6). The 3.7 μm data were not included in Figure 1, since 3.7μm measurements are not available for the lower luminosity galaxies. However, Figure 2 indicates that R(3.7/1.6) is correlated with R(2.2/1.6), indicating that the increase in luminosity beyond 10^{11} $L_{\odot}$ apparently effects the near–infrared flux density ratios at longer wavelengths. Furthermore, the LBGs with $L_{IR} \geq 10^{12}$ $L_{\odot}$ all have R(3.7/1.6) ratios that are amongst the largest in the sample, indicating a significant luminosity dependence of the R(3.7/1.6) ratio.

Included in Figure 2 are representative flux density ratios for normal galaxy emission (N), a "starburst" nucleus (B), and an active galactic nucleus, or AGN (A). R(3.7/1.6) for a normal galaxy is taken to be 0.43 (Lawrence *et al.* 1985). The flux density ratios used for an AGN are those of the quasar 3C273 (from Neugebauer *et al.* 1987); throughout this paper the term AGN will refer specifically to a quasar-like energy source. The flux density ratios used for a starburst nucleus are those of the nucleus of the archetypal starburst galaxy NGC 253. The $1.2 - 2.2$ μm measurements for NGC 253 are from Scoville *et al.* (1985), and the 3.7 μm flux density (taken to be equal to the published 3.5 μm measurement) is from Becklin, Fomalont, and Neugebauer (1973).

Figure 2 presents a direct comparison of the near–infrared continuum emission of the LBGs to that of other extra-galactic sources. It is seen that the near–infrared flux density ratios of most of the LBGs lie roughly between the ratios expected for normal galaxies and those of active nuclei, and are thus consistent with a combination of normal galaxy emission plus direct emission from an AGN. However, based on their near–infrared ratios, many of the LBGs are also consistent with combinations of normal

galaxy emission and emission from a starburst nucleus.

The source of the near–infrared emission in the LBGs is investigated further in Figure 3, where R(1.3/1.6), R(2.2/1.6), and R(10/3.7) are plotted against R(3.7/1.6). The components A and B from Figure 2 are indicated in Figures 3a and b. Since the ratios are plotted on a linear scale, with a common wavelength for the denominator, the flux density ratios for combined contributions from any two components will lie on a straight line connecting the flux density ratios of the two individual components. Also shown in Figures 3a and b are trajectories of the following physical processes:

(*i*) absorption by dust uniformly mixed with the emitting source (line **a**); the line indicates the reddening produced on the flux density ratios of a normal galaxy by gradually increasing the optical depth, using the near–infrared reddening law from Cohen *et al.* (1981);

(*ii*) thermal emission at temperatures of 600 K (line **b**), 800 K (line **c**), and 1000 K (line **d**), with λ^{-1} emissivity, appropriate for dust grains (see, e.g., Draine and Lee 1984). The lines emanate from the point corresponding to a normal galaxy, and indicate the change in the flux density ratios of a normal galaxy as the contribution to the 3.7 μm flux density from thermal emission gradually increases relative to the contribution at 3.7 μm from a normal galaxy. Lines **b**, **c**, and **d** will be taken as representative of contributions from hot dust emission to a normal galaxy component.

From Figures 3a and b, the observed near–infrared ratios of the LBGs are generally consistent with the effects of dust applied to a normal galaxy component. The range in R(1.3/1.6) indicates dust absorption, as seen most clearly in Figure 3a. For most of the galaxies the inferred optical depth at V is between 0 and 10, although for a few objects this number may be much larger. The large dispersion in R(3.7/1.6)cannot be due to extinction (line **a**), but is consistent with contributions from hot dust emission with characteristic temperature $\sim$ 800 K. This contribution is between 0 and 80% of the total 3.7 μm emission for most of the galaxies, while for a few of the objects the data suggest contributions of more than 90%.

If a contribution from direct AGN emission is used to model the flux density ratios of the LBGs, then contributions ranging from 0 to 50% of the total 3.7 μm emission, in combination with dust

absorption and emission, would yield the observed flux density ratios for most of the LBGs. Hence, there is flexibility in modeling the relative contributions from direct AGN emission and hot dust emission, and various combinations are allowed by the data. However, given the quantities of dust expected in these objects, as inferred from the far–infrared emission (Paper I), it is likely that most AGN emission would be absorbed and re-radiated by the dust, and that the dominant factor contributing to the shift in the near–infrared properties of the LBGs relative to those of a normal galaxy is an increase in hot dust emission, with characteristic temperature $T \sim 800\ K$.

In Figure 3c, the R(10/3.7) ratio has been plotted as a diagnostic of the relative contribution from hot dust emission ($T \sim 800\ K$), responsible for the dispersion in R(3.7/1.6), and warm dust emission ($T \sim 300 - 400\ K$), required to produce significant 10 μm emission. The main result from Figure 3c is that, although there is essentially no correlation between R(10/3.7) and R(3.7/1.6) for most of the LBG sample, it appears that those galaxies with the most extreme R(3.7/1.6) ratios, i.e., those postulated in the previous discussion to contain the most hot dust, all have comparatively low R(10/3.7) ratios. This effect can be explained in two ways, as due either to a shift in the temperature of the dust to hotter temperatures in these galaxies, or an increase in silicate absorption at 10 μm, as the result of a larger mass of dust in these galaxies. These two explanations cannot be distinguished based on the data in this paper.

Identifying the observed near–infrared properties as dominated by dust absorption and emission does not severely constrain the intrinsic source of the luminosity in the LBGs. Regions of recent or ongoing star formation would be characterized by large quantities of dust, effecting the near–infrared properties through absorption, as well as emission from hot dust in the environments of very young stars. As was seen in Figure 2, the flux density ratios for many of the LBGs are consistent with a contribution from a starburst nucleus. However, for a heavily dust enshrouded AGN, one would also expect the near–infrared emission to be dominated by dust emission. This is seen in the fact that the LBGs with $L_{IR} \geq 10^{12}\ L_{\odot}$, which Sanders *et al.* (1988) have identified as probably containing active nuclei, have near–infrared flux density ratios which can be readily modeled as due to hot dust emission. Hence, the

near–infrared ratios cannot be used to narrow down the luminosity range wherein the transition to a dominant active nucleus occurs.

There is one galaxy from the LBG sample, IRAS 0857+39, which is clearly distinct, due to its extremely large R(3.7/1.6) ratio of 26.56. This galaxy, with a luminosity of $1.2 \times 10^{12}\ L_{\odot}$, has been studied by Sanders *et al.* (1988), who claim that its primary source of power is an AGN. Such an extreme 3.7 μm excess, although unique in comparison to all of the other LBGs, and certainly inconsistent with direct AGN emission, can be modeled by invoking a substantial emission component from dust at $\sim 500\ K$.

IV.2 IRAS data

The luminosity dependence of the far–infrared emission is shown in Figure 4, where logarithms of the IRAS flux density ratios R(100/60), R(25/60), and R(12/25), are plotted versus L_{IR}. Figure 4a is essentially the high luminosity end of Figure 6a in Paper I, which shows $f_{\nu}(60\ \mu m)/f_{\nu}(100\ \mu m)$ plotted against L_{FIR} for the entire Bright Galaxy Sample. As mentioned previously (Section III), the 60 and 100 μm IRAS data included in this paper do not differ significantly from those given in Paper I.

The effects seen in Figure 4a, namely an apparent minimum R(100/60) ratio which is independent of luminosity, and an apparent maximum R(100/60) which decreases with increasing luminosity, have been attributed to an effective maximum in the radiation field heating the radiating material, which is independent of luminosity, and an effective minimum in the radiation field that increases with luminosity (Paper I). A similar effect has been found for Seyfert galaxies; see, e.g., Miley, Neugebauer, and Soifer (1985).

In Figure 4b, there does not appear to be any change in R(25/60) with luminosity above $10^{11}\ L_{\odot}$. This lack of correlation between R(25/60) and infrared luminosity for infrared galaxies does, in fact, continue down to luminosities $\sim\ 10^{9}\ L_{\odot}$, as demonstrated by Smith *et al.* (1987) using another flux-limited sample of IRAS galaxies.

In Figure 4c, the R(12/25) ratio changes with luminosity in the sense that, although almost half of

the galaxies in the luminosity range $1 - 5 \times 10^{11}\ L_{\odot}$ have $log[R(12/25)] > -0.5$ ($R(12/25) > 0.3$), none of the galaxies with $L_{IR} > 5 \times 10^{11}\ L_{\odot}$ have $log[R(12/25)] > -0.5$. Thus, there appears to be an absence of galaxies with very high luminosities and high R(12/25) ratios.

The far–infrared flux density ratios for the LBGs can be compared to those of other extra-galactic objects in Figure 5, where characteristic flux density ratios for normal (N), starburst (B), and Seyfert (S) galaxies are included. The points N, B, and S were determined based on the data from Rowan-Robinson and Crawford (1986), and are consistent with data from other authors (see, e.g., Sekiguchi 1987; Helou 1986; Miley, Neugebauer, and Soifer 1985). Since all of the LBGs are visually extended sources, Seyfert galaxies were chosen to represent the far–infrared flux density ratios of active galaxies, rather than the quasar 3C273; any far–infrared disk emission detected by the large beam IRAS measurements is thus taken into account in the comparison.

The far–infrared flux density ratios for most of the LBGs are similar to those of normal and starburst galaxies. They are distinct from Seyfert galaxies in the R(25/60) ratio, which is typically larger in Seyfert galaxies, reflecting their relatively flat energy distributions. In particular, it is worth emphasizing that the LBGs with $L_{IR} \geq 10^{12}\ L_{\odot}$, which appear to be powered by active nuclei (Sanders *et al.* 1988), do not have far–infrared emission consistent with typical Seyfert galaxies. One striking feature of Figure 5 is that, for a number of the LBGs, the R(12/25) ratios are considerably smaller than the characteristic ratios for normal, starburst, or Seyfert galaxies, indicating unusually steep energy distributions between 12 and 25 μm.

To investigate the source of the far–infrared emission in the LBGs, Figure 5b shows the locus of points corresponding to the flux density ratios for steady-state emission from dust grains, with λ^{-1} emissivity, at a range of temperatures. It can be readily seen that the far–infrared emission in most of the LBGs cannot be modeled with a single dust temperature, but requires at least two components. The data suggest a cold dust component, with characteristic temperatures $T \sim 30 - 50\ K$, for most of the galaxies, coupled with a contribution from an additional warmer component, at temperatures $T \gtrsim 70\ K$. Such temperatures are in agreement with the results of Sekiguchi (1987) for his sample of starburst

galaxies, but are higher than those expected for lower luminosity IRAS galaxies (see, e.g., Paper I, De Jong *et al.* 1984) and reflect the decrease in R(100/60) with luminosity seen in Paper I. The highest temperature consistent with the data is probably appropriate for the cold dust component, since the mass of dust required to produce a given luminosity scales roughly with temperature as T^{-5}.

As Figure 5b shows, the relative contribution to the far–infrared emission from cold ($T \sim 30 - 50\ K$) dust is primarily reflected in the R(100/60) ratio. Thus, the luminosity dependence seen in Figure 4a indicates that, although galaxies with little or no contribution from cold dust are found over the entire luminosity range, as L_{IR} increases, fewer and fewer galaxies are found which have significant quantities of cold dust contributing to their infrared luminosity. This is essentially equivalent to the result from Paper I mentioned previously. The lack of any correlation between R(25/60) and luminosity seen in Figure 4b suggests that the characteristic temperature of the dust with $T \gtrsim 70\ K$ does not change systematically with luminosity.

Figure 6, which shows log[R(12/25)] versus log[R(100/60)], presents the interesting result that R(12/25) and R(100/60) are correlated. Thus, as R(12/25) increases, indicating a higher characteristic temperature for the dust emitting at 12 and 25 μm, the increase in R(100/60) indicates a colder temperature for the dust emitting at 60 and 100 μm. A plausible explanation for this correlation has been proposed by Helou (1986). Various authors (see, e.g., Desert 1986; Puget, Leger, and Boulanger 1985; Sellgren 1984) have discussed the possibility that very small grains ($\sim$ a few Angstroms in size), transiently heated to roughly 1000 K, can be an important source of emission at wavelengths between 1 and 20 μm. Evidence suggests that these small grains are polycyclic aromatic hydrocarbons, known as PAHs (Leger and Puget 1984). In Helou's model, the R(12/25) ratio reflects the relative contributions from PAHs and from larger, hot dust grains radiating in a steady-state. For relatively quiescent, inactive galaxies, R(12/25) is affected by the emission from PAHs in the 12 μm band, resulting in large R(12/25) ratios. As the intensity of the heating radiation in the galaxy increases, as with increased star formation, the equilibrium temperature of the larger dust grains increases, dominating the far–infrared emission and determining the IRAS colors.

The data used by Helou (1986) in his analysis was taken from a sample of "normal" IRAS galaxies chosen to exclude likely Seyfert candidates by removing from the sample all galaxies with $R(25/60) > 0.18$; Helou's data is indicated by the dashed envelope in Figure 6. For comparison, the LBGs with $R(25/60) > 0.18$ have been identified in Figure 6, although this distinction in R(25/60) does not appear to significantly effect the observed range in R(12/25) or R(100/60) for the LBGs. It is seen that, on average, the LBGs have smaller R(12/25) ratios than do normal IRAS galaxies, which, using Helou's model, implies a higher level of star formation activity in the LBGs. This is consistent with the fact that the LBGs are systematically more luminous than the galaxies in Helou's sample. Furthermore, the luminosity dependence seen in Figure 4c implies that *all* galaxies with $L_{IR} \gtrsim 5 \times 10^{11}\ L_{\odot}$ have sufficient quantities of large dust grains radiating at high temperatures to dominate the 12 and 25 μm emission. This agrees with the earlier result (Section IV.1) that the infrared luminosity is correlated with hot dust emission at near–infrared wavelengths.

IV.3 10 μm measurements: the spatial distribution of the infrared emission

The diameter of the 10 μm measuring beam corresponds to a 3 kpc median diameter at the source and a median d_{10}/D_o of 0.1, where d_{10} is the 10 μm beam diameter and D_o is the visual major axis diameter measured from the Palomar Observatory Sky Survey prints. Since the IRAS detectors typically subtended $1.'5 \times 4.'75$, whereas the visual diameter D_o for the LBGs is typically $0.'2\ to\ 1.'4$, the IRAS data represent the total emission from each source, independent of D_o. Hence, a comparison of the ground-based 10 μm data, $f_\nu(10\ \mu m,\ small\ beam)$, with the IRAS 12 μm data, $f_\nu(12\ \mu m,\ IRAS)$, gives an estimate of the spatial extent of the 10 μm emission in these galaxies. To adjust for the 10 to 12 μm color, a power-law extrapolation through 25 and 12 μm was used to estimate the total 10 μm flux density, $f_\nu(10\ \mu m,\ total)$, for each galaxy, and a second power-law extrapolation through 3.7 and 10 μm was used to estimate the 12 μm flux density which would have been measured in a ground-based beam of the same diameter as the 10 μm beam, $f_\nu(12\ \mu m,\ small\ beam)$. The ratio, R_{10}, of the 10 μm flux density measured in the ground-based beam to the total 10 μm flux density was then taken as the average of $f_\nu(10\ \mu m)/f_\nu(10\ \mu m,\ total)$ and $f_\nu(12\ \mu m,\ small\ beam)/f_\nu(12\ \mu m,\ IRAS)$. Hereafter,

R_{10} will be used to characterize the degree of concentration of the 10 μm emission about the nucleus of each galaxy. R_{10} is tabulated in Table 4.

No attempt has been made to correct the values of R_{10} for silicate absorption, which is known to be strong for at least some of these galaxies. In particular, for Arp 220 the visual extinction corresponding to the depth of the silicate feature observed has been estimated by Becklin and Wynn-Williams (1987) to be $\sim$ 50 mag. In a more detailed analysis than is given here, these authors find that more than 90% of the 12 μm emission from Arp 220 is contained within a 3″ diameter about the nucleus, whereas the value of R_{10} presented in this paper for this galaxy is only 0.63. Arp 220 is most likely a very extreme case, but nevertheless, more accurate values for R_{10} would be somewhat higher than those presented here.

The extent of the 10 μm emission is potentially an effective diagnostic of the relative AGN contribution in a galaxy, since dust sufficiently hot to radiate in a steady-state at 10 μm must be at a temperature of several hundred degrees, and hence must be comparatively close to the luminosity source. For dust at 300 K (which corresponds to a peak in the thermal energy distribution at 10 μm, if the dust emissivity is proportional to frequency), illuminated by a source of luminosity $\sim 5 \times 10^{11} L_{\odot}$, characteristic distances are on the order of one hundred to a few hundred parsecs. Thus, substantial 10 μm emission beyond this distance from the nucleus cannot be due to dust directly heated by an AGN, and should generally be attributed to a distributed luminosity source, such as star formation.

In Figure 7, the fraction of the total 10 μm emission within the ground-based 10 μm beam is shown for the LBGs, by plotting R_{10} versus the 10 μm beam diameter, in kpc at the source. Most of the galaxies have significant 10 μm emission beyond 1 kpc in diameter, providing evidence that enhanced star formation contributes substantially to the intrinsic luminosity in most of the LBGs. The possible exceptions to this are those galaxies with $R_{10} \sim 1$, for which the 10 μm beam diameter is an upper limit on the spatial extent of the 10 μm emission.

An estimate of the extent of the 10 μm emission in the galaxy M 101 has been indicated in Figure 7 by plotting the 12 μm emission within a 9.4 kpc diameter about its nucleus (Rice 1987). It

is clear that the 10 μm emission in M 101 is more extended than that in most of the LBGs. M 101 was chosen for comparison to the LBGs because it is representative of gas-rich spiral galaxies of moderate luminosity detected by IRAS (from Paper I, the luminosity of M 101 is 2×10^{10} $L_{\odot}$), and is large enough for information on the spatial distribution to be obtained. The IRAS data for two other moderate luminosity gas-rich spirals, M 51 and NGC 891, yield very similar results to that of M 101 (Rice).

Also shown in Figure 7 are flux integrals for a brightness distribution proportional to $exp(-r/r_o)$, with r_o = 0.5, 1.0, and 2.0 kpc. An exponential brightness distribution corresponds to the disk emission in normal spiral galaxies (see, e.g., Mihalas and Binney 1968). Most of the LBGs have irregular morphologies, in many cases apparently due to galaxy collisions, so it is unlikely that their brightness profiles would be well represented by an exponential law. Nevertheless, the exponential scale size, r_o, can be a useful number for characterizing the breadth of the light distribution. It is seen that roughly one third of the LBGs have scale sizes $r_o \leq 0.5$ kpc, a size Hill (1987) has shown to be characteristic of a compact nuclear infrared source.

Although 10 μm emission beyond 1 kpc of the center of a galaxy must be due to a distributed source, such emission does not preclude the possibility of an additional, substantial contribution to the total luminosity from a central point source. By assuming that the 10 μm emission coming from *outside* of the ground-based beam has a brightness profile appropriate for normal galaxy disk emission, and by setting a limit to the diameter out to which this 10 μm disk emission originates, one can estimate the maximum possible contribution to the 10 μm emission from a central point source which is consistent with the observed value for R_{10}. Since no galaxies are yet known where significant 12 μm emission is detected beyond the optical disk (Rice *et al.* 1987), D_o can be taken as a limit to the extent of the 10 μm disk emission. An estimate, R_{PS}, of the maximum possible point source contribution to the observed 10 μm flux density for each of the LBGs was thus obtained by modeling the spatial distribution of the 10 μm emission as a central point source coupled with an exponential disk whose surface brightness drops to 1% of its peak brightness at a radius $D_o/2$. The results are shown in Figure 8, for the entire LBG sample and also for the LBGs with $L_{IR} \geq 10^{12}$ $L_{\odot}$. The data for roughly

two-thirds of the LBGs are consistent with a contribution of 20% or more to the total 10 μm emission from a central point source, and half of the galaxies are consistent with a contribution of 50% or more from a point source.

Figure 8 also shows a possible luminosity dependence for the degree of concentration of the 10 μm emission, since 6 of the 7 galaxies with $L_{IR} \geq 10^{12}\ L_{\odot}$ plotted in the histogram have $R_{PS} \geq 0.4$. This possible luminosity dependence has been investigated further in Figure 9, which shows R_{10} plotted against the infrared luminosity for the LBGs. There does not appear to be any luminosity dependence in R_{10}, for luminosities below approximately $7 \times 10^{11}\ L_{\odot}$. However, the population of galaxies with broadly extended 10 μm emission does decrease abruptly above this luminosity. This is not a selection effect since, for galaxies with angular diameter less than 50″ (a size which includes 12 of the 14 LBGs with $L_{IR} > 7 \times 10^{11}\ L_{\odot}$), there is no correlation between R_{10} and optical diameter.

V. CONCLUSIONS

An analysis of 61 IRAS galaxies with infrared luminosities greater than or equal to $10^{11}\ L_{\odot}$ has yielded the following results:

(1) An increase in the total infrared luminosity above $L_{IR} \sim 10^{11}\ L_{\odot}$ is correlated with increased emission from hot dust with characteristic temperatures $\sim 800\ K$. This hot dust contributes a substantial fraction of the 2.2 and 3.7 μm emission, resulting in a greatly increased dispersion in R(3.7/1.6) and R(2.2/1.6) for such galaxies relative to lower luminosity galaxies. This excess hot dust emission appears to "turn on" at luminosities $\sim 10^{11}\ L_{\odot}$. Galaxies with the largest contribution to the near–infrared emission from hot dust have systematically smaller R(10/3.7) ratios, which may represent a shift in the temperature of the dust to hotter temperatures in these galaxies, but can also be explained as an increase in silicate absorption due to an increase in the mass of dust in these galaxies.

(2) The far–infrared flux density ratios of very luminous infrared galaxies generally span the range from normal to "starburst" galaxies, but a number of the galaxies studied have steeper energy distributions between 12 and 25 μm than are expected from normal or starburst galaxies. None of the galaxies presented in this paper have flux density ratios appropriate for typical Seyfert galaxies.

(3) The far–infrared emission in very luminous infrared galaxies cannot be modeled with a single dust temperature, but requires a contribution from cold dust ($T \sim 30 - 50\ K$) coupled with a warmer component with characteristic temperatures $T \gtrsim 70\ K$. Although the maximum cold dust contribution seen in infrared galaxies decreases at luminosities above $10^{11}\ L_{\odot}$, the temperature of the warmer component does not change with luminosity.

(4) If one adopts the model of Helou (1986), the R(12/25) and R(100/60) ratios in the LBGs indicate systematically higher levels of star formation activity in extremely luminous infrared galaxies as compared to "normal" IRAS galaxies. For galaxies with $L_{IR} \gtrsim 5 \times 10^{11}\ L_{\odot}$, the R(12/25) ratio is dominated by emission from large dust grains radiating at high temperatures rather than from PAHs.

(5) Most of the LBGs emit a significant fraction of their 10 μm emission beyond 1 kpc, indicating a substantial contribution to their luminosities from star formation. However, one third of the galaxies have exponential scale sizes characteristic of compact sources, and half of the galaxies have 10 μm emission consistent with a contribution of 50% or more from a central point source.

(6) There is no correlation between the degree of concentration of the 10 μm emission and luminosity for luminosities less than about $7 \times 10^{11}\ L_{\odot}$. However, above this luminosity the population of galaxies with extended 10 μm emission decreases abruptly.

ACKNOWLEDGEMENTS

The authors thank Walter Rice for the data on M 101, and the night assistants at the Palomar 200 inch telescope, Juan Carrasco and Skip Staples. Thanks is also given to the entire staff at IPAC and Palomar Observatory. This work was supported by a grant from the National Science Foundation, and by NASA through the IRAS Extended Mission program.

REFERENCES

Aaronson, J. 1977. Infrared observations of galaxies, Ph.D. thesis, Harvard University.

Becklin, E.E., and C.G. Wynn-Williams, 1987. Ground–based 1 – 32 μm observations of Arp 220: Evidence for a dust–embedded "AGN"?, in *Star Formation in Galaxies*, C.J. Lonsdale (Ed.), US Government Printing Office, Washington D.C., p. 643.

Becklin, E.E., E.B. Fomalont, and G. Neugebauer, 1973. *Astrophys. J. (Letters)*, **181**, L27.

Carico, D.P., B.T. Soifer, C. Beichman, J.H. Elias, K. Matthews, and G. Neugebauer, 1986. Near–infrared observations of *IRAS* minisurvey galaxies, *Astron. J.*, **92**, 1254 (Chapter 1 of this thesis).

Infrared Astronomical Satellite (IRAS) Catalogs and Atlases: *Cataloged Galaxies and Quasars Observed in the IRAS Survey*, 1985. C.J. Lonsdale, G. Helou, J.C. Good, and W. Rice (Eds.), National Aeronautics and Space Administration, Washington D.C..

Cohen, J.G., J.A. Frogel, S.E. Persson, and J.H. Elias, 1981. *Astrophys. J.*, **249**, 481.

de Jong, T., P.E. Clegg, B.T. Soifer, M. Rowan–Robinson, H.J. Habing, J.R. Houck, H.H. Aumann, and E. Raimon, 1984. *IRAS* observations of Shapley–Ames galaxies, *Astrophys. J. (Letters)*, **278**, L67.

Désert, F.X., 1986. In *Light On Dark Matter*, F.P. Israel (Ed.), Reidel, p. 213.

Draine, B.T., and H.M. Lee, 1984. Optical properties of interstellar graphite and silicate grains, *Astrophys. J.*, **285**, 89.

Eales, S.A., Wynn-Williams, C.G., and Beichmann, C.A. 1987, in preparation.

Elias, J.H., J.A. Frogel, K. Matthews, and G. Neugebauer, 1982. Infrared standard stars, *Astron. J.*, **87**, 1029.

Elston, R., M.E. Cornell, and M.J. Lebofsky, 1985. The properties of far–infrared luminous galaxies. I. Spectroscopic and near–infrared observations, *Astrophys. J.*, **296**, 106.

Infrared Astronomical Satellite (IRAS) Catalogs and Atlases: *Explanatory Supplement*, 1988. C.A. Beichman, G. Neugebauer, H.J. Habing, P.E. Clegg, and T.J. Chester (Eds.), National Aeronautics and Space Administration, Washington D.C..

Helou, G., 1986. The IRAS colors of normal galaxies, *Astrophys. J.*, **311**, L33.

Hill, G.J., 1987. Nuclear infrared emission and the colors of *IRAS* galaxies, in *Star Formation in Galaxies*, C.J. Lonsdale (Ed.), US Government Printing Office, Washington D.C., p. 643.

Infrared Astronomical Satellite (IRAS) Catalogs and Atlases: *The Point Source Catalog*, 1985. National Aeronautics and Space Administration, Washington D.C..

Lawrence, A., M. Ward, M. Elvis, G. Fabbiano, S.P. Willner, N.P. Carleton, and A. Longmore, 1985. *Astrophys. J.*, **291**, 117.

Léger, A. and J.L. Puget, 1984. Identification of the unidentified infrared emission features of interstellar dust?, *Astron.strophs.*, **137**, L5.

Mihalas, D., and J. Binney, 1968. *Galactic Astronomy*, Freeman, San Francisco, p. 323.

Miley, G.K., G. Neugebauer, and B.T. Soifer, 1985. *IRAS* observations of Seyfert galaxies, *AstrophysJ. (Letters)*, **293**, L11.

Neugebauer, G., R.F. Green, K. Matthews, M. Schmidt, B.T. Soifer, and J. Bennett, 1987. Continuum energy distributions of quasars in the Palomar–Green survey, *Astrophys. J. Supp.*, **63**, 615.

Pérault, M., F. Boulanger, J.L. Puget, and E. Falgarone, 1989. *Astrophys.J.*, submitted.

Puget, J.L., A. Léger, and F. Boulanger, 1985. Contribution of large polycyclic aromatic molecules to the infrared emission of the interstellar medium, *Astron. Astrophs.*, **142**, L19.

Rice, W., 1987. Private communication.

Rice, W., C.J. Lonsdale, B.T.Soifer, G. Neugebauer, E.L. Kopan, L.A. Lloyd, T. De Jong, and H.J. Habing, 1988. A Catalog of IRAS Observations of Large Optical Galaxies, *Astrophys. J. Supp.*, **68**, 91.

Rieke, G.H., M.J. Lebofsky, R.I. Thompson, F.J. Low, and A.T. Tokunaga, 1980. The nature of the nuclear sources in M 82 and NGC 253, *Astrophys. J.*, **238**, 24.

Rowan-Robinson, M., and Crawford, J. 1986, in *Light On Dark Matter*, ed. F.P. Israel (D. Reidel Publishing Company), p. 421.

Sanders, D.B., B.T. Soifer, J.H. Elias, B.F. Madore, K. Matthews, G. Neugebauer, and N.Z. Scoville, 1988. Ultraluminous infrared galaxies and the origin of quasars, *Astrophys. J.*, **325**, 74.

Scoville, N.Z., B.T. Soifer, G. Neugebauer, J.S. Young, K. Matthews, and J. Yerka, 1985. The inner disk of NGC 253, *Astrophys. J.*, **289**, 129.

Sekiguchi, K, 1987. *IRAS* observations of starburst and non–active spiral galaxies, *AstrophsJ.*, **316**, 145.

Sellgren, K, 1984. The near–infrared continuum emission of visual reflection nebulae, *Astrophs. J.*, **277**, 623.

Smith, B.J., S.G. Kleinmann, J.P. Huchra, and F.J. Low, 1987. *Astrophys. J.*, **318**, 161.

Soifer, B.T., D.B. Sanders, B. Madore, G. Neugebauer, G.E. Danielson, J.H. Elias, C.J. Persson, and W.L. Rice, 1987. The *IRAS* Bright Galaxy Sample. II. The sample and luminosity function, *Astrophys. J.*, **320**, 238 (Paper I).

Soifer, B.T., *et al.*, 1984. Infrared galaxies in the *IRAS* minisurvey, *Astrophys. J. (Letters)*, **278**, L71.

Tokunaga, A., 1984. *Astron. J.*, **89**, 172.

Figure Captions

Figure 1: The near-infrared flux density ratios (a) R(1.3/1.6) and (b) R(2.2/1.6), plotted logarithmically, versus the infrared luminosity, for the LBGs (*circles*) and a sample of IRAS galaxies studied by Carico *et al.* (1986; *squares*). L_{IR} is an estimate of the luminosity between 8 and 1000 μm (see text). The dashed lines indicate representative ratios for normal galaxies (from Aaronson 1977).

Figure 2: The near–infrared flux density ratios R(1.3/1.6), R(2.2/1.6), and R(3.7/1.6). The LBGs previously studied by Sanders *et al.* (1988) are plotted with the symbol *. The data are plotted on the x, y, and z axes of a standard right-handed coordinate system. The smaller circles and stars indicate the projections of the data onto each of the axis planes. Note that, due to the different dispersions in the ratios, different scales have been used for the different axes.

Also shown are the flux density ratios representative of normal galaxies (N), active galactic nuclei (A), and starburst nuclei (B). For point N, R(1.3/1.6) and R(2.2/1.6) are from Aaronson (1977), and R(3.7/1.6) is from Lawrence *et al.* (1985). Point A is from Neugebauer *et al.* (1987). For point B, R(1.3/1.6) and R(2.2/1.6) are from Scoville *et al.* (1985), and R(3.7/1.6) is from Becklin, Fomalont, and Neugebauer (1973).

Figure 3: The flux density ratios R(1.3/1.6), R(2.2/1.6), and R(10/3.7), plotted against R(3.7/1.6). The LBGs previously studied by Sanders *et al.* (1988) are plotted with the symbol *. Galaxies with only limits at 3.7 or 10 μm have been excluded.

The lines **a** through **d** represent the following: **a** = absorption from dust uniformly mixed with the source, labeled as a function of the optical depth at V, τ_V, where $I_\nu \propto \tau_\nu{}^{-1}(1 - e^{-\tau_\nu})$; **b, c,** and **d** = contributions from hot dust emission at $T = 600\ K,\ 800\ K,\ 1000\ K$, respectively; the tick marks indicate the fraction of the total 3.7 μm emission from dust emission, relative to normal galaxy emission, and are drawn at intervals of 10%. The arrows point toward the flux density ratios of pure hot dust emission (no contribution from a normal galaxy). The lines **a** through **d** extend from the point representative of normal galaxies (from Aaronson 1977 and Lawrence 1985; see text). Also shown

are the flux densities representative of an active galactic nucleus (A) and a starburst nucleus (B), as in Figure 2.

The flux density ratios for the galaxy IRAS 0857+39, for which $R(3.7/1.6) = 26.56$, are indicated in each plot by a short arrow extending from an apparent data point; the vertical position of each arrow gives the appropriate flux density ratio for this galaxy.

Figure 4: The IRAS flux density ratios R(100/60), R(25/60), and R(12/25), versus the infrared luminosity for the LBGs. The LBGs previously studied by Sanders *et al.* (1988) are plotted with the symbol *.

Figure 5: The IRAS flux density ratios, R(12/25), R(25/60), and R(100/60), for the LBGs. The LBGs previously studied by Sanders *et al.* (1988) are plotted with the symbol *. Also shown are the flux density ratios representative of normal galaxies (N), Seyfert galaxies (S), and starburst galaxies (B), determined using the data of Rowan-Robinson and Crawford (1986). The curve in (b) is the locus of flux density ratios for dust emission with emissivity proportional to λ^{-1}.

Figure 6: The IRAS flux density ratio R(12/25) versus R(100/60), plotted logarithmically. The LBGs previously studied by Sanders *et al.* (1988) are plotted with the symbol *. The dashed envelope is from a sample of "normal" IRAS galaxies, chosen to exclude likely Seyfert candidates, studied by Helou (1986). Squares indicate LBGs with $R(25/60) > 0.18$ (see text).

Figure 7: The fraction of the total 10 μm emission measured in a 5 " beam plotted as a function of the 10 μm beam diameter, in kpc at the source. Galaxies with only limits at 10 μm or 12 μm (see Table 2) have not been included. The LBGs previously studied by Sanders *et al.* (1988) are plotted with the symbol *. The curves indicate exponential brightness distributions where the surface brightness falls to 1% of its peak brightness at a radius D/2 (see text); curves have been drawn for r_o = 0.5, 1.0, *and* 2.0. The 10 μm emission within a 9.4 kpc diameter about the nucleus of M 101 is shown for comparison (Rice 1987).

Figure 8: Histograms of the maximum possible contribution to the 10 μm emission from a central point source, R_{PS} (see text). *solid line*: the LBG sample, *dotted line*: the LBGs with $L_{IR} \geq 10^{12}\ L_{\odot}$.

Galaxies with only limits at 10 μm or 12 μm (see Table 2) have not been included in either histogram.

Figure 9: The ratio, R_{10}, of the 10 μm emission in the ground-based beam to the total 10 μm emission, versus the infrared luminosity for the LBGs. Galaxies with only limits at 10 μm or 12 μm (see Table 2) have not been included. The LBGs previously studied by Sanders *et al.* (1988) are plotted with the symbol *.

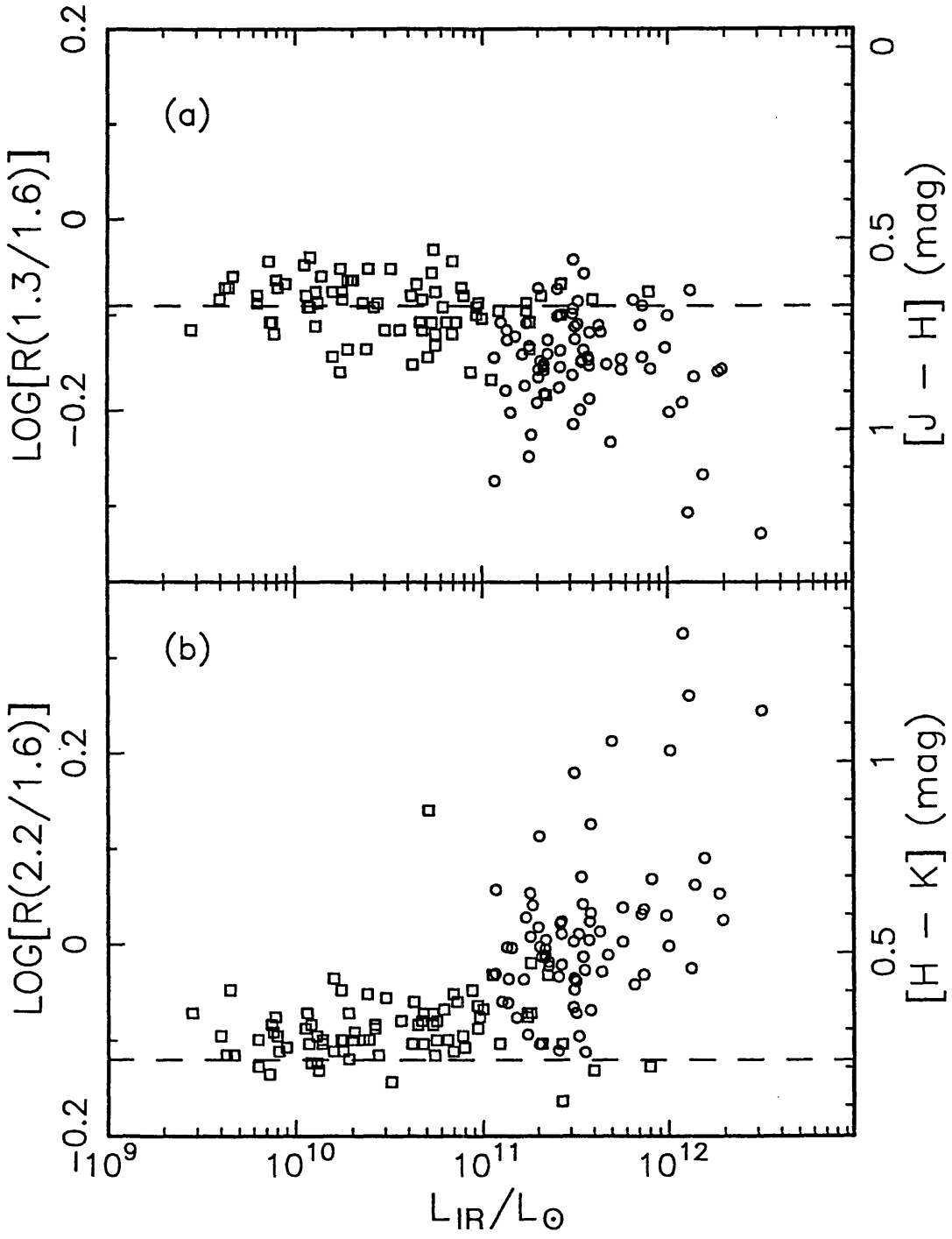
(a)
(b)
LOG[R(1.3/1.6)]
LOG[R(2.2/1.6)]
[J − H] (mag)
[H − K] (mag)
0.2
0
−0.2
0.5
1
10^9
10^{10}
10^{11}
10^{12}
$L_{IR}/L_\odot$

FIGURE 1

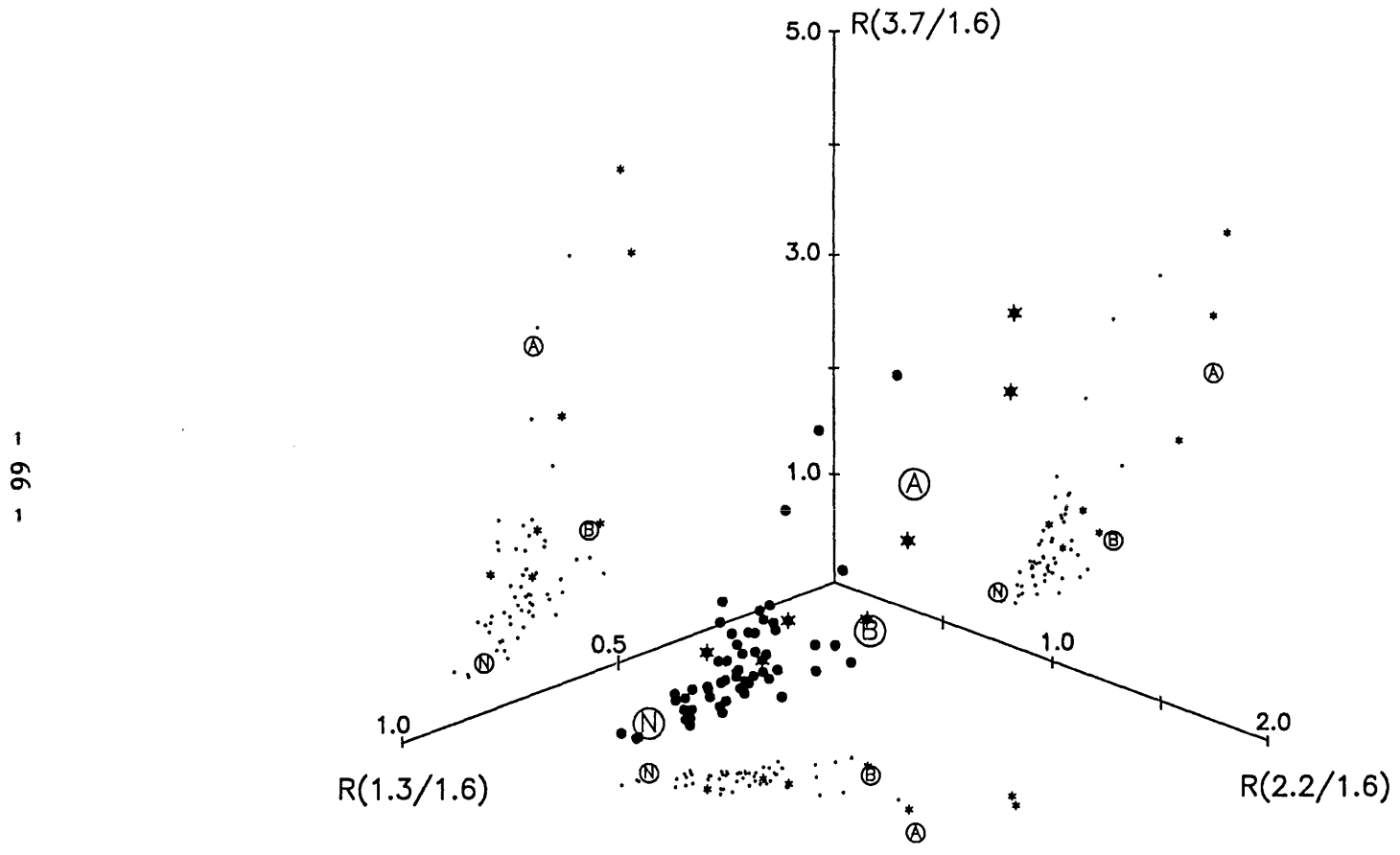

FIGURE 2

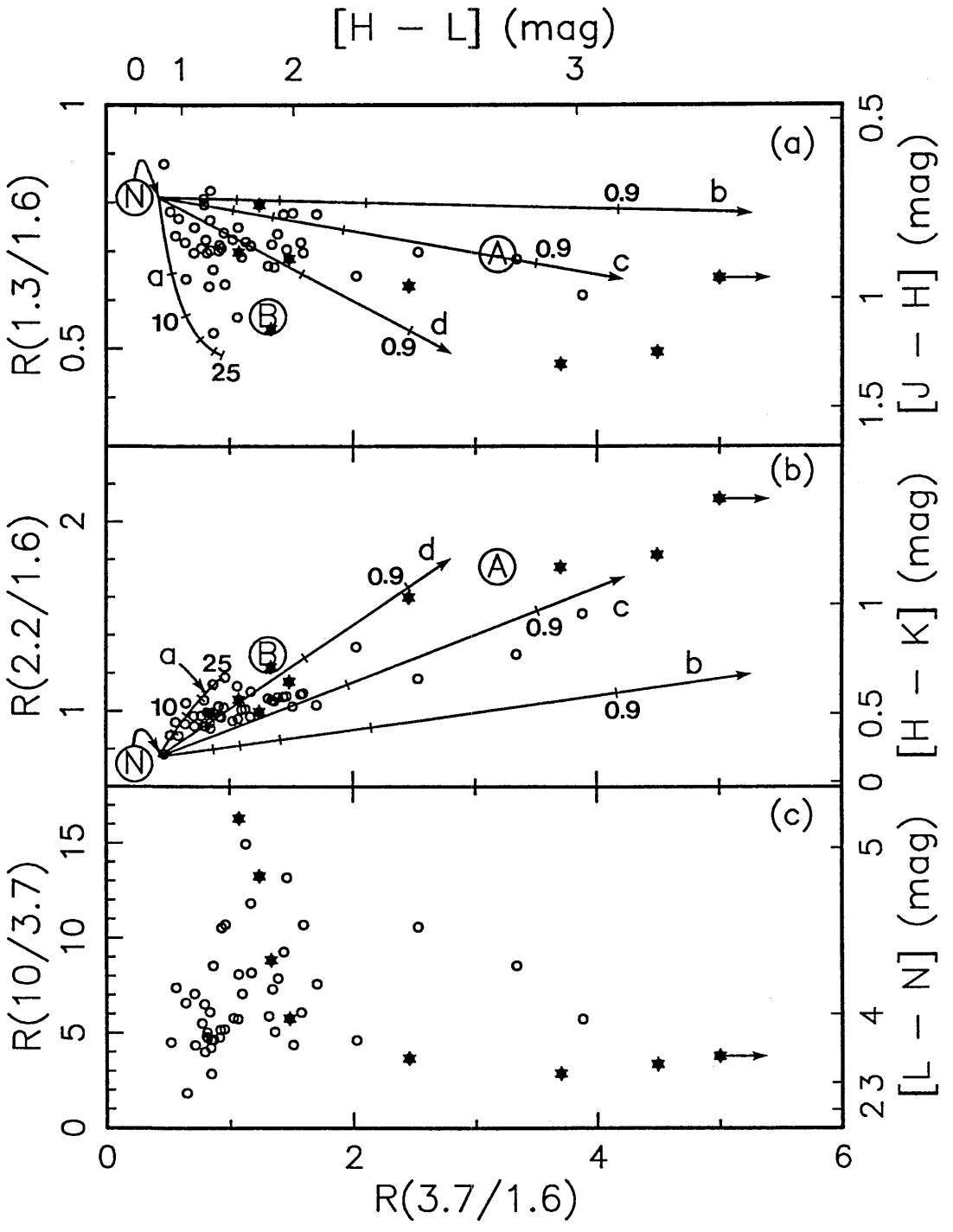
[H − L] (mag)
0 1 2 3
(a)
(b)
(c)
R(1.3/1.6)
R(2.2/1.6)
R(10/3.7)
R(3.7/1.6)
[J − H] (mag)
[H − K] (mag)
[L − N] (mag)
N
A
B
a
b
c
d
10
25
0.9
0 2 4 6

FIGURE 3

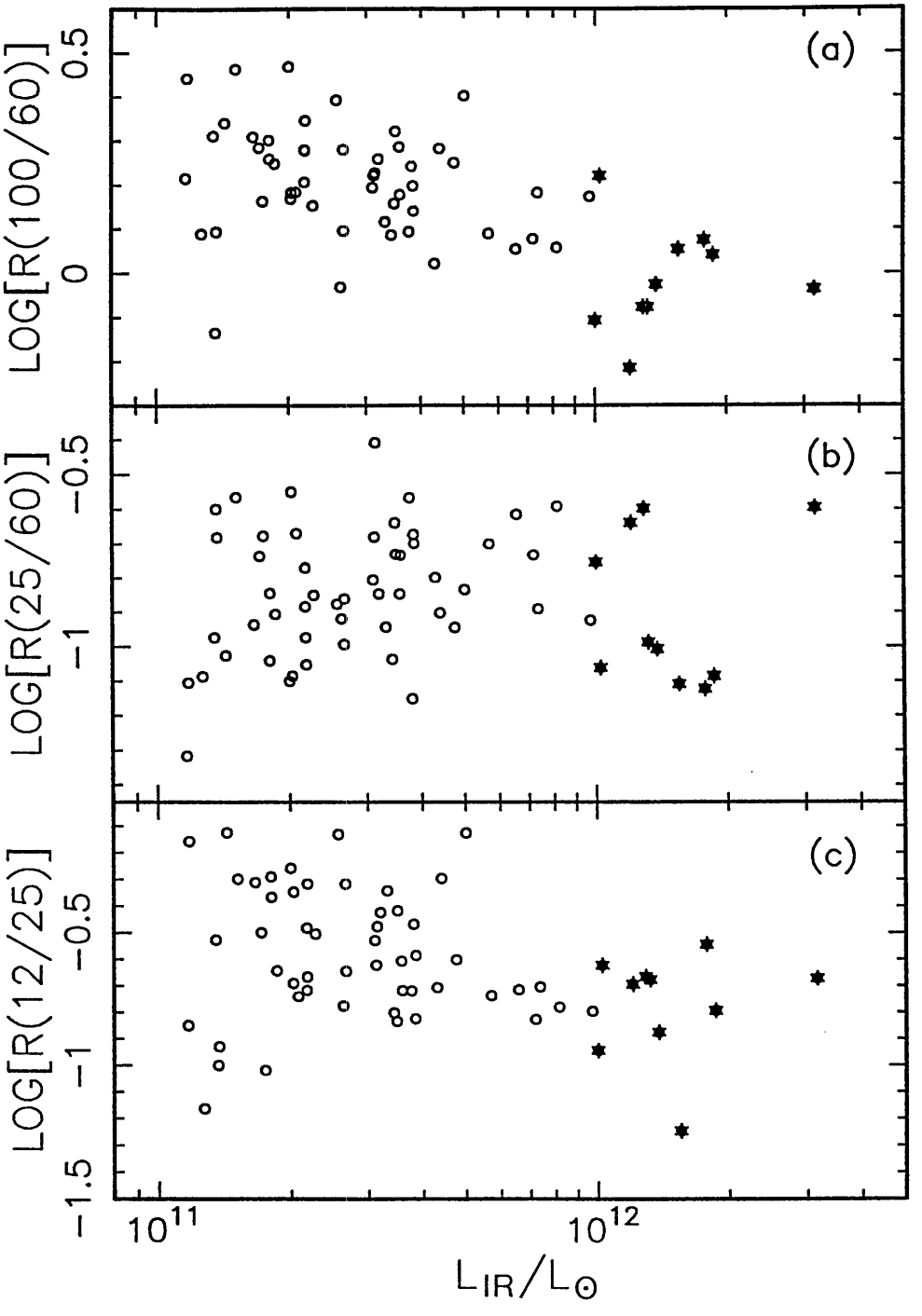
(a)
(b)
(c)
LOG[R(100/60)]
LOG[R(25/60)]
LOG[R(12/25)]
0.5
0
-0.5
-1
-1.5
10^{11}
10^{12}
$L_{IR}/L_{\odot}$

FIGURE 4

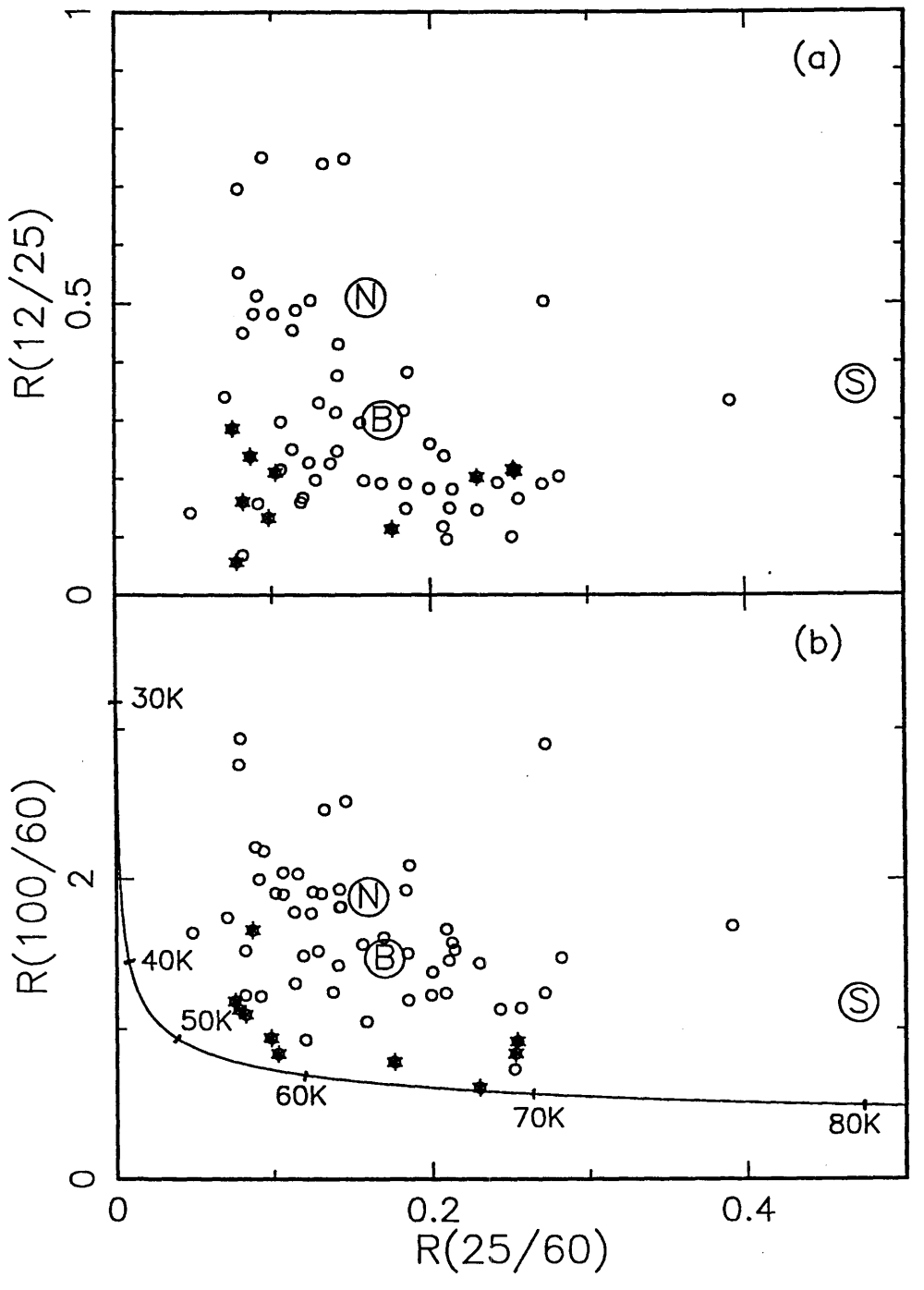

FIGURE 5

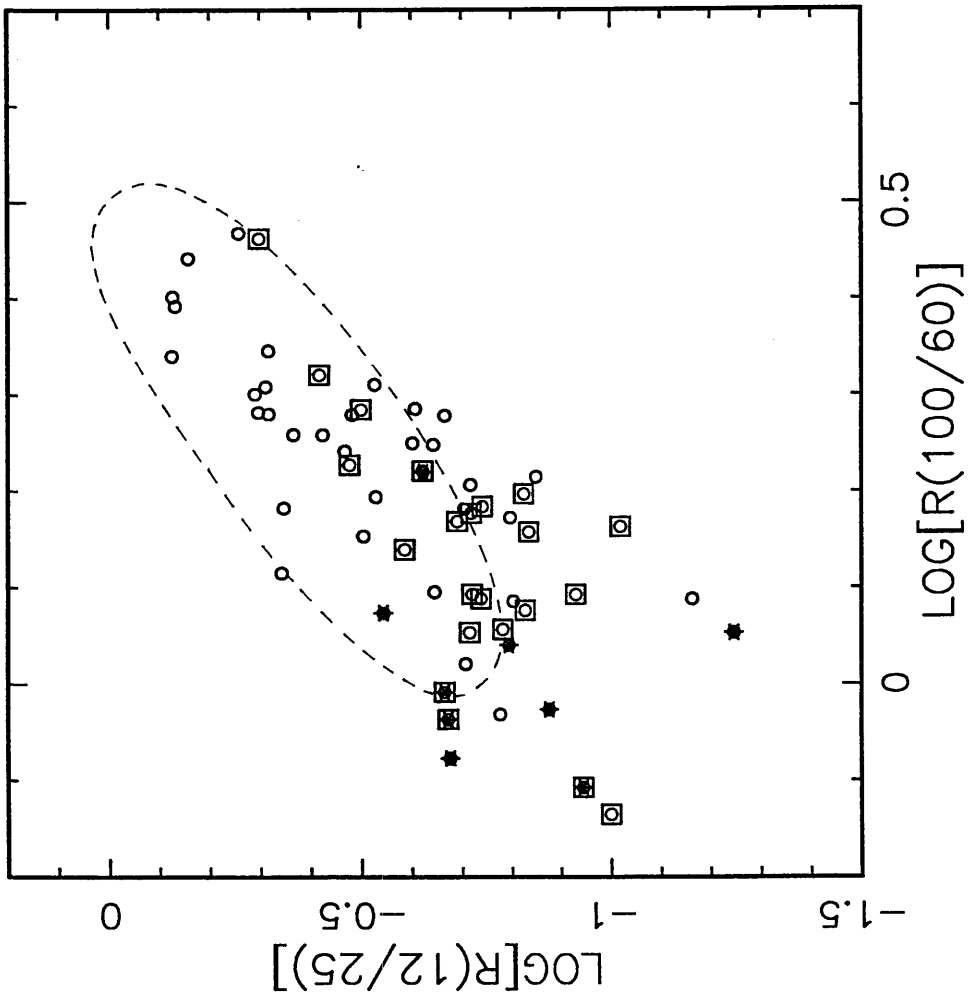

FIGURE 6

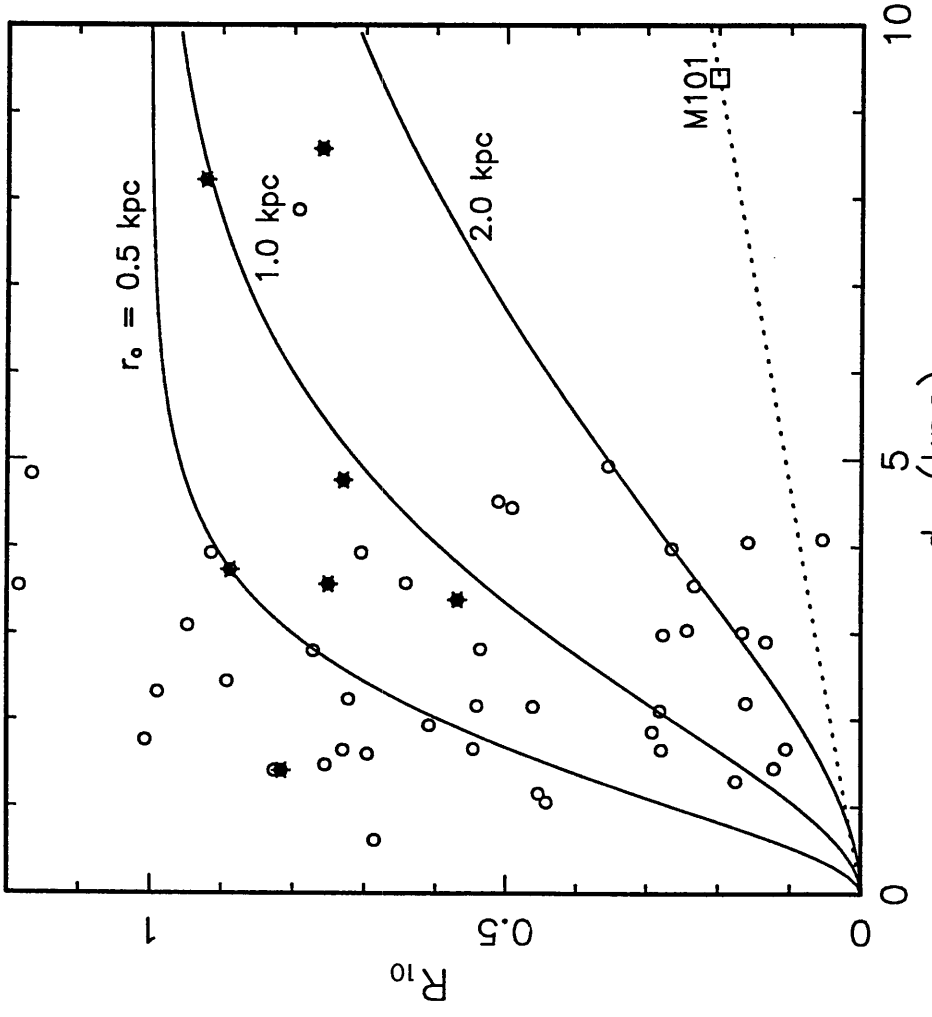

FIGURE 7

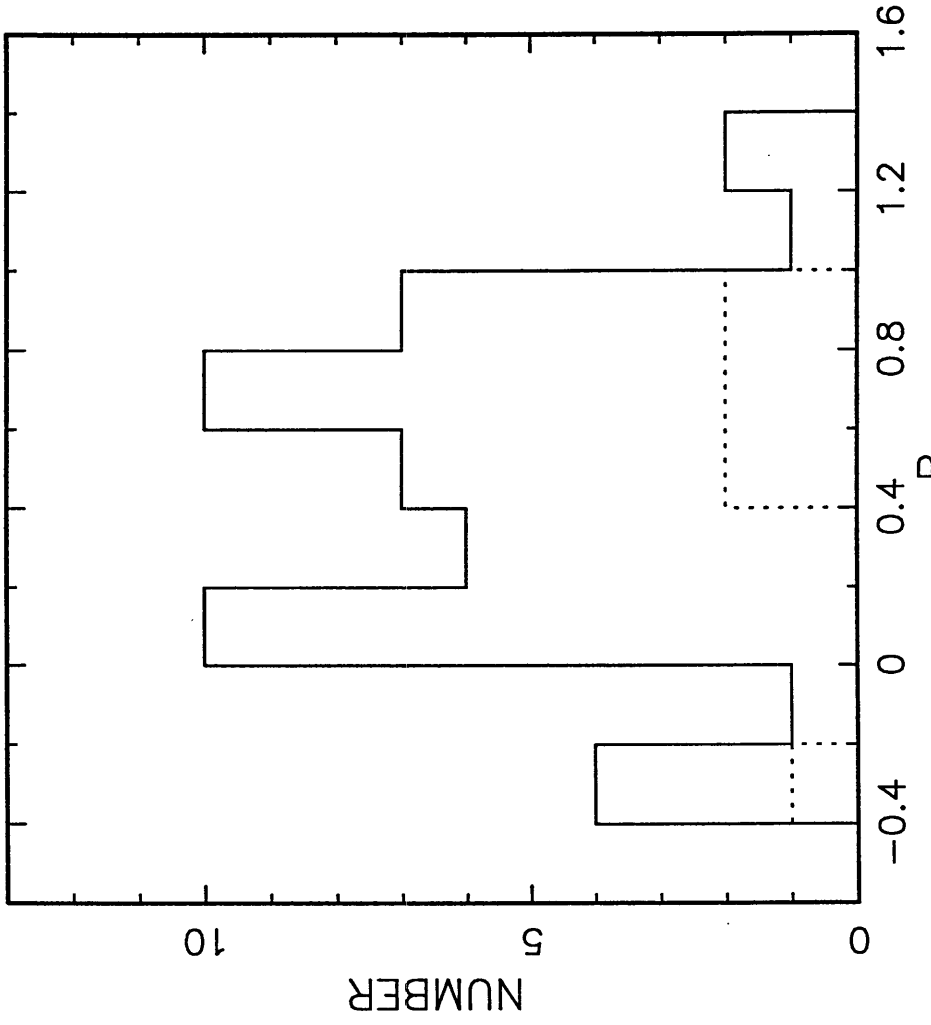

FIGURE 8

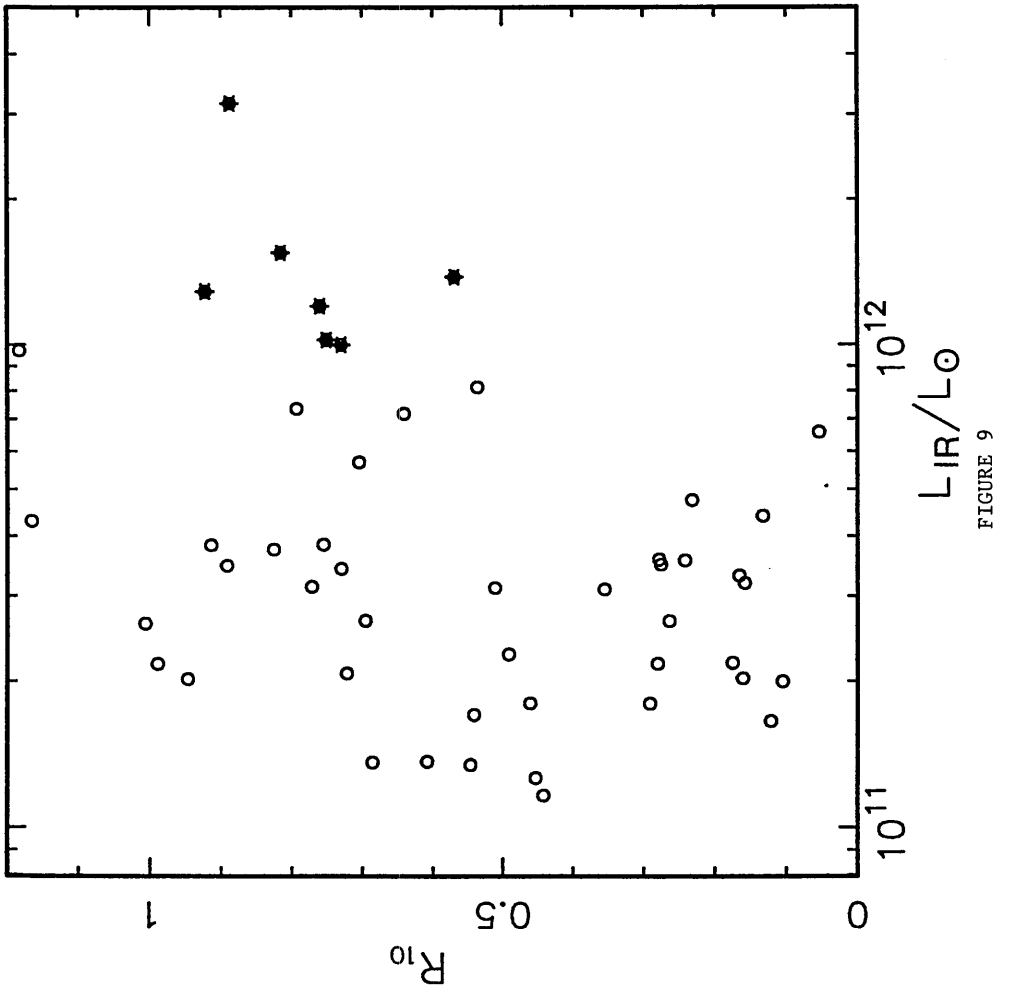

FIGURE 9

TABLE 1 – IDENTIFICATION OF GALAXIES

NAME	OTHER	RA		–1950–	DEC		REDSHIFT[a]	D_o^b
	NAME	(h)	(m)	(s)	(deg)	(arc m)	(arc s)	(z)	(arc s)
NGC 34	Mrk 938	0	8	33.4	–12	23	10	0.0198	35
MCG–02-01-051	Arp 256	0	16	18.0	–10	39	14	0.0250	35
NGC 232†		0	40	17.5	–23	50	2	0.0208	40
IC 1623	VV114	1	5	18.0	–17	46	37	0.0185	40
MCG–03-04-014		1	7	42.0	–17	7	1	0.0335	25
MCG+02-04-025		1	17	22.8	+14	5	53	0.0311	25
IRAS 0136-10†		1	36	24.0	–10	42	25	0.0475	15
III ZW 035†		1	41	48.0	+16	51	7	0.0274	20
NGC 695	UGC 1315	1	48	28.1	+22	20	10	0.0326	35
NGC 958		2	28	11.8	– 3	9	32	0.0192	100
UGC 2238		2	43	33.4	+12	53	10	0.0208	35
IRAS 0243+213		2	43	49.2	+21	22	44	0.0227	20
UGC 2369		2	51	15.6	+14	46	1	0.0312	40
NGC 1143/4	UGC 2388	2	52	38.6	– 0	23	6	0.0285	65
IRAS 0335+15		3	35	57.1	+15	23	6	0.0353	20
UGC 2982		4	9	43.2	+ 5	25	12	0.0177	35
MCG–03-12-002		4	19	6.5	–18	55	48	0.0316	20
NGC 1614	Mrk 617	4	31	35.8	– 8	40	55	0.0158	50
IRAS 0518-25		5	18	58.6	–25	24	40	0.0424	10
NGC 2623	Arp 243	8	35	25.2	+25	55	48	0.0185	35
IRAS 0857+39		8	57	13.0	+39	15	40	0.0583	20
UGC 4881	Arp 55	9	12	39.6	+44	32	20	0.0399	35
UGC 5101		9	32	4.6	+61	34	37	0.0400	30
MGC+08-18-012†		9	33	18.5	+48	41	53	0.0260	30
IC 563/4†		9	43	44.2	+ 3	17	26	0.0203	
NGC 3110		10	1	32.2	– 6	14	2	0.0161	60
IRAS 1017+08		10	17	22.1	+ 8	28	41	0.0480	10
IRAS 1056+24		10	56	35.5	+24	48	43	0.0417	25
A1101+41	V32	11	1	5.8	+41	7	8	0.0345	35
MCG+00-29-023		11	18	38.6	– 2	42	36	0.0241	20
UGC 6436	IC 2810	11	23	9.8	+14	56	53	0.0341	15
NGC 3690	Mrk 171	11	25	42.0	+58	50	17	0.0105	80
IRAS 1211+03		12	11	12.2	+ 3	5	20	0.0723	15
IRAS 1222-06		12	22	29.0	– 6	24	14	0.0250	15
NGC 4418	UGC 7545	12	24	22.1	– 0	36	14	0.0068	60
MCG+08-23-097		12	48	21.4	+48	12	18	0.0294	25
Mrk 231	UGC 8058	12	54	4.8	+57	8	38	0.0421	30
NGC 4922	UGC 8135	12	59	1.0	+29	34	59	0.0245	45
MCG+01-33-036†		12	59	17.8	+ 4	36	4	0.0362	30
IC 860		13	12	40.1	+24	52	52	0.0129	35
UGC 8335	VII Zw 506	13	13	41.3	+62	23	17	0.0312	30
UGC 8387†	Arp 193	13	18	19.0	+34	23	49	0.0229	60
NGC 5104	UGC 8391	13	18	49.2	+ 0	36	14	0.0186	50
NGC 5256	UGC 8632	13	36	14.2	+48	31	52	0.0276	25
NGC 5257/8	UGC 8641	13	37	22.1	+ 1	5	13	0.0227	115
Mrk 273	UGC 8696	13	42	51.6	+56	8	13	0.0380	70
UGC 8739		13	47	1.7	+35	30	14	0.0171	110
NGC 5331†	VV 253	13	49	41.3	+ 2	21	7	0.0332	40
ZW 247.020	Mrk 1490	14	17	53.8	+49	27	54	0.0260	20
IRAS 1434-14		14	34	52.3	–14	47	24	0.0811	15

TABLE 1 – IDENTIFICATION OF GALAXIES (continued)

NAME	OTHER	RA		–1950–	DEC		REDSHIFT[a]	D_o^b
	NAME	(h)	(m)	(s)	(deg)	(arc m)	(arc s)	(z)	(arc s)
UGC 9618	Arp 302	14	54	47.8	+24	48	58	0.0337	80
ZW 049.057		15	10	45.6	+ 7	24	43	0.0118	40
I ZW 107	Mrk 848	15	16	19.0	+42	55	41	0.0401	40
IRAS 1525+36		15	25	3.1	+36	9	0	0.0534	20
Arp 220	UGC 9913	15	32	46.3	+23	40	8	0.0182	50
IRAS 1533-05		15	33	32.4	– 5	13	59	0.0260	40
NGC 6090	UGC 10267	16	10	24.0	+52	35	6	0.0291	25
MCG+01-42-088		16	28	27.4	+ 4	11	24	0.0236	40
NGC 6285/6	Arp 293	16	57	44.9	+59	0	40	0.0187	65
IRAS 1713+53		17	13	14.2	+53	13	52	0.0507	20
MCG–03-57-017		22	28	42.7	–19	17	31	0.0242	50
IRAS 2249-18		22	49	9.6	–18	8	20	0.0760	20
NGC 7469	UGC 12332	23	0	44.6	+ 8	36	18	0.0165	50
ZW 453.062		23	2	28.1	+19	16	55	0.0246	40
ZW 475.056		23	13	31.2	+25	16	48	0.0274	30
NGC 7592	Mrk 928	23	15	47.5	– 4	41	20	0.0244	35
NGC 7674	UGC 12608	23	25	24.7	+ 8	30	14	0.0289	45
NGC 7771		23	48	52.1	+19	49	55	0.0145	110
Mrk 331		23	48	52.8	+20	18	22	0.0180	40

[a] Redshifts are reprinted from Paper I, and are taken as either v/c or DH_o/c where v or D is given in Table 1 or Paper I.

[b] D_o is the optical diameter, as estimated from the Palomar Observatory Sky Survey prints.

TABLE 2 – OBSERVED FLUX DENSITIES

NAME	OBS CODE[a]	BEAM[b] (arc sec)	$f_\nu(\lambda)$, PALOMAR (mJy)[c] 1.3 μm	1.6 μm	2.2 μm	3.7 μm	10 μm	$f_\nu(\lambda)$, IRAS (Jy)[c] 12 μm	25 μm	60 μm	100 μm
NGC 34		5.0	23.02	35.44	37.17	44.84	251.31	0.36	2.15	17.85	16.6
MCG–02-01-051		5.0	5.94	8.66	8.36	9.03	122.52	0.26	1.43	6.68	10.21
IC 1623†	(a)	5.0	8.06	9.41	7.28	4.44		0.80	4.18	22.65	34.08
	(b)	5.0	8.67	14.50	16.53		158.56				
	(c)	10.0	16.52	24.52	27.18	31.89					
	(d)	10.0	15.78	18.43	15.07	<30.46					
MCG–03-04-014		5.0	11.54	16.96	16.68	13.54	83.21	0.39	1.02	5.49	11.49
MCG+02-04-025†	(a)	5.0	1.53	1.88	1.52	1.66	<31.64	0.32	1.63	10.27	10.78
	(b)	5.0	6.40	8.50	8.59	12.70	113.82				
	(c)						128.29				
NGC 695		5.0	10.62	14.50	13.75	10.66	52.99	0.49	0.97	7.75	14.83
NGC 958		5.0	12.77	17.44	14.94	6.60	<32.23	0.76	1.51	5.55	16.10
UGC 2238		5.0	7.76	14.24	16.38	14.05	89.58	0.39	0.76	8.35	16.69
IRAS 0243+213		10.0	13.00	17.92	16.68	11.69	57.04	0.14	1.19	5.71	7.07
UGC 2369†	(a)	5.0	8.91	12.29	10.82	5.24	<31.35	0.25	1.67	7.86	12.38
	(b)	5.0	5.08	7.47	8.06	9.54	150.04				
NGC 1143/4†	(a)	5.0	8.67	10.70	8.52	3.50	<31.64	0.51	0.69	5.19	12.80
	(b)	5.0	11.64	15.19	14.13	11.58	<34.69				
IRAS 0335+15†	(a)	10.0	4.35	5.77	5.84	7.58	39.83	0.3	0.66	5.80	7.56
	(b)	10.0	2.46	3.17	2.57						
UGC 2982	(a)	5.0	8.13	13.35	13.37	10.37	69.22	0.60	0.80	8.5	18.6
	(b)	10.0	17.46	27.89	28.99						
MCG–03-12-002†	(a)	5.0	6.40	8.19	9.00	5.80	27.30	0.27	0.56	5.52	10.52
	(b)	10.0	11.86	16.35	15.21						
	(c)	5.0	4.55	6.75	7.08	5.44	30.49				
	(d)	10.0	6.83	9.58	9.51						
NGC 1614	(a)	5.0	34.21	48.47	49.00	51.01	832.15	1.57	8.24	30.40	37.67
	(b)	10.0	42.28	59.90	59.46	63.05					
IRAS 0518-25	(a)	5.0	12.89	27.38	52.75	122.37	515.47	0.76	3.52	13.94	11.68
	(b)	10.0	14.39	29.75	55.75	123.50					
NGC 2623		5.0	9.33	15.05	18.12	13.54	160.03	0.34	2.16	23.52	28.66
IRAS 0857+39†	(a)	5.0	0.91	1.44	3.68	39.78	207.11	0.35	1.73	7.53	4.59
	(b)	10.0	1.41	1.97	4.35	40.52					
	(c)	10.0	1.80	2.47	4.77	37.64	<51.55				
	(d)	10.0	1.61	2.38	4.47	43.62	288.54				
UGC 4881		5.0	4.35	6.51	6.58	4.24	28.85	0.17	0.68	5.99	10.65
UGC 5101	(a)	5.0	8.59	13.60	22.82	30.46	136.84	0.25	1.05	12.09	20.07
	(b)	10.0	12.89	20.02	27.43	31.02					
NGC 3110		5.0	11.12	15.76	14.53	11.90	61.97	0.64	1.31	11.32	23.03
IRAS 1017+08†	(a)	10.0	17.62	16.50	10.82			0.26	1.35	5.56	6.29
	(b)	10.0	3.27	4.18	3.86	2.88	10.48				
IRAS 1056+24		10.0	11.12	15.76	16.99	18.35	182.05	0.23	1.44	12.09	17.99
A1101+41		5.0	5.42	7.90	8.36	9.20	80.95	<0.16	0.47	6.67	11.63
MCG+00-29-023		7.0	17.30	24.07	24.79	20.88	122.52	0.34	0.79	5.53	10.03
UGC 6436		5.0	5.57	7.97	7.84	3.87	34.37	0.20	0.81	5.70	11.00
NGC 3690†	(a)	5.0	22.81	32.92	38.21	80.11	895.78	4.75	28.71	112.13	127.82
	(b)	5.0	5.78	8.12	14.66	31.60	273.02				
	(c)	5.0	12.42	20.96	25.25	32.48	483.28				

TABLE 2 – OBSERVED FLUX DENSITIES (continued)

NAME	OBS CODE[a]	BEAM[b] (arc sec)	$f_\nu(\lambda)$, PALOMAR (mJy)[c] 1.3 μm	1.6 μm	2.2 μm	3.7 μm	10 μm	$f_\nu(\lambda)$, IRAS (Jy)[c] 12 μm	25 μm	60 μm	100 μm
IRAS 1211+03		5.0	1.80	2.76	3.24	2.09	53.98	<0.18	0.63	8.36	9.91
IRAS 1222-06		10.0	3.33	4.46	3.62		<26.80	<0.11	1.15	5.46	7.95
NGC 4418		5.0	10.72	14.11	12.31	8.01	398.29	1.1	11.0	43.7	32.0
MCG+08-23-097		5.0	7.48	11.21	11.23	7.04	58.10	<0.11	0.51	4.80	9.11
Mrk 231	(a)	5.0	45.51	100.33	182.91	343.30	1213.95	1.81	8.52	33.60	30.89
	(b)	10.0	48.54	101.26	189.77	379.90					
NGC 4922†	(a)	5.0	4.64	6.88	8.75	21.07	205.21	0.31	1.52	5.39	7.95
	(b)	5.0	16.22	19.84	15.93	7.11	<26.31				
IC 860		5.0	8.13	10.60	9.34	5.24	25.13	0.09	1.31	16.0	19.6
UGC 8335†	(a)	5.0	7.62	11.31	12.31	15.84	201.47	0.41	2.24	11.24	13.78
	(b)	5.0	4.23	6.16	6.23	<6.08	27.81				
NGC 5104		5.0	14.13	21.95	21.99	17.69	90.41	0.22	0.74	6.97	14.25
NGC 5256†	(a)	5.0	7.62	9.94	8.59	6.19	<77.30	0.34	1.15	7.36	11.51
	(b)	5.0	7.55	11.41	11.54	11.16	91.24				
NGC 5257/8†	(a)	5.0	4.64	6.39	5.89	4.48	<69.86	0.58	1.54	10.83	19.63
	(b)	5.0	6.22	8.35	7.15	4.36	<46.58				
	(c)						68.58				
Mrk 273		5.0	8.59	12.99	15.21	16.74	118.09	0.31	2.33	23.70	22.31
UGC 8739		5.0	5.04	9.76	11.33	8.70		0.32	0.46	5.86	16.20
ZW 247.020		5.0	8.44	12.40	12.08	10.27	124.80	0.19	0.99	5.84	9.40
IRAS 1434-14		5.0	1.61	2.41	3.18		<151.43	0.09	0.56	6.82	7.49
UGC 9618		5.0	6.70	12.06	14.26			0.68	0.91	6.22	15.68
ZW 049.057		5.0	6.76	9.58	9.00	5.86	40.95	0.14	0.99	20.50	33.63
I ZW 107		5.0	5.62	7.47	8.06	9.03	104.76	0.25	1.68	9.09	10.84
IRAS 1525+36		5.0	2.92	3.89	3.89	3.70	67.33	0.15	1.32	7.50	5.86
Arp 220	(a)	5.0	9.16	17.44	21.79	21.86	212.91	0.46	8.11	104.08	117.69
	(b)	10.0	18.80	30.58	33.90	24.64					
IRAS 1533-05		5.0	7.55	13.23	14.80	12.93	<183.74	0.15	0.66	5.32	9.42
NGC 6090†	(a)	10.0	13.00	16.65	15.50	11.58	87.94	0.31	1.30	6.22	10.35
	(b)	10.0	5.13	5.77	5.18	4.32	<24.00				
	(c)						23.13				
MCG+01-42-088		5.0	10.92	16.05	16.08	12.35	64.30	0.30	0.91	6.97	13.26
NGC 6285/6		10.0	17.62	28.15	30.08	17.21	34.37	0.37	0.67	8.44	24.80
IRAS 1713+53†	(a)	5.0	5.57	8.19	8.92	10.46	83.99	0.15	0.76	5.92	8.99
	(b)	5.0	2.14	2.76	2.69		<28.07				
MCG-03-57-017		5.0	10.14	15.61	16.68	18.69	124.80	0.31	0.98	5.34	10.28
IRAS 2249-18		5.0	2.02	2.59	2.46	<2.21	<38.74	<0.12	0.57	5.54	4.64
NGC 7469		5.0	52.25	81.18	109.20	156.92	787.41	1.41	5.44	27.2	37.5
ZW 453.062		5.0	5.84	8.66	8.75	6.42	34.37	0.27	0.60	7.31	11.13
ZW 475.056		5.0	12.19	17.60	19.69	18.52	175.47	0.30	2.05	8.92	12.83
NGC 7592†	(a)	5.0	6.34	9.07	8.59	8.39	54.98	0.36	1.15	8.15	11.60
	(b)	5.0	6.11	8.42	8.06	8.08	74.51				
NGC 7674		5.0	9.96	16.50	24.79	59.11	394.64	0.68	2.04	5.22	8.81
NGC 7771		5.0	17.79	27.63	28.20	21.27	114.87	0.83	1.72	19.4	43.0
Mrk 331		5.0	25.95	36.43	34.85	29.09	273.02	0.57	2.52	18.3	22.8

[a] Some of the galaxies were measured with more than one beam diameter, and some at more than one position. For such cases, the Observation Code labels the individual measurements, and can be used to identify these measurements in Tables 3 and 4. Galaxies measured at more than one position, indicated by †, are discussed in more detail in the notes to Table 2.

[b] The diameter of the $1.3 - 3.7\ \mu m$ beam; at $10\ \mu m$ the beam diameter was 4.6" for all observations. See the IRAS Explanatory Supplement (1985) for a discussion of the IRAS beam sizes.

[c] The symbol $<$ indicates an upper limit.

† NOTES TO TABLE 2

(Offset positions given here are only approximate)

IC 1623: This object contains a number of visible knot-like structures, although it was not possible at the time of the observations to determine which of these structures are separate nuclei. Measurements (a) and (d) are of the visual (also the $2.2\ \mu m$) peak, lying in the northwestern-most position of the entire object. Measurements (b) and (c) are of the eastern-most position, 15" east of (a) and (d).

MCG+02-24-025: There are three visually obvious nuclei; the nucleus in measurement (a) is the northernmost nucleus, (b) is 10" south of (a), and (c) is 5" east of (b).

UGC 2369: There are two visually obvious nuclei; the nucleus in measurement (a) is 20" northwest of the nucleus in measurement (b).

NGC 1143/4: There are two visually obvious nuclei; the nucleus in measurement (a) is 40" west, 20" north of the nucleus in measurement (b).

IRAS 0335+15: There are two visually obvious nuclei; the nucleus in measurement (a) is 10" east of the nucleus in measurement (b).

MCG–03-12-002: There are two visually obvious nuclei; the nucleus in measurements (a) and (b) is 20" north of the nucleus in measurements (c) and (d).

IRAS 0857+39: There are two visually obvious nuclei; measurements (a), (b), and (c) are centered between the two nuclei; measurement (d) is centered on the northwestern-most nucleus.

IRAS 1017+08: There are two visually obvious nuclei; measurement (a) is to the east of measurement (b).

NGC 3690: This object has a distorted morphology with a number of knot-like structures. Measurement (a) is the visual peak; measurements (b) and (c) are north and east of (a), respectively.

NGC 4922: There are two visually obvious nuclei; the nucleus in measurement (a) is 10" north, 20" east of the nucleus in measurement (b).

UGC 8335: There are two visually obvious nuclei; the nucleus in measurement (a) is 40" southeast of the nucleus in measurement (b).

NGC 5256: There are two visually obvious nuclei; measurement (a) is north of measurement (b).

NGC 5257/8: There are two visually obvious nuclei; the nucleus in measurement (a) is northwest of the nucleus in measurement (b); measurement (c) is of a knot-like structure to the southwest of (b).

NGC 6090: There are two visually obvious nuclei; the nucleus in measurement (a) is 10" northeast of the nucleus in measurement (b); measurement (c) was taken midway between (a) and (b).

IRAS 1713+53: There are two visually obvious nuclei; measurement (a) is northeast of measurement (b).

NGC 7592: There are two visually obvious nuclei; measurement (a) is east of measurement (b).

TABLE 3 – NEAR-INFRARED FLUX DENSITIES CORRECTED FOR REDSHIFT

NAME	OBS CODE[a]	$f_\nu(\lambda)$ (mJy)[b] 1.3 μm	1.6 μm	2.2 μm	3.7 μm
NGC 34		24.21	36.26	38.18	49.48
MCG–02-01-051		6.30	8.85	8.60	10.36
IC 1623	(a)	8.29	9.43	7.29	4.44
	(b)	9.14	14.89	16.53	
	(c)	17.28	25.14	27.84	31.89
	(d)	16.24	18.53	15.74	<30.46
MCG–03-04-014		12.48	17.50	17.01	16.09
MCG+02-04-025	(a)	1.62	1.89	1.58	1.98
	(b)	6.81	8.78	9.07	14.99
NGC 695		11.37	14.89	13.97	12.55
NGC 958		13.29	17.59	14.78	7.25
UGC 2238		8.29	14.68	16.62	15.61
IRAS 0243+213		13.65	18.23	16.80	13.07
UGC 2369	(a)	9.53	12.50	10.69	6.15
	(b)	5.47	7.77	8.39	11.38
NGC 1143/4	(a)	9.11	10.76	8.35	4.07
	(b)	12.30	15.51	14.38	13.24
IRAS 0335+15	(a)	4.66	5.99	6.15	9.07
	(b)	2.63	3.20	2.57	
UGC 2982	(a)	8.54	13.59	13.49	11.34
	(b)	18.31	28.45	28.99	
MCG–03-12-002	(a)	6.79	8.54	9.04	6.79
	(b)	12.69	16.74	15.21	
	(c)	4.91	7.00	7.19	6.39
	(d)	7.31	9.88	9.51	
NGC 1614	(a)	35.44	49.26	49.84	63.05
	(b)	43.80	60.83	60.51	55.65
IRAS 0518-25	(a)	15.04	31.37	58.81	151.26
	(b)	16.73	33.95	61.92	152.62
NGC 2623		9.81	15.51	18.27	14.95
IRAS 0857+39	(a)	1.06	1.83	5.05	54.01
	(b)	1.60	2.43	5.87	40.52
	(c)	2.03	2.98	6.32	48.76
	(d)	1.84	2.86	6.06	59.73
UGC 4881		4.79	6.78	6.62	5.23
UGC 5101	(a)	9.54	15.17	24.25	37.23
	(b)	14.27	21.73	28.79	37.90
NGC 3110		11.53	15.94	14.67	12.88
IRAS 1017+08	(a)	18.26	16.14	10.82	
	(b)	3.57	4.33	3.94	3.66
IRAS 1056+24		12.20	16.59	17.81	23.08
A1101+41		5.87	8.22	8.70	11.06
MCG+00-29-023		18.23	24.71	25.19	23.57
UGC 6436		6.02	8.23	7.75	4.65
NGC 3690	(a)	23.37	33.45	39.19	84.65
	(b)	5.92	8.38	15.04	33.34
	(c)	12.80	21.33	25.64	34.38

TABLE 3 – NEAR-INFRARED FLUX DENSITIES CORRECTED FOR REDSHIFT (continued)

NAME	OBS CODE[a]	$f_\nu(\lambda)$ (mJy)[b] 1.3 μm	1.6 μm	2.2 μm	3.7 μm
IRAS 1211+03		2.15	3.08	3.27	3.31
IRAS 1222-06		3.50	4.49	3.62	
NGC 4418		10.86	14.16	12.32	8.34
MCG+08-23-097		8.04	11.54	11.26	8.22
Mrk 231	(a)	53.33	113.89	200.28	421.43
	(b)	56.41	115.39	208.85	379.90
NGC 4922	(a)	4.92	7.19	9.34	24.00
	(b)	16.91	19.95	15.72	7.99
IC 860		8.34	10.68	9.32	5.58
UGC 8335	(a)	8.21	11.77	12.88	18.82
	(b)	4.55	6.36	6.41	<7.09
NGC 5104		14.82	22.36	22.23	19.38
NGC 5256	(a)	8.04	10.08	8.68	7.20
	(b)	8.08	11.74	11.84	12.90
NGC 5257/8	(a)	4.87	6.49	5.95	5.09
	(b)	6.52	8.43	7.16	4.93
Mrk 273		9.43	13.76	15.90	20.44
UGC 8739		5.33	10.01	11.43	8.70
ZW 247.020		8.97	12.69	12.30	11.84
IRAS 1434-14		1.95	2.81	3.18	
UGC 9618		7.43	12.71	20.77	
ZW 049.057		6.94	9.67	9.02	6.21
I ZW 107		6.09	7.85	8.45	11.29
IRAS 1525+36		3.25	4.09	4.08	5.08
Arp 220	(a)	9.73	18.00	22.19	26.25
	(b)	19.76	31.34	34.14	29.53
IRAS 1533-05		8.16	13.71	15.08	14.94
NGC 6090	(a)	13.73	17.01	15.69	13.48
	(b)	5.34	5.88	5.28	<5.01
MCG+01-42-088		11.54	16.43	16.26	13.89
NGC 6285/6		18.53	28.80	30.04	18.69
IRAS 1713+53	(a)	6.27	8.73	9.51	13.79
	(b)	2.35	2.89	2.69	
MCG-03-57-017		10.78	16.08	17.17	21.15
IRAS 2249-18		2.32	2.75	2.60	<3.53
NGC 7469		54.52	83.92	112.28	170.10
ZW 453.062		6.19	8.88	8.84	7.26
ZW 475.056		12.98	18.27	20.16	21.44
NGC 7592	(a)	6.70	9.25	8.79	9.50
	(b)	6.44	8.60	8.26	9.20
NGC 7674		10.79	17.67	26.75	68.60
NGC 7771		18.46	28.06	28.39	22.83
Mrk 331		27.00	36.98	35.26	31.96

[a] See Table 2.

[b] The symbol < indicates an upper limit.

TABLE 4 – DERIVED QUANTITIES

NAME	OBS CODE[a]	FLUX DENSITY RATIOS[b] R(1.3/1.6)	R(2.2/1.6)	R(3.7/1.6)	R(10/3.7)	R(12/25)	R(25/60)	R(100/60)	$R_{10}^{b,c}$	LOG[$L_{IR}/L_{\odot}$]
NGC 34		0.67	1.05	1.36	5.08	0.17	0.12	0.93	1.01	11.42
MCG–02-01-051		0.71	0.97	1.17	11.83	0.18	0.21	1.53	0.72	11.32
IC 1623	(a)	0.88	0.77	0.47		0.19	0.18	1.50	0.28	11.55
MCG–03-04-014		0.71	0.97	0.92	5.17	0.38	0.19	2.09	0.28	11.54
MCG+02-04-025	(b)	0.78	1.03	1.71	7.59	0.20	0.16	1.05	1.17	11.63
NGC 695		0.76	0.94	0.84	4.22	0.51	0.13	1.91	0.13	11.64
NGC 958		0.76	0.84	0.41	<4.44	0.50	0.27	2.90	<0.04	11.18
UGC 2238		0.56	1.13	1.06	5.74	0.51	0.09	2.00	0.29	11.26
IRAS 0243+213		0.75	0.92	0.72	4.36	0.12	0.21	1.24	0.61	11.14
UGC 2369	(a)	0.76	0.86	0.49	<5.10	0.15	0.21	1.58	0.91	11.58
	(b)	0.70	1.08	1.46	13.18					
NGC 1143/4	(a)	0.85	0.78	0.38	<7.77	0.74	0.13	2.47	<0.15	11.41
	(b)	0.79	0.93	0.85	<2.62					
IRAS 0335+15	(a)	0.78	1.03	1.51	4.39	0.45	0.11	1.30	0.17	11.52
	(b)	0.82	0.80							
UGC 2982	(a)	0.63	0.99	0.83	6.10	0.75	0.09	2.19	0.14	11.15
MCG–03-12-002	(a)	0.80	1.06	0.80	3.20	0.48	0.10	1.91	0.26	11.43
	(c)	0.70	1.03	0.91	4.36					
NGC 1614	(a)	0.72	1.01	1.13	14.95	0.19	0.27	1.24	0.83	11.57
IRAS 0518-25	(a)	0.49	1.82	4.50	3.38	0.22	0.25	0.84	0.92	12.11
NGC 2623		0.63	1.18	0.96	10.70	0.16	0.09	1.22	0.73	11.53
IRAS 0857+39	(d)	0.64	2.12	20.88		0.20	0.23	0.61	20.76	12.08
UGC 4881		0.71	0.98	0.77	5.52	0.25	0.11	1.78	0.23	11.68
UGC 5101	(a)	0.63	1.60	2.45	3.68	0.24	0.09	1.66	0.75	12.01
NGC 3110		0.72	0.92	0.81	4.81	0.49	0.12	2.03	0.12	11.22
IRAS 1017+08	(b)	0.82	0.91	0.85	2.86	0.19	0.24	1.13	0.05	11.82
IRAS 1056+24		0.74	1.07	1.39	7.89	0.16	0.12	1.49	1.18	11.99
A1101+41		0.71	1.06	1.35	7.32	<0.34	0.07	1.74	>0.68	11.58
MCG+00-29-023		0.74	1.02	0.95	5.20	0.43	0.14	1.81	0.46	11.26
UGC 6436		0.73	0.94	0.56	7.39	0.25	0.14	1.93	0.24	11.55
NGC 3690	(a)	0.70	1.17	2.53	10.58	0.17	0.26	1.14	0.54	11.91

TABLE 4 – DERIVED QUANTITIES (continued)

NAME	OBS CODE[a]	FLUX DENSITY RATIOS[b] R(1.3/1.6)	R(2.2/1.6)	R(3.7/1.6)	R(10/3.7)	R(12/25)	R(25/60)	R(100/60)	$R_{10}^{b,c}$	LOG[$L_{IR}/L_{\odot}$]
IRAS 1211+03		0.70	1.06	1.07	16.31	<0.29	0.08	1.19	>0.44	12.25
IRAS 1222-06		0.78	0.81			<0.10	0.21	1.46		11.24
NGC 4418		0.77	0.87	0.59	47.76	0.10	0.25	0.73	0.69	11.13
MCG+08-23-097		0.70	0.98	0.71	7.07	<0.22	0.11	1.90	>0.76	11.34
Mrk 231	(a)	0.47	1.76	3.70	2.88	0.21	0.25	0.92	0.89	12.50
NGC 4922	(a)	0.68	1.30	3.34	8.55	0.20	0.28	1.48	0.95	11.31
	(b)	0.85	0.79	0.40	<3.29					
IC 860		0.78	0.87	0.52	4.50	0.07	0.08	1.23	0.45	11.10
UGC 8335	(a)	0.70	1.09	1.60	10.70	0.18	0.20	1.23	0.70	11.76
	(b)	0.72	1.01	<1.11	>3.92					
NGC 5104		0.66	0.99	0.87	4.66	0.30	0.11	2.04	0.55	11.13
NGC 5256	(a)	0.80	0.86	0.71	<10.74	0.30	0.16	1.56	0.36	11.49
	(b)	0.69	1.01	1.10	7.07					
NGC 5257/8	(a)	0.75	0.92	0.78	<13.72	0.38	0.14	1.81	0.16	11.50
	(b)	0.77	0.85	0.58	<9.45					
Mrk 273		0.69	1.16	1.49	5.78	0.13	0.10	0.94	0.57	12.14
UGC 8739		0.53	1.14	0.87		0.70	0.08	2.76		11.07
ZW 247.020		0.71	0.97	0.93	10.54	0.19	0.17	1.61	0.99	11.34
IRAS 1434-14		0.69	1.13			0.16	0.08	1.10		12.27
UGC 9618		0.58	1.63			0.75	0.15	2.52		11.70
ZW 049.057		0.72	0.93	0.64	6.59	0.14	0.05	1.64	0.44	11.07
I ZW 107		0.78	1.08	1.44	9.28	0.15	0.18	1.19	0.64	11.86
IRAS 1525+36		0.79	1.00	1.24	13.25	0.11	0.18	0.78	0.73	12.00
Arp 220	(a)	0.54	1.23	1.34	8.85	0.06	0.08	1.13	0.82	12.19
IRAS 1533-05		0.60	1.10	1.09	<12.30	0.23	0.12	1.77	<1.83	11.27
NGC 6090	(a)	0.81	0.92	0.79		0.24	0.21	1.66	0.51	11.49
	(b)	0.91	0.90	0.85						
MCG+01-42-088		0.70	0.99	0.85	4.63	0.33	0.13	1.90	0.28	11.34
NGC 6285/6		0.64	1.04	0.65	1.84	0.55	0.08	2.94	0.11	11.30
IRAS 1713+53	(a)	0.72	1.09	1.58	6.09	0.20	0.13	1.52	0.79	11.87
	(b)	0.81	0.93							
MCG–03-57-017		0.67	1.07	1.32	5.90	0.32	0.18	1.93	0.54	11.23

TABLE 4 – DERIVED QUANTITIES (continued)

NAME	OBS CODE[a]	FLUX DENSITY RATIOS[b] R(1.3/1.6)	R(2.2/1.6)	R(3.7/1.6)	R(10/3.7)	R(12/25)	R(25/60)	R(100/60)	$R_{10}^{b,c}$	LOG[$L_{IR}/L_{\odot}$]
IRAS 2249-18		0.84	0.95	<1.28	~10.98	<0.21	0.10	0.84	~0.47	12.12
NGC 7469		0.65	1.34	2.03	4.63	0.26	0.20	1.38	0.76	11.58
ZW 453.062		0.70	1.00	0.82	4.73	0.45	0.08	1.52	0.16	11.31
ZW 475.056		0.71	1.10	1.17	8.18	0.15	0.23	1.44	0.89	11.54
NGC 7592	(a)	0.72	0.95	1.03	5.79	0.31	0.14	1.42	0.49	11.36
	(b)	0.75	0.96	1.07	8.10					
NGC 7674		0.61	1.51	3.88	5.75	0.33	0.39	1.69	0.77	11.50
NGC 7771		0.66	1.01	0.81	5.03	0.48	0.09	2.22	0.17	11.34
Mrk 331		0.73	0.95	0.86	8.54	0.23	0.14	1.25	0.70	11.43

[a] See Table 2.

[b] $R(\lambda_1/\lambda_2) \equiv f_\nu(\lambda_1)/f_\nu(\lambda_2)$. The symbols < and > indicate that the ratios are upper and lower limits, respectively, where a lower limit in the ratio is due to an upper limit in the flux density in the denominator of the ratio; the symbol ~ indicates that both flux densities (numerator and denominator) in the ratio are upper limits.

[c] R_{10} represents the degree of concentration of the 10 μm emission about the nucleus (see text).

Chapter THREE:

The IRAS Bright Galaxy Sample: Multi–Beam Photometry of Galaxies with $L_{IR} \geq 10^{11} L_{\odot}$

This article has previously appeared in
the *Astronomical Journal*, Vol. **100**, p.70 (1990).

Coauthors: D.B. Sanders, B.T. Soifer, K. Matthews, and G. Neugebauer.

ABSTRACT

Forty–seven galaxies from the IRAS Bright Galaxy Sample with infrared luminosities $L_{IR} \geq 10^{11}\ L_{\odot}$ have been measured at 1.3 μm, 1.65 μm, and 2.2 μm with beam diameters of 17″, 33″, and 55″. These measurements, combined with 5″ and 10″ observations presented in an earlier paper, provide an opportunity to study the spatial distribution of the near–infrared emission in luminous IRAS galaxies. It is found that the unusually red near–infrared colors known previously for many of these galaxies are confined to the nuclear regions, whereas the outer disk regions have near–infrared colors essentially appropriate for a normal stellar population. Since dust reddening and emission are required to explain the unusual nuclear colors, it follows that the observed effects of dust in these galaxies are also confined primarily to the nuclei. Thus, it is probable that the far–infrared emission, the bulk of the entire luminosity in infrared luminous galaxies, is highly concentrated about the nuclei, and that *the physical processes responsible for the unusual properties of infrared luminous galaxies tend to occur within the central regions, with diameters* $\lesssim 1 - 3$ *kpc*. The nuclei are found to have considerably higher 2.2 μm luminosities than are found in classical "starburst" nuclei, implying that infrared luminous galaxies are characterized by extremely high radiation densities in their central regions, presumably due to intense star formation activity and/or the presence of a dust–enshrouded quasar. However, the nuclei of the galaxies studied are typically *not* as luminous at 2.2 μm as classical Seyfert nuclei, which may be partly attributable to extinction from dust at near–infrared wavelengths, particularly for those sources in the sample which have been identified in the literature as having Seyfert nuclei. Finally, the large diameter beam measurements are used to obtain estimates of the total near–infrared emission. It is found that, since most of the infrared luminosity is coming from the nuclei, the global near–infrared properties of infrared luminous galaxies are not good tracers of infrared activity. Also, the contribution from the observed stellar emission to the total observed luminosity is found to be $\lesssim$25% for most of the galaxies in the sample, considerably smaller than the value for typical low luminosity spiral galaxies.

I. INTRODUCTION

The IRAS Bright Galaxy Sample (hereafter the BG Sample) was defined by Soifer *et al.* (1987) in order to provide a complete sample of galaxies with strong infrared emission. A revised version of the BG Sample was recently presented by Soifer *et al.* (1989) which contains 313 galaxies and is complete down to a flux limit of 5.24 Jy at 60 μm. The far–infrared emission in virtually all galaxies in the BG Sample appears to be due to thermal emission from dust grains. At the longest IRAS wavelengths (60 and 100 μm) the energy distributions are well modeled by steady–state dust emission. At 12 and 25 μm, however, the IRAS data suggest that significant quantities of very small dust grains (with radii $\lesssim$ a few tens of Angstroms) which are subject to extreme temperature fluctuations from single photon absorption events may be required to explain the observed emission (see e.g. Boulanger *et al.* 1988; Telesco, Decher, and Joy 1989; Helou 1986).

Infrared measurements from 1 to 10 μm for most of the galaxies from the original BG Sample (Soifer *et al.* 1987) with infrared luminosities[1] $L_{IR} \geq 10^{11}\ L_{\odot}$ were presented by Carico *et al.* (1988; hereafter, Paper I), and those galaxies with $L_{IR} \geq 10^{12}\ L_{\odot}$ have been studied extensively by Sanders *et al.* (1988). The results of these studies indicate that the galaxies in the BG Sample include a broad range of galaxy properties, from those seen in normal, optically selected spiral galaxies to those typical of active galactic nuclei (AGN) and quasars. This broad range of properties is seen in the near–infrared colors measured in the central $5'' - 10''$ diameter regions of the galaxies. However, the colors which are significantly different than those seen in normal spiral galaxies appear to be limited to galaxies with infrared luminosities greater than $\sim 10^{11}\ L_{\odot}$ (Paper I).

The cause of the high luminosity for those galaxies with $L_{IR} \sim 10^{11} - 10^{12}\ L_{\odot}$ appears to be star formation (Sanders *et al.* 1986), and the broad range in near–infrared colors is presumably due to the effects of dust absorption (reddening) and emission in the source. For the highest luminosities ($L_{IR} \geq 10^{12}\ L_{\odot}$), Sanders *et al.* (1988) have shown that virtually all of the galaxies from the BG Sample are

[1] L_{IR} is an estimate of the integrated luminosity between 8 and 1000 μm; see Carico *et al.* 1988. Throughout the text, H_o is taken as 75 $km\ sec^{-1}\ Mpc^{-1}$; $L_{\odot}$ is the solar bolometric luminosity, $3.83 \times 10^{26}\ Watts$.

galaxy merger remnants (see also Carico *et al.* 1990), and have suggested that such objects contain dust enshrouded active nuclei and represent a stage in the formation of a "classical" quasar; hence, for these sources the near–infrared colors may also be affected by a contribution from the direct emission from the accretion disk of an active nucleus (see Phinney 1989; Sanders *et al.* 1989).

This paper presents new near–infrared measurements, made with multiple large beam diameters, of a sample of galaxies from the BG Sample with $L_{IR} \geq 10^{11}\ L_{\odot}$. These data, when combined with previously published small–beam measurements, provide a basis for studying the spatial distribution of the near–infrared emission in infrared–luminous galaxies. Throughout this paper, all subsequent references to the BG Sample, unless stated otherwise, will refer to the revised BG Sample (Soifer *et al.* 1989).

II. THE SAMPLE AND OBSERVATIONS

The revised BG Sample contains 79 galaxies with total infrared luminosities $L_{IR} \geq 10^{11}\ L_{\odot}$ (Soifer *et al.* 1989). In early 1987, a program was undertaken to measure as many of these 79 galaxies as possible at near–infrared wavelengths using more than one beam diameter. The goals of the program were (1) to measure the spatial distribution of the near–infrared emission in these galaxies, and (2) to obtain estimates of the *total* near–infrared emission for comparison to the IRAS data, for which typical beam dimensions at 60 μm were $1.'5 \times 4.'75$ (see the *IRAS Explanatory Supplement* 1988).

Three observing runs between June 1987 and April 1988 on the 60 inch telescope at the Palomar Observatory resulted in observations of 47 of the 79 galaxies (59%) at 1.27 μm (*J*), 1.65 μm (*H*), and 2.2 μm (*K*), using 17″, 33″, and 55″ beam diameters. A solid–nitrogen–cooled InSb detector was used for all of the measurements, and sky subtraction was achieved by chopping to reference positions $\sim 90''$ north and south of the source.

The choice of which of the galaxies with $L_{IR} \geq 10^{11}\ L_{\odot}$ to observe was essentially arbitrary. Not all of the galaxies were measured with all three beam sizes at all wavelengths; in particular, it was not possible to measure many of the sources at 2.2 μm with a 55″ diameter beam due to saturation of

the detector from sky background. Also, the largest useful beam diameter was occasionally limited by contamination from extraneous sources near the object of interest.

Optical images indicate that many of the measured sources have severely distorted morphologies evidenced by multiple nuclei (see, for example, Sanders *et al.* 1988). In such cases, an attempt was generally made to measure all apparent nuclei. These considerations are discussed in the notes following Table I.

The uncertainties in the flux densities range from 6% to 28%, with a median uncertainty at each wavelength of less than 10%. No attempt has been made to correct the data for reddening caused by interstellar material in the source or in the Galaxy. For many of the galaxies there is insufficient information to enable an accurate estimation of the internal reddening, and since all of the objects in the BG Sample have Galactic latitude $|b| > 30°$, Galactic reddening in the near–infrared is negligible. Also, the data have not been corrected for source redshift, since the redshift corrections are less than the measurement uncertainties in the data.

The observational data are presented in Table I, and notes on individual sources are given immediately following the table. The column entries for Table I are as follows:

(1) The most commonly used galaxy name.

(2–7) The 1950 coordinates.

(8) The approximate optical diameter of the galaxy, as estimated from the Palomar Observatory Sky Survey prints by Carico *et al.* (1988).

(9) The beam position in the source.

(10–11) The beam diameter, in arc-seconds and in kiloparsecs at the source.

(12–14) The flux density in milli–Janskys[2].

(15–16) Estimates of the total stellar luminosity, L_* (see Section III-*b*), and the infrared luminosity, L_{IR}.

[2] $1\ Jansky \equiv 10^{-26}\ Watts\ m^{-2}\ Hz^{-1}$.

In addition to the large beam measurements from the Palomar 60 inch telescope, Table I also includes 5″ and 10″ measurements from the Palomar 200 inch Hale telescope. These data have all been previously presented in Paper I, but are included here for convenience.

Histograms are shown in Figure 1 of the distribution of galaxy luminosities for the galaxies listed in Table I, and for all galaxies from the BG Sample with $L_{IR} \geq 10^{11}\ L_{\odot}$. The figure shows that the galaxies listed in Table I are not strongly biased towards any particular luminosity range within the luminosities of the Bright Galaxies with $L_{IR} \geq 10^{11}\ L_{\odot}$.

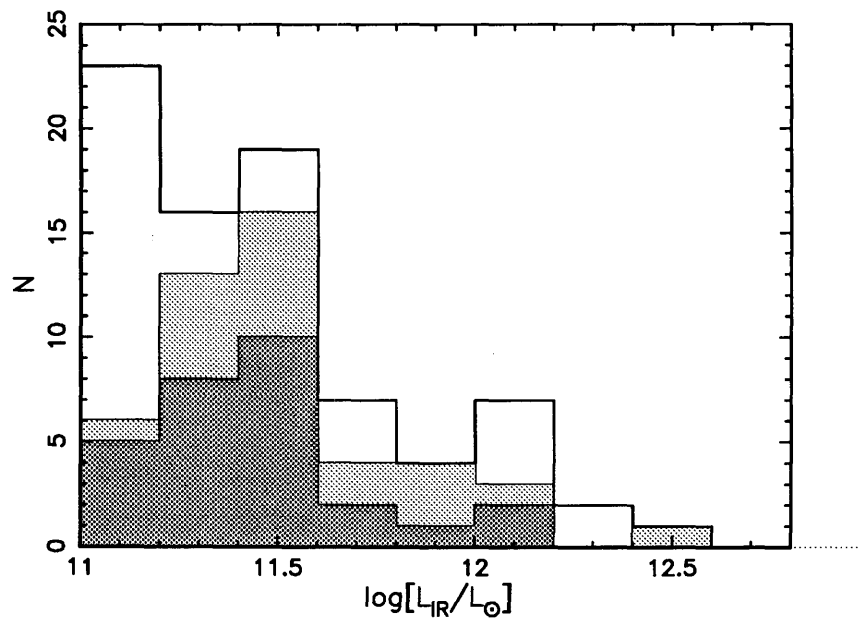

Fig. 1. The distribution of infrared luminosities, L_{IR}, for three samples of galaxies. The *unshaded histogram* includes all galaxies from the BG Sample with $L_{IR} \geq 10^{11}\ L_{\odot}$. The (*light–shaded histogram* includes only those galaxies from the BG Sample which were observed with multiple beam diameters; these galaxies are listed in Table I. The *dark–shaded histogram* includes only those galaxies from Table I for which near–infrared colors for *both* the nucleus and the disk were obtainable (see text, Section III-*a-iii*); these galaxies are listed in Table II.

III. RESULTS AND DISCUSSION

III.1 The Spatial Distribution of the Near–Infrared Emission

III.1.1 Wavelength Dependence

To understand the spatial distribution of the near–infrared emission in infrared–luminous galaxies one would, ideally, use the data in Table I to obtain near–infrared colors in all annuli to determine how these colors change with radial distance from the center of the galaxies. Unfortunately, this is not possible in general. Since the annular colors are determined by subtracting two relatively similar large numbers, the resulting uncertainties for many of the galaxies are larger than the effects attributable to different physical processes.

In order to minimize these uncertainties, the "nuclear" colors of each galaxy were defined to be those obtained with the smallest diameter beam, and the "disk" colors were defined to be those measured in the region between the smallest diameter beam and the largest diameter beam for which measurements were made at all three wavelengths. The results are listed in Table II and plotted in Figure 2, where only those galaxies with *both* nuclear and disk colors with uncertainties less than 33% are presented.

In Figure 2, typical uncertainties in $\log[f_\nu(\lambda_1)/f_\nu(\lambda_2)]$ are estimated to be ± 0.04 for the nuclei and ± 0.09 for the disks (although the fact that the total scatter in the measurements of the disk colors is only $\sim$ 0.1 suggests that the uncertainties is these measurements are actually somewhat less). Because of these uncertainties, a number of the galaxies have colors which are consistent with no change between the nucleus and the surrounding disk. Fifteen of the 28 sources listed in Table II have colors in the nucleus and disk which are clearly distinct. These sources are indicated with a $*$ in Table II, and for all cases the nuclei are considerably redder than the surrounding disks. Furthermore, for all 28 of the sources listed in Table II, the calculated $f_\nu(2.2\mu m)/f_\nu(1.6\mu m)$ color in the nucleus is redder than that calculated for the disk. If the uncertainties are truly statistical, this color difference suggests a tendency towards redder nuclei even amongst the 13 galaxies for which the nuclear and disk colors cannot be formally distinguished individually.

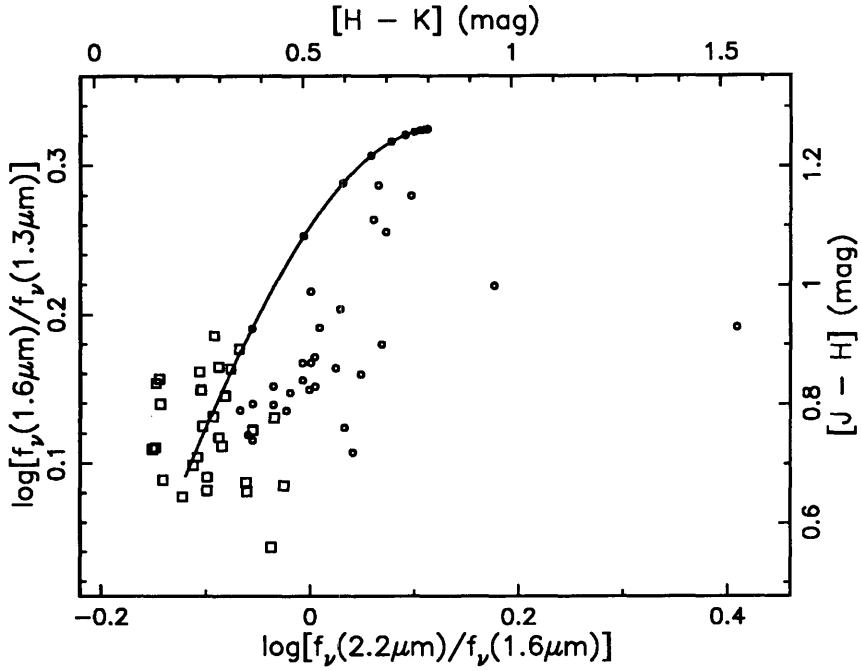

Fig. 2. The near–infrared flux density ratios (colors). *Circles* are the galaxy nuclei, *squares* are the galaxy disks (see text). Only those galaxies which have colors with uncertainties less than 33% for both the nucleus and disk are shown. The *dashed line* indicates the colors of the normal field spiral galaxies measured by Aaronson (1977), and the *dash–dot* line indicates the colors of a sample of lower luminosity IRAS galaxies (Carico *et al.* 1986). The *solid line* indicates the effect on the colors of a normal galaxy due to extinction from dust mixed with the source; the line extends to a total visual extinction A_V = 50 mag, with tick–marks at every 5 magnitudes. Typical uncertainties are ±0.09 for the disks and ±0.04 for the nuclei.

The above result demonstrates that, for those galaxies with the reddest near–infrared continuum emission, as reported and discussed in Paper I, the excess near–infrared emission tends to be confined to the nuclei which, from Table II, puts a limit of 1 – 3 kpc on the diameter of the emitting region. In contrast, the colors of the surrounding regions in those galaxies are similar to the colors of a normal stellar disk. A similar result has been found previously for a number of specific "starburst" and/or active galaxies prior to this study, for example NGC 1068 (Scoville *et al.* 1988), NGC 253 (Scoville *et al.* 1985), and NGC 7469 (Cutri *et al.* 1984). Also, Devereux (1989) put a limit of ~0.5 kpc on the diameter of the region responsible for the excess infrared emission from a sample of nearby, generally lower luminosity starburst galaxies. On the other hand, the result shown in Figure 2 differs significantly from the observed properties of low–luminosity, normal galaxies which typically show no change in near–infrared colors with beam diameter (Aaronson 1977).

Because of the large uncertainties in the large beam measurements, those galaxies for which annular colors are obtainable represent the most extended sources in the current sample. Since the most extended sources tend to be those which are closest, and since the BG Sample is a flux–limited sample, it follows that the galaxies plotted in Figure 2 are biased towards lower luminosities. Figure 1 shows a histogram of the distribution of luminosities for the galaxies included in Figure 2 compared to similar histograms for all of the galaxies in Table I and all of the galaxies from the BG Sample with $L_{IR} \geq 10^{11}\ L_{\odot}$. It is seen that there may be some bias against the highest luminosity galaxies: Figure 2 includes only two of the ten galaxies from the BG Sample with $L_{IR} \geq 10^{12}\ L_{\odot}$, as compared to 26 of the 69 galaxies from the BG Sample with $L_{IR} \geq 10^{11}\ L_{\odot}$. However, if the result in Figure 2 is combined with the results of an analysis of the spatial distribution of the near–infrared emission in nine galaxies from the BG Sample with $L_{IR} \geq 10^{12}\ L_{\odot}$ utilizing near–infrared camera images (Carico *et al.* 1990), it is found that four of the ten galaxies with $L_{IR} \geq 10^{12}\ L_{\odot}$ have nuclei which are significantly redder than their surrounding disks. This fraction is comparable to the fraction of galaxies with $L_{IR} \geq 10^{11}\ L_{\odot}$ in which this effect is seen.

Figure 2 implies that the 2.2 μm emission is more centrally concentrated in infrared luminous galaxies than the 1.3 μm or 1.6 μm emission. This is investigated further in Figure 3, where the availability of multiple beam diameter measurements has been utilized by interpolating between beam diameters to obtain estimates of the emission that would have been measured within a specified diameter about each galaxy nucleus. In this way, distance effects have been eliminated by estimating for each source the quantities $f_{\nu}(\lambda)_{d\ kpc}$, the flux densities which would have been measured with a beam diameter corresponding to a region of diameter d, in kiloparsecs, about the nucleus; the spatial distribution of the near–infrared emission in different sources can then be directly compared.

In Figure 3, the ratio $f_{\nu}(2.2\mu m)_{2\ kpc}/f_{\nu}(2.2\mu m)_{10\ kpc}$ is plotted against the same quantity at 1.3 μm. This ratio is a measure of the compactness of the emission about each nucleus. The solid line indicates the locus of points for which the ratios at 1.3 μm and 2.2 μm are equal. Typical uncertainties in the ratios are on the order of $10 - 15\%$, so that many of the points in Figure 3 are consistent with no

wavelength dependence in the compactness of the emission. Nevertheless, the sample taken as a whole clearly indicates a tendency amongst infrared luminous galaxies towards emission which is more tightly concentrated about the nucleus at 2.2 μm than at 1.3 μm.

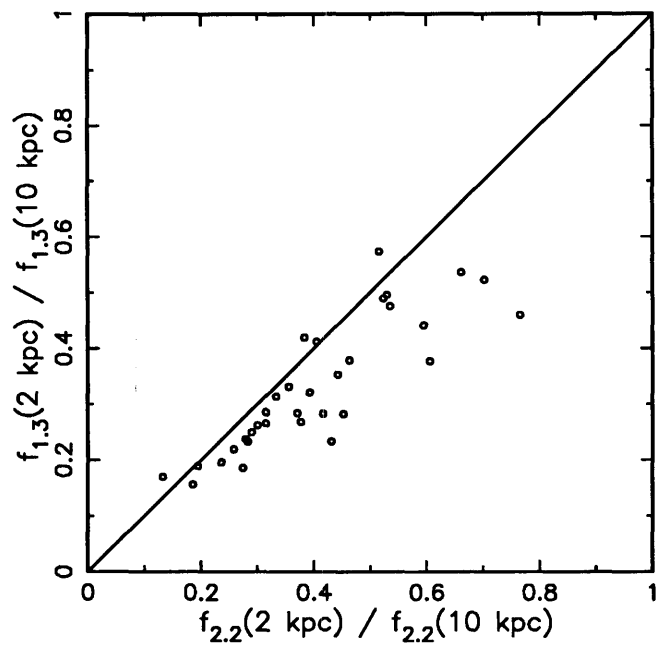

Fig. 3. The concentration of the 1.3 μm emission about the galaxy nucleus, with distance effects removed, plotted against the same quantity at 2.2 μm. $f_\nu(\lambda)_{d\ kpc}$ is an estimate of the flux density that would have been measured with a beam diameter corresponding to a region of diameter d, in kiloparsecs, about the nucleus. The line represents the locus of points for which the concentrations at both wavelengths are equal.

In Figure 4, the analysis of the concentration of the infrared emission has been extended to 10 μm. For this figure, it was not possible to estimate the emission at 10 μm within a region of diameter d in kiloparsecs at the source, since multiple beam diameter measurements are not available for these galaxies at 10 μm. Instead, an estimate of the compactness of the 10 μm emission from Paper I has been used. In that paper, R_{10} was defined as the ratio of the 10 μm emission in a 5″ diameter beam to that which would have been measured at 10 μm in a beam the size of the IRAS 12 μm beam; see Paper I for details of how this quantity was determined. At 2.2 μm, a corresponding quantity, $R_{2.2}$, has been calculated for comparison. $R_{2.2}$ is the ratio of the 2.2 μm flux density measured in a 5″ diameter

beam divided by the 2.2 μm flux density measured in the largest diameter beam. The straight line is the same as in Figure 3. The plot shows that, for those galaxies for which the emission is fairly compact, the 10 μm emission is more centrally concentrated than the near–infrared emission.

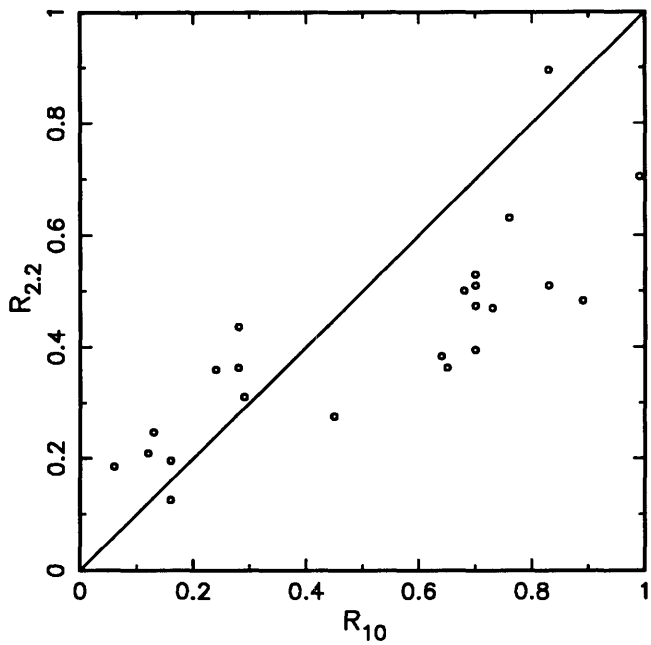

Fig. 4. The concentration of the 10 μm emission about the galaxy nucleus plotted against the concentration of the 2.2 μm emission (see text). The line represents the locus of points for which the concentrations at both wavelengths are equal. The values of R_{10} are from Carico *et al.* (1988).

There is a significant source of uncertainty in the estimates of R_{10} due primarily to the 10 μm silicate absorption feature. No attempt has been made to correct for this effect. Any such correction would tend to increase the values of R_{10}, further strengthening the result seen in Figure 4. Also, there is some uncertainty in the comparison between R_{10} and $R_{2.2}$ due to the fact that the large diameter beams used in calculating $R_{2.2}$ are considerably smaller than the size of the IRAS beam used in calculating R_{10}. However, any correction for this effect would tend to decrease the values of $R_{2.2}$, and thus would also strengthen the result seen in Figure 4.

The red near–infrared colors of the galaxy nuclei in Figure 2 cannot be explained in terms of direct or reddened stellar emission, but suggest the presence of hot dust contributing significant emission at

wavelengths as short as 2.2 μm (Paper I). Figure 2 then suggests that these galaxies have an increased density of dust in their nuclei relative to their outer disks. This conclusion also provides a natural explanation for the result seen in Figs. 3 and 4, since a greater amount of dust in the nucleus would effect the observed spatial distribution of the galaxy emission in the following ways: (1) Extinction by dust of the intrinsic emission would tend to reduce the observed emission from the nucleus more severely than that from the outer disk, thus causing an apparent decrease in the estimated compactness of the emission about the nucleus. Since dust extinction is greater at shorter wavelengths, this would contribute to the result in Figs. 3 and 4. (2) Dust emission from the nucleus would tend to increase the compactness of the emission, and this increase would be more significant at longer wavelengths, where the emission is less contaminated by photospheric emission. This would also contribute to the result in Figs. 3 and 4.

Since the measurements with 5″ and 10″ diameter beams were made by chopping to an angular distance of typically 15″ (Paper I), one would expect that, for many of the sources, the 5″ and 10″ diameter reference beams were contaminated by emission from the extended galaxy. Any such contamination in the smaller diameter beam would tend to reduce the observed compactness of the emission. However, estimates of the amount of flux that would have contaminated the small diameter reference beams for each source indicate that the effect is negligible. Thus, the result seen in Figs. 3 and 4 appears to be a real property of the galaxies.

The conclusion drawn from Figs. 2 – 4, that the unusually red near–infrared colors seen in many infrared luminous galaxies are confined to the nuclei of those galaxies, and hence that the effects of dust required to explain the red near–infrared colors are also confined to the nuclei, has an important implication for the overall distribution of luminosity within infrared luminous galaxies. Since such galaxies tend to radiate most of their power at far–infrared wavelengths, and since far–infrared emission is generally re–radiated emission from dust grains, it is probable that the bulk of the luminosity from infrared luminous galaxies is emitted from their nuclei. Furthermore, since the galaxies in the current sample all have infrared luminosities which exceed the bolometric luminosities of most "normal"

galaxies, their nuclei, if the source of the total luminosity, must be characterized by extremely high radiation densities, presumably due to highly intense star formation activity, or the presence of a central quasar, or both. Confirmation of this idea will require more direct information on the distribution of emission at far–infrared wavelengths than is currently available for these galaxies.

III.1.2 The 2.2 μm Luminosity

The values of $f_\nu(\lambda)_{d\ kpc}$ from the previous section can be used to estimate $L_\nu(\lambda)_{d\ kpc}$, the power emitted at wavelength λ from regions of the same size, centered about the nucleus, in each galaxy. The values of $L_\nu(2.2\mu m)_{2\ kpc} \equiv 4\pi D^2 \nu f_\nu(2.2\mu m)_{2\ kpc}$, where D is the luminosity distance, are given in Table III for 39 of the sources. These values were obtained by simply interpolating linearly between the measurements at the relevant beam diameters, or between the smallest available beam diameter and a diameter of zero. Since the curves of growth generally have negative curvatures, these luminosities have been slightly underestimated. Values of $L_\nu(2.2\mu m)_{2\ kpc}$ were calculated for all sources for which the smallest beam diameter is less than 2 kpc. For the remaining sources, $L_\nu(2.2\mu m)_{2\ kpc}$ was calculated only if a linear fit between the smallest available beam diameter and a diameter of zero represented a reasonable extrapolation of the growth curve from the larger beam diameters.

In addition to the galaxies listed in Table I, Table III includes values of $L_\nu(2.2\mu m)_{2\ kpc}$ for seven more galaxies from the BG Sample using data from Carico *et al.* (1990). All of these additional galaxies have infrared luminosities $L_{IR} \geq 10^{12}\ L_\odot$; thus, they belong to the sub–sample of the BG Sample from which the galaxies in Table I were selected, and have been included in Figs. 5 – 7 without specific identification.

The distribution of $L_\nu(2.2\mu m)_{2\ kpc}$ for the nuclei in Table III is shown in Figure 5, and the distribution of the distance–independent estimate of the compactness of the 2.2 μm emission, $L_\nu(2.2\mu m)_{2\ kpc}/L_\nu(2.2\mu m)_{10\ kpc}$ (which is equivalent to the quantity $f_\nu(2.2\mu m)_{2\ kpc}/f_\nu(2.2\mu m)_{10\ kpc}$, previously plotted in Figure 3), is shown in Figure 6. In both figures, the unshaded histogram includes all nuclei from Table III, whereas the shaded histogram includes only those sources which are classified

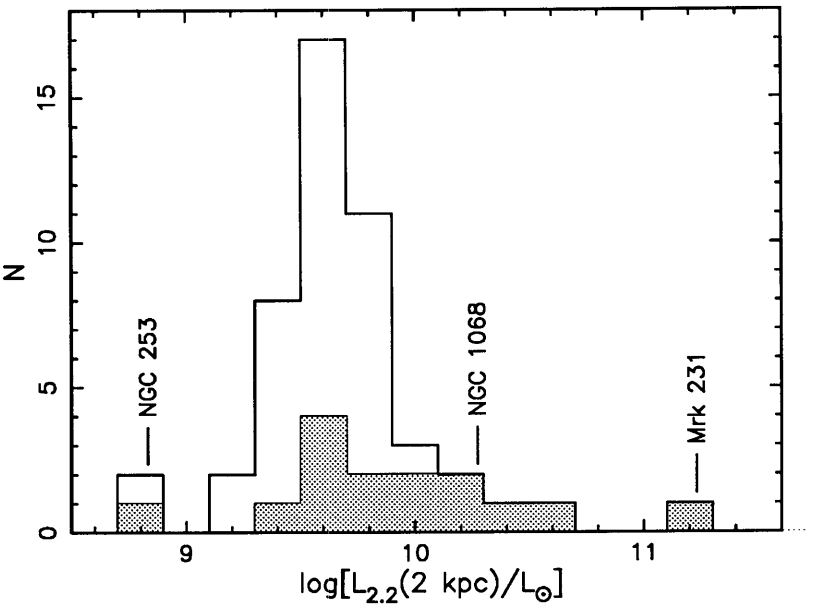

Fig. 5. The 2.2 μm luminosity emitted within a region of diameter 2 kpc about each galaxy nucleus. The ***unshaded histogram*** is the distribution for all galaxies listed in Table III; the ***shaded histogram*** is the distribution for only those galaxies listed in Véron–Cetty and Véron (1989) as Seyferts or quasars, or identified by Sanders *et al.* (1988) as having an AGN. $L_\nu(2.2\mu m)_{2\ kpc}$ for the archetypal Seyfert galaxy *NGC 1068*, included in the current sample, is indicated (see text). Also shown is an estimate of $L_\nu(2.2\mu m)_{2\ kpc}$ for *NGC 253*, obtained from the data of Scoville *et al.* (1985). The median for the unshaded and shaded histograms are $L_\nu(2.2\mu m)_{2\ kpc} = 4.4 \times 10^9\ L_\odot$ and $5.2 \times 10^9\ L_\odot$, respectively.

in Véron–Cetty and Véron (1989) as Seyfert or quasar nuclei,[3] or which were identified by Sanders *et al.* (1988) as having an AGN.

Included in Figs. 5 and 6 are estimates of $L_\nu(2.2\mu m)_{2\ kpc}$ and $L_\nu(2.2\mu m)_{2\ kpc}/L_\nu(2.2\mu m)_{10\ kpc}$ for the archetypal "starburst" galaxy *NGC 253*. These estimates were obtained using the data from the near–infrared mapping of this source by Scoville *et al.* (1985). Also indicated in Figure 5 is $L_\nu(2.2\mu m)_{2\ kpc}$ for the well–studied Seyfert galaxy *NGC 1068*, calculated from the data for this source given in Table I. *NGC 1068* is also indicated in Figure 6; however, since the largest available beam diameter corresponds to only 4.8 kpc at the distance of *NGC 1068*, the estimate of $f_\nu(2.2\mu m)_{10\ kpc}$ was obtained by extrapolating to 10 kpc with an exponential curve fitted to the two largest diameter beams.

[3] Véron–Cetty and Véron (1989) is *not* a complete listing of Seyfert galaxies and/or quasars, but was simply utilized in this analysis as a convenient reference.

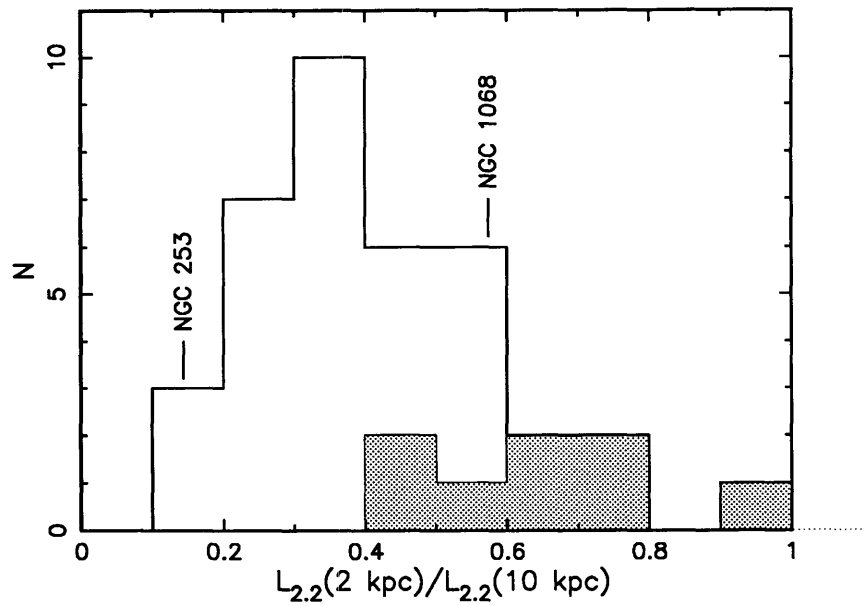

Fig. 6. The concentration of the 2.2 μm emission about the galaxy nucleus, with distance effects removed. $L_\nu(2.2\mu m)_{2\ kpc}/L_\nu(2.2\mu m)_{10\ kpc}$ is defined for each galaxy as the ratio of the 2.2 μm luminosity within a region of diameter 2 kpc about the nucleus to the 2.2 μm luminosity within a region of diameter 10 kpc (see text). The *unshaded histogram* is the distribution for all galaxies from Table III; the *shaded histogram* is the distribution for only those galaxies listed in Véron–Cetty and Véron (1989) as Seyferts or quasars, or identified by Sanders *et al.* (1988) as having an AGN. Also shown are estimates of $L_\nu(2.2\mu m)_{2\ kpc}/L_\nu(2.2\mu m)_{10\ kpc}$ for *NGC 253*, obtained from the data of Scoville *et al.* (1985), and for *NGC 1068* (see text). The median for the unshaded and shaded histograms are $L_\nu(2.2\mu m)_{2\ kpc}/L_\nu(2.2\mu m)_{10\ kpc} = 38\%$ and 63%, respectively.

If *NGC 253* and *NGC 1068* are taken to be typical of classical starburst and Seyfert galaxies, respectively, then Figs. 5 and 6 indicate that infrared luminous galaxies are characterized by a significantly higher density of stars and/or interstellar material emitting at 2.2 μm within their nuclei than exists in classical starburst nuclei, and that the density of this 2.2 μm emitting material falls off much more rapidly with radial distance. However, the nuclei in infrared luminous galaxies are typically *not* as luminous at 2.2 μm, nor is their 2.2 μm emission as centrally concentrated, as that of classical Seyfert galaxies.

This result suggests that, if the intrinsic source of the high luminosity in these galaxies is star formation, then the star formation activity in their nuclei must be extremely intense. Alternatively,

the luminosities in a number of sources may be due to, or at least enhanced by, the presence of a dust–enshrouded quasar. The existence of a quasar energy source is fairly well established in at least two of the sources: *Mrk 231*, which is actually listed as a quasar in Véron–Cetty and Véron (1989; see also the discussion and references in Section III-*a-iii* below), and *NGC 7469*, which is known to have a Seyfert 1 nucleus (Osterbrock 1977; see, for example, Weedman 1986 for a discussion of the correspondence between Seyfert 1 nuclei and quasars). The fact that several other galaxies in the sample have 2.2 μm emission which is comparable in strength and compactness to one or both of these sources suggests that other galaxies in the sample, particularly those listed in Table III as Seyfert 2 or identified by Sanders *et al.* (1988) as having an active nucleus, may also be powered by a quasar. Large amounts of dust in an AGN could cause enough extinction to significantly reduce the observed 2.2 μm nuclear luminosity (see the discusion of *Arp 220* and *NGC 4418* in Section III-*a-iii* below), and may be the reason why a number of the known "infrared–Seyferts" included in Figure 5 have such low 2.2 μm luminosities in their nuclei. However, the evidence for quasar nuclei remains ambiguous, and other emission mechanisms cannot be ruled out, even for the highest luminosity sources (see, e.g., Rieke 1988; Harwit *et al.* 1987).

The relation between the distribution of the 2.2 μm luminosity and the spatial variation of the near–infrared colors is investigated in Figure 7, where $L_\nu(2.2\mu m)_{2\ kpc}$ is plotted against the logarithm of the ratio $f_\nu(2.2\mu m)_{2\ kpc}/f_\nu(1.6\mu m)_{2\ kpc}$ which is the color calculated from the 2.2 μm and 1.65 μm flux densities within a diameter of 2 kpc about the center of each nucleus. The correlation apparent in this figure indicates that the physical mechanism responsible for the red near–infrared colors seen in the nuclei of many of the infrared luminous galaxies is coupled with an increase in 2.2 μm emitting material in those nuclei relative to other, less red nuclei. This is obviously consistent with, though not identical to, the results of Section III-*a-i*, which postulated an increased density of hot–dust emitting at 2.2 μm to account for the color gradient between the galaxy nuclei and their outer disks. Whereas Figure 2 shows that unusually red near–infrared colors in a galaxy imply a higher concentration of hot–dust in that galaxy's nucleus relative to its own outer disk, Figure 7 indicates that those colors also imply a higher concentration of hot–dust in that galaxy's nucleus relative to other galaxy nuclei.

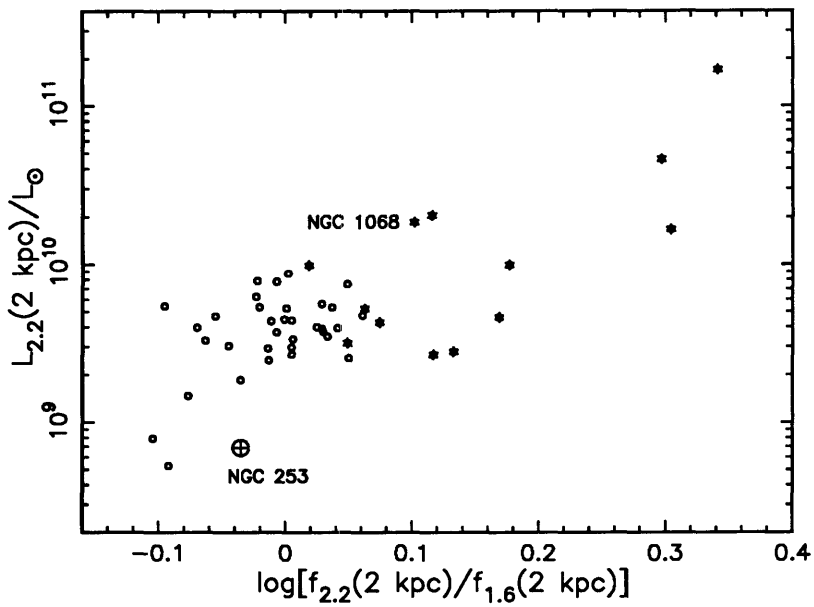

Fig. 7. The logarithm of the 2.2 μm luminosity within a region of diameter 2 kpc about the nucleus, plotted against the logarithm of the ratio $f_\nu(2.2\mu m)_{2\ kpc}/f_\nu(1.6\mu m)_{2\ kpc}$. Galaxies classified in Véron–Cetty and Véron (1989) as Seyfert galaxies, or identified by Sanders *et al.* (1988) as having an AGN, are plotted with the symbol $*$. Included is the starburst galaxy *NGC 253*, its position on the plot having been estimated from the data of Scoville *et al.* (1985).

III.1.3 Individual Sources

The source which stands out most strikingly in Figs. 5 and 6 and Table III is *Mrk 231*. This is not surprising since this source, listed as a quasar in Véron–Cetty and Véron (1989), has long been known to be an extremely luminous, compact galaxy (Young, Knacke, and Joyce 1972; Rieke and Low 1972). With a 2.2 μm luminosity of greater than $10^{11} L_\odot$ within a radius of 1 kpc from its center, its nucleus is nearly an order–of–magnitude more luminous at 2.2 μm than that of *NGC 1068*, and is *250 times* more luminous than the nucleus of *NGC 253*. In fact, the nuclear near–infrared properties of *Mrk 231* are considerably more extreme in comparison to other infrared luminous galaxies than are the properties of its integrated longer wavelength emission. For comparison, the total infrared luminosity, L_{IR}, of *Mrk 231* is only a factor of two greater than that of *Arp 220*, the second most luminous galaxy in the current sample, whereas its nuclear 2.2 μm luminosity, $L_\nu(2.2\mu m)_{2\ kpc}$, is more than a factor of 30

greater than that of *Arp 220*.

These considerations are easily understood in terms of dust extinction in the nuclei of the infrared Seyferts. For a galaxy with a large amount of dust in its nucleus, such as *Arp 220* or *NGC 4418* (see the discussion below), much of the near–infrared emission from within the nucleus would be absorbed and re–radiated at far–infrared wavelengths, reducing the observed 2.2 μm nuclear luminosity. In contrast, for a galaxy with relatively little dust obscuring the central AGN in comparison to other infrared Seyferts, as Sanders *et al.* (1988) have suggested is the case for *Mrk 231*, the energy distribution would more closely resemble the flat distribution typical of a classical quasar, in which a greater fraction of the total luminosity is seen at near–infrared wavelengths than is typical of infrared luminous galaxies.

In addition to *Mrk 231*, a number of other sources stand out in Figs. 5 and 6. Those nuclei forming the high luminosity "tail" in Figure 5, and hence emitting exceedingly high 2.2 μm luminosities from their nuclei, are *Mrk 231*, *IRAS 05189–2524*, *NGC 7469*, *NGC 1068*, *UGC 5101*, *NGC 7674*, *NGC 34*, and *NGC 1614*. *Mrk 231*, *NGC 7469*, *NGC 1068*, and *NGC 7674* are all well studied Seyfert galaxies listed in Véron–Cetty and Véron (1989), and *IRAS 05189–2524* and *UGC 5101* have been studied extensively by Sanders *et al.* (1988), who identified them both as having Seyfert nuclei as well. Hence, the extremely high nuclear luminosities for these galaxies are not surprising. *NGC 34* is also classified in Véron–Cetty and Véron as a Seyfert galaxy, but seems to have received very little attention to date. An (unpublished) image of this source at 6500$\mathring{A}$, taken by the authors, shows a single bright nucleus, with a single tail–like structure extending $\sim$15 kpc away from it, which may suggest that this source is a completed merger (compare optical images of *IRAS 05189–2524* and *Mrk 231* from Sanders *et al.*). This source may be an extremely interesting candidate for further observation.

NGC 1614, although not a Seyfert, was recognized many years ago as an unusual galaxy, with very high luminosity, strong emission lines, and a compact core (Ulrich 1972, and references therein; Rieke and Low 1972). Aitken, Roche, and Phillips (1981) suggested that the infrared emitting region in this source has a diameter $\lesssim$1.5 kpc, and from an analysis presented in Paper I it was found that as much as 80% of the 10 μm emission from this galaxy could be coming from a point source in the nucleus.

From these considerations, it is also not surprising that this source has a value of $L_\nu(2.2\mu m)_{2\ kpc}$ that is amongst the highest in the current sample.

The sources forming the tail at the high end of the distribution in Figure 6, and hence having unusually compact 2.2 μm emission, are *UGC 5101*, *Mrk 231*, *NGC 34*, *NGC 7469*, and *NGC 2623*. The first four have already been discussed and have Seyfert nuclei, which accounts for their highly compact emission. However, *NGC 2623*, which has been studied extensively (see, e.g., Joy and Harvey 1987; Baan *et al.* 1985; Casoli *et al.* 1988), has an optical spectrum which shows no indication of a Seyfert nucleus, and it is not clear from previously published work why this source is so compact at 2.2 μm. It is possible, however, that it contains an AGN which is too heavily shrouded in dust to be identifiable at visible wavelengths; a similar situation is believed to exist in a number of infrared luminous galaxies, including *Arp 220* (Norris 1985; Graham *et al.* 1990) and *NGC 4418* (see Roche *et al.* 1986, and the discussion below). Indeed, such a possibility seems reasonable given the conclusions of Joy and Harvey that *NGC 2623* is the remnant of a completed merger with ~90% of its luminosity emitted by dust.

Finally, *NGC 4418*, listed in Véron–Cetty and Véron (1989) as a *possible* Seyfert galaxy, holds a distinct position in the current sample in that, despite this possible Seyfert classification, it has the second *least* luminous nucleus at 2.2 μm, and is significantly extended at 2.2 μm out to a diameter of at least 4 kpc (the largest 2.2 μm beam diameter for this source; see Table I). *NGC 4418* was studied by Roche *et al.* (1986), who found that it has a compact 10 μm source ($\lesssim$ 0.5 kpc in diameter) containing a tremendous amount of absorbing material, responsible for a visual extinction $A_V \gg 50$ mag which renders the nucleus virtually invisible at optical wavelengths. This unusually high extinction can be predicted simply on the basis of the ratio of infrared to visible luminosities (a measure of the total luminosity re–radiated by dust compared to the observable, hence un–absorbed, intrinsic luminosity) which, for this galaxy, is ~50, placing it at the very highest end of this ratio, not only for the current sample of galaxies, but for the entire BG Sample (see Soifer *et al.* 1989). It is probable that the low 2.2 μm luminosity in this galaxy's nucleus is due to dust extinction at 2.2 μm, which shifts the bulk

of the observed emission to far–infrared wavelengths. All of these considerations are reminiscent of *Arp 220*, which also has a compact infrared core of diameter $\lesssim$ 0.5 kpc (Becklin and Wynn–Williams 1985; Graham *et al.* 1990) containing a (double) active nucleus (Norris 1985; Graham *et al.* 1990) which is heavily enshrouded by dust, responsible for a visual extinction ~50 magnitudes (Becklin and Wynn–Williams), an extremely high infrared–to–visible luminosity ratio ~150 (Soifer *et al.* 1987), and an extended 2.2 μm luminosity profile (Table I). This suggests that *NGC 4418* may be a less luminous version of *Arp 220*, in which case it would also be an interesting case for further study.

III.2 The Total Near–Infrared Emission

The large diameter beam measurements provide an opportunity to estimate the total near–infrared emission in a large sample of high luminosity IRAS galaxies. The optical diameter of the galaxies in the current sample, using visual estimates from the Palomar Observatory Sky Survey prints (Paper I), has a median of 35″, and a maximum of 540″. Thus, although a 55″ diameter beam may not include the total emission in some sources, it should provide a good estimate for the majority. This is also indicated by the curves of growth from which it is clear that, for the majority of the galaxies, the total flux outside of the 33″ diameter beam is a small fraction of the total flux (the median 1.65 μm flux density in a 33 – 55″ annulus is ~ 20% of that inside the 33″ diameter beam).

The luminosity at 1.65 μm (the H wavelength band) can be used as an estimate of the total near–infrared luminosity, where $L_H \equiv 4\pi D^2 \nu f_\nu(1.65\ \mu m)$, D is the luminosity distance, and $f_\nu(1.65\ \mu m)$ is the flux density measured with the largest available beam diameter. The blue luminosity, $L_B \equiv 4\pi D^2 \nu f_\nu(0.43\ \mu m)$, can be obtained for each galaxy from the data of Soifer *et al.* (1987). It is then found that the ratio L_H/L_B has a median of 1.9 for the galaxies in Table I, and ranges from a minimum of 0.7 (for *NGC 34*), up to a maximum of 8.5 (for *UGC 2982*). For this analysis, those galaxies have been excluded for which the largest available beam diameter is too small, as determined from the 1.65 μm curve of growth, to provide a reasonable estimate of the total near–infrared emission; these galaxies are indicated in Table I, in the listing of L_* (see below). A histogram of the values of L_H/L_B for the current sample is shown in Figure 8.

These values of L_H/L_B can be compared to those for lower luminosity galaxies by using the sample of 71 optically selected spiral galaxies measured by Aaronson (1977). Estimates of L_H/L_B for the Aaronson sample, the distribution of which is also shown in Figure 8, were obtained using the magnitudes at H (1.65 μm) and V (0.55 μm) given by Aaronson, and interpolating the V magnitudes to the B wavelength band (0.43 μm) using $B - V = 0.8$ mag, as given by DeVaucouleurs (1959) for spiral galaxies. The distribution has a median of 2.0, and ranges from a minimum of 1.0 up to a maximum of 3.8. The measurements presented by Aaronson were typically done with beam diameters representing a considerably smaller fraction of the galaxy diameter than the measurements presented here. However, Aaronson has shown that the galaxies in his sample exhibit no significant change in galaxy colors with beam diameter.

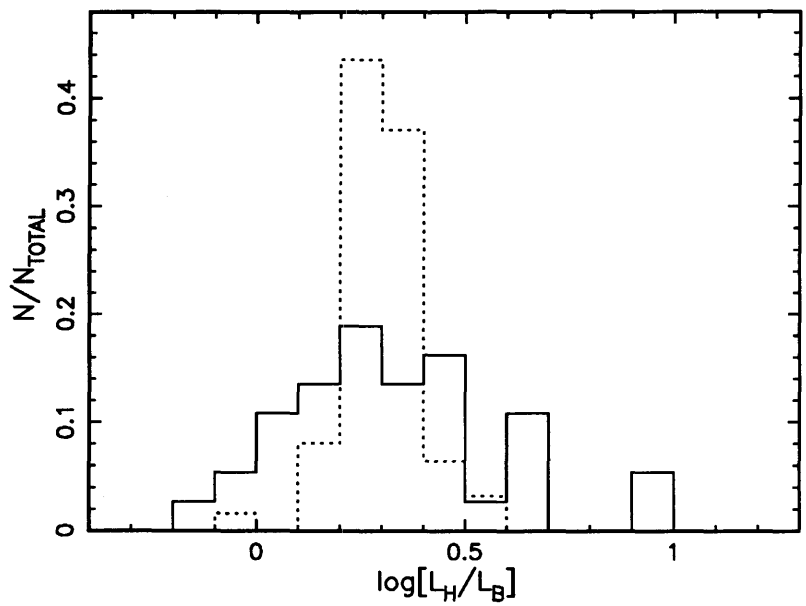

Fig. 8. The ratio of total near-infrared to visible luminosity, L_H/L_B (see text). The *solid-line histogram* is the distribution for the galaxies listed in Table I; the *dotted-line histogram* is the distribution for a sample of low luminosity, optically selected spiral galaxies measured by Aaronson (1977).

As seen in Figure 8, the range of values of L_H/L_B for the galaxies measured by Aaronson (1977) is considerably narrower than the range of values for the galaxies listed in Table I, indicating the

more uniform emission properties expected for a sample of normal galaxies. However, the fact that the median values of L_H/L_B for the two samples are virtually identical demonstrates that the global near–infrared luminosity does not trace the infrared activity in galaxies, a result which provides further evidence that the processes responsible for the unusual properties of infrared luminous galaxies are confined to the nuclear regions.

The estimates of the total near–infrared emission can also be used to estimate the contribution of the stellar luminosity to the total energy budget of infrared–luminous galaxies. The stellar luminosity, L_*, is taken to be $4\pi D^2(F_B + F_{NIR})$, where D is the luminosity distance, $F_B \equiv \nu f_\nu(0.43\mu m)$, and F_{NIR} is an estimate of the stellar near–infrared emission obtained by fitting a single temperature black–body curve to the near–infrared colors for a typical, normal spiral galaxy (Aaronson 1977) and integrating the flux under this curve, normalized to the 1.65 μm flux density from the largest available beam size, for each galaxy. The values of L_* are listed in Table I, along with the values of L_{IR} from Paper I. Galaxies for which L_* is *not* a reasonable estimate of the total stellar emission, based on a 1.65 μm growth curve which is still increasing significantly at the largest available beam diameter, have been flagged with a footnote, and were excluded from the analysis. For sources with obvious double nuclei, estimates of L_{IR} for each nucleus were obtained by assuming that each nucleus contributes the same fraction of the total luminosity at far–infrared wavelengths as at 2.2 μm, where the fraction contributed at 2.2 μm was calculated from the largest available beam size, unless otherwise noted. These estimates for individual nuclei are shown in parentheses in Table I.

A histogram of the logarithm of L_*/L_{TOT} is shown in Figure 9, where $L_{TOT} \equiv L_* + L_{IR}$. The figure indicates that the observed stellar luminosity in infrared luminous galaxies is typically $\lesssim$ 25% of the total luminosity; for the galaxies in Figure 9, the fraction ranges from a minimum of $\sim$ 3% (for *Arp 220*) to a maximum of $\sim$ 37% (for *UGC 6436*, east–nucleus). For comparison, data from Rice *et al.* (1990) give L_*/L_{TOT} = 0.89 for the nearby low–luminosity spiral galaxy *M 33*.

IV. SUMMARY

Forty–seven galaxies from the *IRAS* Bright Galaxy Sample with infrared luminosities $L_{IR} \geq$

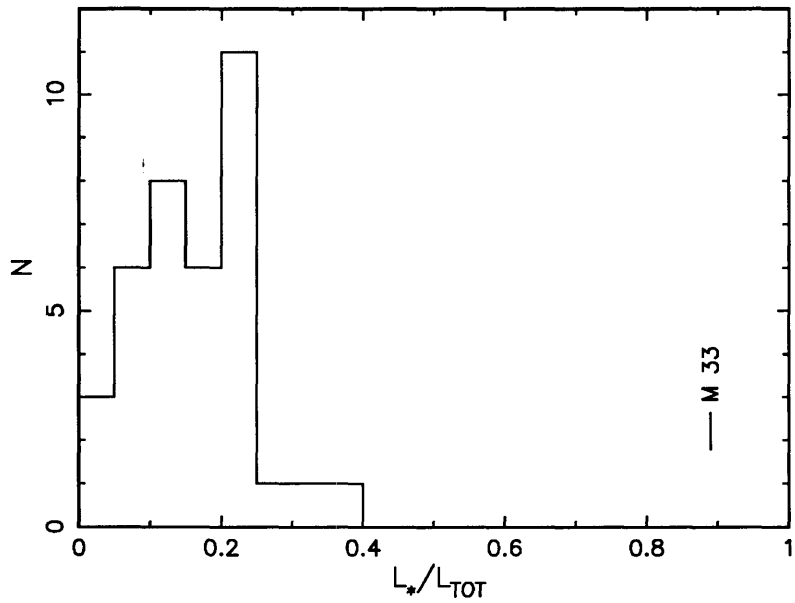

Fig. 9. The distribution of the fraction of the total luminosity attributable to stellar emission in infrared luminous galaxies, defined as the ratio of the stellar luminosity, L_*, as estimated from the blue luminosity and the 1.65 μm flux density (see text), to the total luminosity, $L_{TOT} \equiv L_* + L_{IR}$. An estimate for the low luminosity spiral galaxy *M 33*, calculated from the data in Rice *et al.* (1990), is also shown.

10^{11} $L_\odot$ have been observed at near–infrared wavelengths with multiple large diameter beams.

IV.1 Observational results

1) The unusually red near–infrared colors known previously for many of these galaxies are confined to their nuclei, within regions typically 1 – 3 kpc in diameter, whereas the outer disk regions have colors which are essentially those of a normal stellar population.

2) The 2.2 μm luminosity emitted from the nuclei of infrared luminous galaxies is generally considerably higher and more compact than that seen in classical "starburst" nuclei, but lower and more extended than that seen in classical Seyfert nuclei.

3) The ratio of near–infrared to visible emission for infrared luminous galaxies, calculated from the *total* near–infrared and visible luminosities for each galaxy, is, on average, comparable to that for low luminosity, optically selected galaxies.

4) The observed stellar emission contributes generally $\lesssim 25\%$ of the observed bolometric luminosity in infrared luminous galaxies. This is considerably less than in typical low luminosity galaxies ($\sim 90\%$ in *M 33*).

IV.2 Interpretation

The effects of dust, reddening and thermal re–radiation, required to explain the observed unusual near–infrared colors are confined primarily to the nuclei. Since the far–infrared emission is re–radiated emission from dust grains, it is probable that the far–infrared luminosity, and hence the bulk of the entire luminosity of infrared luminous galaxies, tends to be strongly concentrated about their nuclei. Thus, *the physical processes responsible for the unusual properties of infrared luminous galaxies tend to be confined to the nuclear regions, with diameters* $\lesssim 1 - 3$ *kpc*. This, together with the observation that the 2.2 μm nuclear luminosities of these galaxies are generally higher than those of typical starburst nuclei, implies that the nuclei of infrared luminous galaxies must be characterized by exceedingly high radiation densities which are presumably due to extremely intense star formation activity and, in at least some cases, the presence of a central dust–enshrouded quasar. It is suggested that dust extinction at 2.2 μm is the cause of the comparatively low 2.2 μm nuclear luminosities in a number of galaxies contained in the current sample and identified in the literature as having Seyfert nuclei, and that other galaxies in the sample may also have active nuclei buried in their dusty cores.

Since most of the near–infrared luminosity is concentrated in the nuclei of infrared luminous galaxies, it follows that their global near–infrared properties are poor tracers of their infrared activity, which is why the ratio of total near–infrared to visible emission is similar to that for normal, low luminosity galaxies. Furthermore, since the luminosity source in infrared luminous galaxies is enshrouded in dust, it is not surprising that the observed stellar emission from infrared luminous galaxies is only a minor fraction of the total observed luminosity.

Two galaxies from the current sample appear to be extremely interesting sources for further observation. One of these, *NGC 34*, has received very little attention in the literature, although it has a Seyfert nucleus and is amongst the galaxies with the highest 2.2 μm nuclear luminosities and the most

compact near–infrared emission. The other galaxy, *NGC 4418*, appears distinct in the current analysis in that it has one of the *least* luminous nuclei at 2.2 μm despite its identification in the literature as having many of the characteristics of a Seyfert galaxy. It is suggested that this source may be a low luminosity version of *Arp 220*.

ACKNOWLEDGEMENTS

Special thanks are given to S.E. Persson for the use of his infrared photometer, and to Dave Tennent, John Henning, and Mike Doyle for their much needed help in getting it all working. Thanks are also given to the night assistants at the Palomar 60 inch telescope, Russ Day, Will McKinley, Jeff Phinney, and Skip Staples, and the entire staff at Palomar Observatory. A number of useful comments and references were provided by the anonymous referee, and we greatly appreciate his/her time and effort in reviewing this work. The Palomar 60 inch telescope is owned jointly by the California Institute of Technology and the Carnegie Institution of Washington. Ground based astronomy at Caltech is supported by a grant from the National Science Foundation.

REFERENCES

Aaronson, M., 1977. Infrared observations of galaxies, Ph.D. thesis, Harvard University.

Aitken, D.K., P.F. Roche, and M.M. Phillips, 1981. *Mon. Not. R. Astron. Soc.*, **196**, 9p.

Baan, W.A., A.D. Haschick, D. Buckley, and J.T. Schmelz, 1985. *Astrophys. J.*, **293**, 394.

Becklin, E.E., and C.G. Wynn-Williams, 1987. Ground–based 1 – 32 μm observations of Arp 220: Evidence for a dust–embedded "AGN"?, in *Star Formation in Galaxies*, C.J. Lonsdale (Ed.), US Government Printing Office, Washington, D.C., p. 643.

Boulanger, F., C. Beichman, F.X. Désert, G. Helou, M. Pérault, and C. Ryter, 1988. Small grains and IRAS colors, *Astrophys. J.*, **332**, 328.

Carico, D.P., J.R. Graham, K. Matthews, T.D. Wilson, B.T. Soifer, G. Neugebauer, and D.B. Sanders, 1990. The near–infrared morphology of ultraluminous infrared galaxies, *Astrophys. J. (Letters)*, **349**, L39 (*Chapter 5*).

Carico, D.P., D.B. Sanders, B.T. Soifer, J.H. Elias, K. Matthews, and G. Neugebauer, 1988. The *IRAS* Bright Galaxy Sample. III. $1 - 10\ \mu m$ observations and coadded *IRAS* data for galaxies with $L_{IR} \geq 10^{11}\ L_{\odot}$, *Astronom. J.*, **95**, 356 (Paper I; also Chapter 2 of this thesis).

Carico, D.P., B.T. Soifer, C. Beichman, J.H. Elias, K. Matthews, and G. Neugebauer, 1986. Near–infrared observations of *IRAS* Minisurvey Galaxies, *Astronom. J.*, **92**, 1254 (Chapter 1 of this thesis).

Casoli, F., F. Combes, C. Dupraz, M. Gerin, P. Encrenaz, and M. Salez, 1988. *Astron. Astrophys.*, **192**, L17.

Cutri, R.M., R.J. Rudy, G.H. Rieke, A.T. Tokunaga, and S.P. Willner, 1984. The spatial extent of the 3.3 micron emission feature in the Seyfert galaxy NGC 7469, *Astrophys. J.*, **280**, 521.

de Vaucouleurs, G., 1959. *Handb. Phys.*, **53**, 275.

Devereux, N.A., 1989. Nearby starburst galaxies, *Astrophys. J.*, **346**, 126.

Graham, J.R., D.P. Carico, K. Matthews, G. Neugebauer, B.T. Soifer, and T.D. Wilson, T.D., 1990. The double nucleus of Arp 220 unveiled, *Astrophys. J. (Letters)*, **354**, L5.

Harwit, M., J.R. Houck, B.T. Soifer, and G.G.C. Palumbo, 1987. The most luminous far–infrared extragalactic sources, *Astrophys. J.*, **315**, 28.

Helou, G., 1986. The IRAS colors of normal galaxies, *Astrophys. J.*, **311**, L33.

Infrared Astronomical Satellite (IRAS) Catalogs and Atlases: *Explanatory Supplement*, 1988. C.A. Beichman, G. Neugebauer, H.J. Habing, P.E. Clegg, and T.J. Chester (Eds.), National Aeronautics and Space Administration, Washington, D.C..

Joy, M., and P.M. Harvey, 1987. A near–infrared study of the luminous merging galaxies NGC 2623 and Arp 148, *Astrophys. J.*, **315**, 480.

Norris, R.P., 1985. *Mon. Not. R. Astron. Soc.*, **216**, 701.

Osterbrock, D.E., 1977. *Astrophys. J.*, **215**, 733.

Phinney, E.S., 1989. Dusty disks and the infrared emission from AGN, in *Theory of Accretion Disks*, W. Duschl, F. Meyer, and J. Frank (Eds.), Kluwer, Dordrecht, p.457.

Rice, W., F. Boulanger, F. Viallefond, B.T. Soifer, and W.L. Freedman, 1990. The infrared structure of M 33, *Astronom. J.*, (in press).

Rieke, G.H., 1988. Hard X–ray observations of ultraluminous infrared galaxies, *Astrophys. J. (Letters)*, **331**, L5.

Rieke, G.H., and F.J. Low, 1972. *Astrophys. J. (Letters)*, **176**, L95.

Roche, P.F., D.K. Aitken, C.H. Smith, and S.D. James, 1986. NGC 4418; a very extinguished galaxy, *Mon. Not. R. Astron. Soc.*, **218**, 19p.

Sanders, D.B., E.S. Phinney, G. Neugebauer, B.T. Soifer, and K. Matthews, 1989. Continuum energy distributions of quasars: shapes and origins, *Astrophys. J.*, **347**, 29.

Sanders, D.B., N.Z. Scoville, J.S. Young, B.T. Soifer, F.P. Schloerb, W.L. Rice, and G.E. Danielson, 1986. *Astrophys. J.*, **305**, L45.

Sanders, D.B., B.T. Soifer, J.H. Elias, B.F. Madore, K. Matthews, G. Neugebauer, and N.Z. Scoville, 1988. Ultraluminous infrared galaxies and the origin of quasars, *Astrophys. J.*, **325**, 74.

Scoville, N.Z., K. Matthews, D.P. Carico, and D.B. Sanders, 1988. The stellar bar in NGC 1068, *Astrophys. J. (Letters)*, **327**, L61.

Scoville, N.Z., B.T. Soifer, G. Neugebauer, J.S. Young, K. Matthews, and J. Yerka, 1985. The inner disk of NGC 253, *Astrophys. J.*, **289**, 129.

Soifer, B.T., L. Boehmer, G. Neugebauer, and D.B. Sanders, 1989. The *IRAS* Bright Galaxy Sample. IV. Complete *IRAS* observations, *Astronom. J.*, **98**, 766.

Soifer, B.T., D.B. Sanders, B. Madore, G. Neugebauer, G.E. Danielson, J.H. Elias, C.J. Persson, and W.L. Rice, 1987. The *IRAS* Bright Galaxy Sample. II. The sample and luminosity function, *Astrophys. J.*, **320**, 238 (Paper I).

Telesco, C.M., R. Decher, and M. Joy, 1989. Small grains in M 82: a dusty halo surrounding the starburst, *Astrophys. J. (Letters)*, **343**, L13.

Ulrich, M., 1972. *Astrophys. J.*, **178**, 113.

Véron–Cetty, M.P., and P. Véron, 1989. *A Catalog of Quasars and Active Nuclei*, 4th Edition, European Southern Observatory, München.

Weedman, D. W., 1986. *Quasar Astronomy*, Cambridge University Press, Cambridge.

Young, E.T., R.F. Knacke, and R.R. Joyce, 1972. *Nature*, **238**, 263.

TABLE I – FLUX DENSITIES

NAME(S)[a]	RA –1950–			DEC			D_o	POS[b]	BEAM DIAM		$f_\nu(\lambda)$(mJy)[c]			LOG[$L/L_\odot$][d]	
	(h)	(m)	(s)	(°)	(′)	(″)	(″)		(″)	(kpc)	1.27 μm	1.65 μm	2.23 μm	L_*	L_{IR}
NGC 34	0	8	33.4	−12	23	10	35		5	1.9	23.02	35.44	37.17	10.85	11.41
(Mrk 938)									17	6.5	38.20	57.19	48.55		
									33	12.7	49.44	66.31	56.78		
									55	21.1	51.30	66.29			
MCG–02-01-051[†]	0	16	18.0	−10	39	14	35	S	5	2.4	6.17	8.76	8.48		(11.07)
(Arp 256)									17	8.2	13.00	20.49	14.94		
									33	16.0	19.15	22.92	18.80		
								N	5	2.4	1.53	1.88	1.52		(10.94)
									17	8.2	5.73	9.50	8.13		
									33	16.0	13.25	17.05	13.87		
									55	26.7	17.79	20.39			
MCG–03-04-014	1	7	42.0	−17	7	1	25		5	3.2	11.54	16.96	16.68	10.77	11.58
									17	11.0	24.33	36.61	32.98		
									33	21.4	32.07	41.70	38.21		
									55	35.7	34.21				
MCG+02-04-025[†]	1	17	22.8	+14	5	53	25		17	10.3	10.52	13.25	11.54	10.61	11.63
									33	19.9	21.98	17.63	18.98		
									55	33.2	16.99	23.20	21.99		
NGC 695	1	48	28.1	+22	20	10	35		5	3.2	10.62	14.50	13.75	11.19	11.63
(UGC 1315)									17	10.7	28.71	40.06	31.79		
									33	20.9	46.79	58.16	48.55		
									55	34.8	47.22	62.93	55.75		
NGC 958	2	28	11.8	− 3	9	32	100		5	1.9	12.77	17.44	14.94	11.36[e]	11.13
									17	6.3	45.51	61.86	49.92		
									33	12.3	89.97	127.96	102.38		
									55	20.5	134.93	195.89	160.78		
NGC 1068[†]	2	40	7.2	+20	13	30	540		5	0.5	193.24	300.23	769.54	10.92[e]	11.26
									10	0.9	375.07	546.32	899.98		
									17	1.5	605.49	850.06	1175.53		
									33	3.0	1153.74	1532.68	1730.74		
									55	5.0	1520.92	2096.29	2219.38		
UGC 2238	2	43	33.4	+12	53	10	35		5	2.0	7.76	14.24	16.38	10.60	11.23
									17	6.9	20.05	30.39	29.80		
									33	13.3	34.84	47.74	42.29		
									55	22.2	37.51	57.57	52.75		

TABLE I (continued)

NAME(S)[a]	RA −1950−			DEC			D_o	POS[b]	BEAM DIAM		$f_\nu(\lambda)$(mJy)[c]			LOG[$L/L_\odot$][d]	
	(h)	(m)	(s)	(°)	(′)	(″)	(″)		(″)	(kpc)	1.27 μm	1.65 μm	2.23 μm	L_*	L_{IR}
IRAS 0243+213	2	43	49.2	+21	22	44	20		10	4.4	13.00	17.92	16.68		11.05
									17	7.5	13.00	25.57	20.81		
									33	14.5	21.98	28.04	25.48		
									55	24.2	22.19	33.61	23.89		
UGC 2369†	2	51	15.6	+14	46	1	40	MID	55	33.3	54.21	68.78	59.46	11.06	11.57
								N	5	3.0	8.91	12.29	10.82	10.78[e]	(11.40)
									17	10.3	23.02	27.94	24.34		
									33	20.0	35.16	45.64	36.83		
								S	5	3.0	5.08	7.47	8.06	10.65[e]	(11.08)
									17	10.3	8.13	14.66	14.13		
									33	20.0	16.68	27.71	17.79		
IRAS 0335+15†	3	35	57.1	+15	23	6	20		10	6.8	4.35	5.77	5.84		11.44
									17	11.6	3.65	6.39	6.00		
									33	22.6	6.00	11.22	9.69		
									55	37.7	9.77	10.60	10.05		
UGC 2982	4	9	43.2	+ 5	25	12	35		5	1.7	8.13	13.35	13.37	10.60	11.15
									10	3.4	17.46	27.85	28.99		
									17	5.8	23.23	41.00	37.52		
									33	11.3	46.36	69.80	63.42		
									55	18.9	58.90	84.26	72.15		
MCG-03-12-002†	4	19	6.5	−18	55	48	20	N	5	3.1	6.40	8.19	9.00	10.91[e]	(11.26)
									10	6.1	11.86	16.35	15.21		
									17	10.4	14.93	22.35	18.98		
									33	20.2	26.68	34.28	27.43		
									55	33.7	39.64	51.70			
								S	5	3.1	4.55	6.75	7.08	10.41[e]	(10.95)
									10	6.1	6.83	9.58	9.51		
									17	10.4	6.00	11.87	9.34		
NGC 1614 (Mrk 617)	4	31	35.8	− 8	40	55	50		5	1.5	34.21	48.47	49.00	10.66	11.58
									10	3.1	42.28	59.90	59.46		
									17	5.2	50.36	73.66	65.80		
									33	10.1	75.53	104.25	100.52		
									55	16.9	83.58	122.01	95.99		
NGC 2623 (Arp 243)	8	35	25.2	+25	55	48	35		5	1.8	9.33	15.05	18.12	10.49	11.55
									17	6.1	19.87	27.75	27.68		
									33	11.8	28.98	45.91	32.08		
									55	19.7	29.25	46.20	38.57		

TABLE I (continued)

NAME(S)[a]	RA −1950−			DEC			D_o	POS[b]	BEAM DIAM		$f_\nu(\lambda)$(mJy)[c]			LOG[$L/L_\odot$][d]	
	(h)	(m)	(s)	(°)	(′)	(″)	(″)		(″)	(kpc)	1.27 μm	1.65 μm	2.23 μm	L_*	L_{IR}
MGC+08-18-012	9	33	18.5	+48	41	53	30		5	2.5	8.83	12.45	12.42	10.61	11.31
									10	5.0	14.00	18.45	17.79		
									17	8.6	14.66	19.64	14.94		
									33	16.6	21.58	28.89	24.11		
									55	27.7	21.78	32.02			
NGC 3110	10	1	32.2	− 6	14	2	60		5	1.6	11.12	15.76	14.53	10.73	11.22
									17	5.3	31.20	46.70	39.65		
									33	10.3	63.40	85.44	69.54		
									55	17.2	79.82	104.10			
IRAS 1056+24[†]	10	56	35.5	+24	48	43	25		10	8.1	11.12	15.76	16.99		11.99
									17	13.7	12.89	17.36	17.47		
									33	26.7	14.39	20.42	19.69		
									55	44.5	16.99	23.41			
A1101+41	11	1	5.8	+41	7	8	35		5	3.3	5.42	7.90	8.36	10.69	11.58
(V 32)									17	11.4	12.65	16.83	14.53		
									33	22.1	14.00	18.67	16.68		
									55	36.8	15.64	17.92			
UGC 6436[†]	11	23	9.8	+14	56	53	15	W	5	3.3	5.57	7.97	7.84	10.59	(11.38)
(IC 2810)									17	11.2	14.00	17.28	16.38		
									33	21.8	15.49	16.11	21.79		
									55	36.4	22.39	30.86			
								E	17	11.2	4.90	4.09	3.39	10.30	(10.84)
									33	21.8	5.57	4.43	3.89		
									55	36.4	15.64	21.35			
NGC 3690[†]	11	25	42.0	+58	50	17	80		5	1.0	22.81	32.92	38.21	10.91[e]	11.90
(Mrk 171)									17	3.5	43.86	68.50	68.90		
									33	6.7	115.37	173.01	166.81		
									55	11.2	196.84	268.81			
NGC 4418	12	24	22.1	− 0	36	14	60		5	0.7	10.73	14.11	12.31	9.82	11.10
(UGC 7545)									17	2.2	28.45	35.49	27.68		
									33	4.4	42.67	52.29	41.14		
									55	7.3	51.77	68.78			
Mrk 231	12	54	4.8	+57	8	38	30		5	4.1	45.51	100.33	182.91	11.54	12.52
(UGC 8058)									10	8.2	48.54	101.26	189.77		
									17	13.9	48.54	110.05	177.92		
									33	26.9	64.58	124.23	204.28		
									55	44.9	66.39	114.14			

TABLE I (continued)

NAME(S)[a]	RA −1950− (h)	(m)	(s)	DEC (°)	(′)	(″)	D_o (″)	POS[b]	BEAM DIAM (″)	(kpc)	$f_\nu(\lambda)$(mJy)[c] 1.27 μm	1.65 μm	2.23 μm	LOG[$L/L_\odot$][d] L_*	L_{IR}
NGC 4922† (UGC 8135)	12	59	1.0	+29	34	59	45	MID	55	26.1	77.64	103.15		11.03	11.31
								SW	5	2.4	16.22	19.84	15.93	10.76[e]	(11.11)
									17	8.1	35.49	44.11	32.98		
									33	15.7	57.82	68.09	51.79		
								NE	5	2.4	4.64	6.88	8.75	10.61[e]	(10.89)
									17	8.1	13.25	17.39	15.93		
									33	15.7	27.17	36.75	31.21		
IC 860	13	12	40.1	+24	52	52	35		5	1.3	8.13	10.60	9.34	10.15	11.11
									17	4.3	24.33	30.95	24.56		
									33	8.3	35.82	44.58	33.90		
									55	13.8	35.16	45.86			
UGC 8335† (VII ZW 506)	13	13	41.3	+62	23	17	30	SE	5	3.0	7.62	11.31	12.31	10.76	(11.53)
									17	10.3	8.83	15.71	15.93		
									33	20.0	12.65	19.01	23.24		
									55	33.3	19.87	22.36			
								NW	5	3.0	4.23	6.16	6.23	10.73	(11.37)
									17	10.3	6.89	11.37	10.33		
									33	20.0	10.43	13.13	15.78		
									55	33.3	13.62	19.30			
NGC 5256† (UGC 8632)	13	36	14.2	+48	31	52	25	MID	17	9.1	27.68	38.99	34.53	10.98	11.47
									33	17.7	43.46	57.54	47.23		
									55	29.4	48.99	62.15			
								SW	5	2.7	7.55	11.41	11.54	10.61[e]	(11.23)
								NE	5	2.7	7.62	9.94	8.59	10.59[e]	(11.10)
NGC 5257† (UGC 8641)	13	37	22.1	+ 1	5	13	115		5	2.2	4.64	6.39	5.89	10.90	11.50
									17	7.5	18.12	21.78	18.80		
									33	14.5	43.06	56.06	46.80		
									55	24.2	53.72	70.71			
Mrk 273 (UGC 8696)	13	42	51.6	+56	8	13	70		5	3.7	8.59	12.99	15.21	10.83	12.14
									17	12.5	16.07	24.63	27.43		
									33	24.3	22.19	33.84	32.08		
UGC 8739	13	47	1.7	+35	30	14	110		5	1.7	5.04	9.75	11.33	10.52	11.04
									17	5.6	16.37	30.98	30.64		
									33	10.9	35.82	55.96	50.84		
									55	18.2	43.06	63.89			
ZW 247.020 (Mrk 1490)	14	17	53.8	+49	27	54	20		5	2.5	8.44	12.40	12.08	10.46	11.32
									17	8.6	13.49	18.97	18.29		
									33	16.6	13.62	21.98	17.15		
									55	27.7	15.49	22.15			

TABLE I (continued)

NAME(S)[a]	RA –1950–			DEC			D_o	POS[b]	BEAM DIAM		$f_\nu(\lambda)$(mJy)[c]			LOG[$L/L_\odot$][d]	
	(h)	(m)	(s)	(°)	(′)	(″)	(″)		(″)	(kpc)	1.27 μm	1.65 μm	2.23 μm	L_*	L_{IR}
UGC 9618† (Arp 302)	14	54	47.8	+24	48	58	80	N	5	3.3	6.70	12.06	14.26	10.93[e]	(11.36)
									17	11.1	11.43	16.72	14.94		
									33	21.6	34.21	48.50	46.37		
								S	17	11.1	9.16	11.05	7.98	10.73[e]	(11.31)
									33	21.6	14.93	17.87	13.25		
I ZW 107 (Mrk 848)	15	16	19.0	+42	55	41	40		5	3.9	5.62	7.47	8.06	10.91	11.85
									17	13.2	6.28	12.49	11.54		
									33	25.7	18.80	23.71	21.00		
									55	42.8	17.79	23.20			
IRAS 1525+36†	15	25	3.1	+36	9	0	20		5	5.2	2.92	3.89	3.89	10.73	12.00
									10	10.4	3.48	4.72	4.55		
									17	17.6	3.24	3.97	4.39		
									33	34.2	6.76	7.17	8.92		
									55	35.7	9.25	9.67			
Arp 220 (UGC 9913)	15	32	46.3	+23	40	8	50		5	1.8	9.16	17.44	21.79	10.67	12.19
									10	3.5	18.80	30.58	33.90		
									17	6.0	27.93	43.33	40.39		
									33	11.6	51.77	70.08	60.01		
									55	19.4	59.99	78.97			
NGC 6090† (UGC 10267)	16	10	24.0	+52	35	6	25	MID	17	9.6	25.71	23.76	21.59	10.89	11.48
									33	18.6	30.63	32.93	28.20		
									55	31.0	31.49	35.76			
								NE	10	5.6	13.00	16.65	15.50	10.74[e]	(11.35)
								SW	10	5.6	5.13	5.77	5.18	10.62[e]	(10.89)
MCG+01-42-088	16	28	27.4	+ 4	11	24	40		5	2.3	10.92	16.05	16.08	10.62	11.34
									17	7.8	27.17	35.61	32.08		
									33	15.1	35.49	45.93	44.28		
									55	25.2	30.63	41.06			
NGC 6286† (Arp 293)	16	57	44.9	+59	0	40	65		10	3.6	17.62	28.15	30.08	10.73	11.32
									17	6.2	28.45	48.06	45.94		
									33	12.0	48.54	72.98	65.20		
									55	19.9	57.29	85.01			
IRAS 1713+53†	17	13	14.2	+53	13	52	20	MID	33	32.4	8.44	16.31	15.07	10.83	11.88
									55	54.1	14.00	14.77			
								NE	5	4.9	5.57	8.19	8.92	10.65[e]	(11.77)
								SW	5	4.9	2.14	2.76	2.69	10.39[e]	(11.24)
MCG–03-57-017	22	28	42.7	–19	17	31	50		5	2.3	10.14	15.61	16.68	10.62[e]	11.25
									17	8.0	22.19	34.78	29.53		

TABLE I (continued)

NAME(S)[a]	RA −1950−			DEC			D_o	POS[b]	BEAM DIAM		$f_\nu(\lambda)$(mJy)[c]			LOG[$L/L_\odot$][d]	
	(h)	(m)	(s)	(°)	(′)	(″)	(″)		(″)	(kpc)	1.27 μm	1.65 μm	2.23 μm	L_*	L_{IR}
NGC 7469	23	0	44.6	+ 8	36	18	50		5	1.6	52.25	81.18	109.20	10.99	11.59
(UGC 12332)									17	5.4	75.53	121.97	131.29		
									33	10.6	105.22	167.75	173.07		
									55	17.6	131.25	191.18			
ZW 453.062	23	2	28.1	+19	16	55	40		5	2.4	5.84	8.66	8.75	10.71	11.28
									17	8.1	13.62	16.32	13.62		
									33	15.7	32.37	43.41	37.17		
									55	26.2	38.20	50.88	44.69		
ZW 475.056	23	13	31.2	+25	16	48	30		5	2.7	12.19	17.60	19.69	10.79	11.53
									17	9.0	23.48	32.38	31.31		
									33	17.5	29.89	41.98	37.52		
									55	29.2	32.97	47.20	40.76		
NGC 7592†	23	15	47.5	− 4	41	20	35	MID	55	26.0	39.27	52.08	43.47	10.81	11.32
(Mrk 928)								E	5	2.4	6.34	9.07	8.59	10.46[e]	(11.03)
								W	5	2.4	6.11	8.42	8.06	10.45[e]	(11.00)
NGC 7674†	23	25	24.7	+ 8	30	14	45		5	2.8	9.96	16.50	24.79	11.16[e]	11.48
(UGC 12608)									17	9.5	24.11	34.52	41.14		
									33	18.5	43.46	61.17	66.41		
									55	30.8	57.32	84.40	73.49		
NGC 7771†	23	48	52.1	+19	49	55	110		5	1.4	17.79	27.63	28.20	10.99[e]	11.34
									17	4.8	65.78	95.92	82.84		
									33	9.3	126.50	182.24	152.14		
									55	15.5	190.84	271.48	219.90		
Mrk 331	23	48	52.8	+20	18	22	40		5	1.7	25.95	36.43	34.85	10.63	11.40
									17	5.9	47.22	61.79	54.73		
									33	11.5	61.11	79.41	72.15		
									55	19.2	60.57	82.96	68.27		

[a] The symbol † indicates that a comment regarding that source appears at the end of the table.

[b] Refer to the notes to Table I for an explanation of specific beam positions.

[c] The 5″ and 10″ measurements are from Carico *et al.* (1988).

[d] Parentheses indicate estimates for individual nuclei within sources containing multiple nuclei (see Section III-*b*).

[e] This value of L_* is *not* a reasonable estimate of the total stellar luminosity – the largest available beam diameter was too small.

† NOTES TO TABLE I

(Angular separations given here are only approximate)

MCG–02-01-051 and MCG+02-04-025 It was recently discovered that, due to a mis-identification in the observing logs, the data reported by Carico *et al.* (1988) for MCG+02-04-025 were actually measurements of MCG–02-01-051. Hence, the 5″ measurements reported here for MCG–02-01-051, N, are those previously reported as MCG+02-04-025(a), and those for MCG–02-01-051, S, are the average of the previously reported measurements for MCG–02-01-051 and MCG+02-04-025(b). The designations N and S for MCG–02-01-051 refer to the two distinct nuclei in a N–S orientation separated by 50″. There are no 5″ measurements available for MCG+02-04-025.

NGC 1068 The near–infrared data were previously published by Scoville *et al.* (1988).

UGC 2369 There are two visually obvious nuclei in a N–S orientation separated by 30″. The 5″, 17″, and 33″ measurements are of the respective nuclei; the 55″ measurements are of a position midway between the nuclei, encompassing both.

IRAS 0335+15 There are two visually obvious nuclei separated by 15″ in an E–W orientation. All measurements are of the E nucleus. Due to the close association of the two nuclei, all measurements with beam diameters greater than 17″ contain emission from the companion (W) nucleus. No attempt has been made to correct for this effect, as this nucleus is considerably fainter than the east nucleus.

MCG–03-12-002 There are two visually obvious nuclei in a north–south orientation separated by 15″. Thus, although all measurements are centered on the respective nuclei, the 33″ and 55″ measurements of the N nucleus include emission from from both nuclei.

IRAS 1056+24 There are two nuclei in a NW–SE orientation separated by 10″. All measurements are of the NW nucleus, which is the dominant source.

UGC 6436 There are two visually distinct nuclei in an E–W orientation separated by 20″. The measurements are of the respective nuclei; however, the 55″ measurements contain emission from both nuclei. Hence, the luminosities have been estimated from the 33″ measurements.

NGC 3690 The visual image of this sources shows two apparently merging galaxies in an E–W orientation separated by 25″; the galaxy to the west is NGC 3690. The other galaxy, not measured in this analysis, is IC 694.

NGC 4922 There are two visually obvious nuclei in a NE–SW orientation separated by 20″. The 5″, 17″, and 33″ diameter beam measurements are of the respective nuclei; the 55″ diameter beam measurements are centered at a position midway between the two nuclei.

UGC 8335 There are two visually obvious nuclei in a NW–SE orientation separated by 30″. The measurements are of the respective nuclei.

NGC 5256 There are two visually obvious nuclei in a NE–SW orientation separated by 10″. The 5″ measurements are of the SW nucleus; the larger beam measurements are centered midway between the two nuclei, encompassing both.

NGC 5257 This source was reported by Carico *et al.* (1988) as NGC 5257/8; it has since been determined that NGC 5257 alone is the IRAS source, rather than in combination with NGC 5258, which lies 80″ to the NW.

UGC 9618 There are two merging galaxies in a N–S orientation separated by 40″. There appears to be a bright foreground star roughly midway between the two nuclei, and it is likely that this star is causing the anomolous increase in the 33″ measurements of the N nucleus. For this reason, the luminosities for that nucleus have been estimated from the 17″ measurements.

IRAS 1525+36 This object consists of a compact central source, with a diameter of 10″($\sim$ 10 kpc), and a faint surrounding ring-like structure extending out to a radius of roughly 20″($\sim$ 20 kpc; see Sanders *et al.* 1988). The measurements are consistent with this morphology. However, the 33″ and 55″ beams may also have been contaminated by emission from the nearby galaxy and/or foreground star lying 20″ N and NE, respectively.

NGC 6090 There are two visually obvious nuclei in a NE–SW orientation separated by 10″. The 10″ measurements are of the respective nuclei; the larger beam measurements are centered midway between

the two nuclei, encompassing both.

NGC 6286 This source was reported by Carico *et al.* (1988) as NGC 6285/6; it has since been determined that NGC 6286 alone is the IRAS source, rather than in combination with NGC 6285, which lies 80″ to the NW.

IRAS 1713+53 There are two visually obvious nuclei in a NE–SW orientation separated by 10″. The 5″ measurements are of the respective nuclei; the larger beam measurements are centered midway between the two nuclei, encompassing both.

NGC 7592 There are two visually obvious nuclei in an E–W orientation separated by 10″. The 5″ measurements are of the respective nuclei; the 55″ measurement is centered midway between the two nuclei, encompassing both.

NGC 7674 There are two visually obvious nuclei in a NE–SW orienation separated by 30″. All measurements are of the dominant SW nucleus.

NGC 7771 There are two visually obvious nuclei in a NE–SW orientation separated by 50″. All measurements are of the dominant NE nucleus.

TABLE II – FLUX DENSITY RATIOS

NAME	POS[a]	D_1[b]	D_2[b]	LOG[$f_\nu(1.6\mu m)/f_\nu(1.3\mu m)$][c]		LOG[$f_\nu(2.2\mu m)/f_\nu(1.6\mu m)$]	
		(kpc)	(kpc)	NUCLEUS	DISK	NUCLEUS	DISK
MCG–03-04-014		3.2	21.4	0.16	0.08	-0.01	-0.06
NGC 695		3.2	20.9	0.14	0.08	-0.02	-0.10
NGC 958		1.9	20.5	0.14	0.16	-0.07	-0.09
NGC 1068		0.4	4.8	* 0.19	0.13	0.41	-0.09
UGC 2238		2.0	22.2	* 0.26	0.16	0.06	-0.08
UGC 2369	N	3.0	20.0	0.14	0.10	-0.06	-0.11
UGC 2982		1.7	18.9	* 0.22	0.15	0.00	-0.08
MCG-0312002	N	3.1	20.2	* 0.11	0.11	0.04	-0.15
NGC 1614		1.5	10.1	0.15	0.13	0.00	-0.03
MCG+08-18-012		2.5	16.6	* 0.15	0.11	-0.00	-0.15
NGC 3110		1.6	10.3	0.15	0.12	-0.04	-0.10
A1101+41		3.3	22.1	* 0.16	0.10	0.02	-0.11
UGC 6436	W	3.3	11.2	0.16	0.04	-0.01	-0.04
NGC 4418		0.7	4.4	0.12	0.08	-0.06	-0.12
IC 860		1.3	8.3	0.12	0.09	-0.06	-0.14
NGC 5257		2.2	14.5	0.14	0.11	-0.04	-0.08
Mrk 273		3.7	24.3	* 0.18	0.19	0.07	-0.09
UGC 8739		1.7	10.9	* 0.29	0.18	0.07	-0.07
UGC 9618	N	3.3	21.6	* 0.26	0.12	0.07	-0.05
I ZW 107		3.9	25.7	0.12	0.09	0.03	-0.10
ARP 220		1.8	6.0	* 0.28	0.14	0.10	-0.14
MCG+0142088		2.3	15.1	0.17	0.09	0.00	-0.03
NGC 6286		3.6	12.0	* 0.20	0.16	0.03	-0.11
ZW 453.062		2.4	15.7	* 0.17	0.12	0.00	-0.09
ZW 475.056		2.7	29.2	* 0.16	0.15	0.05	-0.15
NGC 7674		2.8	30.8	* 0.22	0.16	0.18	-0.14
NGC 7771		1.4	15.5	* 0.19	0.15	0.01	-0.10
Mrk 331		1.7	11.5	0.15	0.09	-0.02	-0.06

[a] The beam position in the source; refer to the notes to Table I.

[b] D_1 and D_2 are the inner and outer diameters, respectively, of the annulus used to calculate the colors of the disk; the units are kiloparsecs at the source.

[c] A * preceding the color measurements indicates a source for which the error ellipses for the nuclear and disk colors do *not* overlap; for these sources the nuclear and disk colors are clearly distinct.

TABLE III – LUMINOSITIES WITHIN FIXED PHYSICAL DIAMETERS

NAME[a]	POS[b]	$L_\nu(2.2\mu m)_{2\ kpc}$ [c] / $L_\odot$	$L_\nu(2.2\mu m)_{2\ kpc}$ [d] / $L_\nu(2.2\mu m)_{10\ kpc}$	AGN[e]	NAME[a]	POS[b]	$L_\nu(2.2\mu m)_{2\ kpc}$ [c] / $L_\odot$	$L_\nu(2.2\mu m)_{2\ kpc}$ [d] / $L_\nu(2.2\mu m)_{10\ kpc}$	AGN[e]
NGC 34		9.99	0.70	VV/2	Mrk 231		11.23	0.77	VV/Q
MCG–02-01-051	S	9.47	0.44		NGC 4922	SW	9.73	0.36	
	N	8.72	0.13		IC 860		9.17		
MCG–03-04-014		9.89	0.33		UGC 8335	NW	9.43	0.41	
NGC 695		9.79	0.29			SE	9.73	0.52	
NGC 958		9.60	0.19		NGC 5256	SW	9.65		
NGC 1068		10.27		VV/1		NE	9.52		
UGC 2238		9.67	0.45		NGC 5257		9.27	0.19	
UGC 2369	N	9.67	0.30		UGC 8739		9.41	0.27	
	S	9.54	0.38		ZW 247.020		9.64	0.53	
UGC 2982		9.53	0.28		IRAS 14348–1447†	SW	9.66		S88
MCG–03-12-002	N	9.60	0.32			NE	9.45		S88
NGC 1614		9.94	0.52		IRAS 15250+3609†		9.50	0.37	S88
IRAS 05189–2524†		10.66		S88	Arp 220		9.72	0.43	VV/2
NGC 2623		9.63	0.61		MCG+01-42-088		9.72	0.39	
IRAS 08572+3915†		9.70	0.51	S88	NGC 6286		9.59	0.28	
UGC 5101†		10.22	0.92	S88	MCG–03-57-017		9.75		
MGC+08-18-012		9.65	0.59		NGC 7469		10.31	0.66	VV/1
NGC 3110		9.48	0.26		ZW 453.062		9.48	0.38	
A1101+41		9.60	0.37		ZW 475.056		9.87	0.46	
UGC 6436	W	9.57	0.32		NGC 7674		10.00	0.42	VV/2
NGC 3690		9.57			NGC 7771		9.73	0.24	
IRAS 12112+0305†		9.43		S88	Mrk 331		9.90	0.53	
NGC 4418		8.90							

[a] A † indicates sources for which the data from Carico *et al.* (1990) were used in calculated $L_\nu(2.2\mu m)_{2\ kpc}$ and $L_\nu(2.2\mu m)_{2\ kpc}/L_\nu(2.2\mu m)_{10\ kpc}$.

[b] The beam position in the source; refer to the notes to Table I.

[c] The 2.2 μm luminosity emitted from a region about the nucleus 2 kpc in diameter (see text).

[d] The ratio of the luminosities emitted from regions about the nucleus 2 kpc in diameter and 10 kpc in diameter (see text).

[e] Sources listed in Véron–Cetty and Véron (1989) as Seyfert 1 (VV/1), Seyfert 2 (VV/2), or a quasar (VV/Q), or identified by Sanders *et al.* (1988) as having an AGN (S88).

Chapter FOUR:

The Near–Infrared Morphology of Ultraluminous Infrared Galaxies

This article has previously appeared in
the *Astrophysical Journal (Letters)*, Vol. **349**, p.L39 (1990).
Coauthors: J.R. Graham, K. Matthews, T.D. Wilson,
B.T. Soifer, G. Neugebauer, and D.B. Sanders.

ABSTRACT

Near–infrared images at 1.25 μm, 1.65 μm, and 2.2 μm have been obtained of nine galaxies from the IRAS Bright Galaxy Sample with infrared luminosities $L_{IR} \geq 10^{12}\ L_{\odot}$. Two of the 2.2 μm images reveal previously undetected double nuclei, increasing the number of close double nuclei known for this sample from two to four. For three of these four sources, the colors of *both* nuclei are substantially different from those of normal spiral galaxies, indicating that the high activity state in high luminosity mergers tends to occur in both nuclei. Three sources show 2.2 μm emission that is more centrally concentrated than the emission at 1.3 μm, a result that can be explained as the effects of dust emission and/or extinction, or alternatively, as the result of direct emission at 2.2 μm from the accretion disk of a central active galactic nucleus. Implications of these results for the model that galaxy collisions lead to quasar formation are briefly discussed. Finally, from the frequency and separation of the double nucleus sources, the lifetime of the ultraluminous phase of galaxies is estimated to be $\sim\ 4 \times 10^8$ years.

Subject headings: galaxies: interactions – galaxies: nuclei – infrared: general – quasars

I. INTRODUCTION

The most luminous galaxies from the IRAS Bright Galaxy Sample (Soifer *et al.* 1989) are the "ultraluminous" infrared galaxies with infrared luminosities† $L_{IR} \geq 10^{12}\ L_{\odot}$. Sanders *et al.* (1988, hereafter S88) made an extensive study of the ultraluminous galaxies, and have presented a model in which these galaxies represent a phase in the formation of quasars. This *Letter* presents near–infrared images of nine of the ten ultraluminous infrared galaxies studied by S88. These are the first high–resolution images available of the nuclei of these galaxies at infrared wavelengths, and since these objects are known to be heavily obscured by dust, it is clear that knowledge of their infrared morphologies is essential to an understanding of their nature.

II. OBSERVATIONS

The images were obtained using a near–infrared camera at the Cassegrain focus of the 200 inch Hale telescope at the Palomar Observatory. The camera uses a 58 × 62 array of InSb photodiodes held to a temperature of 32 K, and has a scale of $0.31''\ pixel^{-1}$ at the f/70 Cassegrain focus, giving a field–of–view approximately 19″ square. The images were all obtained between October 1988 and July 1989 in both photometric and non–photometric conditions. The 2.2 μm seeing ranged from 0.8″ to 2.5″, with a mean of $\sim$ 1.3″. Broad–band 1.25 μm (J), 1.65 μm (H), and 2.2 μm (K) filters were used, with typical integration times between 30 and 120 seconds, depending primarily on radiation background (the ambient temperature). In all cases, sky subtraction was achieved by imaging the sky near the source immediately after the source was observed. Most of the objects were imaged more than once, and for those cases the multiple images were coadded by aligning the centroids of the brightest 2.2 μm peak. The galaxies observed are listed in Table I.

III. RESULTS

Contour maps of the 2.2 μm images are shown in Figure 1, and magnitudes for 2.5″ and 5″ diameter beams are given in Table I. The 5″ photometry is from S88. The 2.5″ magnitudes were calculated from the sky–subtracted images shown in Figure 1, and were calibrated by defining the flux

† L_{IR} is an estimate of the integrated luminosity between 8 and 1000 μm; see Sanders *et al.* 1988.

in a 5″ diameter beam, reconstructed in software on each image, to be that measured by S88 for that source. Hence the *difference* in flux between the 2.5″ and 5″ diameter beams is given directly by the images. The near–infrared colors are plotted in Figure 2.

A brief discussion is now given of those sources for which the near–infrared images are significantly different than the visible images. Note that frequent reference is made to the visible wavelength images which were presented by S88.

IRAS 05189–2524 – This source has a single nucleus at visible wavelengths with faint tails, and was identified by S88 as possibly a nearly completed merger. The 2.2 μm image also shows a single nucleus, with near–infrared colors which do not change significantly with beam size. There is an apparent elongation in the northwest(NW)–southeast(SE) direction, not seen in the visible image, with a full–width at half–maximum (FWHM) of 1.9″, compared to 1.0″ in the orthogonal direction. Stellar images taken during the night of observation appear circular, suggesting that this elongation is a genuine feature of the galaxy; however, an effect this small requires further confirmation.

IRAS 08572+3915 – The visible image shows two galaxies of roughly comparable brightness separated by ~6″ (6 kpc at the source). The 2.2 μm image also shows both galaxies, but the NW source appears much brighter than the SE source; the color differences between the two nuclei are $\Delta(J - H) = 0.45 \pm 0.1$ mag and $\Delta(H - K) = 1.15 \pm 0.4\ mag$. The SE nucleus has colors significantly redder than those expected for a "normal" galaxy, with a ~0.4 mag excess at K. The NW source shows the most extreme $H - K$ color of any source in this sample, a fact representative of its extremely unusual near–infrared energy distribution (see Carico *et al.* 1988); furthermore, this nucleus is more compact at 2.2 μm than at 1.3 μm, as evidenced by the change in near–infrared colors with beam diameter (see Figure 2). Note however that the 10″ diameter beam presumably contains emission from both nuclei.

UGC 5101 – The visible image shows a nearby companion ~50″ to the west, and considerable tidal structure. The 2.2 μm image shows a single nucleus (the companion is well outside of the field–of–view of the image) which is more compact at 2.2 μm than at 1.3 μm, as seen in a color difference of almost 0.5 mag in $H - K$ between the 2.5″ and 10″ diameter beams (see Figure 2).

IRAS 12112+0305 – The visible image is dominated by a single bright nucleus; there appears to be a second, much fainter nucleus about 6″ (~9 kpc) south, and the morphology is highly distorted at low light levels. The 2.2 μm image does not show this faint nucleus, but does show two clearly distinct nuclei separated by 3″ (4 kpc). These nuclei are roughly similar in their near–infrared colors, both being considerably redder than normal galaxies.

IRAS 14348–1447 – The visible image shows two nuclei, separated by ~3.5″ (6 kpc), with extended tidal structure. In the 2.2 μm image, the two nuclei are more clearly delineated, presumably due to the improved resolution of the near–infrared images. The nuclei have similar near–infrared colors, both being considerably redder than normal galaxies.

Arp 220 – The visible image shows extended tidal structure, and two apparent peaks separated by ~7″ (2.6 kpc); the dominant visible peak is to the north. The infrared peak is located roughly midway between the visible peaks (Joy *et al.* 1986), and is extended in the E–W direction, with a FWHM in that direction of ~2″ (0.7 kpc). No evidence is seen at 2.2 μm for the second visible peak, adding further support to the interpretation of this peak as an effect of a dust lane in the galaxy. Also, the 2.2 μm emission is more centrally concentrated than the 1.3 μm emission, as seen in the color change between the 2.5″ and 10″ diameter beams (see Figure 2); this fact was noted earlier by Neugebauer *et al.* (1987).

IRAS 22491–1808 – This galaxy is the only one of the galaxies studied by S88 with an HII region spectrum rather than that of an active galactic nucleus (AGN). The visible image shows tidal tails, but only a single nucleus, whereas the 2.2 μm image clearly shows two distinct nuclei, separated by ~1.6″ (2.5 kpc). The near–infrared colors of the two nuclei are similar to those of normal galaxies, with evidence for a small amount of reddening.

IV. DISCUSSION

The 2.2 μm emission in these systems is a combination of reddened starlight, thermal emission by hot dust, and possibly direct emission by the accretion disk of the dust enshrouded AGN. As is clear from the energy distributions of these objects presented by S88, the relative contributions of these components varies significantly from source to source.

Three of the galaxies – *IRAS 05189–2524*, *Mrk 231*, and *Arp 220* – were classified by S88 as probably completed mergers, based on the presence of tidal tails extending from a single nucleus. Neither *IRAS 05189–2524* nor *Mrk 231* show any clear evidence for more than one nucleus at 2.2 μm either, adding further support for the hypothesis that these mergers are essentially complete. However, for *Arp 220* the 2.2 μm peak seen in Figure 1 is clearly extended, and recent higher resolution images have succeeded in resolving this feature into two distinct 2.2 μm peaks, which may indicate a double nucleus for this source (Graham *et al.* 1989).

The colors in Table I and Figure 2 show a clear increase in the central concentration of the 2.2 μm emission relative to that at 1.3 μm for three of the sources – *IRAS 08572+3915*, *UGC 5101*, and *Arp 220*. There are three possible causes for this effect: (1) Extinction from dust in the central 1 – 2 kpc would deplete the observed 1.3 μm emission relative to the 2.2 μm emission. (2) Emission from dust in the interstellar medium within the central 1 – 2 kpc can contribute at 2.2 μm. The dust would have to be extremely hot, or the emission dominated by fluctuations in small grains. (3) It is possible that direct 2.2 μm emission from the accretion disk of the AGN is being seen at the smallest radii (cf. Phinney 1989; Sanders *et al.* 1989).

In three of the four sources which show double nuclei at 2.2 μm – *IRAS 08572+3915*, *IRAS 12112+0305*, and *IRAS 14348-1447* – the near–infrared colors of *both* nuclei exhibit unusually red energy distributions at near–infrared wavelengths. Thus the formation of an ultraluminous infrared galaxy appears to be generally a process of the collision of two galaxies wherein both galaxy nuclei undergo a high activity phase. This result should be contrasted with the result for more widely separated interacting galaxies, where typically only one member of the pair shows unusual infrared colors (Joseph *et al.* 1984). In the fourth double–nucleus source, *IRAS 22491-1808*, the near–infrared colors in a 5″ diameter beam were known to be only slightly redder than those of normal galaxies (S88), and the present analysis shows that both nuclei have essentially normal colors.

The results of these observations have several implications which are relevant to the model proposed by S88 that the ultraluminous IRAS galaxies represent a stage in the formation of a quasar.

First of all, the strongest evidence for galaxy collisions is the presence of close double nuclei. With the current results, the number of close double nuclei in the ultraluminous galaxies has been increased to four, and ultimately five (referring to the results mentioned above for Arp 220 from Graham *et al.* 1989). Secondly, the fact that three of the four confirmed double–nucleus sources have excessively red near–infrared colors in *both* nuclei implies a high gas/dust content in both nuclei, which is what was hypothesized in the statement of the theory by S88. Finally, the increased compactness of the 2.2 μm emission relative to the 1.3 μm emission in *IRAS 08572+3915*, *UGC 5101*, and *Arp 220* suggests an increase in the concentration of gas and dust with decreasing radius in these sources, which may be evidence for the funneling of molecular gas into the nuclear regions as a result of the dissipation of orbital angular momentum, as required by the galaxy collision model.

From the frequency of double nuclei in the current sample one can estimate crudely the lifetime of the ultraluminous phase of infrared bright galaxies. The starting point is the assumption that the ultraluminous galaxies represent snapshots at different stages of an evolutionary sequence, in which two galaxies undergo a collisional interaction. Then, if there is no change in luminosity with time during the ultraluminous phase (there is certainly no obvious ordering of luminosity with the double nuclei or single nuclei in Table I, and in any case the range in luminosity in Table I is only a factor of ~ 3), the fraction of the sources in a particular phase is proportional to the lifetime of the sources in that phase. The four double–nucleus sources of Figure 1 represent roughly half of all the ultraluminous infrared galaxies in the IRAS Bright Galaxy Sample, a complete, flux limited sample. The remaining ultraluminous galaxies in this sample appear to be either completely merged, as with the single–nucleus sources, or in a post–collision phase, as with the galaxies with nearby companions seen in the visible wavelength images in S88. This suggests that the lifetimes of the pre–merged and post–merged (or post–collision) phases of the ultraluminous stage are roughly the same.

One can get an order of magnitude estimate of the lifetime for the pre–merged phase from the average separations. N–body simulations indicate that a reasonable approximation for the time scale for orbital decay of two merging nuclei from dynamical friction is given by $t_{dyn} \sim \frac{M}{m}\ x\ t_{orb}$, where M and

m are the masses of the nuclei, M referring to the more massive of the two, and t_{orb} is the orbital period (Phinney, private communication). The average separation of the nuclei in the current sample (projected onto the plane of the sky) is $\sim$ 4.5 kpc, so that a typical orbital velocity of 300 $km\ s^{-1}$ gives $t_{orb} \sim 10^8$ years. One can then assume that M/m is equal to the ratio of observed fluxes of the two nuclei at 1.65 μm, where the stellar continuum from the nuclei presumably dominates. For the four double nuclei in this sample, the ratios of the 1.65 μm flux densities lie in the range $1 - 3$. Using $M/m \sim 2$, one then obtains $t_{dyn} \sim 2x10^8$ years, which gives a total lifetime for the ultraluminous infrared galaxy phase of $\sim 4x10^8$ yrs.

If this estimate for the lifetime of the ultraluminous infrared phase in galaxies is accepted, and if one adopts the model proposed by S88 that such systems evolve into quasars, it is possible to make an order of magnitude estimate of the lifetime of quasars. Sanders *et al.* (1989) show that the space density of the ultraluminous infrared galaxy phase essentially equals or slightly exceeds that of the optically selected quasars at the same bolometric luminosity. Thus the lifetime of the quasar phase roughly equals that of the ultraluminous phase, i.e., $t_{qso} \sim 4x10^8$yrs. This estimate is the same as the Eddington lifetime of such objects (see, e.g., Rees 1984).

ACKNOWLEDGEMENTS

We thank the night assistants at the Hale telescope, J. Carasco and S. Staples, and the entire staff at Palomar Observatory. S. Lin made substantial contributions to the construction of the near infrared camera and V. Heron wrote most of the data acquisition software for the camera. Discussions with S. Phinney and W. Sargent were most helpful, as were the suggestions provided by the referee, G. Wynn–Williams. Ground–based infraredastronomy at Caltech is supported by a grant from the NSF.

REFERENCES

Carico, D.P., D.B. Sanders, B.T. Soifer, J.H. Elias, K. Matthews, and G. Neugebauer, 1988. The *IRAS* Bright Galaxy Sample. III. $1 - 10$ μm observations and coadded *IRAS* data for galaxies with $L_{IR} \geq 10^{11}$ $L_{\odot}$, *Astronom. J.*, **95**, 356 (Chapter 2 of this thesis).

Graham, J.R., D.P. Carico, K. Matthews, G. Neugebauer, and B.T. Soifer, 1989. The double nucleus of Arp 220 unveiled, *Astrophys. J. (Letters)*, **354**, L5.

Joseph, R.D., W. Meikle, N.A. Robertson, and G.S. Wright, 1984. Recent star formation in interacting galaxies. I. Evidence from JHKL photometry, *Mon. Not. R. Astron. Soc.*, **209**, 111.

Joy, M., D.F. Lester, P.M. Harvey, and M. Frueh, 1986. *Astrophys. J.*, **307**, 110.

Neugebauer, G., J. Elias, K. Matthews, J. McGill, N.Z. Scoville, and B.T. Soifer, 1987. High spatial resolution, near–infrared observations of Arp 220, *Astron.J.*, **93**, 1057.

Phinney, E.S., 1989. Dusty disks and the infrared emission from AGN, in *Theory of Accretion Disks*, W. Duschl, F. Meyer, and J. Frank (Eds.), Kluwer, Dordrecht, p. 457.

Rees, M.J. 1984, *Ann. Rev. Astron. Astrophys.*, **22**, 471.

Sanders, D.B., E.S. Phinney, G. Neugebauer, B.T. Soifer, K. Matthews, and R.F. Green, 1989. Continuum energy distributions of quasars: shapes and origins, *Astrophys. J.*, **347**, 29.

Sanders, D.B., B.T. Soifer, J.H. Elias, B.F. Madore, K. Matthews, G. Neugebauer, and N.Z. Scoville, 1988. Ultraluminous infrared galaxies and the origin of quasars, *Astrophys. J.*, **325**, 74 (S88).

Soifer, B.T., L. Boehmer, G. Neugebauer, and D.B. Sanders, 1989. The *IRAS* Bright Galaxy Sample. IV. Complete *IRAS* observations, *Astronom. J.*, **98**, 766.

FIGURE CAPTIONS

Fig. 1: Images at 2.2 μm of nine ultraluminous infrared galaxies listed in Table I. In all plots, north is towards the top of the figure, east is to the left. The horizontal bars in the upper left corner of each plot represent an angular distance of 2″; the contours are logarithmic with a factor of $\sqrt{2}$ between levels.

Fig. 2: The near–infrared colors of the ultraluminous galaxies. Two of the sources which show essentially no change in near–infrared colors with beam size – *IRAS 05189–2524* and *IRAS 15250+3609* – have been left out to simplify the figure. The smallest circles represent the colors measured from the near–infrared images using a 2.5″ diameter "beam" (see text); the mid–sized and largest circles are the colors obtained from Sanders *et al.* (1988) using their 5″ and 10″ diameter beam measurements, respectively. Lines connect the colors for each source determined from the various beam sizes. For sources with two nuclei, colors corresponding to the brightest nucleus are connected with a solid line, and those corresponding to the fainter nucleus are connected with a dashed line. Note that the larger diameter beams encompass *both* nuclei in *IRAS 12112+0305*, *IRAS 14348-1447*, and *IRAS 22491-1808*, but only the brighter (NW) nucleus in *IRAS 08572+3915*.

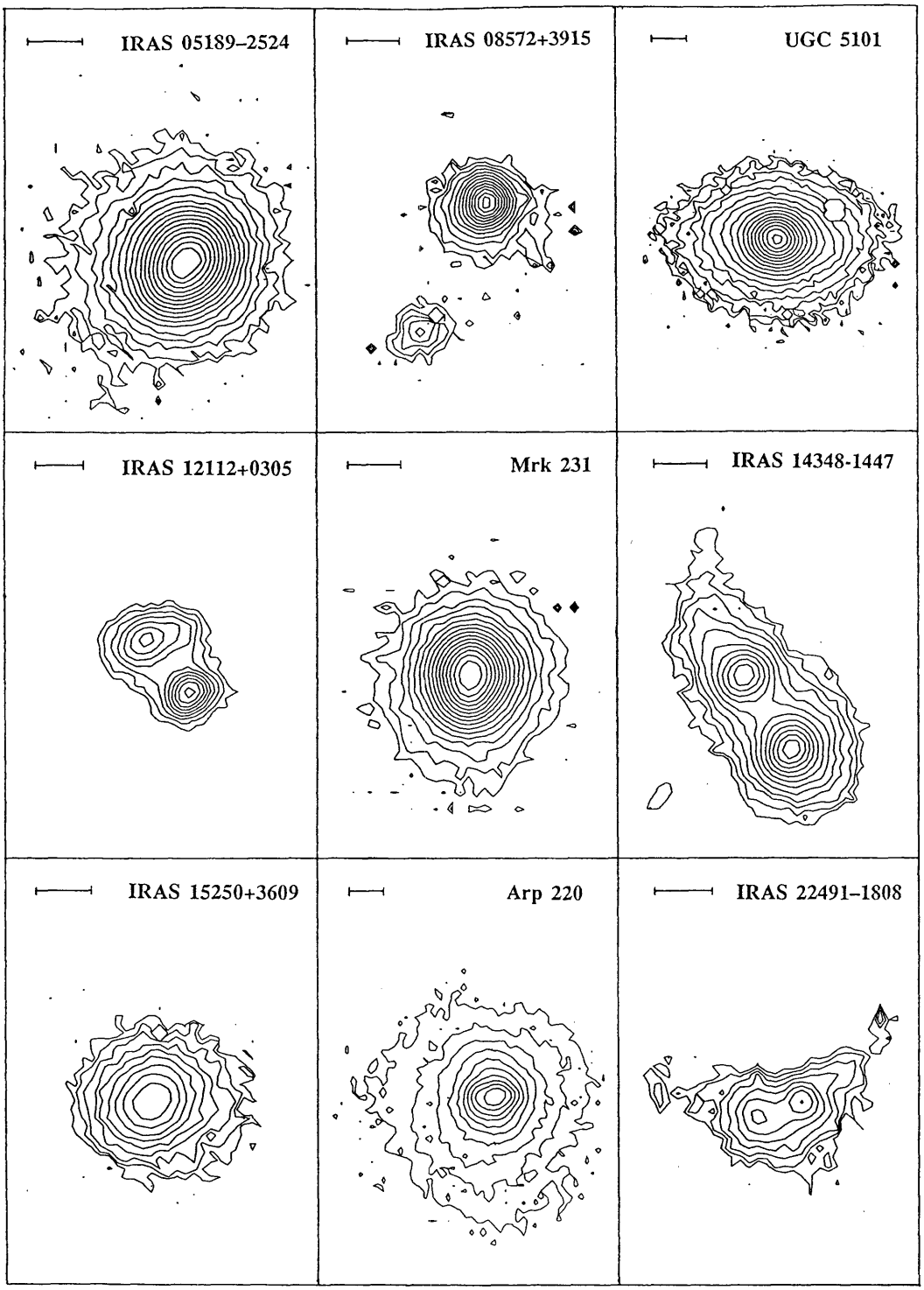
IRAS 05189-2524
IRAS 08572+3915
UGC 5101
IRAS 12112+0305
Mrk 231
IRAS 14348-1447
IRAS 15250+3609
Arp 220
IRAS 22491-1808

Fig. 1

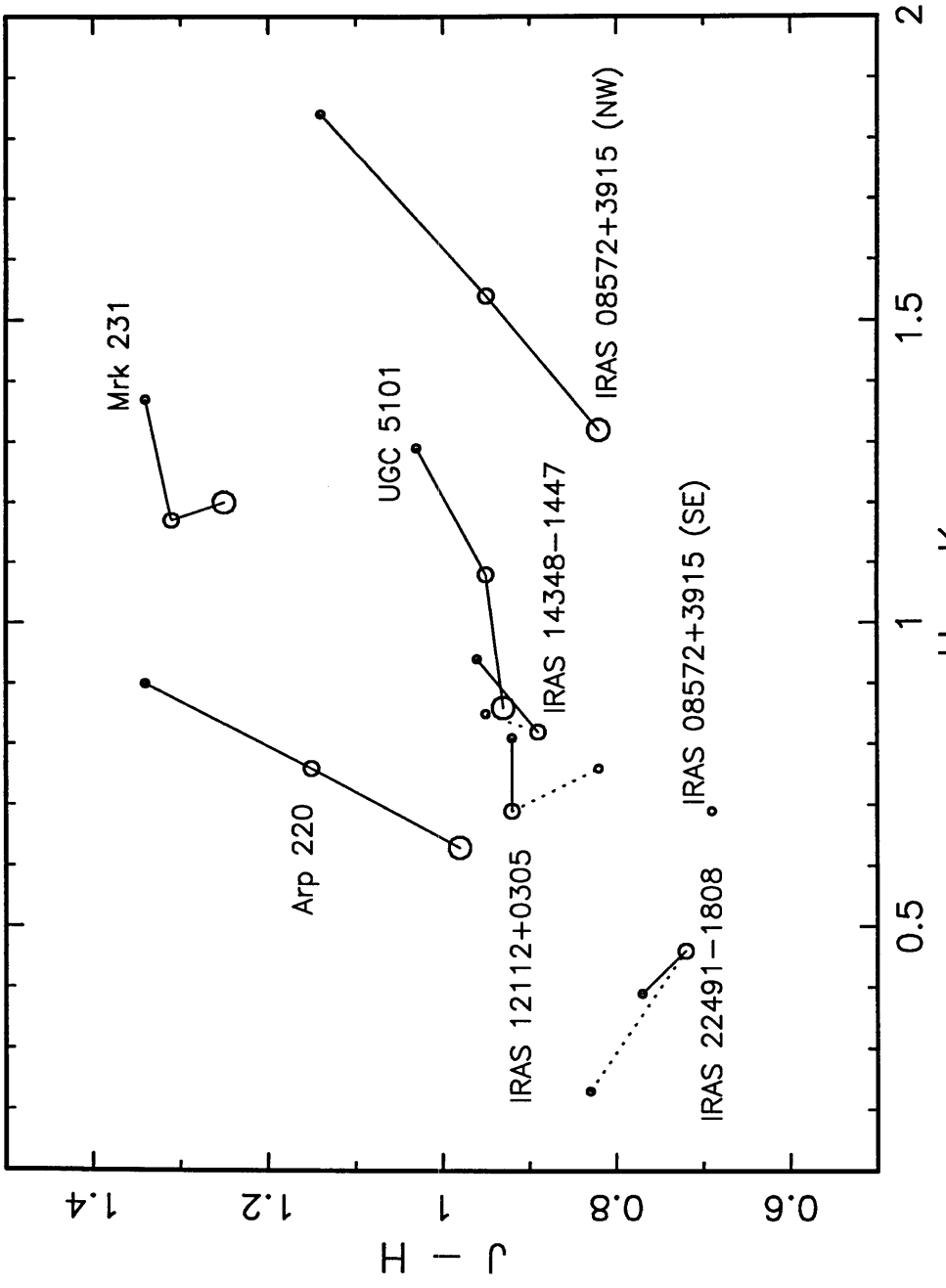
J − H
H − K
0.6
0.8
1
1.2
1.4
0.5
1
1.5
2
Mrk 231
UGC 5101
IRAS 08572+3915 (NW)
IRAS 14348−1447
IRAS 08572+3915 (SE)
Arp 220
IRAS 12112+0305
IRAS 22491−1808

Fig. 2

TABLE I

Object Name	$Log[L_{IR}/L_{\odot}]$	Separation Between Nuclei (kpc)	Position[a]	Beam Diameter (″)	Near Infrared Colors[b] (mag) K	H–K	J–H
IRAS 05189–2524	12.10	<1.6		5.0	10.22	1.23	1.27
				2.5	10.55	1.26	1.33
IRAS 08572+3915	12.09	6.3	NW	5.0	13.11	1.54	0.95
				2.5	13.29	1.84	1.14
			SE	2.5	15.52	0.69	0.69
UGC 5101	12.01	<0.6		5.0	11.13	1.08	0.95
				2.5	11.57	1.29	1.03
IRAS 12112+0305	12.29	4.0	MID	5.0	13.25	0.69	0.92
			SW	2.5	14.21	0.81	0.92
			NE	2.5	14.42	0.76	0.82
Mrk 231	12.52	<1.0		5.0	8.87	1.17	1.31
				2.5	9.12	1.37	1.34
IRAS 14348–1447	12.29	5.3	MID	5.0	13.27	0.82	0.89
			SW	2.5	13.75	0.94	0.96
			NE	2.5	14.29	0.85	0.95
IRAS 15250+3609	12.00	<2.0		5.0	13.05	0.52	0.76
				2.5	13.70	0.64	0.74
Arp 220	12.19	<0.7		5.0	11.18	0.76	1.15
				2.5	11.80	0.90	1.34
IRAS 22491–1808	12.13	2.4	MID	5.0	13.55	0.46	0.72
			W	1.9	14.97	0.39	0.77
			E	1.9	15.07	0.23	0.83

[a] The position of the beam relative to the two nuclei for sources with a double–nucleus. "MID" refers to a position midway between the two nuclei, encompassing both; all other designations refer to a position centered on the indicated nucleus.

[b] Uncertainties in the 2.5″ photometry are $\sim$ 0.07 mag, except for the southeast nucleus of IRAS08572+3915 for which the uncertainty at K is $\sim$ 0.4 mag. The data for a 5″ diameter beam are from Sanders *et al.* (1988).

Chapter FIVE:

The Temperature Distribution of Dust in Infrared Galaxies

ABSTRACT

A method has been developed for deriving the distributions of dust mass and luminosity as a function of the dust temperature from measurements of the thermal dust emission. Newly reported measurements at 1.25 mm and previously published near–infrared data are then utilized to apply the method to a sample of 25 high–luminosity galaxies selected from the IRAS Bright Galaxy Sample. It is shown that estimates of the mass of cold dust are severely dependent upon the assumed long–wavelength spectral index for the absorption efficiency, $Q(\lambda)$, where $Q \propto \lambda^{-\beta}$. From the 1.25 mm measurements, it is found that $\beta \gtrsim 1$ for luminous infrared galaxies, from which it is determined that *all of the galaxies are consistent with no detectable emission from cold dust*, provided a suitable value of β is adopted from the range $1 \lesssim \beta \lesssim 2$. On the other hand, for most of the galaxies (70% of those studied), a value of $\beta = 2$ results in an upper limit to the total mass of cold dust which is roughly an order–of–magnitude greater than the mass of dust estimated from a single–temperature fit to the *IRAS* 60 μm and 100 μm measurements. Thus, *for most of the galaxies the measurements are also consistent with a mass of cold dust which completely dominates the entire mass of dust in the galaxy.*

At higher temperatures, the dust mass varies with temperature approximately as a power–law, $M(T) \propto T^{-\alpha}$, over a range of temperatures from ~30 K up to more than 1000 K. Values of α range from a minimum of 5.1 to a maximum of 6.7; however, for ~70% of the galaxies studied, $6 \leq \alpha \leq 6.5$ Emission from hot dust is found to provide a significant contribution to the energy budget of luminous infrared galaxies: At dust temperatures 100 K above the temperature corresponding to the peak in the energy distribution, the luminosity from the dust is generally 10 – 30% of the luminosity at the peak temperature; for most of the galaxies, this contribution drops to only a few percent at temperatures 300 K above the peak temperature, but for 25% of those studied the contribution is still significant, at the level of 10 – 20% of the peak luminosity. This contribution to the luminosity from hot dust is seen clearly in the difference between the far–infrared luminosity estimated from the IRAS 60 μm and 100 μm measurements, and the dust luminosity integrated over the entire relevent temperature range. It

is found that the far–infrared luminosity under–estimates the total luminosity from dust by typically 20%, although for some sources this difference is as high as 50%.

I. INTRODUCTION

The infrared emission from most[1] galaxies is thought to be dominated by thermal emission from "dust" at wavelengths between a few microns (μm) and roughly 1000 μm. In this context, "dust" refers to particles with linear dimensions ranging from a few tens of angstroms up to $0.1 - 0.2$ μm, presumably of graphite and/or silicate composition, which are found in HII regions and planetary nebulae, circumstellar shells, molecular clouds, and throughout the interstellar medium, particularly in regions of enhanced star formation. These dust grains preferentially absorb visible and ultra–violet (UV) energy from the incident radiation field, and are thereby heated to a steady–state temperature which is determined by the balance between the energy absorbed and the thermal energy lost through radiation by the grains.[2] The temperature of an individual dust grain thus depends on its environment through the intensity of the incident radiation field. A lower limit of a few $(10 - 20)$ degrees Kelvin can be adopted for any dust grain, this being a typical steady–state temperature appropriate for a quiescent region of the interstellar medium (Draine and Lee 1984). Also, a maximum dust grain temperature of $1500 - 2000$ K can be determined based on the sublimation properties of typical astrophysical grain materials (Watson and Salpeter 1972; Salpeter 1974). Hence, for *any* dust grain, the spectrum of its own thermal radiation will peak somewhere between a few microns and roughly 1 mm – that is, at infrared wavelengths. Since, as stated before, the energy of the incident radiation is generally primarily at visible and UV wavelengths, the net effect of the presence of dust in an astropysical environment is a "re–distribution" of the intrinisic luminosity, from comparatively high–energy, optical and UV photons, to lower energy infrared photons.

Because of this re–distribution of energy due to dust grains, the far–infrared luminosity, L_{FIR}, or more directly, the ratio of the luminosity at far–infrared wavelengths to that at visible wavelengths, L_{FIR}/L_{VIS}, can be used to infer the presence of significant quantities of dust. In the most extreme

[1] Galaxies with quasar–like nuclei may have infrared emission which is dominated by non–thermal emission. See, e.g., Weedman (1986); Edelson and Malkan (1986).

[2] Gas–grain collisions may also play a role in regions of very dense gas, but this process will not be considered in this analysis.

cases, an entire galaxy's bolometric luminosity can be dominated by dust emission at far–infrared wavelengths. For these sources, an understanding of the nature and distribution of the dust is clearly of critical importance.

As mentioned previously, dust grains have been observed in a wide range of astrophysical environments, from regions characterized by high–intensity radiation fields, such as HII regions and areas of high–density star formation, to regions of relatively low–intensity radiation fields, such as quiescent molecular clouds and the general interstellar medium. This wide range of environments suggests a wide range of steady–state temperatures of the dust in these differing regions, and hence a wide range of temperatures contributing to the observed infrared emission from any given galaxy. In fact, many galaxies have far–infrared energy distributions which can be approximated quite well by a single dust temperature, enabling a simplified analysis of the typical radiation intensities within those galaxies and reasonable estimates of their total dust masses. However, no galaxy has an infrared energy distribution which can be even approximately modeled by a single dust temperature over the entire range of relevent wavelengths, and even at far–infrared wavelengths, many galaxies have energy distributions which are sufficiently broad to require a range of dust temperatures for any meaningful analysis.

This chapter presents a method for determining the distribution of dust mass as a function of temperature. The method is then applied to a selection of galaxies from the *IRAS* Bright Galaxy Sample (Soifer *et al.* 1989; hereafter referred to as the BG Sample). This sample is a complete, flux–limited, infrared selected sample of 313 galaxies. It thus contains a high percentage of galaxies which are distinguishable by their high ratio of infrared to visible luminosities, and is ideally suited to a study of dust emission from galaxies. Section II presents a brief discussion of the relevent physics underlying the temperature distribution analysis. Section III then details the numerical solution. In Section IV, the sources for the various infrared data are discussed, and in Section V the results of the temperature distribution analysis are presented and discussed.

II. THE ANALYTIC SOLUTION

(i.e., The Basic Physics)

II.1 Statement of the problem

Consider a cloud of dust grains, each grain being at a temperature T, where T may vary throughout the cloud. We wish to determine the thermal emission from the cloud, as a function of both the wavelength of the emission and the temperature of the individual dust grains, measured by an observer at a distance d, where d is much greater than the linear dimensions of the cloud. The detailed calculation would require knowledge of not only the properties of the individual dust grains and the variations in those properties from one grain to the next, but also the spatial distribution of the dust grains within the cloud, and the shape and extent of the cloud. Such a calculation is clearly impossible within the current analysis, since none of these factors is known with any accuracy for any of the galaxies being studied; all of the available data represent mean properties, generally averaged over an entire galaxy. Hence, the following two fundamental simplifying assumptions will be made, in order to establish a tractable problem:

Assumption 1: All of the dust grains are "seen," unobscured, by the observer; that is, the absorption of the radiation from the individual dust grains by the other grains in the cloud is negligible.

Assumption 2: The dust grains are spherical and small compared to the wavelength of radiation.

Since the thermal emission from the grains is at infrared wavelengths, and since, as will be shown later in this section, the absorption efficiency for the grains decreases with increasing wavelength, *Assumption 1* is probably reasonable for most of the galaxies in the BG Sample, in that there is simply not enough dust in the galaxies to absorb an appreciable amount of the infrared radiation coming from within the galaxy. However, there are almost certainly exceptions to this; in particular, *Arp 220* and *NGC 4418*, have both been measured to have significant internal extinction well into the infrared (Becklin and Wynn–Williams 1987; Roche *et al.* 1986).

Assumption 2 is almost certainly incorrect, in that there is no evidence that astrophysical dust grains should be expected to be spherical. Nevertheless, this is a common assumption in studies of dust emission, and the degree to which it may affect the results will be discussed further below (Section II.2.2).

Consider, therefore, a spherical dust grain at temperature T, with an effective cross–section $\sigma_{em}(\lambda)$ for emission of radiation of wavelength λ. Then, the power, P_ν^g, radiated by the grain at wavelength λ, per frequency interval, is given by[3]

$$P_\nu^g(\lambda, T) = 4\pi\sigma_{em}(\lambda)B_\nu(\lambda, T), \tag{2}$$

where $B_\nu(\lambda, T)$ is the Planck function describing thermal radiation, and it has been assumed that the grain emits isotropically at all wavelengths. Let the number of dust grains as a function of temperature be $N_T(T)$; that is, $N_T(T)dT$ is the number of dust grains with temperatures between T and $T + dT$. Then, the total power per frequency interval at wavelength λ emitted by the entire dust cloud is simply

$$P_\nu(\lambda) = \int_T P_\nu^g(\lambda, T)N_T(T)dT = 4\pi\sigma_{em}(\lambda)\int_T B_\nu(\lambda, T)N_T(T)dT. \tag{3}$$

Hence, the flux of radiation per frequency interval at wavelength λ (referred to as the flux density), measured by the observer at a distance d is

$$f_\nu(\lambda) = \frac{P_\nu(\lambda)}{4\pi d^2} = \frac{1}{d^2}\sigma_{em}(\lambda)\int_T B_\nu(\lambda, T)N_T(T)dT. \tag{4}$$

It is a well–known result that the effective cross–section for emission of light of a particular frequency is equal to the effective cross–section for absorption at that same frequency (a result known as *Kirchoff's law*; see Bohren and Huffman 1983, p. 125); one is thus free to treat σ_{em} and the corresponding absorption cross–section interchangeably, and dispense with the subscripts. Furthermore, as will be demonstrated shortly, it is convenient to define an *absorption efficiency per unit area*, $Q(\lambda)$,

[3] Note that $B_\nu(\lambda, T)$ and $P_\nu^g(\lambda, T)$ are both functions of *wavelength*, but expressed per unit *frequency* interval. This somewhat unfortunate mixture of wavelength and frequency will be used throughout this analysis in order to coincide with standard convention. In infrared astronomy, the *energy* of the observed radiation is generally quoted in terms of wavelength in microns, whereas the *amount* of radiation is quoted in Janskies, which is power per unit area per unit *frequency* interval.

defined to be the absorption cross–section for radiation of wavelength λ, divided by the geometrical cross–section of the grain. Thus, for spherical grains of radius a,

$$Q(\lambda) \equiv \frac{\sigma(\lambda)}{\pi a^2}.$$

Eq. (4) then becomes

$$f_\nu(\lambda) = \pi \left(\frac{a}{d}\right)^2 Q(\lambda) \int_T B_\nu(\lambda, T) N_T(T) dT. \tag{5}$$

Note that, in keeping with the simplified nature of this analysis, the temperature dependence of $Q(\lambda)$ has been ignored (see Bohren and Huffman 1983, p. 281, for a discussion of the possible effects of temperature on $Q(\lambda)$).

Eq. (5) can be put into a somewhat more interesting form by replacing $N_T(T)$ with the total *mass* of dust per degree, $M_T(T)$ (the *mass density*), given by

$$M_T(T) = m_g N_T(T) = \frac{4}{3}\pi a^3 \rho N_T(T), \tag{6}$$

where m_g is the mass per dust grain, and ρ is the mean mass density of the grain material. Then,

$$\begin{aligned} f_\nu(\lambda) &= \pi \left(\frac{a}{d}\right)^2 Q(\lambda) \int_T B_\nu(\lambda, T) \left(\frac{3}{4\pi a^3 \rho} M_T(T)\right) dT \\ &= \frac{1}{d^2} \left(\frac{3Q(\lambda)}{4a\rho}\right) \int_T B_\nu(\lambda, T) M_T(T) dT, \end{aligned} \tag{7}$$

The ultimate intent of the analysis is to solve this equation for $M_T(T)$, given a set of measurements of the energy distribution, $f_\nu(\lambda)$. However, before any such solution can be obtained, a form for the absorption efficiency, $Q(\lambda)$, must be adopted. This is almost certainly the source of the greatest uncertainty in the entire analysis, and hence a discussion will now be given of the theoretical considerations behind a determination of $Q(\lambda)$, and the related empirical evidence. The discussion will, of necessity, be brief; the reader is referred to Bohren and Huffman (1983), or van de Hulst (1957), for a more complete discussion of this material.

II.2 Determination of the absorption efficiency

II.2.1 Theoretical considerations

The calculation of an analytic expression for the absorption efficiency, $Q(\lambda)$, for an arbitrary

irregularly shaped grain is quite complicated, and, although some intriguing approximation methods have been developed (Purcell and Pennypacker 1973; Pollack and Cuzzi 1980; Wright 1987), no general theory exists. However, for the case of a uniform sphere, exact solutions can be obtained for the absorption efficiency of the grain as a function of the dielectric properties of the grain material, using what is commonly known as Mie theory (Mie 1908; see also Bohren and Huffman 1983, p. 82, or van de Hulst 1957, p. 114). Then the problem of obtaining accurate numerical values for $Q(\lambda)$ becomes a problem of understanding sufficiently well the dielectric properties of that material. The case for a uniform sphere will be presented here, subject to the condition that the size of the sphere is much smaller than the wavelength of the radiation ("Rayleigh scattering") – a condition which is expected to be satisfied for infrared emission from astrophysical dust grains. However, it should be kept in mind that the degree to which astronomers have traditionally adopted the spherical dust grain model and applied it, virtually unquestioningly, to so many astrophysical situations, is almost certainly more justifiable from an aesthetic perspective than a scientific one; hence, a discussion of the possible limitations of this model will also be presented (Section II.2.2.1).

For a sphere of radius a, in the approximation that a is much smaller than the wavelength of the radiation, Mie theory gives

$$Q = \frac{8\pi a}{\lambda} Im\left\{\frac{\epsilon - 1}{\epsilon + 2}\right\} = \frac{4a\omega}{c} Im\left\{\frac{\epsilon(\omega) - 1}{\epsilon(\omega) + 2}\right\}, \tag{8}$$

for the absorption efficiency of the sphere. $\epsilon(\omega) = \epsilon'(\omega) + i\epsilon''(\omega)$ is the complex dielectric function (or relative permittivity) of the material of which the grain is composed, and λ has been written in terms of the angular frequency, $\omega = 2\pi c/\lambda$, to simplify the equations that follow. In terms of ϵ' and ϵ'', Eq. (8) becomes

$$\begin{aligned} Q(\omega) &= \frac{4a\omega}{c} Im\left\{\frac{[\epsilon'(\omega) - 1] + i\epsilon''(\omega)}{[\epsilon'(\omega) + 2] + i\epsilon''(\omega)}\right\} \\ &= \frac{12a\omega}{c} \frac{\epsilon''(\omega)}{[\epsilon'(\omega) + 2]^2 + [\epsilon''(\omega)]^2}. \end{aligned} \tag{9}$$

To obtain an estimate of the dielectric function for the grain material, a standard approach is to use the so–called *Lorentz model*, which basically treats the solid as a collection of simple harmonic

oscillators, each with resonant frequency ω_o. This model gives quite good results (one might even say surprisingly good, given the simplicity of the premise) for a number of *crystalline* materials. The resulting dielectric function is given by

$$\epsilon'(\omega) = 1 + \frac{\omega_p^2(\omega_o^2 - \omega^2)}{(\omega_o^2 - \omega^2)^2 + \gamma^2\omega^2} \tag{10a}$$

$$\epsilon''(\omega) = \frac{\gamma\omega_p^2\omega}{(\omega_o^2 - \omega^2)^2 + \gamma^2\omega^2}, \tag{10b}$$

where ω_p is the plasma frequency of the material, and γ is a parameter expressing the "damping" of the oscillators.[4] In the long–wavelength limit, that is for ω much less than the resonance frequency ω_o,

$$\epsilon' \approx 1 + \frac{\omega_p^2}{\omega_o^2} \tag{11a}$$

$$\epsilon'' \approx \frac{\gamma\omega_p^2\omega}{\omega_o^4}. \tag{11b}$$

Plugging these into Eq. (9),

$$Q(\omega) = \frac{12a\gamma}{c} \frac{\omega_p^2\,\omega^2}{(\omega_p^2 + 3)^2 + \gamma^2\left(\frac{\omega_p}{\omega_o}\right)^4\omega^2}. \tag{12}$$

Then, as $\omega \to 0$,

$$Q(\lambda) \to \frac{48\pi^2 ac\gamma\omega_p^2}{(\omega_p^2 + 3)^2}\,\lambda^{-2},$$

and hence

$$Q(\lambda) \propto \frac{a}{\lambda^2}. \tag{13}$$

For conducting spheres, one need only set $\omega_o = 0$ in Eq. (10), which is equivalent to removing the "springs" from the electronic oscillator. The result is the *Drude model*:

$$\epsilon' = 1 - \frac{\omega_p^2}{\omega^2 + \gamma^2} \tag{14a}$$

[4] It is comforting to note that the results of the Lorentz model, although strictly classical, are formally identical to those obtained from quantum mechanics. However, one should recognize that the interpretation of the quantities ω_o and γ is quite different. In the quantum mechanical treatment, ω_o becomes ω_{ij}, where $\hbar\omega_{ij}$ is the transition energy between the initial and final states, and γ becomes γ_j, which is a measure of the transition probabilities to other quantum states. See Bohren and Huffman (1983), p. 232, or Heitler (1954).

$$\epsilon'' = \frac{\omega_p^2 \gamma}{\omega(\omega^2 + \gamma^2)} \tag{14b}$$

Plugging these into Eq. (9),

$$Q(\lambda) = \frac{12a\gamma}{c} \frac{\omega_p^2(\omega^2 + \gamma^2)\omega^2}{\omega^2[3(\omega^2 + \gamma^2) - \omega_p^2]^2 + \omega_p^4\gamma^2}, \tag{15}$$

which, in the long–wavelength limit, gives

$$Q \rightarrow \frac{12a\gamma}{c} \frac{\omega^2}{\omega_p^2} \propto \frac{a}{\lambda^2}. \tag{16}$$

Eqs. (13) and (16) contain two important results, the first being that $Q(\lambda)$ is proportional to the grain size, a, and the second that $Q(\lambda)$ goes as λ^{-2} at long wavelengths. However, the validity of both of these results depends on the degree to which the assumptions which went into the derivation of $Q(\lambda)$ are valid for astrophysical dust grains. These assumptions are:

(1) the grain is *spherical*

(2) the grain material is *crystalline*

(3) the absorption properties of the small grain are well–approximated by those of the *bulk* grain material.

The importance of the result that $Q \propto a$ can be immediately seen from Eq. (7): Since the only place that a appears in the equation is through the ratio $Q(\lambda)/a$, it is this result that effectively removes a as a parameter in the problem, and enables the solution by the current methods. Hence, throughout the remainder of the analysis, it will be *assumed* that the grain–size dependence of $Q(\lambda)$ is not strongly effected by the above assumptions. Although this approach is motivated primarily by the need to maintain a tractable problem, it is not expected that any variation of the grain–size dependence of $Q(\lambda)$ would be severe enough to greatly effect the results which will be presented (see Draine and Lee 1984).

In contrast, the long–wavelength dependence of $Q(\lambda)$ can have a critical effect on the results of the analysis. Hence, the validity of the above assumptions will now be discussed in the context of the predicted λ^{-2} dependence of $Q(\lambda)$ at long wavelengths.

II.2.2 The absorption efficiency at long wavelengths

II.2.2.1 Variations of the theory

It is often stated that theory predicts a λ^{-2} dependence for $Q(\lambda)$ at long wavelengths, based on the results presented in Eqs. (13) and (16). However, if one steps beyond the constraints imposed by the assumptions presented in the previous section, the "theoretical prediction" can be quite different. As an example, consider the first assumption, that the grains are spherical. Various studies have shown that, *even in the Rayleigh limit*, the shape of a particle can have a strong effect on its absorption properties. Bohren and Huffman (1983) have calculated the absorption efficiency for a distribution of small ellipsoidal aluminum particles, and found a roughly λ^{-1} dependence, as compared to the λ^{-2} dependence obtained when the particles are treated as spheres. Also, Wright (1987) has shown that if conducting spheres are randomly aggregated into various irregular shapes, the resulting "fractal grains" have absorption efficiencies with long–wavelength spectral indices given by $0.4 < \beta < 1.6$.

One way in which grain shape can severely effect the absorption efficiency is through the interaction of light with the *surface* of the grain. The development of Eq. (9) assumes that the size of the particle is large enough that edge effects can be ignored (this is the third assumption given above). However, if the particle is sufficiently small, that is if the surface–to–volume ratio for the grain is sufficiently large, such effects can become significant, and even dominant. These effects are generally described by "surface modes," which depend on the shape of the grain; hence, a *small, non–spherical* grain can have an absorption efficiency which is quite different from that of the parent material. Hence, *from considerations of grain shape alone*, the "λ^{-2} law" need not necessarily apply to actual dust grains; rather, from the analytic results mentioned in the previous paragraph, an absorption efficiency with $\beta < 2$ at long wavelengths may be favored.

As another example, consider the second assumption, that the grain material is crystalline – that is, that it has regular periodic lattice structure. There is considerable evidence that amorphous (non–crystalline) materials may be a significant element in astrophysical dust (see, e.g., Whittet 1988, and references therein). For such materials, the Lorentz and/or Drude models do not apply, and other

methods must be adopted. Schlömann (1964) developed such a method for treating the optical properties of amorphous materials, and Seki and Yamamoto (1980) have utilized this model to determine the absorption efficiency for amorphous interstellar grains. They find that, for spherical grains with radii $a \gtrsim 100$ Å, the λ^{-2} wavelength dependence of $Q(\lambda)$ is reproduced by the amorphous grains; however, for smaller grains, $Q(\lambda)$ approaches a λ^{-1} wavelength dependence. Tielens and Allamandola (1987) have presented a lucid discussion of the physical basis for a predicted $Q \propto \lambda^{-1}$ relation in certain amorphous grains.

Finally, Aannestad (1975) has shown that the presence of an ice mantel can significantly effect the far–infrared absorption efficiency of dust grains. He compared uncoated silicate grains to grains containing a silicate core with an ice mantle, and found that the presence of the ice mantle changed the "normal" λ^{-2} dependence of $Q(\lambda)$ to a λ^{-3} dependence at wavelengths longer than 100 μm.

It is thus clear that *only in the simplest case does theory predict a λ^{-2} dependence for $Q(\lambda)$ at long wavelengths*. Once slightly more realistic conditions are imposed, the calculations can yield a whole range of values for β. Given this fact, the empirical determinations of β are of critical importance, and some of these determinations will now be discussed.

II.2.2.2 Empirical considerations

Numerous attempts have been made to estimate the far–infrared absorption efficiency of astrophysical dust grains and, in contrast to Eqs. (13) and (16), the results tend to favor values of $\beta < 2$. This is generally attributed to the effects of amorphous structure in the grains, although, as mentioned in the previous section, grain shape can have a similar effect.

As examples of determinations of β based on astrophysical sources, one has the observations of the evolved infrared star *IRC+10216* by Campbell *et al.* (1976), from which they find $\beta \sim 1$; observations of the Galactic center at wavelengths out to 100 μm by Gatley *et al.* (1977), from which the authors also find $\beta \sim 1$; sub–millimeter and millimeter measurements of compact HII regions by Gear, Robson, and Griffin (1988), who find find $\beta \sim 0.7 - 1.3$ for $350\mu m \leq \lambda \leq 800\mu m$, and $\beta \sim 1.0 - 2.6$ for

$800\mu m \leq \lambda \leq 1100\mu m$; and the sub–millimeter measurements presented by Sopka *et al.* (1985) of evolved stars, from which they estimate $\beta \sim 1.2$.

In addition, laboratory measurements of small amorphous silicate particles by Day (1976) and small amorphous graphite particles by Koike, Hasegawa, and Manabe (1980), have both yielded values of $\beta \sim 1$.

Not all empirical estimates of $Q(\lambda)$ result in $\beta \sim 1$, however. As already mentioned, the measurements of HII regions by Gear, Robson, and Griffin (1988) include some sources for which $\beta > 2$. Also, Schwartz (1982) studied three molecular clouds at millimeter wavelengths with the specific intent of determining the long–wavelength absorption efficiency for the dust in these clouds, and found $\beta \sim 2.2 - 2.6$ for all three sources.

It is clear from both the theoretical and empirical considerations, that values of β given by $1 \lesssim \beta \lesssim 3$ can be expected for astrophysical dust grains. The preponderance of evidence suggests that, although individual sources exist in which the dust grains are best characterized by $\beta > 2$, it is probable that, on the scale of an entire galaxy, $\beta < 2$ is appropriate. A discussion of the analytic form of $Q(\lambda)$ actually used for the current analysis is deferred to Section III.4.

II.3 The luminosity as a function of temperature

Once $M_T(T)$ has been obtained from Eq. (8), another quantity of interest can be derived. Given a sufficient number of measurements at different wavelengths to enable a reasonable estimate of the entire infrared energy distribution, one can integrate Eq. (8) over frequency (note that the integration is *not* over wavelength, since the flux density is defined per unit frequency) to obtain the infrared luminosity, L_{IR}:

$$\begin{aligned} L_{IR} &= 4\pi d^2 \int_{\nu,IR} f_\nu(\nu) d\nu \\ &= 4\pi d^2 \int_{\nu,IR} \frac{1}{d^2} \left(\frac{3Q(\nu)}{4a\rho} \right) \int_T B_\nu(\nu,T) M_T(T) dT d\nu. \end{aligned} \tag{17}$$

Reversing the order of integration,

$$L_{IR} = 4\pi d^2 \int_T \left\{ \frac{1}{d^2} M_T(T) \int_{\nu,IR} \frac{3Q(\nu)}{4a\rho} B_\nu(\nu,T) d\nu \right\} dT,$$

$$= 4\pi d^2 \int_T f_T(T) dT, \tag{18}$$

where

$$f_T(T) \equiv \frac{1}{d^2} M_T(T) \int_{\nu,IR} \frac{3Q(\nu)}{4a\rho} B_\nu(\nu,T) d\nu. \tag{19}$$

$f_T(T)$ is the observed flux of energy per degree of dust grain temperature. Multiplying this by $4\pi d^2$, one obtains

$$L_T(T) \equiv 4\pi d^2 f_T(T) = 4\pi M_T(T) \int_{\nu,IR} \frac{3Q(\nu)}{4a\rho} B_\nu(\nu,T) d\nu. \tag{20}$$

$L_T(T)$ is effectively the bolometric luminosity of the dust cloud per interval of dust grain temperature T, and is exactly analogous to the more commonly used quantity $L_\nu(\nu) = 4\pi d^2 f_\nu(\nu)$; that is,

$$L_{IR} = \int_\nu L_\nu(\nu) d\nu = \int_T L_T(T) dT.$$

However, unlike L_ν, L_T provides *direct* information on the physical properites within the source by showing in what proportion the dust grains at different temperatures contribute to the total energy output of the source.

As was shown in Section II.2, the wavelength dependence of the absorption efficiency of astrophysical dust grains at sufficiently long wavelengths is expected to go as $Q(\lambda) \propto \lambda^{-\beta}$, where $1 \lesssim \beta \lesssim 2$. If one is willing to adopt this form for $Q(\lambda)$ over the entire range of infrared wavelengths, Eq. (19) can be considerably simplified. Although this approach was *not* taken in the current analysis (see Section III.4), the result is worth presenting in that it provides an extremely simple and fairly accurate means of calculating $L_T(T)$ from $M_T(T)$.

Following Hildebrand (1983), one can write

$$Q(\lambda) = Q_{250} \left(\frac{250}{\lambda_{\mu m}} \right)^\beta = Q_{250} \left(\frac{250}{c_{\mu m}} \right)^\beta \nu^\beta, \tag{21}$$

where $Q_{250} = Q(250\mu m)$, $\lambda_{\mu m}$ is the wavelength measured in μm, and $c_{\mu m}$ is the speed of light measured in microns per second. Then,

$$L_T(T) = 4\pi M_T(T) \int_{\nu,IR} \left[\frac{3Q_{250}}{4a\rho} \left(\frac{250}{c_{\mu m}} \right)^{\beta} \nu^{\beta} \right] B_\nu(\nu, T) d\nu,$$

$$= 4\pi \left(\frac{3Q_{250}}{4a\rho} \right) \left(\frac{250}{c_{\mu m}} \right)^{\beta} M_T(T) \int_{\nu,IR} \nu^{\beta} B_\nu(\nu, T) d\nu. \tag{22}$$

Since the Planck function at the relevent dust temperatures is negligible for frequencies outside of the infrared range, one can treat the integral as ranging over all positive frequencies, enabling it to be solved analytically:

$$\int_0^\infty \nu^{\beta} B_\nu(\nu, T) d\nu = \frac{2h}{c^2} \int_0^\infty \frac{\nu^{\beta+3} d\nu}{e^{\frac{h\nu}{kT}} - 1}$$

$$= \frac{2h}{c^2} \left(\frac{k}{h} \right)^{\beta+4} T^{\beta+4} \int_0^\infty \frac{u^{\beta+3} du}{e^u - 1} \qquad \left(u \equiv \frac{h\nu}{kT} \right)$$

$$= \frac{2h}{c^2} \left(\frac{k}{h} \right)^{\beta+4} T^{\beta+4} \, \Gamma(\beta+4) \left[1 + \frac{1}{2^{\beta+4}} + \frac{1}{3^{\beta+4}} + \ldots \right].$$

Thus, Eq. (15) becomes

$$L_T(T) = \frac{8\pi h}{c^2} \left(\frac{k}{h} \right)^{\beta+4} \Gamma(\beta+4) \left[1 + \frac{1}{2^{\beta+3}} + \frac{1}{3^{\beta+3}} + \ldots \right] \left(\frac{250}{c_{\mu m}} \right)^{\beta} \left(\frac{3Q_{250}}{4a\rho} \right) M_T(T) T^{\beta+4}. \tag{23}$$

Normalizing the absorption efficiency as

$$\frac{3Q_{250}}{4a\rho} = 10 \ cm^2/g, \tag{24}$$

obtained empirically by Hildebrand (1983) for $a = 0.1 \ \mu m$ and $\rho = 3 \ g \ cm^{-3}$, one obtains the following numerical expressions for $L_T(T)$ as a function of $M_T(T)$ and T:

$$\underline{\text{For } \beta = 1}: \qquad L_T(T) = 8.02 \times 10^9 \left(\frac{3Q_{250}/4a\rho}{10 cm^2/g} \right) \left(\frac{M_T(T)}{10^6 M_\odot} \right) \left(\frac{T}{40K} \right)^5 \ L_\odot \tag{25a}$$

$$\underline{\text{For } \beta = 2}: \qquad L_T(T) = 2.73 \times 10^{10} \left(\frac{3Q_{250}/4a\rho}{10 cm^2/g} \right) \left(\frac{M_T(T)}{10^6 M_\odot} \right) \left(\frac{T}{40K} \right)^6 \ L_\odot \tag{25b}$$

III. THE NUMERICAL SOLUTION

Eq. (8) is of the form

$$f(x) = \int \xi(x, y) g(y) dy, \tag{25}$$

and can thus be identified as an inhomogenous Fredholm equation of the first kind. There tends to be comparatively little attention given to equations of this form in most standard references on integral equations, the reason presumably being that the Fredholm equation of the first kind is, in general, an *ill–posed problem* – that is, its solution may not exist and, if it exists, may not be unique. However, Pajot *et al.* (1986) have shown that, if the kernel in Eq. (25) is of the form

$$\theta(x,y) \propto \frac{y^n}{(e^y - 1)},$$

then a unique solution does exist. Hence, if one adopts the standard power–law form for $Q(\lambda)$ (or if one is willing to assume that Q is sufficiently close in form to a power–law that thorny mathematical details can be ignored), it is safe to conclude that a unique solution to Eq. (25), and hence to Eq. (8), exists and one can use a standard least–squares approach to obtain $M_T(T)$. Numerically, one uses the method of least–squares to minimize the quantity

$$\Phi \equiv \sum_i \left\{ f(x_i) - \sum_j \xi(x_i, y_j) g(y_j) \Delta y_j \right\}^2 ,$$

where the $f(x_i)$ are the measured quantities, $g(y_j)$ are free parameters, and the form of $\xi(x_i, y_j)$ is assumed known from theoretical and/or empircal considerations. This is what has been used to produce the results presented throughout the rest of this paper. The method, which will now be presented in detail, is similar to that discussed previously by Pajot *et al.*

III.1 Determining the relevent wavelengths

The range of wavelengths appropriate for the study of thermal emission from astrophysical dust grains in a particular galaxy is limited by two factors: (1) the temperatures of the dust grains, and (2) contamination from other sources of emission. These considerations will now be discussed in their relation to the determination of the long– and short–wavelength limits appropriate for the current analysis.

In determining the long–wavelength limit, one must consider the coldest grain temperatures which, in a galaxy, are those determined by the general interstellar radiation field, far from any localized heating source. The results of Draine and Lee (1984) for such a case give grain temperatures $T \sim 10$ –

20 K, depending on grain size and composition; similar results were obtained by Mathis, Mezger, and Panagia (1983). Thus, significant dust emission is not expected beyond wavelengths of a few hundred microns. Furthermore, it will be assumed throughout this analysis that, for infrared selected galaxies, any non–thermal emission which may dominate the energy distributions at radio wavelengths is negligible in comparison to the dust emission for wavelengths less than about 1 mm. Hence, $\lambda \sim 1$ mm will be taken as an appropriate long–wavelength limit.

The appropriate short wavelength limit is somewhat more complicated to determine. It is known that dust emission cannot contribute at indefinitely short wavelengths since, at sufficiently high temperatures, dust grains are destroyed by evaporation. Although the temperature above which this begins to occur is not accurately known for astrophysical dust grains (see, e.g., Fadeyev (1987) for a discussion of the relevent physics), values commonly adopted throughout the literature are 1000 – 2000 K (as determined, for example, from modeling of circumstellar dust shells; see, e.g., Bode 1988. Also, Watson and Salpeter 1972; Salpeter 1974); in any case, it is generally accepted that dust grains can be heated to a high enough temperature to emit at near–infrared wavelengths. However, for wavelengths less than a few microns, the emission from most galaxies is dominated by stars (see, e.g., Aaronson 1977), making the determination of the emission attributable to dust at the shortest infrared wavelengths uncertain at best.

There is another consideration which provides an even more severe complication for many galaxies, namely, the now well established contribution to the near– and mid–infrared emission from dust grains which are small enough so as to be susceptible to extreme temperature fluctuations resulting from single–photon absorption events (see, e.g., Draine and Anderson 1985). These small grains are generally attributed to various types of polycyclic aromatic hydrocarbon molecules (PAHs; see Allamandola, Tielens, and Barker 1989, for a comprehensive up–to–date review of this rapidly expanding field of research), although other possibilities exist (see Donn, Allen, and Khanna 1989, and references therein). In any case, they have characteristic sizes on the order of a few angstroms up to a few tens of angstroms, and are believed to populate a wide range of astrophysical environments. Their small size

results in a very low heat capacity, which precludes their maintaining a steady state temperature; instead, they fluctuate between a temperature of perhaps a few degrees kelvin and a few hundred degrees. In order to include the emission from such grains in the current analysis, one would have to separate out the contributions at each wavelength from the "small" dust grains and the "large" dust grains, where the distinction between "small" and "large" is the grain size for which the method used to determine $Q(\lambda)$ for the largest grains fails to apply. However, even if this were possible, the correct form of $Q(\lambda)$ for the "small" grains is not well understood (see Désert, Boulanger, and Puget 1990, for the current state of our understanding of the absorption properties of PAHs).

Rather than attempt such an analysis of the contribution from single–photon heating, the problem has basically been ignored herein by recognizing that, *if* the emission from this heating process is dominant in some source, it is *primarily* dominant at the shorter wavelengths ($\lambda \lesssim 30\ \mu m$); then, although an analysis at short wavelengths would not be appropriate for that source, the results based on the far–infrared emission should remain reliable. The only problem, then, is that of determining for which sources this heating process produces the short wavelength emission. A good educated guess of the solution to this problem can be found in the work of Helou (1986), who showed that such emission is evidenced by an increase in the ratio of the *IRAS* 12 μm emission to the 25 μm emission, $f_\nu(12\mu m)/f_\nu(25\mu m)$, which in turn is coupled with a decrease in the ratio of the 60 μm emission to the 100 μm emission, $f_\nu(60\mu m)/f_\nu(100\mu m)$. The idea is that the single–photon heating process results in a thermal continuum which peaks between 1 and 10 μm; this continuum is seen in a galaxy [resulting in a large value of $f_\nu(12\mu m)/f_\nu(25\mu m)$] to the extent that the steady–state thermal emission is cold enough that its contribution at short wavelengths is negligible [resulting in a small value of $f_\nu(60\mu m)/f_\nu(100\mu m)$].

The relevent point behind this idea is that galaxies whose infrared emission contains a significant contribution from the single–photon heating process show energy distributions characterized by two separate components, one which peaks at near– to mid–infrared wavelengths, the other which peaks at far–infrared wavelengths. Evidence for these two–components is most easily seen in the shape of the

distribution in the $\sim 10 - 50\ \mu m$ wavelength range, and can be read from the *IRAS* 12 μm, 25 μm, and 60 μm flux densities: If both components are present, the distribution, which is falling between 60 μm and 25 μm, will begin to flatten between 25 μm and 12 μm; otherwise, the distribution will show a constant or increasing slope in going from 60 μm to 25 μm to 12 μm. Another way of stating this is that an indication that a contribution from single–photon heating is significant at the shorter wavelengths is that the *spectral curvature*, defined to be $\alpha_{12,25} - \alpha_{25,60}$, is less than zero, where $\alpha_{\lambda_1,\lambda_2}$ is defined by the relation

$$\frac{f_\nu(\lambda_1)}{f_\nu(\lambda_2)} = \left(\frac{\lambda_1}{\lambda_2}\right)^{\alpha_{\lambda_1,\lambda_2}} .$$

Based on the above considerations, the appropriate short–wavelength limit for the galaxies in this analysis will be taken as 12 μm *unless* the spectral curvature $\alpha_{12,25} - \alpha_{25,60} \leq 0$, in which case available near–infrared data will be considered.

III.2 Interpolating between the available data

In order for a meaningful solution to the temperature inversion to exist, the number of points known in the energy distribution must exceed the number of unknown temperatures. Thus, if one were to insist that the *only* information available on the energy distributions are the flux densities at the measured wavelengths, then the number of temperatures for which Eq. (26) could be solved would be severely limited; for the current sample, the number of appropriate infrared measurements is at most 7, and in many cases is only 5.

This approach, however, would be neglecting an additional source of information – namely, the assumption that the infrared emission is thermal. This assumption translates into a starting premise which states that, *regardless of what emission/absorption features may exist in the galaxy's infrared spectrum, there is validity to the consideration of an underlying, smooth continuum which can be modelled with thermal emission curves (Planck curves) over some set of temperatures.* Once this premise has been assumed, a considerable source of new information about the galaxies' continuum emission has been provided. For example, consider a galaxy for which the flux densities at 25 μm, 60 μm, and 100 μm are all close to a single temperature Planck curve (many galaxies in the BG

Sample satisfy this criterion). Then, *the very fact that one is modelling the emission with Planck curves constrains the flux densities at all wavelengths between 25 μm and 100 μm to an accuracy which is almost equal to that of the actual measurements.*

In a more general sense, the assumption of thermal emission constrains the underlying continuum to be smooth – that is, at least as broad everywhere as a corresponding Planck curve. Since, for all of the galaxies in the current analysis, the wavelength spacings between adjacent measured flux densities are comparable to or smaller than the "width" of a Planck curve, large oscillations in the thermal continuum are not possible; hence, *any* smooth, continuous fit to the available data points should provide a fairly good estimate of the emission at any relevent wavelength.

For the current analysis, the available data points were fit with a smooth curve using a "canned" cubic–spline curve–fitting routine.[5] Then, a set of $n = 20$ wavelengths, equally spaced logarithmically between the shortest and longest available wavelengths, was chosen and, for each wavelength, the curve–fit to the data was used to estimate the emission at that wavelength.

III.3 Determining the temperatures for the analysis

A minimum and maximum for the temperatures to be used in the analysis was selected for each galaxy so as to be consistent with the maximum and minimum wavelengths being used. This temperature range was then divided into $m - 1$ logarithmically equal intervals, giving a total of m temperatures to be used in the temperature inversion, where, to enable a solution by the least–squares method, $m < n$.

Generally, it is desirable to have m as small as possible. For one thing, the necessary computing time goes up rapidly with m. Also, as m approaches n, the program begins to be unstable; the reason for this is that, given the relatively broad shape of the Planck curves as a function of wavelength and the continuous nature of $Q(\lambda)$, if the temperatures are too close together, the program will begin to improve on the least–squares criterion artificially by invoking arbitrarily large weighting factors, which

[5] The IMSL library routine ICSSCU was used.

are consequently "fine–tuned" with comparably large negative values, the result being an unphysical distribution of dust mass with temperature.

For most galaxies, a value of $m = 7$ was found to work well, but as few as five temperatures were employed in some cases.

III.4 The form of the absorption efficiency

The theoretical and empirical considerations in establishing the appropriate form for $Q(\lambda)$ were discussed in Section II.2. There it was shown that, for the simplified approximation considered in this analysis, $Q(\lambda) \propto \lambda^{-\beta}$. The values of β were seen to range anywhere between roughly 1 and 3, but it was suggested that $1 \lesssim \beta \lesssim 2$ was probably appropriate when averaged over an entire galaxy. Motivated by these results, and the calculations presented by Draine and Lee (1984) for graphite and silicate grains, a value of $\beta = 1$ was adopted for wavelengths less than 50 μm. For wavelengths longer than 50 μm, an additional factor had to be considered, namely the decision that, for purposes of the current analysis, a single absorption efficiency law should be adopted for *all* of the galaxies, so as to enable direct comparison of the results for different galaxies. With this criterion, the form for $Q(\lambda)$ was essentially set by the 1.25 mm measurements for a sample of the Bright Galaxies presented in Section V.1. For this sample, lower limits for β range between 1.3 and 2.0. To accomodate all of the galaxies with the same absorption efficiency, the largest limit was required; hence, the adopted form for the absorption efficieny is

$$Q(\lambda) = \begin{cases} Q_{250}\left(\dfrac{250}{\lambda_{\mu m}}\right)^2, & \text{for } \lambda \geq 50\mu m. \\ 5 \cdot Q_{250}\left(\dfrac{250}{\lambda_{\mu m}}\right), & \text{for } \lambda < 50\mu m. \end{cases} \tag{28}$$

III.5 Obtaining the initial temperature distribution

The equivalent form of Eq. (8) for purposes of numerical calculation is

$$f_\nu(\lambda_i) = \frac{1}{d^2}\left(\frac{3Q(\lambda_i)}{4a\rho}\right)\sum_{j=1}^{m} B_\nu(\lambda_i, T_j) M_T(T_j)\Delta T_j, \qquad i = 1, 2, \ldots, n. \tag{26}$$

After obtaining values of $f_\nu(\lambda)$ for each galaxy (see Section IV), as well as luminosity distances, d, from Soifer *et al.* (1987), Eq. (26) was solved, using a standard least–squares fitting routine,[6] to obtain $M_T(T)$ at m different temperatures over an appropriate temperature range (see Section III.3).

III.6 Obtaining the smoothed temperature distribution

The intent of this analysis is to obtain an estimate of the continuous mass density function $M_T(T)$, where M_T is defined so that the total mass of dust, M_d, is given by

$$M_d = \int_T M_T(T)dT. \tag{29}$$

Throughout the following discussion, this *continuous* function $M_T(T)$ will be referred to as the *true* function, denoted $M_T(T)$, or simply M_T. To avoid confusion, the numerical approximation to $M_T(T)$ will be denoted $M_T(T_j)$.

As discussed in Section III.3, the number of temperatures, m, used in obtaining $M_T(T_j)$ from Eq. (26) was at most 7, and as low as 5. However, if one is willing to make the reasonable assumption that, when averaged over an entire galaxy, the amount of dust plotted as a function of temperature is smooth and continuous,[7] one can interpolate between the values of $M_T(T_j)$ obtained from the solution to Eq. (26) to find $M_T(T_j)$ for *any* temperature, within the available temperature range. This was done for each galaxy by fitting a cubic–spline curve to the values of $M_T(T_j)$,[8] and then using this curve to identify the values of $M_T(T_j)$ at any desired temperature.

Unfortunately, a problem develops when one proceeds in this way. Although the original approximation $M_T(T_j)$ may provide a good fit to the energy distribution when used in Eq. (26), one finds that, in general, the *smoothed* $M_T(T_j)$ function (e.g., that obtained by interpolating between the original $M_T(T_j)$ values) will *not* provide as good a fit to the energy distribution. To see the reason for

[6] The subroutine GRIDLS from Bevington (1969) was used.

[7] This assumption is obviously a corollary to the assumption of a smooth energy distribution discussed in Section III.2, and hence its validity depends upon the same reasoning presented in that section.

[8] The IMSL library routine ICSSCU was used.

this, consider that, if one had *a priori* knowledge of the true function M_T from which the values of $M_T(T_j)$ could be determined, one could reproduce each $f_\nu(\lambda_i)$ to any desired accuracy by choosing a small enough temperature interval ΔT_j, and summing over a very large number of closely spaced temperatures T_j in Eq. (26), so as to approximate the integral in Eq. (8) with sufficient accuracy. However, if one were to then use the same function M_T with only a few temperatures, and hence fairly large values for the ΔT_j, the summation in Eq. (26) would give a comparatively poor approximation to the integral in Eq. (8), and hence a poor approximation to the energy distribution would result. In a sense, the reverse situation holds in this analysis. One *starts* with a comparatively crude approximation to the integral to obtain each flux density *to the desired accuracy.* Then, when $M_T(T_j)$ is smoothed, the resulting values of $f_\nu(\lambda_i)$ are changed and no longer provide as good an approximation to the real data.

To deal with this problem, a spline–curve was fit to the initial values of $M_T(T_j)$, and the resulting energy distribution generated from the smoothed M_T function was compared to the original measured flux densities. At wavelengths where the computed energy distribution did not reproduce the measured flux densities, the computed values of $M_T(T_j)$ at the appropriate temperatures were adjusted. A spline–curve was then fit to the adjust values of $M_T(T_j)$, a new energy distribution was generated, and this was compared to the flux densities at the measured wavelengths. If necessary, further adjustments were made in the appropriate $M_T(T_j)$ values, and this process was iterated until the computed energy distribution reproduced all of the measured flux densities to within 10%. The final values of $M_T(T_j)$ were then fitted with a spline–curve to obtain the desired function $M_T(T)$.

III.7 Summary

A summary of the steps used to obtain the mass density function $M_T(T)$ for each galaxy is now presented:

1. All relevent data for the galaxy are obtained.

2. A smooth continuous curve of $f_\nu(\lambda)$ is fitted through the data points, extending between the shortest and longest wavelengths for which appropriate data are available.

3. A set of n wavelengths is chosen to span the entire available wavelength range; the flux density corresponding to the emission at each of the n wavelengths is obtained from the continuous curve fitted to the original data.

4. A set of m temperatures, where $m < n$, is chosen to span a range of temperatures appropriate for the available wavelength range.

5. The thermal emission curves at the m different temperatures are weighted and summed to obtain the best fit, in a least–squares sense, to the set of n flux densities calculated from the continuous curve fitted to the original data.

6. The weighting factors, converted into the quantity $M_T(T)$, are plotted versus temperature, and a smooth continuous curve is fitted through these points to obtain the value of $M_T(T)$ at any desired temperature.

IV. THE SAMPLE, SOURCES OF DATA, AND OBSERVATIONS

The galaxies in this analysis were all selected from the *IRAS* Bright Galaxy (BG) Sample, a complete, flux–limited sample of 313 galaxies with 60 μm flux densities $>$ 5.24 Jy[9] developed by Soifer *et al.* 1989. Two subsets of galaxies have been drawn from this sample, based on various criteria; these subsets, and the data utilized in the corresponding analysis, will now be described.

IV.1 Galaxies with measurements at 1.25 mm

As discussed in Section III.1, the effective long wavelength limit for dust emission in galaxies is roughly 1 mm, and measurements at or near this wavelength are required to enable a study of the coldest dust in infrared galaxies. To this end, measurements at 1.25 mm have been made of 17 galaxies from the BG Sample using the Caltech Submillimeter Observatory on Mauna Kea. Most of these galaxies have infrared luminosities $L_{IR} \geq 10^{11}\ L_{\odot}$, but some lower luminosity galaxies are included as well. The observations were made on three separate observing runs between January and September, 1988; a beam diameter of 20″ was used, and calibration was achieved by using the temperatures of Uranus and Mars.

[9] 1 Jy = 1 Jansky $\equiv 10^{-26}\ W\ m^{-2}\ Hz^{-1}$.

The results are presented and analyzed in Section V.1. [Note that the results for 10 of the 17 galaxies were presented by Keene *et al.* (1990); the remainder are being reported for the first time].

IV.2 Galaxies with near–infrared measurements

In order to study the short wavelength dust emission from galaxies, two factors must be considered. First, appropriate near–infrared data must be available. Although near–infrared measurements are available for many of the Bright Galaxies, the large dimensions of the *IRAS* beams (typically greater than 1′; see the *IRAS Explanatory Supplement* 1988) require that any near–infrared measurements used be reasonable estimates of the *total* near–infrared emission. Because of this, the source for the short wavelength measurements has been limited to the large–diameter beam measurements presented in Chapter 3 of this thesis. The second factor to be considered is that, as discussed in Section III.1, an analysis of the short–wavelength dust emission from a galaxy is problematic *unless* the spectral curvature, $\alpha_{12,25} - \alpha_{25,60}$, is small.

Based on these considerations, a subset was compiled of 19 galaxies from the BG Sample, all of which satisfy the following criteria:

1. Near–infrared data are available from Chapter 3.
2. The largest beam diameter measurements from Chapter 3 provide a reasonable estimate of the total near–infrared emission, based on the near–infrared growth curves.
3. The spectral curvature $\alpha_{12,25} - \alpha_{25,60} \leq 0$.

These galaxies are analyzed in Section V.2.

V. RESULTS AND DISCUSSION

V.1 Cold dust in infrared galaxies

The infrared emission from infrared–selected galaxies, measured out to a long–wavelength limit of 100 μm, tends to be dominated by thermal emission at temperatures $T \sim 30 - 40$ K. For the BG Sample, single temperatures fit to the 60 and 100 μm flux densities (for $Q \propto \lambda^{-2}$) range from 23 K

to 45 K, with a median at 30 K. One of the important questions concerning such galaxies is whether or not they also contain significant quantities of dust that is cold enough to have been undetectable by *IRAS*. Chini *et al.* (1986) claimed that such dust was necessary to explain their 1.3 mm measurements of 26 infrared–selected galaxies, whereas Eales, Wynn–Williams, and Duncan (1989), on the basis of $350 - 1100\ \mu m$ measurements of 11 *IRAS* galaxies, found that, although cold dust could not be ruled out as a component in such galaxies, the energy distributions could also be satisfactorily modelled without it.

The ability to determine the existence or non–existence of significant quantities of cold dust in galaxies depends critically on our understanding of the functional form for the absorption efficiency, $Q(\lambda)$. To see this, consider two dust components in a galaxy, one consisting of cold dust at temperature T_c, whose emission, $f_c(\lambda)$, peaks at a wavelength λ_c, and the other consisting of warm dust at temperature T_w, whose emission, $f_w(\lambda)$, peaks at a wavelength λ_w. Let $f_\nu(\lambda)$ represent the measurement of the combined emission from the two dust components at wavelength λ. Then,

$$f_\nu(\lambda_c) = f_c(\lambda_c) + f_w(\lambda_c).$$

Assuming the absorption efficiency of the dust grains is given by $Q(\lambda) \propto \lambda^{-\beta}$, and adopting values of $T_w = 30\ K$, $\lambda_w = 100\ \mu m$, and $\lambda_c = 1250\ \mu m$, the fraction, $\Delta f_c(1250\mu m)$, of the emission at 1250 μm that is actually attributable to dust colder than 30 K is given by

$$\Delta f_c(1250\mu m) \equiv \frac{f_c(1250\mu m)}{f_\nu(1250\mu m)} = 1 - 257.70 \cdot (0.08)^{\beta+3} \frac{f_\nu(100\mu m)}{f_\nu(1250\mu m)}.$$

It has been assumed that the emission from the warm dust component at 100 μm, $f_w(100\mu m)$, is approximately equal to the measured total flux density, $f_\nu(100\mu m)$. A plot of this curve is shown in Figure 1 for $\beta = 1$, 1.5, and 2. It is clear that, for a given value of the ratio $f_\nu(100\mu m)/f_\nu(1250\mu m)$, the fraction of the long wavelength emission that is due to cold dust depends critically on the assumed value for β. As one example, for *NGC 3310*, which has a single–temperature fit to the 60 and 100 μm flux densities of 30 K, $f_\nu(100\mu m)/f_\nu(1250\mu m) = 290$; hence, if $\beta = 2$, 75% of the emission at 1250 μm can be attributed to dust colder than 30 K, whereas if $\beta = 1$, the existence of dust colder than 30 K is completely ruled out, since even the 30 K dust provides too much emission at 1250 μm.

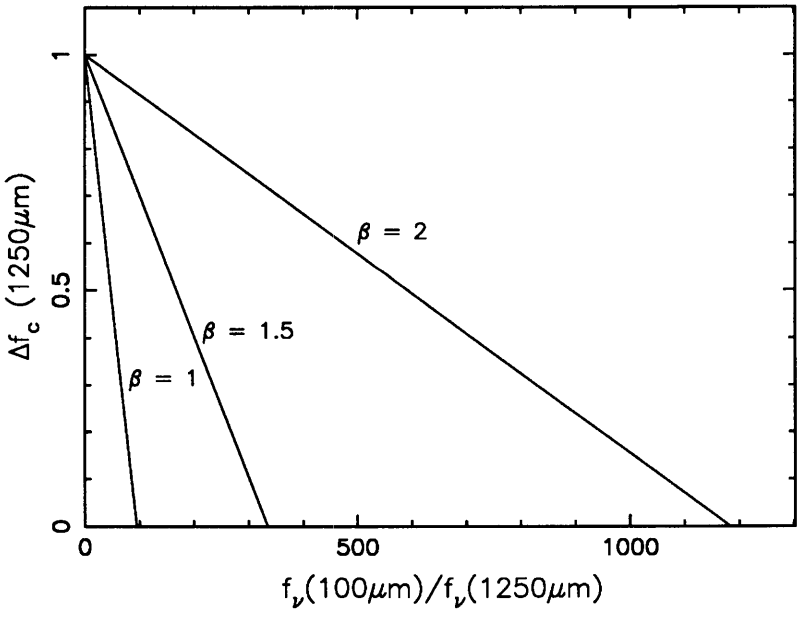

Fig. 1. An estimate of the fraction of the emission at 1250 μm which could be attributed to cold dust, $\Delta f_c(1250\mu m)$ (see text), plotted as a function of the measured flux density ratio $f_\nu(100\mu m)/f_\nu(1250\mu m)$. The dust is assumed to have an absorption efficiency given by $Q(\lambda) \propto \lambda^{-\beta}$. The plot shows the strong effect of the choice of β on the determination of the existence of significant quantities of cold dust.

V.1.1 The 1.25 mm data: Constraints on the absorption efficiency

The results of the 1.25 mm measurements of 17 galaxies from the BG Sample are presented in Table I, along with the *IRAS* data for each source from Soifer *et al.* (1989). The data are shown graphically in Figure 2 (Figure 2 appears at the end of this chapter), which also includes single–temperature thermal emission curves, $f_\nu(\lambda) \propto Q(\lambda)B(\lambda,T)$, for $Q(\lambda) \propto \lambda^{-2}$ (*solid line*) and $Q(\lambda) \propto \lambda^{-1}$ (*dashed line*); the curves are fit to the 60 μm and 100 μm data points for each source.

It is clear from Table I and Figure 2 that, for all of the galaxies, the *measured* flux densities at 1250 μm are inconsistent with an absorption efficiency $Q(\lambda) \propto \lambda^{-1}$. Values of β required for a single–temperature fit to the 60 μm, 100 μm, and 1250 μm flux densities are given in Table I (along with the corresponding temperatures, T_β), and their distribution is shown by the solid line histogram in Figure 3.

TABLE I – 1.25 mm observations

NAME	$f_\nu(\lambda)$ (Jy)[a] 12 μm	25 μm	60 μm	100 μm	1250 μm	$f_{est}(1250\mu m)$[b]	T_3^c	β^d
NGC 337	0.40	0.75	9.33	19.18	0.024		30.3	1.8
MCG–03-04-014	0.47	0.88	6.76	10.20	0.026	0.030	37.1	1.3
NGC 958	0.59	0.95	5.90	14.99	0.034		29.3	1.6
NGC 1055	2.20	2.89	23.27	60.09	0.073		27.3	2.0
UGC 2982	0.57	0.86	8.70	17.32	0.042	0.083	32.2	1.5
NGC 1614	1.44	7.82	33.12	36.19	0.011	0.017	35.2	2.2
UGC 5101	0.26	1.08	13.03	21.25	<0.018		32.7	1.8
NGC 3110	0.58	1.10	11.68	23.16	0.080	0.178	33.7	1.3
NGC 3690	3.90	24.14	121.64	122.45	0.095		40.3	1.7
Mrk 231	1.93	8.80	35.40	32.28	0.029	0.029	44.4	1.5
Mrk 273	0.23	2.30	22.09	22.44	<0.030	0.038	40.0	1.7
Zw 049.057	<0.08	0.93	21.06	29.88	0.047		33.9	1.6
Arp 220	0.64	7.92	103.33	113.95	0.225	0.410	42.5	1.3
NGC 6286	0.50	0.64	9.87	22.01	<0.054		30.3	1.7
NGC 7469	1.60	5.84	27.68	34.91	<0.099	0.155	37.6	1.6
NGC 7541	1.49	1.99	20.59	40.63	0.067		31.7	1.6
NGC 7771	0.87	2.18	20.46	37.42	0.070	0.140	32.7	1.6

[a] The flux densities at 12μm, 25μm, 60μm, and 100μm are the *IRAS* data from Soifer *et al.* (1989); the 1250μm measurements identified with a * were previously published by Keene *et al.* (1990), whereas the remainder are herein being presented for the first time.

[b] An estimate of the *total* emission at 1250μm, based on the growth curves at 1.65μm (see text).

[c] The temperature required to fit a single thermal emission curve through the 60μm, 100μm, and 1250μm points simultaneously.

[d] The spectral index for the absorption efficiency ($Q \propto \lambda^{-\beta}$) required to fit a single temperature thermal emission curve through the 60μm, 100μm, and 1250μm points simultaneously.

Unfortunately, any conclusions drawn from these results must be tempered by a consideration of possible beam size effects due to the use of a relatively small 20″ beam diameter for the 1250 μm measurements, in comparison to the 1 – 5 arc–minute size of the *IRAS* detectors (see the *IRAS Explanatory Supplement* 1988). The significance of this effect is difficult to assess, since information on the spatial distribution of the far–infrared emission in these galaxies is not available. However, for 12 of the 17 sources, multiple beam diameter measurements at near–infrared wavelengths have been presented by Carico *et al.* (1990), which can be used to generate near–infrared growth curves for these galaxies. There is, of course, little reason to suspect that the near–infrared emission would be a reasonable tracer of the emission at 1250 μm. However, Carico *et al.* concluded from their analysis that the dust in infrared galaxies tends to be more tightly concentrated about their nuclei than the stars. If this is true, then the 1.65 μm emission, which is believed to be dominated by star light, should provide an upper

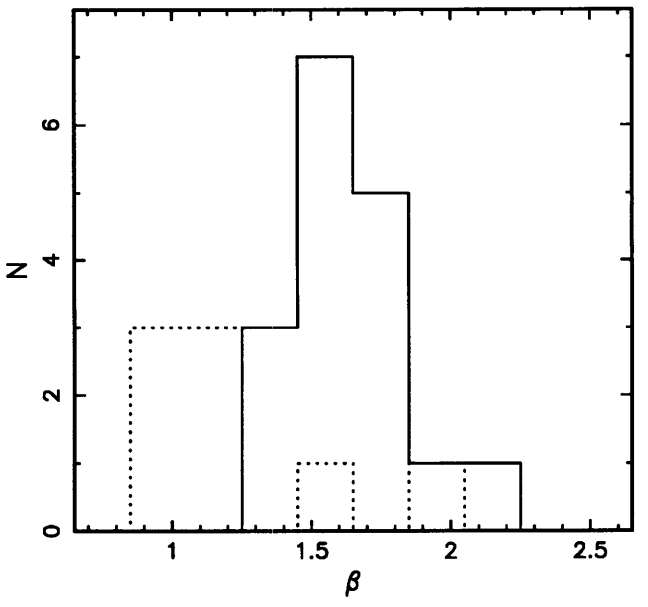

Fig. 3. *solid–line*: The distribution of β, where $Q \propto \lambda^{-\beta}$, for a single temperature fit to the *IRAS* 60 μm and 100 μm flux densities and the measured 1250 μm flux density. *dashed–line*: The distribution of β for a single temperature fit to the *IRAS* 60 μm and 100 μm flux densities and an estimate of the *total* emission at 1250 μm (see text).

limit to the spatial extent of the 1250 μm emission, which is due to dust.

Motivated by the reasoning just given, and a desire to have some handle on the amount of 1250 μm emission which could have been missed by the 20″ diameter beam, the measurements from Carico *et al.* (1990) have been used to obtain estimates of the total emission at 1.25 mm. The method used for each of the galaxies studied was to first determine from the near–infrared data and the optical size of the galaxy, whether or not the largest beam diameter measurements presented by Carico *et al.* represent reasonable estimates of the total near–infrared emission. If so, the estimate of the total emission at 1250 μm was taken to be

$$f_{est}(1250\mu m) \equiv \left[\frac{f_\nu(1.65\mu m)_{large}}{f_\nu(1.65\mu m)_{17''}}\right] \cdot f_\nu(1250\ \mu m),$$

where $f_\nu(1.65\mu m)_{17''}$ and $f_\nu(1.65\mu m)_{large}$ are the flux densities from Carico *et al.* measured with their 17″ and largest diameter beams, respectively, and $f_\nu(1250\mu m)$ is the 1250 μm flux density from Table I. It should be kept in mind that, since the emission near 1 mm is expected to be considerably

more concentrated than the near–infrared emission in most galaxies, *the values of* $f_{est}(1250\mu m)$ *should be considered as conservative upper limits on the possible total flux density at 1250* μm. The estimates of $f_{est}(1250\mu m)$, which were obtained for 8 of the galaxies, are included in Table I and plotted in Figure 2.

It is readily seen from Figure 2 that, even using the values of $f_{est}(1250\mu m)$, most of the galaxies are, at best, just barely consistent with a λ^{-1} dependence for the absorption efficiency. Such a model would have to assume that *all* of the emission at 1250 μm is due to the dust at the peak temperature responsible for the 60 μm and 100 μm emission. The exception to this is *Mrk 231*, for which even beam size effects cannot account for sufficient emission at 1250 μm to allow for $\beta \sim 1$. The distribution of β calculated for a single temperature fit using $f_{est}(1250\mu m)$ rather than $f_\nu(1250\mu m)$ is shown by the dashed–line histogram in Figure 3.

V.1.2 Temperature distribution results

The conclusion from the previous section regarding constraints on the absorption efficiency is that, for *all* of the galaxies studied, the dust grains are characterized by $\beta \gtrsim 1$. Since, as discussed in Section V.1.1, theory easily allows for values of β as small as 1, it follows that *all of the 1250* μm *measurements in Table I are consistent with the hypothesis that these galaxies contain no dust colder than that responsible for the 60* μm *and 100* μm *emission.* That is, the lower limit to the amount of cold dust in each of these galaxies is *no* cold dust; one can simply tailor the absorption efficiency for each galaxy so that the 1250 μm emission is exactly accounted for by the dust needed for the 60 μm and 100 μm emission.

One must also consider the possible *upper* limit to the amount of cold dust, which will be obtained by taking $\beta = 2$. For five of the galaxies – *NGC 337, NGC 1055, NGC 1614, UGC 5101*, and NGC 6286 – the measured 1250 μm flux densities are low enough as to *require* $\beta \approx 2$, and hence these galaxies cannot contain cold dust in sufficient quantities to provide any detectable emission unless beam size effects are invoked. However, for the remaining 12 galaxies, the measurements allow room for significant emission at 1250 μm from cold dust. For these 12 sources, dust temperature distributions

TABLE II
Temperature distribution results for galaxies with 1.25 mm measurements

NAME	T^a_{IRAS} $\beta=2$	T^a_{IRAS} $\beta=1$	$TM_T(20K)$ / $TM_T(T_{IRAS})$	$log[\ M_{cold}\ ]$	M_{cold} / M_d
MCG-03-04-014	32.47	8.01	8.12	8.88	0.96
NGC 958	27.59	3.53	7.97	5.68	0.95
UGC 2982	29.79	5.68	8.04	10.76	0.96
NGC 3110	29.54	7.14	8.22	13.89	0.97
NGC 3690	36.13	3.83	7.80	6.47	0.93
Mrk 231	39.31	6.88	8.40	8.85	0.95
Mrk 273	38.82	5.79	8.12	7.75	0.94
Zw 049.057	31.74	6.47	7.68	10.72	0.94
Arp 220	36.13	9.62	8.51	13.84	0.96
NGC 7469	34.67	3.16	7.71	5.53	0.93
NGC 7541	29.79	3.72	7.65	6.97	0.94
NGC 7771	30.52	5.92	7.95	6.69	0.94

have been obtained using Eq. (21) for $Q(\lambda)$ (for which $\beta = 2$ at the wavelengths appropriate for the emission from the coldest dust); the results are shown in Figure 4 (Figure 4 appears at the end of this chapter). In each plot, the *solid–line curve* represents the quantity $\log[TM_T(T)]$, shown on the left–hand vertical axis, and the *dashed–line curve* represents the quantity $\log[TL_T(T)]$, shown on the right–hand vertical axis. The quantities $TM_T(T)$ and $TL_T(T)$ are shown, rather than $M_T(T)$ and $L_T(T)$, since they provide an easier visualization of the significance of the dust at a given temperature. To see this, consider that, for $M_T(T)$,

$$M_d = \int_T M(T)dT = \int_T TM_T(T)\left(\frac{dT}{T}\right) = \log[e]\int_T TM_T(T)d(\log T).$$

Hence, on a log–log plot, the relative contribution to the total dust mass from dust within any two temperature bands of equal width is given directly by $TM_T(T)$; furthermore, the total mass of dust within any temperature decade is simply the mean value of $TM_T(T)$ within that decade.

Also shown in Figure 4 are vertical bars indicating the values of $TM_T(T)$ and $TL_T(T)$ at the temperature T_{IRAS} appropriate for a single–temperature fit to the *IRAS* 60 μm and 100 μm flux densities for $Q \propto \lambda^{-2}$. It is readily seen that a single temperature fit to the *IRAS* flux densities does *not* necessarily provide a good estimate of the temperature distribution of the dust mass. That is, for the galaxies in Figure 4, although the temperature distributions of the dust *luminosity* peak at or very near T_{IRAS}, as would be expected, the dust *mass* in each case is dominated by dust at temperatures $T < T_{IRAS}$. This has been quantified in Table II (Column 3), where the quantity $M_T(20K)/M_T(T_{IRAS})$ has been tabulated. This ratio ranges from 3.2 to 9.6, and has a median of 5.9.

Table II also contains, in Column 4, estimates of the quantity M_{cold}, the total integrated dust mass between temperatures T_{min}, the minimum temperature used in the analysis, and T_{IRAS}:

$$M_{cold} \equiv \int_{T_{min}}^{T_{IRAS}} M_T(T)dT.$$

In Column 5 of Table II, the values of M_{cold} are compared to M_{IRAS}, the dust mass estimated from a single temperature fit using T_{IRAS}, and in Column 6, M_{cold} is compared to M_d, the total dust mass estimated from the integral of $M_T(T)$:

$$M_d \equiv \int_{T_{min}}^{T_{max}} M_T(T)dT,$$

where T_{max} is the maximum temperature used in the analysis. It is again clear that the dust at temperatures $T < T_{IRAS}$ is dominant: The ratio of cold dust, M_{cold}, to single–temperature "warm" dust, M_{IRAS}, ranges from about 5 up to almost 14, with a median of 8.3; also, for all of the galaxies, the cold dust represents more than 90% of the total dust mass obtained by integrating over the entire range of temperatures.

V.1.3 Conclusions regarding cold dust in infrared galaxies

The results of Sections V.1.1 and V.1.2 can be summarized as follows:

1. The 1250 μm measurements imply that the dust grains in all of the galaxies have absorption efficiencies characterized by $\beta \gtrsim 1$ at far–infrared wavelengths.

2. A model which includes *no* dust colder than the dust responsible for the 60 μm and 100 μm emission can be adopted for all of the galaxies, provided the appropriate wavelength dependence for the absorption efficiency is included in the model, with $1 \lesssim \beta \lesssim 2$.

3. If β is taken to be 2, an upper limit is obtained for the possible amount of cold dust in each galaxy, and in most cases the resulting mass of cold dust is roughly an order–of–magnitude greater than found by *IRAS*, and dominates the total dust mass.

These results illustrate the difficulty in obtaining accurate estimates of cold dust masses based on millimeter continuum measurements, and the critical importance of the absorption efficiency, $Q(\lambda)$, in any such analysis. The problem is simply in the nature of the Planck function: A body at temperature T_2 emits more radiation at *all* wavelengths than a similar body at temperature T_1, for $T_2 > T_1$; in the Rayleigh–Jeans region of the spectrum, the ratio of the emission from the two bodies at a given wavelength is T_2/T_1. It follows that, in order to attribute *any* detectable emission at 1250 μm to dust colder than that responsible for the 60 μm and 100 μm emission, one must invoke a very large mass of this cold dust. Since, as Figure 1 shows, the emission at 1250 μm which is attributable to cold dust depends critically on the value of β for the absorption efficiency, any uncertainty in β quickly translates into a very large uncertainty in the mass of cold dust.

It is interesting to compare the 1250 μm measurements being presented in this analysis with other submillimeter and millimeter studies of infrared–selected galaxies. This has been done in Figure 5; at each wavelength, the "data" point represents the *mean* flux density for the appropriate sample of galaxies, normalized to a value of 100 at 100 μm, and the "error bars" indicate the minimum and maximum (normalized) flux densities for the sample at that wavelength. The *squares* at the *IRAS* wavelengths and at 1250 μm are the flux densities for the galaxies in the current sample, given in Table I; the *circles* at 350 μm and 450 μm are from samples of 8 and 5 galaxies, respectively, detected by Eales, Wynn–Williams, and Duncan (1989); the *triangle* at 1300 μm is from the sample of 17 galaxies detected by Chini *et al.* (1986). The only overlap between the current sample and those of the other authors is *Arp 220*, which appears in all of the samples. The curve in Figure 5 is the energy distribution for 33 K emission with $Q \propto \lambda^{-2}$, appropriate for a single–temperature fit to the 60 μm and 100 μm points in the figure.

It is readily seen that the data from Eales, Wynn–Williams, and Duncan (1989) agree well with the measurements presented herein. Although their samples were quite small, diluting somewhat any statistical results, it is worth noting that, even with a beam diameter of 104″, their 350 μm and 450 μm flux densities provide no evidence that our 20″ beam missed any significant fraction of the emission at

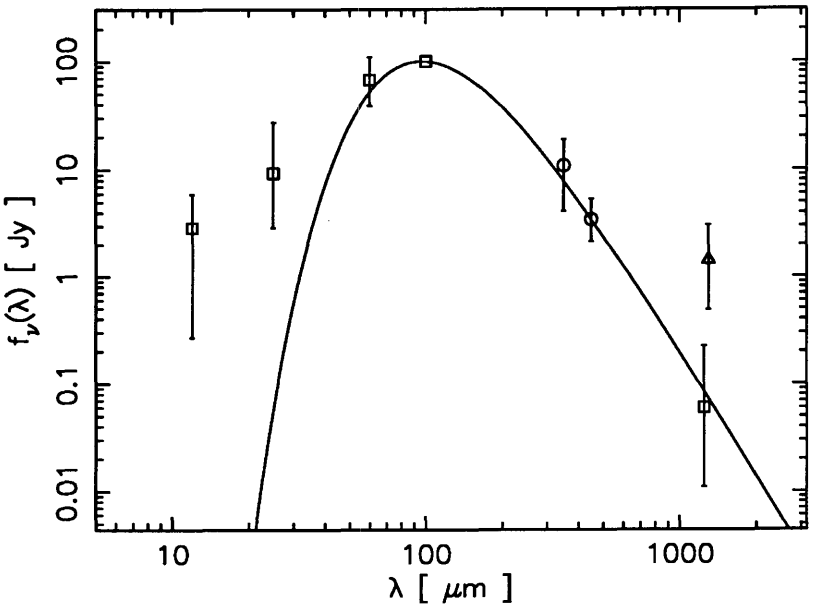

Fig. 5. A comparison of millimeter and sub–millimeter measurements for various samples of infrared–selected galaxies. For each sample, the "data" point represents the mean flux density, normalized to 100 Jy at 100 μm, and the "error bars" represent the minimum and maximum flux densities for that sample. The *squares* are for the current sample; the *circles* are for the sample of Eales, Wynn–Williams, and Duncan (1989); the *triangle* is for the sample of Chini *et al.* (1986). The curve is the energy distribution for 33 K thermal emission, with $Q \propto \lambda^{-2}$, as determined by fitting a single temperature to the 60 μm and 100 μm points in the figure.

longer wavelengths.

In contrast, the results of Chini *et al.* (1986) are grossly discrepent with those of the current analysis. Eales, Wynn–Williams, and Duncan (1989) also remarked on the discrepancy between their 350 μm measurements and the 350 μm measurements from Chini *et al.* In particular, measurements of *Arp 220* at millimeter and/or submillimeter wavelengths have been reported by Emerson *et al.* (1984) and Thronson *et al.* (1987), in addition to those given by Eales, Wynn–Williams, and Duncan (see the latter paper for a comparison). All of these measurements are consistent with each other, and with those in this analysis, but are discrepent with the measurements given for this source by Chini *et al.* We shall not comment on this discrepancy further, but will simply state that, given the general agreement between the measurements presented herein and those given by other authors for similar galaxies, we believe that

the 1250 μm flux densities presented in Table I are correct, and that the general energy distribution implied by the data in Figure 5 (other than those of Chini *et al.*) is appropriate for infrared selected galaxies.

V.2 Hot dust in infrared galaxies

Although the far–infrared emission for all of the galaxies discussed in Section V.1 can be successfully modelled with a single–temperature dust component providing the observed 60 μm, 100 μm, and 1250 μm emission, the same is not true for the shorter–wavelength emission; for all of the galaxies in the BG Sample, the *IRAS* 12 μm and/or 25 μm flux densities imply the existence of dust at temperatures greater than those inferred from the 60 μm and 100 μm flux densities.[10] It is this "hot dust" which will now be considered, using the temperature distribution analysis developed previously (Sections II and III).

V.2.1 Interpretation of the near–infrared data

As discussed in Section III.1, there are 19 galaxies from the BG Sample for which the near–infrared measurements presented by Carico *et al.* (1990) were deemed appropriate for consideration in the current analysis. However, before using the near–infrared data, an attempt was made to identify in each galaxy the component of the near–infrared emission at wavelength λ which is actually attributable to dust; this quantity will be designated $f_\nu^d(\lambda)$.

To determine the values of $f_\nu^d(\lambda)$ at each wavelength, a near–infrared color–color plot was made ($log[f_\nu(1.65)/f_\nu(1.25)]$ versus $log[f_\nu(2.2)/f_\nu(1.65)]$), and the near–infrared colors of each galaxy were compared to those of normal, optically selected galaxies, as given by Aaronson (1977). The following three cases were then considered:

Case 1:

[10] Note that this statement doesn't necessarily apply to *steady–state* temperatures, since temperature fluctuations in individual grains may also contribute at the shorter wavelengths; see Section III.1.

If the colors were consistent with emission from a normal galaxy, plus a component due to emission from dust at a temperature $\leq$ 1500 K, then the values of $f_\nu^d(\lambda)$ were calculated as follows: First, the flux density at 1.25 μm was assumed to be due entirely to stellar emission. Then, the contributions from stars at 1.65 μm and 2.2 μm were taken to be the flux densities at those wavelengths which would be appropriate for a normal, optically–selected galaxy. The estimates of the values for $f_\nu^d(\lambda)$ were then calculated from

$$f_\nu^d(1.65\mu m) = f_\nu(1.65\mu m) - f_\nu(1.25\mu m)\left[\frac{f_\nu(1.65\mu m)}{f_\nu(1.25\mu m)}\right]_{normal}$$

$$f_\nu^d(2.2\mu m) = f_\nu(2.2\mu m) - f_\nu(1.25\mu m)\left[\frac{f_\nu(2.2\mu m)}{f_\nu(1.25\mu m)}\right]_{normal},$$

where the flux–density ratios for normal galaxies were taken to be

$$\left[\frac{f_\nu(1.65\mu m)}{f_\nu(1.25\mu m)}\right]_{normal} = 1.26$$

$$\left[\frac{f_\nu(2.2\mu m)}{f_\nu(1.25\mu m)}\right]_{normal} = 0.96,$$

as given by Aaronson (1977).

Case 2:

If the colors were consistent with a combination of normal galaxy emission, dust emission, and "reddening" (extinction), the measured flux densities were "de–reddened," that is the conjectured extinction effects were removed by assuming an extinction proportional to λ^{-1}, but only enough so as to bring the colors in line with a combination of normal galaxy emission and emission from 1500 K dust. Then, the values of $f_\nu^d(\lambda)$ were determined as in *Case 1*. This approach assumes the minimum amount of extinction for a 1500 K upper limit on the dust temperature, and hence yields an upper limit for the values of $f_\nu^d(\lambda)$.

Case 3:

If the colors were not consistent with any combination of normal galaxy emission, emission from dust at a temperature $\leq$ 1500 K, and extinction, the near–infrared flux densities were

not used in the analysis, and the galaxy was removed from the list of sources which can be analyzed at short wavelengths.

This process resulted in the elimination of 7 of the 19 galaxies from the original candidate list of galaxies with large–beam near–infrared measurements. The remaining 12 galaxies which will be studied in this section are listed in Table III, along with the values of $f_\nu^d(\lambda)$ at 1.65 μm and 2.2 μm, and all other flux densities used in the analysis. The results of the temperature distribution analysis for each of the 12 galaxies are shown in Figure 6, where, in each plot, the *solid–line curve* represents the quantity $log[TM_T(T)]$, shown on the left–hand vertical axis, and the *dashed–line curve* represents the quantity $log[TL_T(T)]$, shown on the right–hand vertical axis; the corresponding energy distributions generated from these temperature distributions are shown in Figure 7 (Figures 6 and 7 appear at the end of this chapter), along with the flux densities from Table III.

TABLE III
Near–infrared flux densities

NAME	$f_\nu^d(\lambda)$[a] (mJy)		$f_\nu(\lambda)$[b] (Jy)				
	1.65 μm	2.2 μm	12 μm	25 μm	60 μm	100 μm	1250 μm
NGC 34	4.57	9.21	0.36	2.38	16.08	16.97	
MCG–02-01-051†, N	0.39	1.21	0.23	1.18	7.35	9.48	
MCG+02-04-025	1.84	5.76	0.27	1.41	10.72	9.60	
UGC 2369†	0.63	7.67	0.22	1.75	7.68	11.10	
MCG+08-18-012	0.58	2.01	0.10	0.78	6.39	8.83	
Mrk 231	43.05	142.59	1.93	8.80	35.40	32.28	0.029
Mrk 273	2.48	6.30	0.23	2.30	22.09	22.44	<0.030
I Zw 107	0.08	3.04	0.22	1.40	9.15	10.04	
Arp 220	2.54	7.36	0.64	7.92	103.33	113.95	0.225
NGC 7469	23.19	55.48	1.60	5.84	27.68	34.91	<0.099
Zw 475.056	0.65	2.80	0.32	1.88	8.75	11.64	
Mrk 331		1.69	0.51	2.56	17.32	20.86	

[a] $f_\nu^d(\lambda)$ is an estimate of the contribution to the flux density at wavelength λ from dust emission (see text); the values given were estimated from the data of Carico *et al.* (1990).

[b] The flux densities at 12 μm, 25 μm, 60 μm, and 100 μm are the *IRAS* data from Soifer *et al.* (1989); the 1250 μm measurements are from Table I, and are discussed in Section V.1.3.

V.2.2 Temperature distribution results

It is readily seen from Figure 6 that, for virtually all of the galaxies studied, the dependence of dust mass on temperature is approximately a power–law, from a few tens of degrees up to over 1000 K.

This result must be tempered with the fact that all of the galaxies listed in Table III were chosen under a very strict selection criterion which effectively filtered out any galaxies which do not have straight (i.e., power–law) energy distributions between 12 μm and 60 μm, as seen in Figure 7 (refer to Section III.1). Because of the correlation between the *IRAS* $f_\nu(12\mu m)/f_\nu(25\mu m)$ color and the $f_\nu(60\mu m)/f_\nu(100\mu m)$ color, and the correlation between these colors and galaxy luminosity (see Soifer *et al.* 1989), the galaxies in Table III are biased towards both high $f_\nu(60\mu m)/f_\nu(100\mu m)$ color temperatures, T_{IRAS}, and high infrared luminosity, L_{IR}. For comparison, T_{IRAS} ranges from 23 K to 46 K, with a median of 30 K for the entire BG Sample, whereas for the galaxies in Table III, T_{IRAS} has a much narrower range, from 33 K to 44 K, with a higher median of 36 K; also, the logarithm of the infrared luminosity for the entire BG Sample ranges from 8.54 to 12.52, with a median of 10.56, whereas for the galaxies in Table III, $log[L_{IR}]$ ranges from 11.05 to 12.52, and has a median of 11.53 (this bias towards high luminosity also reflects the fact that Carico *et al.* (1990) only reported near–infrared measurements for galaxies with $L_{IR} \geq 10^{11}\ L_\odot$; however, a consideration of all of the Bright Galaxies satisifying the selection criterion on the *IRAS* colors yields a similar bias towards high luminosity, with a median $log[L_{IR}] = 11.32$). Thus, the results in Figure 6 should not be taken as representative of the entire BG Sample, or infrared galaxies in general. Nevertheless, these results are still of interest for the following reasons.

First, the selection criterion was applied only to the *IRAS* data; thus, although a power–law dependence for $M_T(T)$ could be predicted from the outset for the dust temperatures between ~40 K and 300 K which contribute between 12 μm and 60 μm, it is not obvious that this simple temperature dependence would continue so smoothly up through the highest temperatures, particularly since the stellar correction applied to the near–infrared flux densities was, at best, a crude approximation.

Second, the intent of the selection criterion was to enable the analysis of only those galaxies for which the energy distributions are dominated everywhere by emission from dust grains at steady–state temperatures, rather than grains undergoing extreme random temperature fluctuations due to single–photon absorption events (see Section III.1). *To the extent that this selection process was*

successful, the results of Figure 6 show the distribution of dust mass with steady–state temperature for the most luminous infrared galaxies.

TABLE IV
Temperature distribution results for galaxies with near–infrared measurements

NAME	α[a]	T^b_{IRAS} $\beta=2$	T^b_{IRAS} $\beta=1$	T^c_L	$log[\, TL_T(T)\,]_{T_L}$	$\Delta L_T[(T_L+\Delta T)/T_L]$[d] $\Delta T=100K$	$300K$	$1000K$	$log[L_d]$[e]	L_d/L_{FIR}	L_d/L_{IR}
(1)	(2)	(3)	(4)	(5)	(6)	(7)	(8)	(9)	(10)	(11)	(12)
NGC 34	6.1	37.11	46.89	44.20	11.22	0.20	0.06	0.024	11.37	1.22	0.90
MCG–02-01-051, N†	6.5	34.42	42.48	37.06	11.08	0.30	0.08	0.007	11.27	1.22	0.91
MCG+02-04-025	6.1	39.79	51.27	44.20	11.51	0.16	0.08	0.022	11.59	1.13	0.92
UGC 2369†	5.9	32.96	40.04	67.42	11.23	0.24	0.09		11.56	1.37	0.97
MCG+08-18-012	6.5	33.69	41.02	37.06	11.14	0.15	0.05	0.014	11.28	1.18	0.93
Mrk 231	5.2	39.55	50.78	46.33	12.31	0.33	0.16	0.151	12.54	1.55	1.05
Mrk 273	5.8	37.60	47.85	42.18	12.08	0.09	0.02	0.010	12.07	1.08	0.88
I Zw 107	6.0	36.62	45.90	42.92	11.65	0.20	0.09		11.79	1.18	0.87
Arp 220	6.5	36.62	45.90	38.39	12.07	0.07	0.01	0.003	12.10	0.97	0.84
NGC 7469	5.1	34.67	42.97	34.26	11.45	0.31	0.17	0.069	11.58	1.47	0.97
Zw 475.056	6.5	33.94	41.99	48.27	11.19	0.39	0.14	0.016	11.50	1.34	0.92
Mrk 331	6.7	35.16	43.95	37.06	11.21	0.27	0.06	0.004	11.35	1.20	0.89

[a] The spectral index of the dust mass temperature distribution: $M_T(T) \propto T^{-\alpha}$.

[b] The temperature determined from the *IRAS* 60 μm and 100 μm flux densities.

[c] The temperature corresponding to the peak in the $L_T(T)$ distribution.

The spectral indices, α, for the power–law temperature dependence of the dust mass for the galaxies in Table III, are listed in Table IV, and their distribution is shown in Figure 8. α is defined such that

$$M_T(T) \propto T^{-\alpha}.$$

Table IV also contains additional numerical results from the temperature distribution analysis. In Columns 3 – 5, the temperature obtained from a single–temperature fit to the *IRAS* 60 μm and 100 μm flux densities, T_{IRAS}, obtained using $\beta = 2$ and 1, is shown for comparison to the temperature, T_L, corresponding to the peak in the $TL_T(T)$ curves in Figure 6. It is clear that, for most of the sources, T_L is comparable to the estimates of the dust temperature obtained from a single–temperature fit, falling somewhere between the two values of T_{IRAS}. The two exceptions are *UGC 2369* and *Zw 475.056*, for which T_L is significantly larger than the largest value of T_{IRAS}. As is seen in Figure 6, this discrepancy in each case is due to an exceptionally broad $TL_T(T)$ distribution at the relevent temperatures.

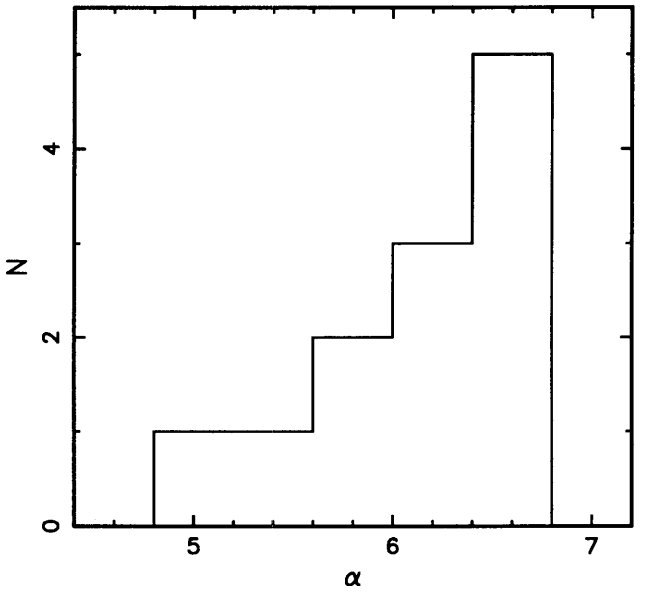

Fig. 8. The distribution of the spectral index, α, for the dust mass temperature distributions in Figure 6; $M_T(T) \propto T^{-\alpha}$.

Column 6 of Table IV lists the luminosity per logarithmic temperature interval at the temperature T_L, $[TL_T(T)]_{T_L}$, where $L_T(T)$ is expressed in units of solar luminosities,[11] $L_\odot$, and in Columns 7 – 9 the luminosity from dust at temperatures T', relative to that at T_L, is shown for $T' = T_L + 100\ K$, $T_L + 300\ K$, and $T_L + 1000\ K$; this quantity is designated $\Delta L_T(T'/T_L)$, where

$$\Delta L_T(T'/T_L) \equiv \frac{T' L_T(T')}{T_L L_T(T_L)}.$$

It is clear that, for most of the galaxies, there is a significant contribution to the observed luminosity, at the level of ~10 – 30% of the luminosity at the peak temperature T_L, from dust at temperatures ~100 K above T_L. Furthermore, in three of the sources (25% of the sample), dust at 300 K above the peak temperature contributes significantly to the luminosity at the 10 – 20% level. These results are shown graphically in Figure 9, where histograms of the $\Delta L_T(T'/T_L)$ distributions for $T' = T_L + 100\ K$ and $T_L + 300\ K$ are plotted. From Table IV it is also seen that, at temperatures

[11] $L_\odot = 3.83 \cdot 10^{33}\ ergs\ s^{-1}$.

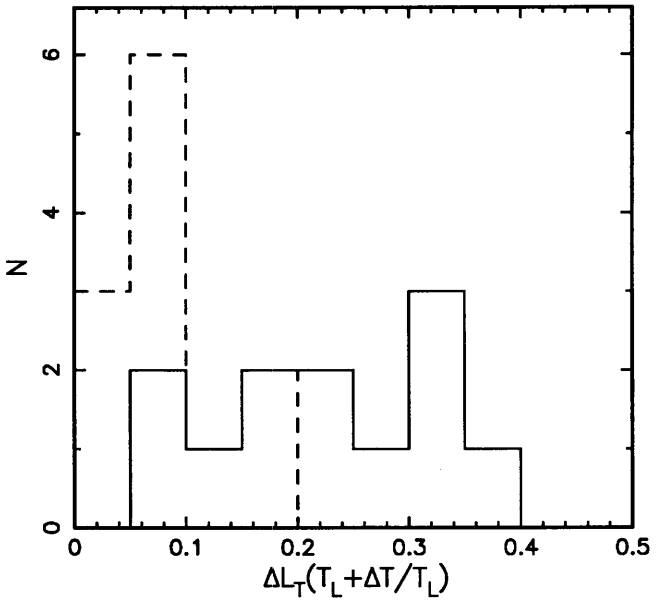

Fig. 9. The distributions of the ratio of the luminosity from dust at temperatures $T' = T_L +$ 100 K (*solid–line*) and $T' = T_L + 300$ K (*dashed–line*), to the luminosity from dust at the temperature, T_L, where T_L corresponds to the peak in the $TL_T(T)$ curves.

$\sim$1000 K above the peak temperature, the contribution to the luminosity is small, only a few percent of the peak luminosity. The one exception to this is *Mrk 231*, for which $\Delta L_T(T_L + 1000K/T_L) = 15\%$.

In Column 10 of Table IV, the integrated luminosity from dust, L_d, is given for each source, where

$$L_d \equiv \int_{T_{min}}^{T_{max}} L_T(T)dT,$$

and in Figure 10 the distribution of L_d is plotted. Also shown in Table IV are the ratios L_d/L_{FIR} (Column 11) and L_d/L_{IR} (Column 12), where L_{FIR} is an estimate of the far–infrared luminosity between 40 μm and 1000 μm obtained using the *IRAS* 60 μm and 100 μm flux densities, and L_{IR} is an estimate of the infrared luminosity between 8 μm and 1000 μm obtained using the *IRAS* 12 μm, 25 μm, 60 μm, and 100 μm flux densities. The values for L_{FIR} in Table IV are from Soifer (private communication), and the values of L_{IR} are from Carico *et al.* (1988).

The distributions of the fractional difference between L_d and L_{FIR}, $(L_d - L_{FIR})/L_{FIR}$, and between L_d and L_{IR}, $(L_d - L_{IR})/L_{IR}$, are shown in Figure 11. It is not expected that L_d and L_{FIR}

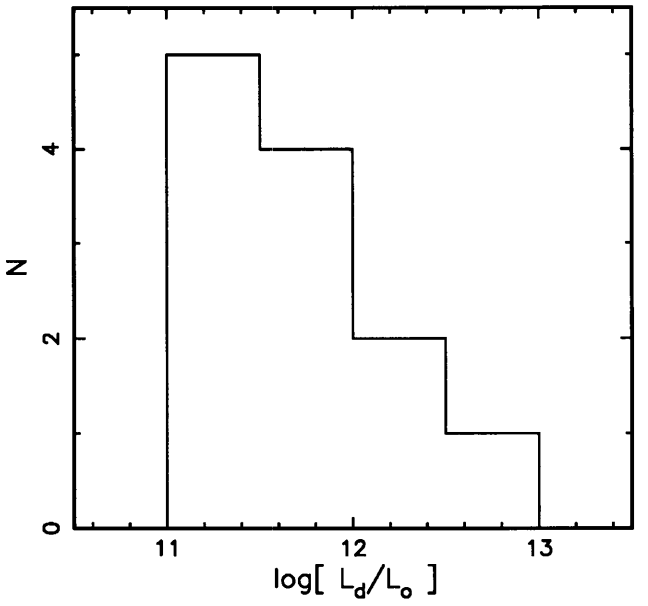

Fig. 10. The distribution of the integrated luminosity from dust at all available temperatures.

should agree, since L_{FIR} is calculated over a much smaller wavelength range. The comparison is given to illustrate the contribution to the total integrated dust emission from hot dust, and the degree to which any estimate based only on the far–infrared emission underestimates the total infrared luminosity. It is seen that, for most of the galaxies, the estimate of the far–infrared luminosity is significantly less than the total integrated luminosity from dust. For the 12 galaxies studied, the median fractional difference between L_d and L_{FIR} is 21%, and ranges up to 55% (for *Mrk 231*). The one exception to this is *Arp 220*, for which the far–infrared luminosity is essentially equal to the integrated luminosity from dust. This is perhaps not surprising for this source, given its extreme infrared–to–visible luminosity ratio of $\sim$150 (Soifer *et al.* 1987), and the extreme degree of internal extinction known to effect its intrinsic emission (Becklin and Wynn–Williams 1987).

In contrast, the estimates of the $8 - -1000$ μm luminosity, L_{IR}, given by Carico *et al.* (1988), agree fairly well with the integrated dust luminosity, differing in most cases by no more than 10%.

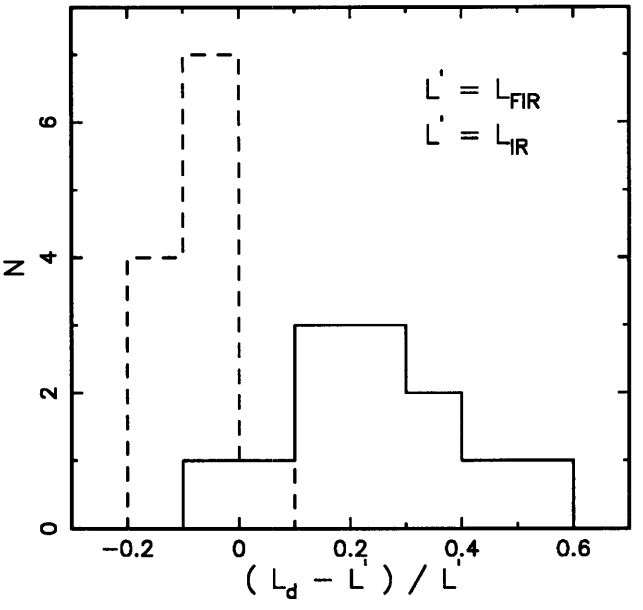

Fig. 11. The distributions of the ratio of the total integrated luminosity from dust at all available temperatures, L_d, to estimates of the far–infrared luminosity, L_{FIR} (*solid–line*), obtained from the *IRAS* 60 μm and 100 μm flux densities by Soifer *et al.* (1987), and estimates of the total infrared luminosity, L_{IR}(*dashed–line*), obtained from the *IRAS* 12 μm, 25 μm, 60 μm, and 100 μm flux densities by Carico *et al.* (1988).

V.2.3 Conclusions regarding hot dust in infrared galaxies

The results of Section V.2 can be summarized as follows:

1. The distribution of dust mass as a function of temperature tends to follow a power–law, from temperatures corresponding to the peak in the luminosity, up to temperatures over 1000 K. The spectral index for this power–law ranges from ~5 – 7, with most of the galaxies studied (67% of the sample) showing indices between 6 and 6.5.

2. Dust at temperatures ~100 K above the temperature of peak emission contributes significantly to the total luminosity, at a level of 10 – 30% of the luminosity at the peak temperature for most of the sample. At 300 K above the peak temperature, dust still contributes significantly to the total luminosity, at the level of 10 – 20% of the peak luminosity, in 25% of the sample. At 1000 K above the peak temperature, the dust emission is down to the level of a few percent in all but one galaxy, *Mrk 231*, in which

the luminosity from dust at temperatures ~1000 K is 15% of the peak luminosity.

3. The contribution from hot dust to the infrared luminosity is summarized in the result that the integrated luminosity from dust at temperatures between 20 K and 1500 K is, for most of the sources, significantly greater than the far–infrared luminosity estimated from the *IRAS* 60 μm and 100 μm flux densities. On average, the far–infrared luminosities are 21% below the estimates of the integrated luminosity from dust at all relevent temperatures, and run as low as 55% below the total luminosity. In contrast, previous estimates of the total infrared luminosity based on the entire *IRAS* energy distribution agree well with the estimates obtained from the integrated dust luminosity, usually to within ~10%.

ACKNOWLEDGEMENTS

Thanks are extended to Jocelyn Keene and Gerry Neugebauer, who worked with me in obtaining the millimeter observations, and especially to Jocelyn for her patience in guiding a sometimes dense mind through the methods and confusions of working in what was for me a foreign field of astronomical research. Thanks are also given to Tom Soifer for many helpful discussions throughout the development of this work; to Todd Groesbeck for helpful discussions and for his truly invaluable computer expertise; to James Graham for a particular *extremely* well–timed suggestion; and to Jean–Loup Puget for a number of helpful discussions, and most importantly for his enthusiastic support during the early stages of this work.

REFERENCES

Aannestad, P.A., 1975. Absorptive properties of silicate core–mantle grains, *Astrophys. J.*, **200**, 30.

Aaronson, M., 1977. Infrared observations of galaxies, Ph.D. thesis, Harvard University.

Allamandola, L.J., A.G.G.M. Tielens, and J.R. Barker, 1989. Interstellar polycyclic aromatic hydrocarbons: the infrared emission bands, the excitation/emission mechanism, and the astrophysical implications, *Astrophys. J. Supp.*, **71**, 733.

Becklin, E.E., and C.G. Wynn-Williams, 1987. Ground–based $1 - 32\ \mu m$ observations of Arp 220: Evidence for a dust–embedded "AGN"?, in *Star Formation in Galaxies*, C.J. Lonsdale (Ed.), US Government Printing Office, Washington, D.C., p. 643.

Bevington, P.R., 1969. *Data Reduction and Error Analysis for the Physical Sciences*, McGraw–Hill, New York.

Bode, M.F., 1988. Observations and modelling of circumstellar dust, in *Dust in the Universe*, Bailey, M.E., and Williams, D.A. (Eds.), Cambridge University Press, Cambridge, p. 73.

Bohren, C.F., and D.R. Huffman, 1983. *Absorption and Scattering of Light by Small Particles*, Wiley–Interscience, New York.

Campbell, M.F., J.H. Elias, D.Y. Gezari, P.M.Harvey, W.F. Hoffmann, H.S. Hudson, G. Neugebauer, B.T. Soifer, M.W. Werner, and W.E. Westbrook, 1976. Far–infrared observations of IRC+10216, *Astrophys. J.*, **208**, 396.

Carico, D.P., D.B. Sanders, B.T. Soifer, K. Matthews, and G. Neugebauer, 1990. The *IRAS* Bright Galaxy Sample. V. Multi–beam photometry of galaxies with $L_{IR} \geq 10^{11}\ L_{\odot}$, *Astronom. J.*, **100**, 70 (Chapter 3 of this thesis).

Carico, D.P., D.B. Sanders, B.T. Soifer, J.H. Elias, K. Matthews, and G. Neugebauer, 1988. The *IRAS* Bright Galaxy Sample. III. $1 - 10\ \mu m$ observations and coadded *IRAS* data for galaxies with $L_{IR} \geq 10^{11}\ L_{\odot}$, *Astronom. J.*, **95**, 356 (Chapter 2 of this thesis).

Chini, R., E. Kreysa, E. Krügel, P.G. and Mezger, 1986. Sub–mm observations of IRAS galaxies, *Astron. Astrophys.*, **166**, L8.

Day, K.L., 1976. Further measurements of amorphous silicates, *Astrophys. J.*, **210**, 614.

Désert, F.X., F. Boulanger, and J.L. Puget, 1990. Very small grains and interstellar dust models, *Astron. Astrophys.*, in press.

Donn, B.D., J.E. Allen, and R.K. Khanna, 1989. A critical assessment of the PAH hypothesis, in *Interstellar Dust*, L.J. Allamandola and A.G.G.M. Tielens (Eds.), Kluwer, Dordrecht, p. 181.

Draine, B.T., and H.M. Lee, 1984. Optical properties of interstellar graphite and silicate grains, *Astrophys. J.*, **285**, 89.

Draine, B.T., and N. Anderson, 1985. Temperature fluctuations and infrared emission from interstellar grains, *Astrophys. J.*, **292**, 494.

Eales, S.A., C.G. Wynn–Williams, and W.D. Duncan, 1989. Cold dust in galaxies, *Astrophys. J.*, **339**, 859.

Edelson, R.A., and M.A. Malkan, 1986. Spectral energy distributions of active galactic nuclei between 0.1 and 100 microns, *Astrophys. J.*, **308**, 59.

Emerson, J.P., P.E. Clegg, G. Gee, C.T. Cunningham, M.J. Griffin, L.M.J. Brown, E.I. Robson, and A. Longmore, 1984. *Nature*, **311**, 237.

Fadeyev, Yu.A., 1987. Formation and destruction of dust grains in circumstellar regions, in *Circumstellar Matter*, Appenzeller, I., and Jordan, C. (Eds.), D. Reidel, Dordrecht, p. 515.

Heitler, W., 1954. The Quantum Theory of Radiation, Dover, New York.

Gatley, I., E.E. Becklin, M.W. Werner, and C.G. Wynn–Williams, 1977. Airborne far–infrared observations of the galactic center region, *Astrophys. J.*, **216**, 277.

Gear, W.K., E.I. Robson, and M.J. Griffin, 1988. Millimetre and submillimetre observations of the emission from dust in compact HII regions, *Mon. Not. R. Astron. Soc.*, **231**, 55p.

Helou, G., 1986. The IRAS colors of normal galaxies, *Astrophys. J.*, **311**, L33.

Infrared Astronomical Satellite (IRAS) Catalogs and Atlases: *Explanatory Supplement*, 1988. C.A. Beichman, G. Neugebauer, H.J. Habing, P.E. Clegg, and T.J. Chester (Eds.), National Aeronautics and Space Administration, Washington, D.C..

Keene, J., D.P. Carico, G. Neugebauer, B.T. Soifer, 1990. Millimeter observations of luminous IRAS galaxies, in *Submillimetre Astronomy*, Watt, G.D., and Webster, A.S. (Eds.), Kluwer, Dordrecht, p. 209.

Koike, C., H. Hasegawa, and A. Manabe, 1980. Extinction coefficients of amorphous carbon grains from 2100 Å to 340 μm, *Astrophys. Space Sci.*, **67**, 495.

Mathis, J.S., P.G. Mezger, and N. Panagia, 1983. *Astron. Astrophys.*, **128**, 212.

Mie, G., 1908. Beitrage zur Optik trüber Medien speziell kolloidaler Metallösungen, *Ann. Phys.*, **25**, 377.

Pajot, F., P. Boissé, R. Gispert, J.M. Lamarre, J.L. Puget, and G. Serra, 1986. Temperature distribution of interstellar dust, *Astron. Astrophys.*, **157**, 393.

Pollack, J.B., and J.N. Cuzzi, 1980. Scattering by nonspherical particles of size comparable to a wavelength: a new semi–empirical theory and its application to tropospheric aerosols, *J. Atmospher. Sci*, **37**, 868.

Purcell, E.M., and C.R. Pennypacker, 1973. Scattering and absorption of light by non–spherical dielectric grains, *Astrophys. J.*, **186**, 705.

Roche, P.F., D.K. Aitken, C.H. Smith, and S.D. James, 1986. NGC 4418; a very extinguished galaxy, *Mon. Not. R. Astron. Soc.*, **218**, 19p.

Salpeter, E.E., 1974. Formation and flow of dust grains in cool stellar atmospheres, *Astrophys. J.*, **193**, 585.

Schlömann, E., 1964. Dielectric losses in ionic crystals with disordered charge distributions, *Phys. Rev.*, **135**, A413.

Schwartz, P.R., 1982. The spectral dependence of dust emissivity at millimeter wavelengths, *Astrophys. J.*, **252**, 589.

Seki, J., and T. Yamamoto, 1980. Amorphous interstellar grains: Wavelength dependence of far–infrared emission efficiency, *Astrophys. Space Sci.*, **72**, 79.

Soifer, B.T., L. Boehmer, G. Neugebauer, and D.B. Sanders, 1989. The *IRAS* Bright Galaxy Sample. IV. Complete *IRAS* observations, *Astronom. J.*, **98**, 766.

Soifer, B.T., D.B. Sanders, B. Madore, G. Neugebauer, G.E. Danielson, J.H. Elias, C.J. Persson, and W.L. Rice, 1987. The *IRAS* Bright Galaxy Sample. II. The sample and luminosity function, *Astrophys. J.*, **320**, 238.

Sopka, R.J., R. Hildebrand, D.T. Jaffe, I. Gatley, T. Roellig, M. Werner, M. Jura, and B. Zuckerman, 1985. Submillimeter observations of evolved stars, *Astrophys. J.*, **294**, 242.

Thronson, H.A., C.K. Walker, C.E. Walker, and P. Maloney, 1987. Observations of 1.3 millimeter continuum emission from the centers of galaxies, *Astrophys. J.*, **318**, 645.

Tielens, A.G.G.M., and L.J. Allamandola, 1987. Composition, structure, and chemistry of interstellar dust, in *Interstellar Processes*, Hollenbach, D.J., and Thronson, H.A., (Eds.), D. Reidel, Dordrecth, p.397.

van de Hulst, H.C., 1957. *Light Scattering by Small Particles*, Dover, New York.

Watson, W.D., and E.E. Salpeter, 1972. Molecule formation on interstellar grains, *Astrophys. J.*, **174**, 321.

Weedman, D. W. (1986). *Quasar Astronomy* (Cambridge, Cambridge University Press).

Whittet, D.C.B., 1988. The observed properties of interstellar dust in the infrared, in *Dust in the Universe*, Bailey, M.E., and Williams, D.A. (Eds.), Cambridge University Press, Cambridge, p. 25.

Wright, E.L., 1987. Long–wavelength absorption by fractal dust grains, *Astrophys. J.*, **320**, 818.

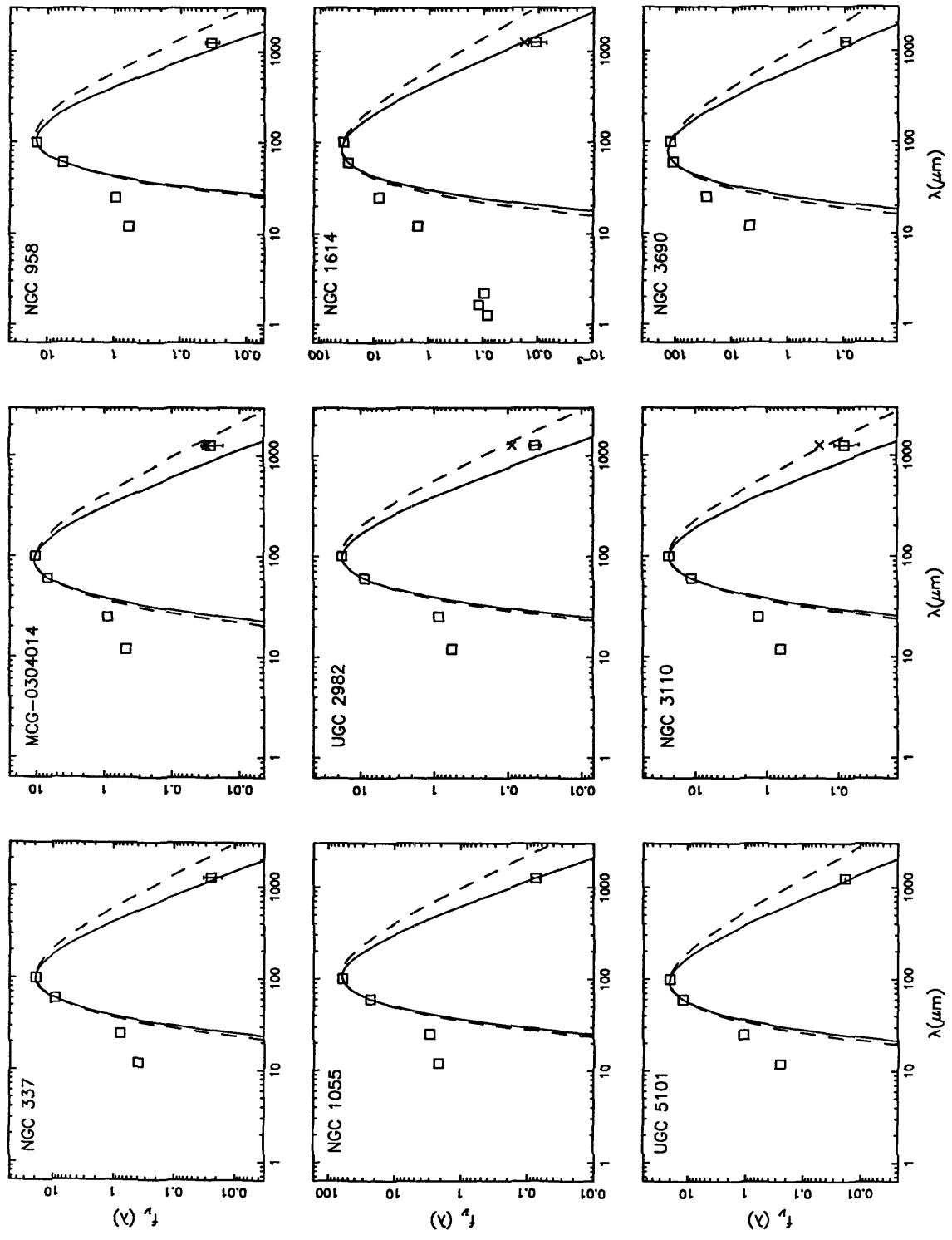
NGC 337
NGC 1055
UGC 5101
MCG-0304014
UGC 2982
NGC 3110
NGC 958
NGC 1614
NGC 3690
f_ν (λ)
λ(μm)

Fig. 2

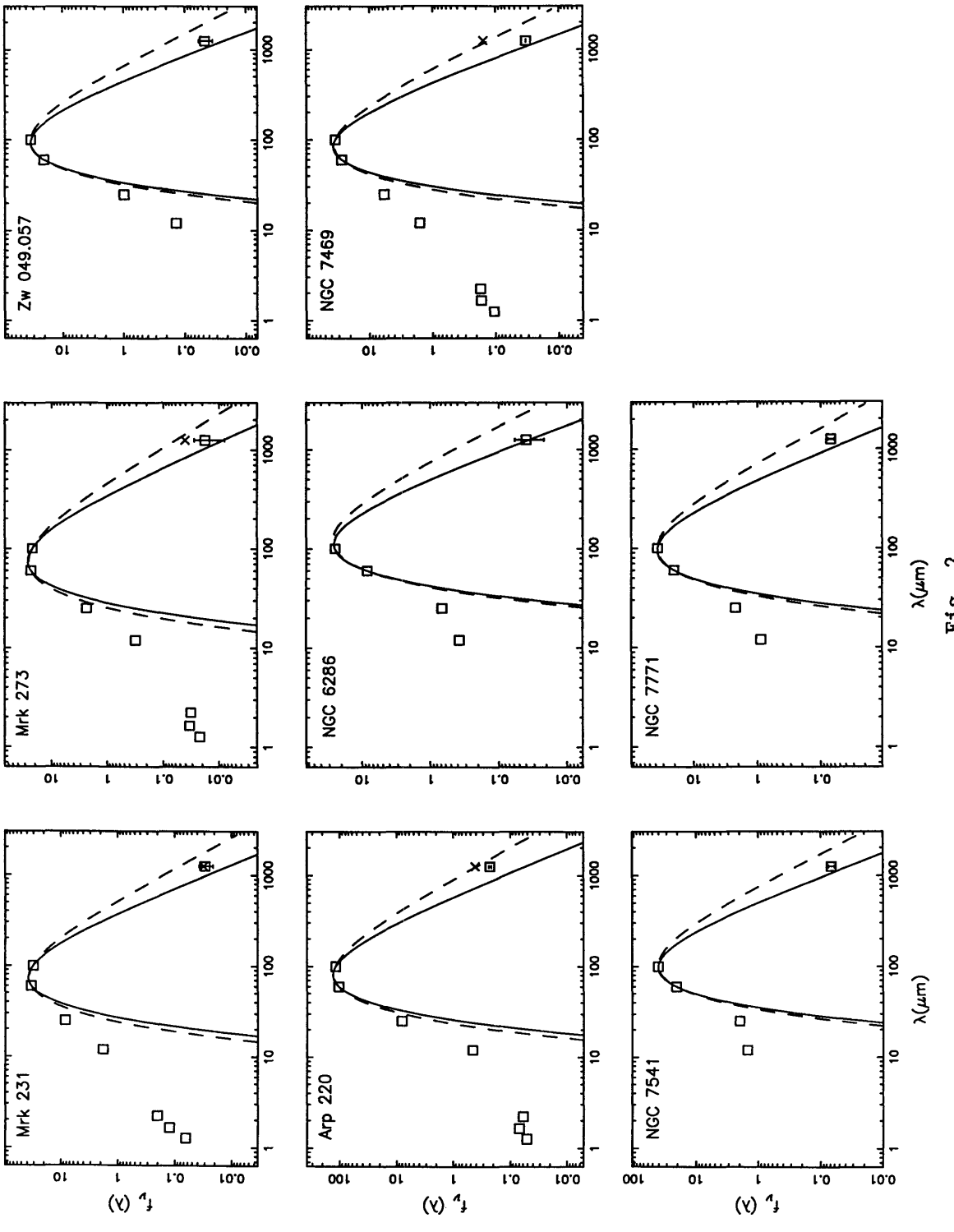
Mrk 231
Arp 220
NGC 7541
Mrk 273
NGC 6286
NGC 7771
Zw 049.057
NGC 7469
f_ν (λ)
λ(μm)

Fig. 2

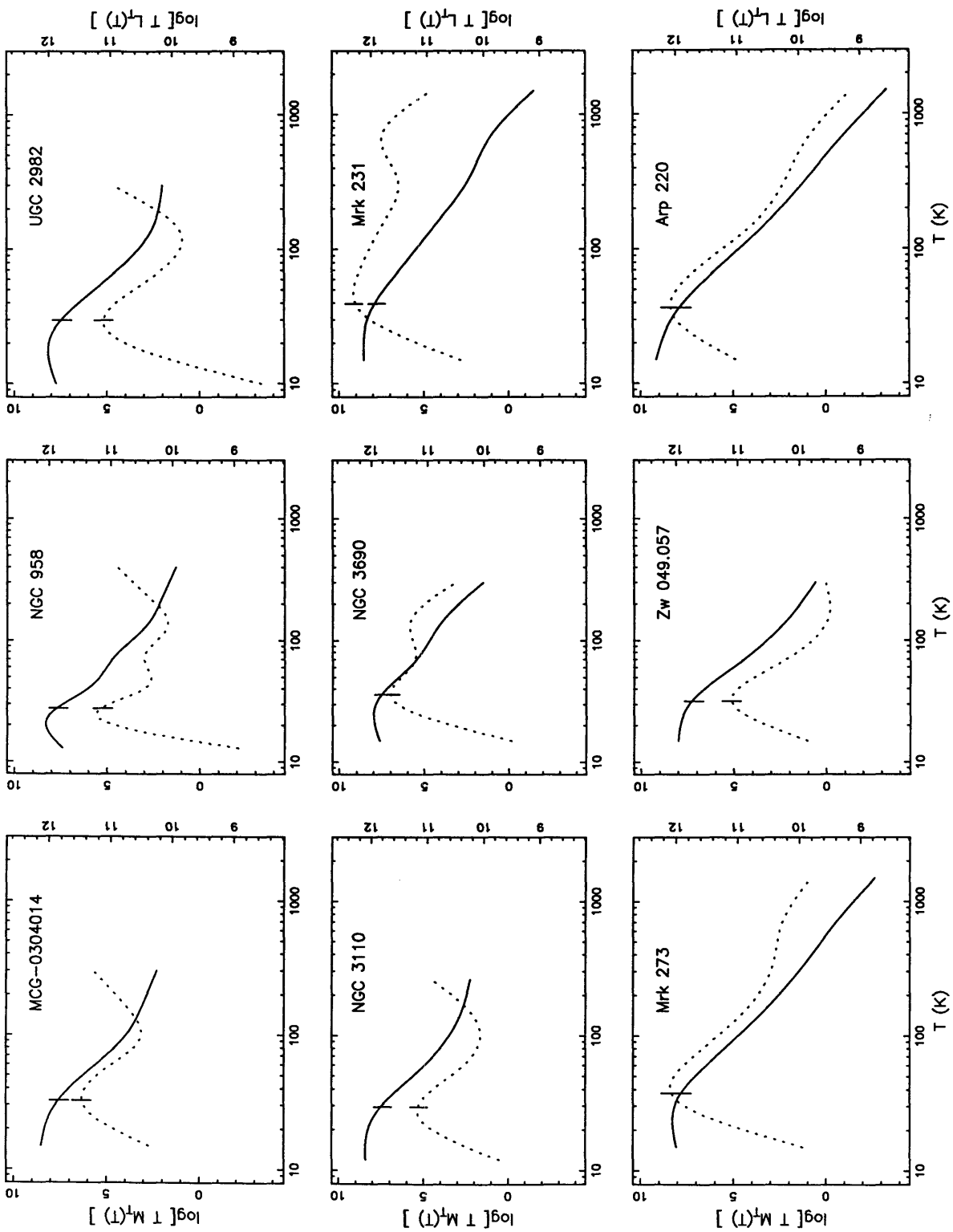
Arp 220
Mrk 231
UGC 2982
Zw 049.057
NGC 958
NGC 3690
Mrk 273
NGC 3110
MCG-0304014
log[T L_T(T)]
log[T M_T(T)]
T (K)

Fig. 4

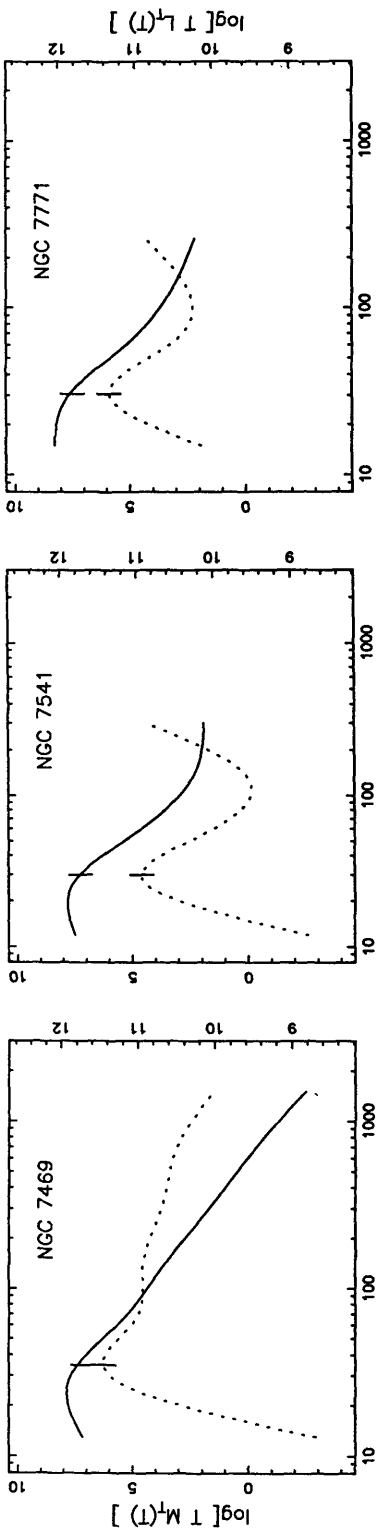
log[T $M_t(T)$]
log[T $L_t(T)$]
NGC 7469
NGC 7541
NGC 7771
0
5
10
9
10
11
12
10
100
1000

Fig. 4

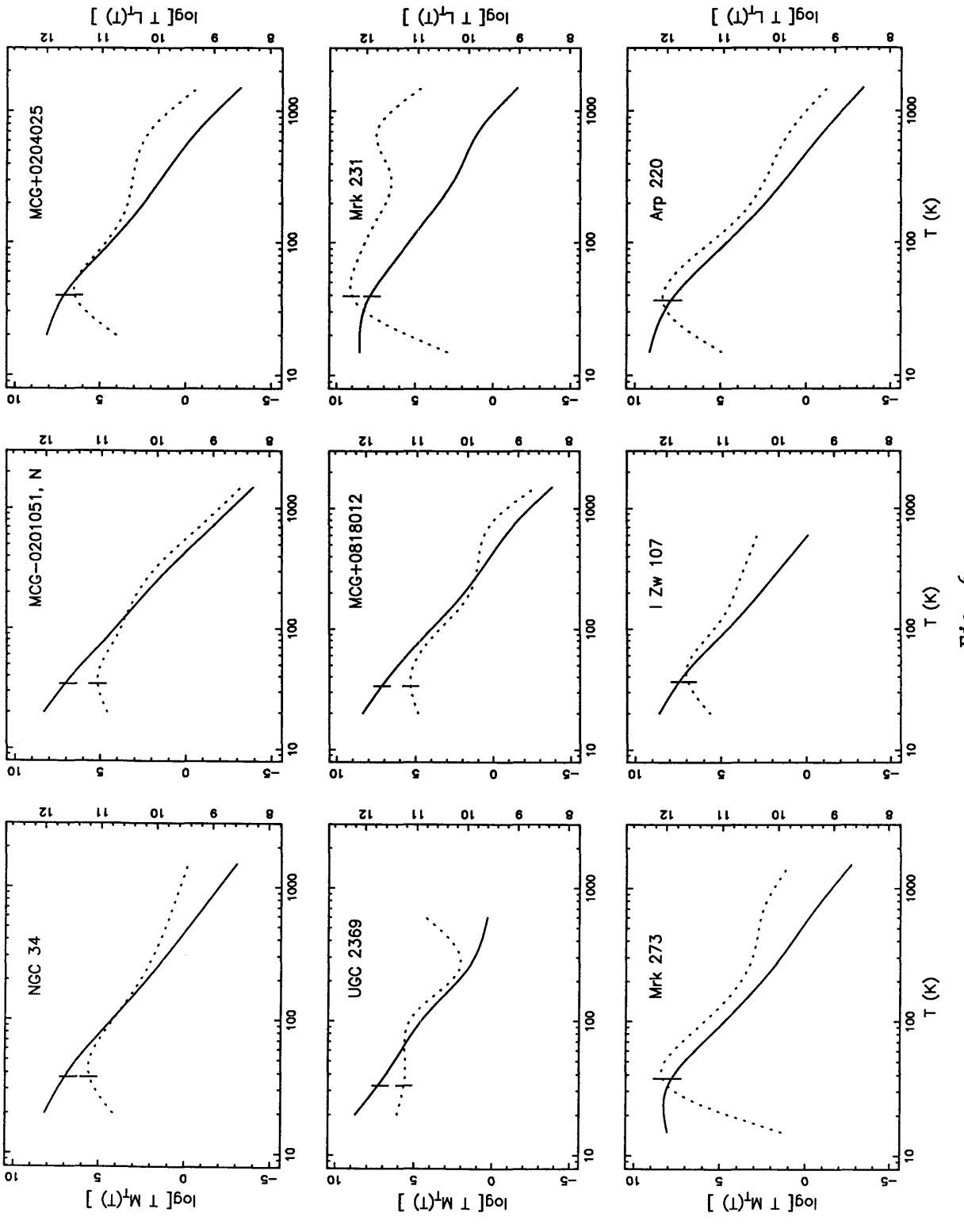
Mrk 273
UGC 2369
NGC 34
I Zw 107
MCG+0818012
MCG-0201051, N
Arp 220
Mrk 231
MCG+0204025
T (K)
log[T M_T(T)]
log[T L_T(T)]

Fig. 6

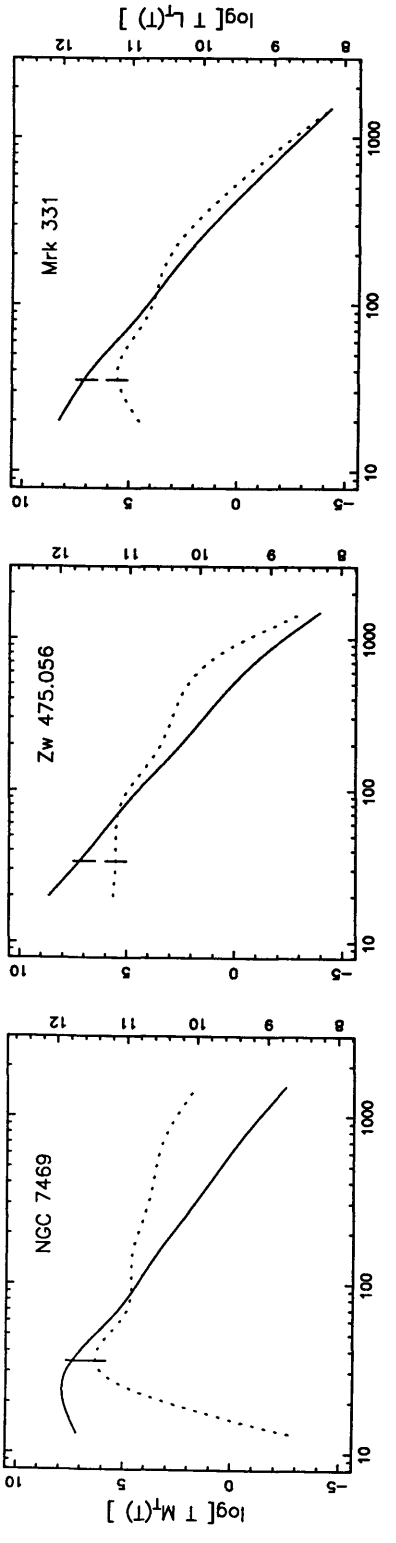

Fig. 6

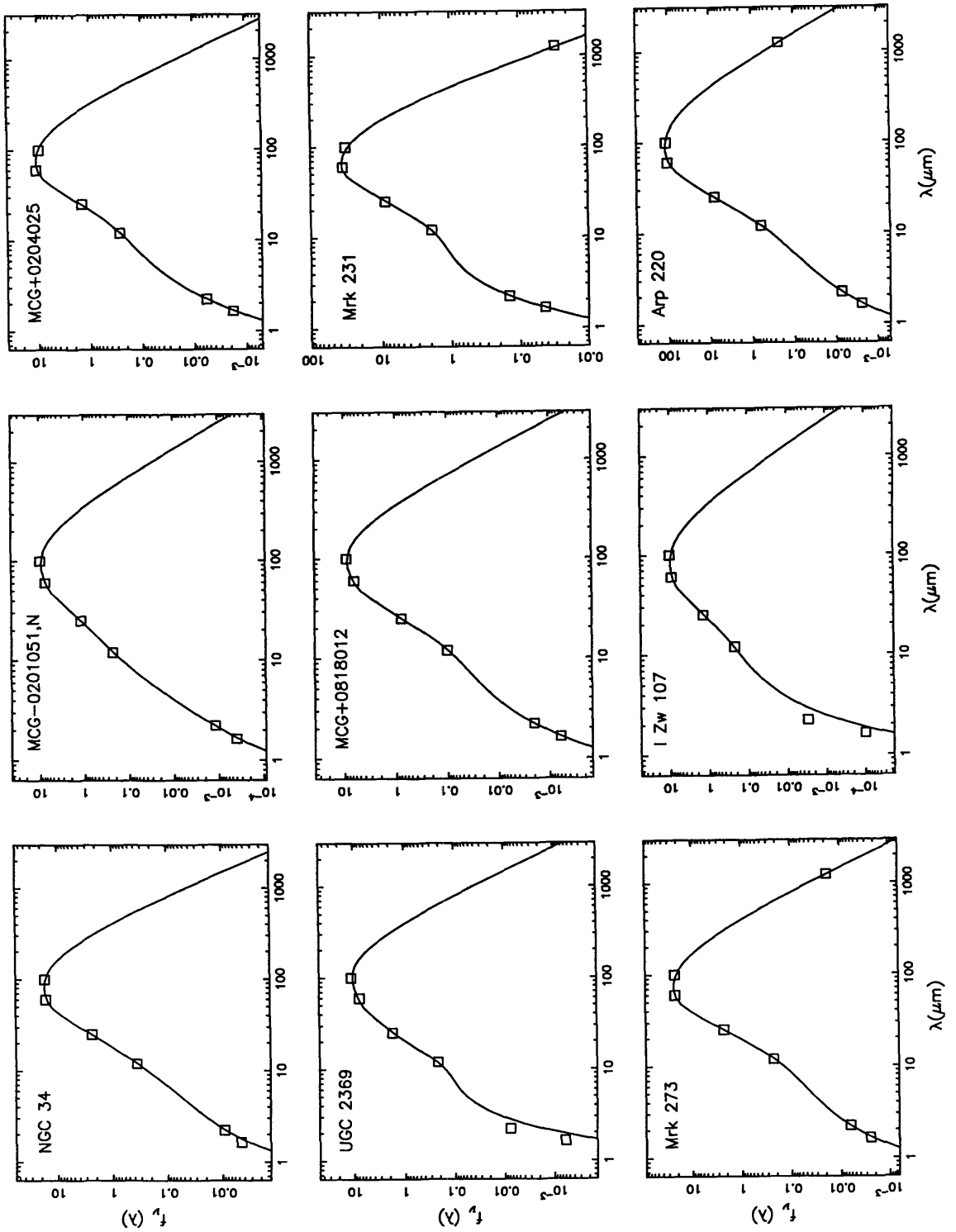
NGC 34
UGC 2369
Mrk 273
MCG-0201051,N
MCG+0818012
I Zw 107
MCG+0204025
Mrk 231
Arp 220
λ(μm)
λ(μm)
λ(μm)
f_ν (λ)
f_ν (λ)
f_ν (λ)

Fig. 7

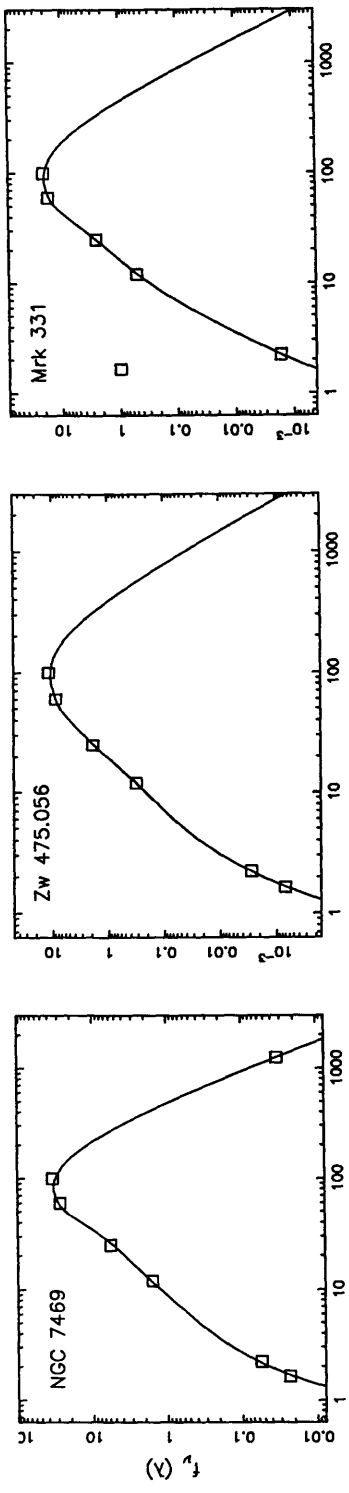

Fig. 7